

2019

A multisensor and multiscale methodological framework for the management of complex natural ecosystems

# A MULTISENSOR AND MULTISCALE METHODOLOGICAL FRAMEWORK FOR THE MANAGEMENT OF COMPLEX NATURAL ECOSYSTEMS

Tesis Doctoral

Programa de Oceanografía y Cambio Global

Edurne Ibarrola Ulzurrun

Las Palmas de Gran Canaria

Febrero 2019













UNIVERSIDAD DE LAS PALMAS  
DE GRAN CANARIA

**D. SANTIAGO HERNÁNDEZ LEÓN COORDINADOR DEL PROGRAMA DE  
DOCTORADO DE OCEANOGRAFÍA Y CAMBIO GLOBAL DE LA  
UNIVERSIDAD DE LAS PALMAS DE GRAN CANARIA,**

**INFORMA,**

Que la Comisión Académica del Programa de Doctorado, en su sesión de fecha 25 de febrero de dos mil diecinueve tomó el acuerdo de dar el consentimiento para su tramitación, a la tesis doctoral titulada *A multisensor and multiscale methodological framework for the management of complex natural ecosystems* presentada por la doctoranda D<sup>a</sup> Edurne Ibarrola Ulzurrun y dirigida por el Dr. Javier Marcello Ruiz y la Dra. Consuelo Gonzalo Martín.

Asimismo, se acordó el informar favorablemente la solicitud para optar a la Mención Internacional del Título de Doctor, por cumplir los requisitos reglamentarios.

Y para que así conste y a efectos de lo previsto en el Artº 11 del reglamento de Estudios de Doctorado (BOULPGC 7/10/2016) de la Universidad de Las Palmas de Gran Canaria, firmo la presente en Las Palmas de Gran Canaria, a 25 de febrero de diecinueve.



**A MULTISENSOR AND MULTISCALE METHODOLOGICAL  
FRAMEWORK FOR THE MANAGEMENT OF COMPLEX  
NATURAL ECOSYSTEMS**

**METODOLOGÍA MULTISENSOR Y MULTIESCALA PARA LA  
GESTIÓN DE ECOSISTEMAS NATURALES COMPLEJOS**

Tesis doctoral presentada por Edurne Ibarrola Ulzurrun

Programa de Oceanografía y Cambio Global

Instituto de Oceanografía y Cambio Global (IOCAG), Universidad de Las Palmas de  
Gran Canaria (ULPGC)

Dirigida por el Dr. Javier Marcello Ruiz (ULPGC) y la Dra. Consuelo Gonzalo  
Martín (UPM)

La doctoranda

Director

Co-directora

Las Palmas de Gran Canaria, Febrero de 2019





## AGRADECIMIENTOS

Deseo expresar en este apartado mis agradecimientos a las personas e instituciones que han hecho posible, con su ayuda y apoyo, la realización de esta Tesis Doctoral.

En primer lugar, agradecer al programa de Formación de Personal Investigador (FPI) del Ministerio de Economía y Competitividad por la financiación recibida para el desarrollo de la Tesis, así como para la movilidad internacional. También a todos los miembros del proyecto ARTEMISAT, por apostar por la chica del norte, y acogerme desde la primera reunión del proyecto a la que asistí. ¡Gracias por la oportunidad!

Por supuesto, a mis directores, el Dr. Javier Marcello (ULPGC) y la Dra. Consuelo Gonzalo (UPM), no solo por todo el tiempo que han dedicado en dirigir mi trabajo y la confianza que han depositado en mí, sino por sus consejos y contribuciones, que me han hecho crecer profesional y personalmente. También merecen unas palabras, por su paciencia y por los buenos ratos, Dioni y Ángel, ¡qué hubiese sido de mí sin vuestra ayuda!

Agradecer también sus consejos y aportaciones durante toda la Tesis a los gestores del Parque Nacional del Teide, sobre todo a José Luis Martín Esquivel, por su colaboración en estos últimos meses. Gracias también al INTA, por la imagen hiperespectral prestada, que fue de gran ayuda para el desarrollo de la Tesis.

Recordar y agradecer a todos los miembros de MIDAS de la UPM por los buenos ratos pasados y por haberme acogido durante mi primer año de doctorado, ¡qué lejos quedaba este día!

Moreover, I would like to thank to Jocelyn Chanussot from GIPSA-Lab (Grenoble, France), not only for hosting and guiding me during the international exchange, but for his support and suggestions made afterwards. Besides, I want to say some words for all the people working at GIPSA-Lab, which made that stay unforgettable. Sobre todo, a las bonitas casualidades, Lara, Miguel y María, no hubiese sido lo mismo sin vosotr@s.

Hablando de estancias, no olvidar a María González de Audicana, del Departamento de Ingeniería de la Universidad Pública de Navarra (UPNA), que me ha acogido durante estos últimos meses de doctorado en mi ciudad natal, por compartir conmigo su experiencia, ¡seguimos colaborando!. No olvidar a todas las personas del grupo de investigación THERRAE, por muchos más seminarios y cafés. Sobre todo a los compis de laboratorio, que han hecho que escribir la memoria no fuese tan duro.

Fuera del ámbito académico, a todas las personas que se han cruzado y aparecido durante mi periodo en Madrid, Las Palmas, Grenoble y Pamplona, y han

mostrado interés sobre mi Tesis (cerveza o cuerda en mano), aguantado la “chapa”, sin entender bien que era eso de la teledetección.

Quienes sí entienden todo el proceso de realizar la Tesis Doctoral son “Biologakada”, por ser ya doctores (zorionak!), por estar en proceso de ser doctor, o por qué nos tienen que aguantar día sí y día también. ¡Gracias por haber aparecido hace ya 13 años y seguir ahí!

Mis últimas palabras son para mi familia. A mi hermano, por nuestro apoyo mutuo, y a mis padres, por todo su amor y comprensión desde el principio, en los buenos y malos momentos, y a pesar de la distancia. A mi segunda familia, por su cariño, a pesar de que el “txikito” de la familia se fue lejos. Y sobre todo a Asier, por tu “hasta el fin del mundo”, siendo este fin del mundo Madrid y Las Palmas. Por estar desde el principio hasta el final en esta aventura, aguantando altibajos y entendiéndolos. ¡Gracias por estar ahí siempre!

A todas las personas que han estado presentes...

¡GRACIAS!

ESKERRIK ASKO!

Las Palmas de Gran Canaria, febrero de 2019

## PREFACIO

La tesis doctoral, titulada *Metodología multisensor y multiescala para la gestión de ecosistemas naturales complejos*, se ha desarrollado dentro del Programa de Doctorado en Oceanografía y Cambio Global, bajo la supervisión del Dr. Javier Marcello Ruiz, del Grupo de Procesado de Imágenes y Teledetección perteneciente al Instituto de Oceanografía y Cambio Global (IOCAG) de la Universidad de Las Palmas de Gran Canaria (ULPGC), y de la Dra. Consuelo Gonzalo Martín, profesora del Departamento de Arquitectura y Tecnología de Sistemas Informáticos, de la Universidad Politécnica de Madrid (UPM).

El trabajo desarrollado se enmarca dentro de los proyectos ARTEMISAT (CGL2013-46674-R) y ARTEMISAT-2 (CTM2016 77733-R), del Programa Estatal de Investigación, Desarrollo e Innovación Orientada a los Retos de la Sociedad, así como de las estancias realizadas en el Laboratorio de Análisis de Datos del Centro de Biotecnología Médica, en la Universidad Politécnica de Madrid (UPM); en *Grenoble Institute of Engineering, GIPSA-lab* de la Universidad Grenoble Alpes CNRS (Francia) y en el grupo de investigación THERRAE del Departamento de Ingeniería en la Universidad Pública de Navarra (UPNA). La Tesis ha recibido el apoyo financiero de los programas de Ayudas a la Formación de Personal Investigador en Formación del MINECO (Gobierno de España) (BES-2014-069426), de la Agencia Estatal de Investigación (AEI), y del Fondo Europeo de Desarrollo Regional (FEDER).

La Tesis está compuesta por una recopilación de cinco trabajos originales, publicados o en proceso de revisión en revistas indexadas en el *Journal Citations Reports*, y organizada según el Reglamento de Estudios de Doctorado de la ULPGC (BOULPGC, Cap. III, Art. 11 y 12, 7 de octubre de 2016) en lengua inglesa, incluyendo una introducción general que presenta los objetivos de la Tesis y los trabajos publicados, a continuación se detallan las cinco contribuciones científicas siguiendo el formato de artículo científico convencional y, por último, se sintetizan las principales conclusiones. En cumplimiento de la normativa del Reglamento de Estudios de Doctorado de la ULPGC (BOULPGC, Cap. III, Art. 10, 7 de octubre de 2016), la Tesis también incluye una sección en lengua castellana detallando los objetivos desarrollados y las principales conclusiones.



## PREFACE

The Doctoral Thesis, entitled *A multisensor and multiscale methodological framework for the management of complex natural ecosystems*, has been developed within the Oceanography and Global Change Doctoral Program, under the supervision of Ph.D. Javier Marcello Ruiz, of the Image Processing and Remote Sensing Group belonging to *the Instituto de Oceanografía y Cambio Global (IOCAG)* of the *Universidad de Las Palmas de Gran Canaria (ULPGC)*, and Ph.D. Consuelo Gonzalo Martín, belonging to the *Departamento de Arquitectura y Tecnología de Sistemas Informáticos*, of the *Universidad Politécnica de Madrid (UPM)*.

This work has been accomplished in the frame of the ARTEMISAT (CGL2013-46674-R) and ARTEMISAT-2 (CTM2016 77733-R) projects within the *Programa Estatal de Investigación, Desarrollo e Innovación Orientada a los Retos de la Sociedad*, as well as stays at the Data Mining Laboratory at the Center of Biomedical Technologies, *Universidad Politécnica de Madrid (UPM)*; Grenoble Institute of Engineering, GIPSA-lab in the University Grenoble Alps, CNRS (France) and in the THERRAE research group at the *Departamento de Ingeniería* of the *Universidad Pública de Navarra (UPNA)*. The Thesis has received the financial support of the programs of *Ayudas a la Formación de Personal Investigador en Formación* of MINECO (*Gobierno de España*) (BES-2014-069426), and *Agencia Estatal de Investigación (AEI)*, and the *Fondo Europeo de Desarrollo Regional (FEDER)*.

The Thesis is composed of a compilation of five original works, published or under revision in indexed journals (Journal Citations Reports) and organized according to the *Reglamento de Estudios de Doctorado* of the ULPGC (BOULPGC, Chap. III, Art. 11 and 12, October 7<sup>th</sup>, 2016) in English language, including a general introduction presenting the main objectives of the Thesis and the articles published or under revision, then adding the five scientific contributions following the conventional scientific article format and, finally, summarizing the main conclusions. In compliance with the regulations of the *Reglamento de Estudios de Doctorado* of the ULPGC (BOULPGC, Chap. III, Art. 11 and 12, October 7<sup>th</sup>, 2016), the Thesis also includes a section in Spanish explaining the objectives developed and the main conclusions.



---

**TABLE OF CONTENT**

Resumen .....	1
Abstract.....	11
Chapter 1. Introduction and objectives .....	13
1.1. Objectives of the Thesis .....	16
1.2. Publications .....	19
1.3. Thesis structure.....	20
1.4. References .....	22
Chapter 2. Study areas and methodology.....	25
2.1. Study areas and ecosystem description.....	27
2.2. Datasets .....	31
2.3. Pre-processing techniques .....	34
2.4. Spectral unmixing.....	47
2.5. Classification techniques.....	50
2.6. Applications of remote sensing.....	54
2.7. References .....	57
Chapter 3. Fusion of high resolution multispectral images in vulnerable coastal and land ecosystems .....	77
Chapter 4. Influence of pansharpening in obtaining accurate vegetation Maps .....	105
Chapter 5. Assessment of component selection strategies in hyperspectral Imagery .....	127
Chapter 6. Hyperspectral classification through unmixing abundances maps addressing the spectral variability.....	149
Chapter 7. Temporal dynamic analysis of a mountain ecosystem based on multi-source and multi-scale remote sensing data .....	169
Chapter 8. Conclusions and future research .....	197
8.1. Conclusions and contributions.....	199
8.2. Future research.....	201
8.3. Scientific contributions.....	202
Acronyms .....	205





## RESUMEN

Los ecosistemas naturales proporcionan una amplia variedad de recursos naturales que mejoran el bienestar humano. Sin embargo, en las últimas décadas, ha habido una disminución en dichos recursos, así como en la biodiversidad en los ecosistemas, debido a la intensificación del uso agrícola, el desarrollo turístico, el cambio climático y otras actividades. Por ello, el estudio del estado de conservación de áreas naturales es esencial para guiar a los gestores ambientales en su toma de decisiones.

Hasta ahora, las observaciones de campo han sido la principal fuente de información para la evaluación del estado de conservación de los distintos tipos de hábitat. Sin embargo, son costosas y requieren de una mano de obra intensiva, por lo tanto, no son adecuadas para ser repetidas con frecuencia, ni para aplicarlas en zonas con una gran extensión. En este contexto, los datos de teledetección pueden proporcionar información valiosa y complementar dichas observaciones de campo. Así, la teledetección ofrece la oportunidad de proporcionar información constante en el tiempo y el espacio, al ser una herramienta precisa y repetible, para ayudar en el mapeo y vigilancia de los ecosistemas y su estado de conservación. Sin embargo, es de gran importancia el desarrollo de técnicas avanzadas de procesado de imágenes para obtener metodologías fiables para el análisis, la conservación y la gestión de entornos terrestres y marinos, de forma automática, continua, económica, y a la resolución espacial, espectral y temporal adecuada.

De este modo, la teledetección se ha convertido en una tecnología importante debido al progreso que los sensores han experimentado en las últimas décadas, proporcionando una gran cantidad de imágenes con alta resolución espacial y espectral. Como ya se ha indicado, la teledetección ofrece un medio práctico y rentable para una buena gestión ambiental, especialmente cuando se deben monitorizar grandes áreas o se necesita información periódica. En definitiva, la vigilancia de los ecosistemas de forma detallada y fiable, a través de la teledetección, sigue siendo un desafío, ya que requiere sensores y métodos que puedan tratar con zonas de transición complejas presentes en la vegetación natural. Un factor a considerar cuando se cartografían hábitats naturales es la complejidad de la estructura del paisaje. Además, el estado de conservación se evalúa por las estructuras del hábitat, la presencia de especies características, los factores abióticos y las presiones o perturbaciones en el ecosistema de estudio.

Los nuevos sensores hiperespectrales a bordo de plataformas aéreas, junto con los sensores multispectrales de muy alta resolución espacial, permiten analizar ecosistemas complejos, siendo en un tema actual y de elevado interés para la comunidad de teledetección y conservación.

Específicamente, la disponibilidad de nuevos sensores, a bordo de satélites o aerotransportados, puede ayudar a generar mapas precisos de vegetación en zonas

naturales protegidas, especialmente en áreas insulares que, en general, son más pequeñas y, habitualmente, con ecosistemas más complejos y heterogéneos. Por lo tanto, estas áreas deben ser estudiadas a través de sensores de última generación con las máximas resoluciones espaciales y espectrales.

El contexto de la Tesis se abarca el análisis de los ecosistemas terrestres utilizando imágenes de muy alta resolución, concretamente imágenes multiespectrales, pancromaticas e hiperespectrales, para la obtención de productos de alta calidad que permitan el análisis exhaustivo de los recursos naturales. La Tesis se ha centrado en varios ecosistemas que se encuentran en la región de la Macaronesia, en las Islas Canarias (España), ya que se considera un importante foco geológico y de biodiversidad debido a su origen volcánico.

El objetivo general de la Tesis es el análisis y desarrollo de metodologías avanzadas de procesamiento de imágenes multiespectrales e hiperespectrales de muy alta resolución, que permita la obtención de información precisa para la conservación de ecosistemas terrestres complejos y vulnerables. Por lo tanto, se han implementado técnicas avanzadas en cada etapa de procesamiento para corregir o mejorar la calidad de las imágenes y permitir la generación de productos de valor añadido de utilidad para los gestores de las zonas protegidas.

Para lograr el objetivo global, se han abordado los siguientes objetivos a un nivel más específico:

- Selección de los datos de teledetección y auxiliares adecuados para la caracterización de los ecosistemas a analizar.
- Análisis y aplicación de algoritmos avanzados de pre-procesado para proporcionar información espacial y espectral de alta calidad.
- Evaluación y aplicación de técnicas clásicas y avanzadas de desmezclado y clasificación para la discriminación de cubiertas vegetales.
- Desarrollo de la metodología óptima para la generación de productos específicos para la gestión de los ecosistemas analizados.
- Estudio de variabilidad de los recursos naturales en los ecosistemas analizados.

La Tesis se ha escrito como compendio de 5 artículos, 4 de ellos ya publicados en revistas científicas internacionales indexadas y 1 artículo en fase de revisión. La intención de cada artículo es que se pueda leer de forma independiente; por consiguiente, puede haber cierta superposición de contenidos entre los diferentes artículos.

El Capítulo 1 proporciona una introducción general en la que se presentan los objetivos de la Tesis, así como la estructura de la misma. El Capítulo 2 describe el marco general de la metodología utilizada durante la Tesis. Los siguientes cinco capítulos corresponden a los artículos publicados o en revisión. La unidad temática de esta Tesis se justifica al comienzo de cada uno de estos cinco capítulos.

Específicamente, los Capítulos 3 y 4 tratan sobre el procesado de imágenes multiespectrales. Concretamente, el Capítulo 3 presenta una evaluación de las diferentes técnicas de *pansharpening* para las imágenes multiespectrales de muy alta resolución, mostrando las técnicas más adecuadas según el tipo de ecosistema. El Capítulo 4 evalúa la influencia de las diferentes técnicas de mejora de la calidad espacial (*pansharpening*) al obtener mapas temáticos precisos aplicando clasificadores, a nivel de píxel y objeto, en imágenes multiespectrales. Los Capítulos 5 y 6 se centran en las imágenes hiperespectrales. El Capítulo 5 compara estrategias de reducción de la dimensionalidad y evalúa diferentes estrategias de selección de componentes en imágenes hiperespectrales, mientras que el Capítulo 6 presenta un marco de clasificación hiperespectral a través de mapas de abundancia obtenidos a partir de modelos avanzados de *unmixing*, que consideran la variabilidad espectral de las clases. En el Capítulo 7 se propone una metodología para la detección de cambios en el ecosistema seleccionado, utilizando los mapas temáticos precisos tanto multiespectrales como hiperespectrales, obtenidos durante la Tesis. Finalmente, las conclusiones generales derivadas de este trabajo, así como las investigaciones futuras, se presentan en el Capítulo 8.

El área de estudio se ha centrado principalmente en el Parque Nacional del Teide, ubicado en la isla de Tenerife. Sin embargo, en el Capítulo 3, se incluyen imágenes multiespectrales adicionales en otras áreas protegidas de las Islas Canarias: la Reserva Natural de Maspalomas, en el sur de la isla de Gran Canaria, y un área del norte de Fuerteventura, que cubre los Parques Naturales de Corralejo e Islote de Lobos. Finalmente, en el Capítulo 5 se utiliza una imagen hiperespectral que fue adquirida por el INTA (Instituto Nacional de Técnica Aeroespacial) en Reborio (Asturias, España). Aunque la Tesis no se ha enfocado en esta área de estudio, se usó para evaluar diferentes estrategias para la selección de componentes, antes de que las imágenes hiperespectrales finales del Parque Nacional del Teide fueran adquiridas por el mismo instrumento CASI (*Compact Airborne Spectrographic Imager*).

Los datos de teledetección utilizados para la Tesis han sido, en primer lugar, imágenes multiespectrales de satélites de muy alta resolución espacial, concretamente tanto imágenes Worldview-2, como Quickbird. Ésta última solamente se ha utilizado en el estudio de detección de cambios llevado a cabo en el Parque Nacional del Teide al requerirse datos con mayor antigüedad. En segundo lugar, también se han utilizado imágenes hiperespectrales obtenidas por el Instituto Nacional de Técnica Aeroespacial (INTA) mediante el sensor CASI 1550i embarcado en la aeronave CASA C-2012-200, que logra la resolución espacial requerida para estudiar el complejo ecosistema del Parque Nacional del Teide.

A lo largo de la Tesis se han llevado a cabo tres campañas de campo, durante las cuales se adquirieron datos para validar la corrección atmosférica, a partir de medidas de las distintas clases de interés con el espectroradiómetro *ASD Field-Spec*,

así como muestras de vegetación para el entrenamiento y la validación en la clasificación supervisada. Todas las campañas de campo se llevaron a cabo en la misma fecha que la adquisición de las imágenes multiespectrales e hiperspectrales.

Normalmente, los proveedores de datos de teledetección realizan un pre-procesado preliminar; sin embargo, es necesario aplicar técnicas adicionales de pre-procesado y procesado para corregir y mejorar los datos del sensor y, para la generación de los productos finales. En particular, los algoritmos de pre-procesado son críticos para mejorar la calidad de la información disponible.

Durante la Tesis se han abordado distintas técnicas de pre-procesado: corrección atmosférica de las imágenes de partida; fusión de imágenes para aumentar la calidad de la imagen fusionada en comparación con las imágenes de origen; ortorectificación y co-registro de las imágenes; y, finalmente, reducción de la dimensionalidad en las imágenes hiperespectrales, necesaria ya que las variables dependientes redundantes no proporcionan información adicional sobre las clases, afectando negativamente a la eficiencia del clasificador.

Seguidamente, una vez pre-procesadas las imágenes, se han aplicado distintas técnicas de procesado. Concretamente, técnicas de desmezclado espectral (*spectral unmixing*), para descomponer los espectros de los píxeles en una colección de firmas espectrales puras, denominadas *endmembers*, y un conjunto de fracciones correspondientes o abundancias, que indican la proporción de cada *endmember* presente en el píxel. Otra técnica de procesado llevada a cabo durante la Tesis es la clasificación supervisada. Se presentan dos enfoques para la clasificación y el monitoreo de ecosistemas con datos de detección remota: el enfoque tradicional basado en píxeles y el enfoque novedoso basado en objetos. Como se mencionó anteriormente, el Parque Nacional del Teide es un ecosistema montañoso vulnerable y heterogéneo. Se analizaron diferentes algoritmos y, seguidamente, la clasificación se llevó a cabo utilizando el clasificador óptimo, agregando diferentes características (texturas, abundancias, índices de vegetación, etc.) al modelo de clasificación para obtener el mapa temático más preciso.

Finalmente, se propone una metodología precisa para analizar los cambios producidos en el Parque Nacional del Teide, utilizando los productos cartográficos obtenidos durante la Tesis.

En la Figura R.1 se presenta el diagrama de bloques simplificado de los diferentes procesos que componen la metodología del procesado.

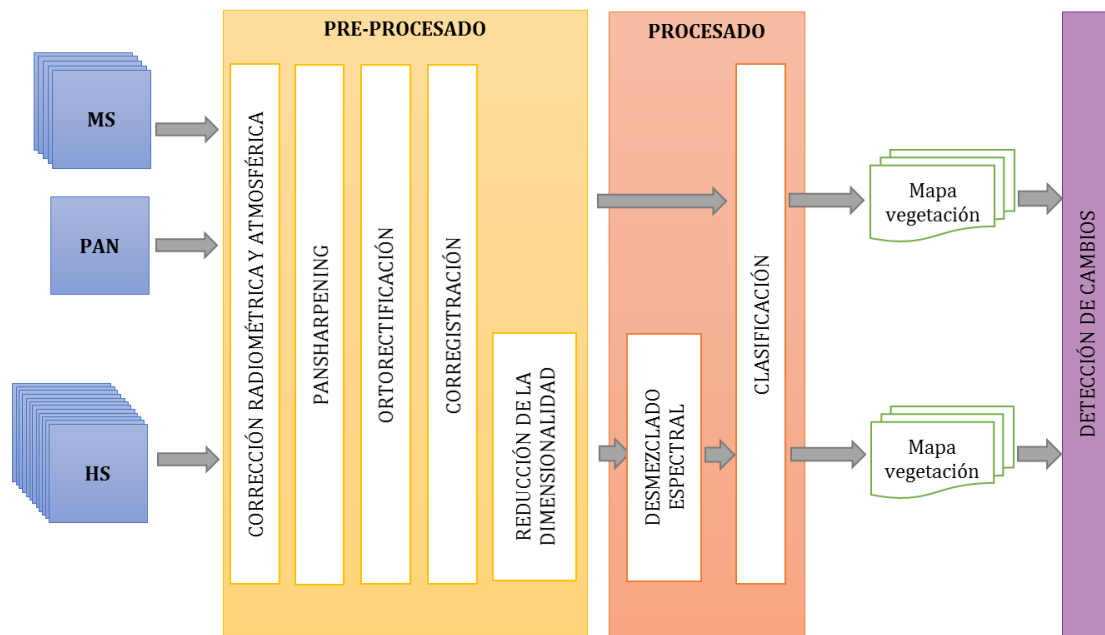


Figura R.1. Diagrama de bloques de la metodología de procesamiento llevada a cabo en la Tesis.

A continuación se resumen brevemente los artículos desarrollados en el marco de esta Tesis.

- **1. Fusion of high resolution multispectral imagery in vulnerable coastal and land ecosystems** (Sensors, 2017. Factor de impacto: 2.475).

En este artículo se estudian tres zonas vulnerables, que incluyen ecosistemas de matorral, áreas costeras con sistemas de dunas y zonas de aguas poco profundas. El objetivo de este análisis consiste en evaluar e identificar las técnicas de *pansharpening* que proporcionan la mejor imagen fusionada para los diferentes tipos de ecosistemas. Se utilizaron imágenes de alta resolución Worldview-2 debido a sus excelentes características espaciales y espectrales. Después de una evaluación preliminar de doce algoritmos de fusión, se analizaron un total de cuatro algoritmos de *pansharpening* (*Fast Intensity Hue Saturation*, *Hyperspherical Color Sharpening*, *Modulation Transfer Function – Generalized Laplacian Pyramid – High Pass Modulation* y *Weighted Wavelet ‘à trous’ through Fractal Dimension Maps*), usando seis índices de calidad (*Spectral Angle Mapper*, *Spectral and Spatial Relative Dimensionless Global Error* o *ERGAS*, *Frequency Comparison*, *Zhou* y *Q8*). La evaluación de la calidad se abordó no solo para todo el conjunto de bandas multiespectrales, sino también para el subconjunto de bandas espectrales cubiertas por el rango de longitudes de onda de la imagen pancromática y fuera de ella. Se observa una mejor calidad en la imagen fusionada utilizando sólo las bandas cubiertas por el rango de banda pancromática. Es importante resaltar el uso de estas

técnicas no solo en áreas urbanas y de tierra, sino en un análisis novedoso en áreas de ecosistemas de aguas poco profundas. Aunque las prestaciones de cada algoritmo no muestran una gran diferencia en las áreas terrestres y costeras, los ecosistemas costeros requieren algoritmos más simples, como el *Fast Intensity Hue Saturation*, mientras que los ecosistemas más heterogéneos, como los mixtos y de matorral, necesitan algoritmos avanzados: *Weighted Wavelet 'à trous' through Fractal Dimension Maps*. Además del estudio de calidad global, se realizó un análisis basado en mapas de calidad para estudiar el resultado de la fusión en cada banda a nivel local. Por último, para demostrar el rendimiento de estas técnicas de *pansharpening*, se llevó a cabo una clasificación basada en objetos, usando el clasificador *Support Vector Machine*. El resultado fue un mapa temático para el ecosistema de matorrales, que corrobora al algoritmo *Weighted Wavelet 'à trous' through Fractal Dimension Maps* como el mejor método de fusión para este ecosistema.

- **2. Influence of pansharpening in obtaining accurate vegetation maps** (Canadian Journal of Remote Sensing, 2017. Factor de impacto: 2.000).

El objetivo principal de este artículo consistió en evaluar la influencia de las técnicas de *pansharpening* en la obtención de mapas de vegetación precisos. Para ello, se implementaron y compararon diferentes técnicas de clasificación basadas en píxeles y objetos (*Maximum Likelihood, Mahalanobis Distance, Support Vector Machine, Bayes, Nearest Neighbor y K-Nearest Neighbor*) y se aplicaron a las imágenes fusionadas obtenidas a partir del estudio anterior. El Parque Nacional del Teide, en las Islas Canarias (España), fue elegido como área de estudio debido a que es un ecosistema heterogéneo vulnerable y que no dispone de cartografía detallada a nivel de especies vegetales. Las clases de vegetación de interés consideradas fueron establecidas por los gestores de conservación del Parque Nacional, previamente a la clasificación de las imágenes. Se aplicaron los diferentes pre-procesados (fusión, corrección atmosférica y ortorectificación). El algoritmo *Weighted Wavelet 'à trous' through Fractal Dimension Maps* demostró un rendimiento superior en la etapa de fusión de imágenes. El clasificador más adecuado para generar mapas temáticos de vegetación precisos en ecosistemas heterogéneos y mixtos fue el método *Bayes*, tras realizar la segmentación necesaria (*Multiresolution Segmentation*) para la clasificación a través de objeto, aunque *Support Vector Machine* logró una precisión general ligeramente más alta, el tiempo de cómputo era mucho mayor.

- **3. Assessment of component selection strategies in hyperspectral imagery** (Entropy, 2017. Factor de impacto: 2.305).

Las imágenes hiperespectrales integran muchas bandas continuas y estrechas que cubren diferentes regiones del espectro electromagnético. Sin embargo, el principal desafío es su alta dimensionalidad debido al fenómeno *Hughes*. Por lo tanto, la reducción de la dimensionalidad es necesaria antes de aplicar algoritmos de clasificación para obtener mapas temáticos precisos. El estudio se basó en datos

del sensor hiperespectral CASI y se centró en los siguientes algoritmos de extracción de características: análisis de componentes principales (PCA), fracción de ruido mínimo (MNF) y análisis de componentes independientes (ICA). Tras una revisión del estado del arte, se observó la carencia de un estudio comparativo sobre estas técnicas, así como de estrategias precisas para determinar el número de componentes adecuado. Por lo tanto, el primer objetivo fue comparar las técnicas tradicionales de reducción de dimensionalidad (PCA, MNF e ICA) para el sensor CASI y evaluar diferentes estrategias para seleccionar el número óptimo de componentes en el espacio transformado. El segundo objetivo fue analizar un nuevo enfoque de reducción de dimensionalidad dividiendo la imagen hiperespectral con respecto a las regiones espectrales que cubren el espectro electromagnético. Se apilaron las componentes seleccionadas del espacio transformado de las diferentes regiones espectrales de forma independiente. Este nuevo espacio transformado apilado se evaluó observando que enfoque propuesto mejoraba la clasificación final.

- **4. Hyperspectral classification through unmixing abundance maps addressing spectral variability** (IEEE Transactions on Geoscience and Remote Sensing, 2018. Factor de impacto: 4.662).

Como ya se ha mencionado, la teledetección y, en concreto, las imágenes hiperespectrales pueden contribuir a la generación de mapas de vegetación para la vigilancia de los ecosistemas. Para obtener correctamente dicha información y solucionar el inconveniente de los píxeles mixtos con contribuciones procedentes de diferentes materiales, la riqueza de los datos hiperespectrales permite la aplicación de técnicas de desmezclado. En este sentido, un problema encontrado tanto en el modelo de mezcla lineal tradicional (LMM), como en el algoritmo *Fully Constrained Least Squared Unmixing* (FCLSU), es la falta de capacidad para afrontar la variabilidad espectral de las clases. Este estudio se centra en evaluar el rendimiento de diferentes modelos de mezcla espectral en función de la calidad y la cantidad de los *endmembers*. Se seleccionó el Parque Nacional del Teide, al ser un complejo ecosistema montañoso con alta variabilidad espectral para una misma clase, principalmente causada por la topografía y las diferencias radiométricas en cada pasada del sensor aeroportado. Concretamente, para la imagen CASI, se comparó el algoritmo FCLSU con respecto a otros tres que sí consideran la variabilidad espectral: *Scaled Constrained Least Squares Unmixing* (SCLSU), *Extended LMM* (ELMM) y *Robust ELMM* (RELMM). El análisis incluye dos casos de estudio: (i) *endmembers* robustos y (ii) *endmembers* no robustos. Las prestaciones de cada algoritmo se calcularon utilizando el error cuadrático medio (RMSE) y los mapas tras la clasificación, los cuales se obtuvieron usando los mapas de abundancia como datos de entrada al clasificador. Se demostró que se necesitan técnicas avanzadas de desmezclado para abordar la variabilidad espectral y así obtener estimaciones de abundancia precisas. RELMM obtuvo excelentes valores de RMSE y mapas de clasificación más precisos, incluso en escenarios con poco conocimiento



del área de estudio y un esfuerzo mínimo en la selección de *endmembers*, evitando el problema de la dimensionalidad que se encuentra en las imágenes hiperespectrales.

- **5. Temporal dynamic analysis of a mountain ecosystem based on multi-source and multi-scale remote sensing data** (Ecosphere, en revisión. Factor de impacto: 2.671).

Durante las últimas décadas, el Parque Nacional del Teide ha sufrido importantes variaciones en los recursos naturales debido al cambio climático y a la presión antropogénica y de los herbívoros. Específicamente, el conejo europeo introducido por los humanos, así como los episodios de sequía, han llevado a un cambio en la estructura de dicho ecosistema. Los gestores del Teide estudiaron, con métodos tradicionales de campo y en pequeñas parcelas del Parque, cómo están cambiando su dinámica las dos especies de vegetación más importantes en este ecosistema vulnerable y heterogéneo, la retama del Teide (*Spartocytisus supranubius*) y el rosalillo de cumbre (*Pteroccephalus lasiospermus*). Este artículo propone un marco metodológico para analizar los cambios producidos en este ecosistema y su problemática mediante el uso de imágenes de teledetección. Los resultados obtenidos fortalecen y amplían el análisis realizado por los gestores del Teide, lo que demuestra que la retama del Teide ha disminuido su población, mientras que la cobertura del rosalillo ha aumentado. Además, este estudio proporciona mapas temáticos de las especies de interés, así como su cobertura específica en diferentes fechas, proporcionando datos cuantitativos en zonas extensas que no son posibles de obtener con los enfoques tradicionales.

Finalmente, a continuación, se presentan las principales conclusiones obtenidas durante la Tesis:

- Se puede concluir la importancia de la elección de las imágenes adecuadas, en base a sus características espaciales, espectrales, radiométricas y temporales, dependiendo del propósito final del estudio. Además, las medidas *in situ* y los datos auxiliares han sido esenciales durante el procesamiento de los datos. Específicamente, los datos reales obtenidos en las campañas de campo para la clasificación supervisada, los DEM (*Digital Elevation Models*) para la ortorectificación precisa, las ortofotos para la fusión hiperespectral, etc.
- Se ha demostrado la importancia de las técnicas de pre-procesado, siendo necesaria la aplicación de métodos adecuados para mejorar la calidad espectral y espacial en las imágenes (corrección atmosférica, fusión de imágenes, ortorectificación, etc.). Específicamente, los métodos avanzados de fusión en las imágenes multispectrales son importantes para obtener imágenes con mejor calidad espacial. Además, tras realizar diversos estudios exhaustivos de algoritmos de *pansharpening*, se demostró que es una etapa

esencial para obtener imágenes de alta resolución espacial que son imprescindibles dado el pequeño tamaño de la vegetación estudiada, y permitir la generación de mapas precisos a nivel de especies. Por otro lado, la reducción de la dimensionalidad en las imágenes hiperespectrales es esencial para obtener mapas temáticos precisos, excepto cuando se utilizan técnicas avanzadas de desmezclado espectral. En definitiva, se han utilizado los algoritmos más adecuados para cada una de las etapas de la cadena de procesado.

- Se ha comprobado la dificultad de obtener un mapa de especies vegetales preciso en el Parque Nacional del Teide, al ser un ecosistema complejo y heterogéneo. Como se menciona en los objetivos, la dificultad de la investigación radica en la generación de una metodología robusta, semi-automática y eficiente para el mapeado sistemático de ecosistemas heterogéneos. En este contexto, como se ha indicado, la primera observación es que los ecosistemas heterogéneos y mixtos necesitan datos de elevada riqueza espacial y espectral, así como la aplicación de técnicas de procesado avanzadas. Por ejemplo, la clasificación basada en objetos proporciona mejores resultados en ecosistemas heterogéneos utilizando imágenes de alta resolución espacial. Por otro lado, en imágenes hiperespectrales, se necesitan técnicas avanzadas de desmezclado para abordar la variabilidad espectral de ecosistemas heterogéneos y mixtos. Se ha demostrado la viabilidad de obtener estimaciones de abundancia adecuadas y mapas temáticos precisos sin aplicar técnicas de reducción de la dimensionalidad. En cuanto a las técnicas de clasificación, no sólo se han utilizado para obtener los mapas de vegetación a nivel de especie, sino también como un método indirecto para evaluar la importancia de los algoritmos de *pansharpening* para evaluar el número adecuado de componentes en los datos hiperespectrales y para analizar el rendimiento de las técnicas de desmezclado espectral
- Se puede concluir que la teledetección es una herramienta fundamental para detectar cambios en áreas extensas de manera semi-automática, continua y económica. Tras un estudio combinando datos de teledetección multiplataforma, se obtuvieron resultados cuantitativos de la cobertura de cada especie y su variabilidad durante el período temporal analizado.

Se puede afirmar que esta Tesis ha logrado desarrollar un marco general de procesado que podría utilizarse como referencia para la generación de productos terrestres, usando imágenes multispectrales e hiperespectrales de alta resolución, en cualquier tipo de ecosistema complejo. Se ha demostrado que los mapas temáticos a nivel de especie vegetal, obtenidos aplicando diferentes metodologías, son lo suficientemente precisos. Este hecho ha conllevado la posibilidad de su utilización por los responsables de conservación del Parque Nacional del Teide.

En definitiva, la consecución de los objetivos de la Tesis permite a la comunidad científica contar con una serie de técnicas de procesado de imágenes para permitir el desarrollo de estudios con una resolución muy elevada y aumentando el potencial de investigación para la gestión ambiental, especialmente en ecosistemas complejos vulnerables.

Finalmente, la investigación futura podría orientarse hacia:

- La obtención de productos terrestres precisos utilizando imágenes de drones hiperspectrales de muy alta resolución espacial (aprox. 10 cm).
- La modificación de la metodología para la inclusión de datos auxiliares, como ortofotos, datos LiDAR o SAR.
- Estudiar en mayor detalle el Parque Nacional del Teide y otros ecosistemas. Especialmente su dinámica usando un mayor número de imágenes de alta resolución y analizando su posible relación con diversos factores naturales o antropogénicos.

## **ABSTRACT**

Biodiversity conservation on ecosystems is an essential task to protect them from the anthropogenic pressure and climate change, among others. In the last decades, remote sensing has become an important tool to complement field observations in the study of ecosystems and offers different types of sensors to carry out these tasks. Specially, very high spatial resolution sensors are trending for performing conservation studies and monitoring ecosystems.

In this context, the general objective of the Thesis is to analyze complex and vulnerable ecosystems, using advanced multi-sensor remote sensing imagery, specifically, very high spatial resolution multispectral and hyperspectral data, to obtain high quality products which allow the comprehensive analysis of natural resources. Thus, advanced processing methodologies are analyzed and applied in ecosystems of Canary Islands (Spain), mainly in the Teide National Park.

In particular, pre-processing techniques, specially adapted for this specific type of imagery and study area, were investigated and assessed. Specifically, apart from the radiometric calibration and the removal of the atmospheric effects, image fusion techniques were applied to the multispectral and hyperspectral imagery to improve its spatial quality. In addition orthorectification, co-registration and hyperspectral dimensionality reduction methods were also considered in the methodology. Regarding the processing steps, advanced spectral unmixing and classification algorithms were reviewed, applied and tested. The final objective of the comprehensive study carried out was to obtain a robust, automatic, and effective methodology for the accurate and systematic mapping of endemic and colonizing plants species, to obtain specific products for the management of complex and heterogeneous land ecosystems. Finally, a change detection study was performed to monitor and analyze the changes of Teide National Park.

The Thesis offers a methodological framework ecological relevant, effective, flexible and transferable to other systems that could be used as a reference for the generation of land products, important not only at ecological level, but also at social and economic level.





# CHAPTER 1. INTRODUCTION AND OBJECTIVES





Ecosystems provide a wide variety of useful services that enhance the human welfare. However, in last decades, there has been a decline in these ecosystems services, as well as in the biodiversity, due to intensification of agricultural land use, tourism development and other activities (Bock 2003, Pagiola et al. 2004, Mùcher et al. 2013, Khare and Ghosh 2016). Thus, knowledge on the conservation status of natural areas is essential to guide site managers in their decisions (Delalieux et al. 2012). Up till now, field observations have been the main source of information for the assessment of the conservation status of habitat types, being time-consuming, labor-intensive, and hence, not suitable to be repeated frequently. In this context, remote sensing data can provide valuable information and complement field observations. Remote sensing offers a synoptic view and the opportunity to provide consistent information in time and space, being an accurate and repeatable tool to aid in the mapping and monitoring of habitat types and their conservation status (Turner et al. 2003, Rocchini et al. 2010, Delalieux et al. 2012, Mùcher et al. 2013, Förster et al. 2014, Corbane et al. 2015). However, it is of great importance the development of advanced image processing techniques to obtain reliable methodologies for the analysis, conservation and management of terrestrial and marine environments, in an automatic, continuous and effective way, and at the suitable spatial, spectral and temporal resolution.

At this point, remote sensing has become an important technology due to the considerable progress that remote sensed sensors have experience in recent decades, providing a huge amount of images with high spatial and spectral resolution. As indicated, it offers a practical and cost-effective means for a good environmental management, especially when large areas have to be monitored (Reinke and Jones 2006, Xie et al. 2008, Spanhove et al. 2012) or periodic information is needed.

The reliable and detailed monitoring of habitats, using remote sensing data, remains a challenging application, as it requires sensors and methods which can deal with complex transitional zones present in natural vegetation. A factor to consider when mapping habitats, is the complexity of the landscape structure, which becomes more challenging when ecosystems are more heterogeneous. Moreover, the conservation status is assessed by habitat structures, presence of typical species in the habitat, abiotic factors and pressures on, or disturbances (Corbane et al. 2013).

Mùcher et al. 2013 stated that new spaceborne hyperspectral (HS) sensors, in parallel to the existing very high spatial resolution (VHSR) multispectral (MS) sensors, can be used for habitat and vegetation monitoring, becoming a hot topic for the remote sensing and conservation community in the coming years. Mapping of broad habitat types, using remote sensing, is a common practice from the perspective of land cover mapping, and is generally done at different analysis of coarse scale. For instance, global mapping using MODIS (250 m, 500 m or 1000 m of



spatial resolution) (Friedl et al. 2002, Xiao et al. 2005, Gao et al. 2017), regional level mapping using LANDSAT or SPOT (Chavez Jr 1988, Wang et al. 2004, MacAlister and Mahaxay 2009, Thomas et al. 2011, Mouginot et al. 2017) or more local mapping with very high resolution sensors, such as Worldview and GeoEye (Dennison et al. 2010, Longbotham et al. 2011, Eugenio et al. 2013, Medina et al. 2018).

At this point, the availability of new sensors on board satellites and airbornes, with improved capabilities, can assist in the generation of precise vegetation maps in natural protected areas (Marcello et al. 2013), especially in insular areas which, in general, are smaller and, usually, with more complex and heterogeneous habitats. Therefore, these areas need to have sensors with the maximum spatial and spectral resolutions.

### 1.1. OBJETIVES OF THE THESIS

The Thesis context was the analysis of land ecosystems, using VHSR MS, panchromatic (PAN) and HS remote sensing imagery, in order to obtain high quality products which will allow the comprehensive analysis of natural resources. Specifically, the Thesis was focused on ecosystems found in the Macaronesia region, in Canary Islands (Spain), since it is considered a geologic and a biodiversity hotspot due to their volcanic origin (Fig. 1.1).

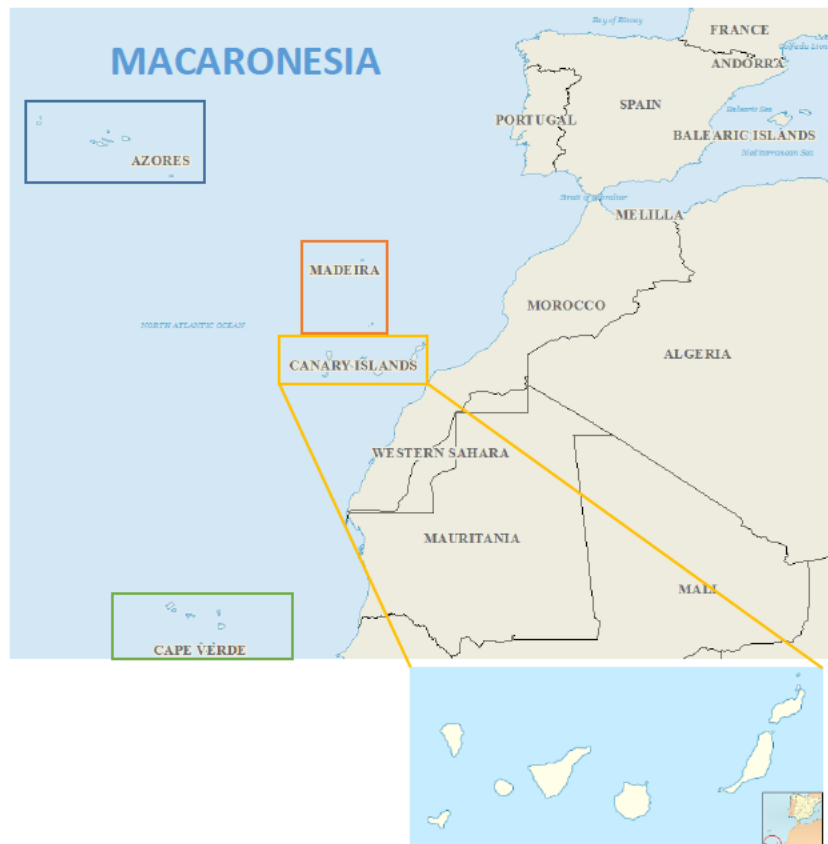


Figure 1.1. Macaronesia region and Canary Islands Map.

The general Thesis objective was the analysis of advanced processing methodologies which, when applied to very high resolution remote sensing imagery, serve to obtain accurate information for the conservation of natural resources. Thus, advanced techniques were implemented in each processing stage to correct or enhance the quality of the imagery and to extract useful value-added products. Techniques for image fusion, dimensionality reduction, segmentation, spectral unmixing and classification of MS, PAN and HS imagery were studied and implemented, as well as algorithms for topographic corrections and co-registration. Figure 1.2 shows a general flowchart of the processing steps involved in the Thesis.

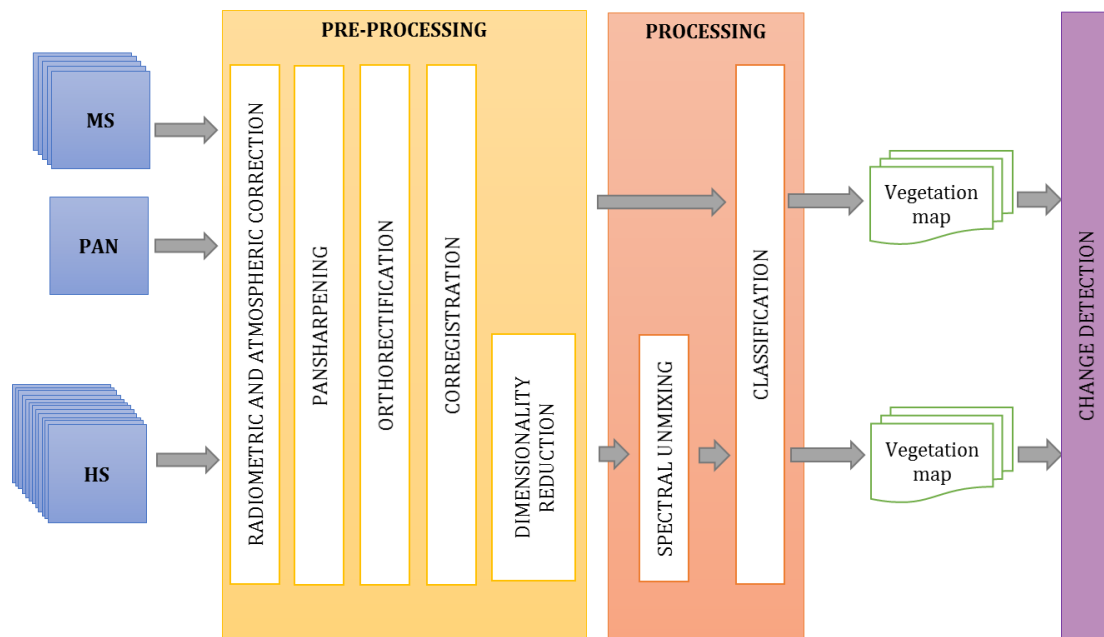


Figure 1.2. General flowchart followed in the Thesis.

To achieve the global objective, the following objectives at more specific level have been addressed:

1. Selection of the appropriate data for the characterization of the ecosystems to be analyzed.

A fundamental task before addressing any remote sensing study is to select and acquire the appropriate remote sensing imagery, *in-situ* and ancillary data, suitable for characterizing the ecosystems under study, as well as for setting and evaluating the algorithms. This objective is addressed through the following tasks:

- Selection of remote sensing imagery with high spatial and spectral resolution.
- Selection of *in-situ* measurements and ancillary data. Specifically, the ground field measurements and auxiliary data (Digital Elevation Models, orthophotos, etc.) were obtained or collected in specific campaigns performed during the Thesis.

2. Analysis and application of advanced pre-processing algorithms to provide spatial and spectral information of high quality.

Appropriate algorithms have to be applied and evaluated for the correction and enhancement of the MS and HS imagery recorded from the sensors to eliminate the radiometric, atmospheric and geometric disturbances to the signal and to increase the spatial detail of the imagery. The most important techniques studied and applied during the Thesis for the generation of the final products were:

- Atmospheric correction algorithms to remove the effects of the atmosphere in different spectral bands.
- Image sharpening to improve the spatial quality of the MS and HS imagery.
- Orthorectification, in order to remove the effects of the relief on the signal received by the sensor.
- Co-registration of multi-sensor data to guarantee data superposition for the fusion of each type of information or for a change detection analysis.
- Dimensionality reduction for HS imagery, in order to reduce the high number of spectral bands and thus, reduce the redundant information of the data.

3. Development and validation of specific products for the management of land resources.

Once the previous pre-processing steps were performed, land products were generated. In the Thesis, the challenging detection, classification and analysis of plant species by remote sensing was addressed. The research difficulty was the generation of a robust, automatic, and effective methodology for the systematic mapping of endemic and colonizing plants species, using remote sensing in complex and heterogeneous ecosystems. In order to accomplish this objective, the following tasks were carried out:

- Detection of plant coverage. The cartography of vegetation covers (vegetation and no-vegetation maps) were generated and evaluated using specialized indexes based on MS and HS data. The goal was to obtain high resolution maps of vegetation distribution in the ecosystems studied.
- Classification of plant species. Precise thematic maps of species were generated and evaluated using advanced classification techniques on multisensor data. Hence, in order to obtain reliable high-resolution cartography of the distribution and abundance of each plant species, it was necessary to apply classification algorithms that process the available MS and HS information, both at pixel and object level to obtain a robust framework for the different zones.
- Apply advanced unmixing models which consider the spectral variability of the classes in the HS imagery. Then, accurate classification maps were

obtained from the abundance maps, which were used as the input data in the classification model.

4. Studies of the variability of natural resources in the ecosystems analyzed.

As indicated, the intense changes in land use, the pressure on ecosystems due to the development of tourism, and the repeated introduction of exotic species, are important threats that make certain land ecosystems, especially insular ones, more sensitive to climate change. In this context, techniques for detecting changes were applied, performing a quantitative analysis of the temporal and spatial variability of each species of interest, on multi-temporal and multi-sensor products. The main task to undertake this objective was:

- Development of a framework for the detection of changes in land ecosystems based on the products generated for the analyzed ecosystem. An approach that allows characterizing the changes occurred in the study area, as well as their quantification, was developed in this Thesis.

## 1.2. PUBLICATIONS

In accordance with the modality offered in University of Las Palmas de Gran Canaria (ULPGC) in the Doctorate Program in Oceanography and Climate Change, this Thesis is presented as a compendium of publications. The PhD candidate, Edurne Ibarrola Ulzurrun, is the first author and responsible for each and every one of the articles. The complete list of articles published in indexed scientific journals that make up the body of the Thesis are:

- E. Ibarrola-Ulzurrun, C. Gonzalo-Martín, J. Marcello-Ruiz, García-Pedrero, A., Rodríguez-Esparragón, D. *Fusion of high resolution multispectral images in vulnerable coastal and land ecosystems*. *Sensors* 2017, 17(2), pp. 228.  
Impact Factor: 2.475.
- E. Ibarrola-Ulzurrun, C. Gonzalo-Martín, J. Marcello. *Influence of pansharpening in obtaining accurate vegetation maps*. *Canadian Journal of Remote Sensing*, 2017, pp. 1-17.  
Impact Factor: 2.000.
- E. Ibarrola-Ulzurrun, J. Marcello, C. Gonzalo-Martín. *Assessment of component selection strategies in hyperspectral imagery*. *Entropy*, 2017, 19(2).  
Impact Factor: 2.305.
- E. Ibarrola-Ulzurrun, L. Drumetz, J. Marcello, C. Gonzalo-Martín, J. Chanussot. *Hyperspectral classification through unmixing abundances maps addressing the*

*spectral variability*. IEEE Transactions on Geoscience and Remote Sensing. Accepted.

Impact Factor: 4.662.

- E. Ibarrola-Ulzurrun, J. Marcello, C. Gonzalo-Martín, J. Martín-Esquivel. *Temporal dynamic analysis of a mountain ecosystem based on multi-source and multi-scale remote sensing data*. Ecosphere. Under review. Impact Factor: 2.671.

### 1.3. THESIS STRUCTURE

As it was mentioned above, this Thesis has been written as a compendium of articles published or submitted to indexed international scientific journals. Each article was intended to be read independently, therefore, some overlap may occur between the different papers, especially in the “Introduction” and the “Materials and Methods” sections.

This **Chapter 1** provides a general introduction in which the objectives of the Thesis are presented, as well as the structure. **Chapter 2** describes a general framework of the methodology used in this Thesis. The next five chapters correspond to the articles published or under revision. The thematic unit of this Thesis is justified at the beginning of each of these five chapters. **Chapters 3 and 4** deal about the processing of MS imagery. Specifically, **Chapter 3** presents an assessment of the different pansharpening techniques for the VHSR MS imagery, showing the most suitable ones, depending on the ecosystem type. **Chapter 4** evaluates the influence of the different pansharpening techniques when obtaining accurate thematic maps applying classifiers, at pixel and object-based level, in MS imagery. The fifth and the sixth chapters are focused in HS imagery. **Chapter 5** compares and assesses different component selection strategies in HS imagery, while **Chapter 6** presents a framework of HS classification through abundance maps obtained from advanced spectral mixing models, which consider the spectral variability of the classes. **Chapter 7** studies the ecosystem changes using the MS and HS accurate thematic maps obtained during the Thesis. Finally, the general conclusions derived throughout this Thesis, as well as future research, are presented in **Chapter 8**.

**Chapters 3 to 6** do not follow the same page numbering as the original published article is included in this document. Moreover, references appear in each chapter, as the articles have their own references and, this way, the same format is used throughout the manuscript.

Table 1.1 links the steps followed in the Thesis related with the chapters while Figure 1.3 shows a detailed flowchart with all the steps followed in the Thesis.

Table 1.1. Steps followed in the Thesis related with the chapters.

	CHAPTER 2	CHAPTER 3	CHAPTER 4	CHAPTER 5	CHAPTER 6	CHAPTER 7
Atmospheric Correction						
Pansharpening						
Orthorectification						
Co-registration						
Dimensionality Reduction						
Spectral Unmixing						
Classification						
Change Detection						

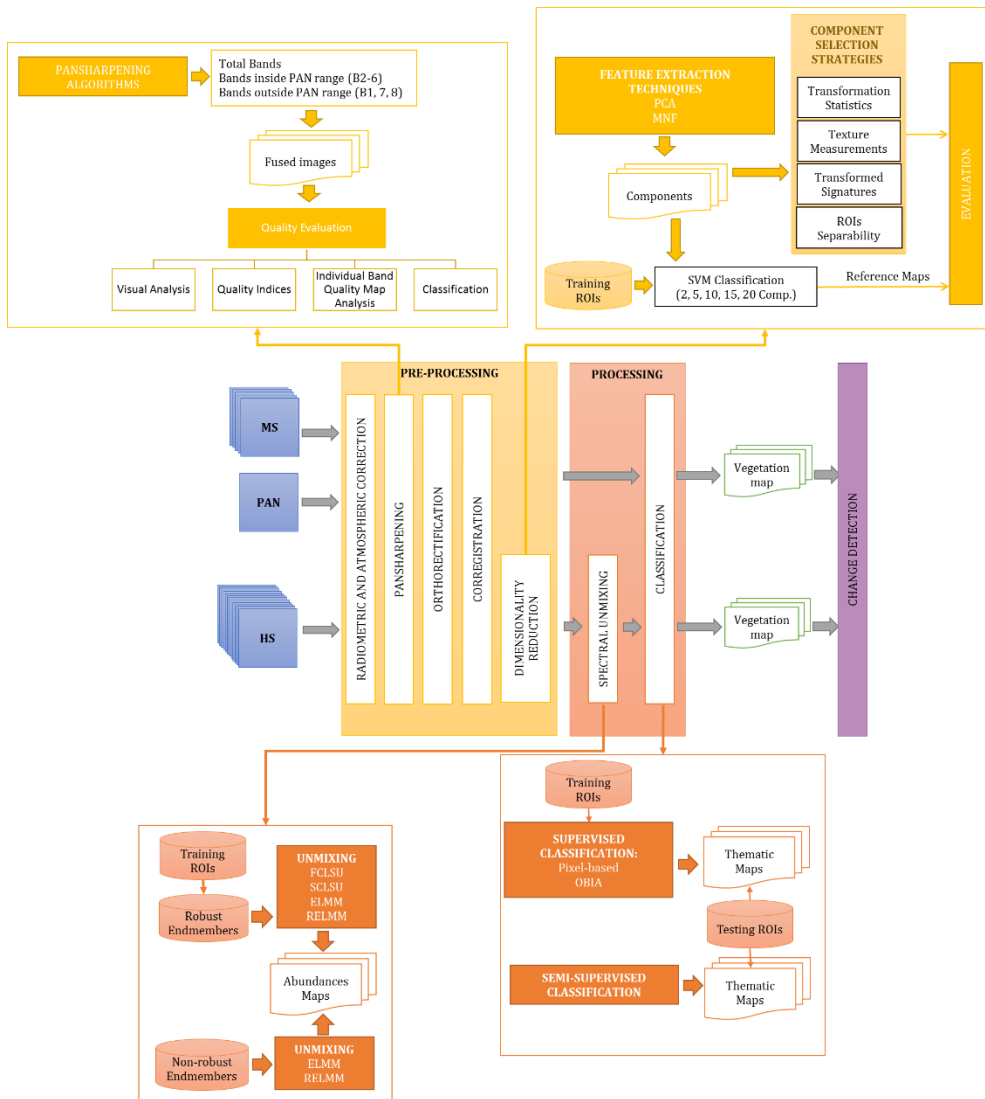


Figure 1.3. Detailed flowchart followed in the Thesis.

## 1.4. REFERENCES

- Bock, M. 2003. Remote sensing and GIS-based techniques for the classification and monitoring of biotopes: Case examples for a wet grass-and moor land area in Northern Germany. *Journal for Nature Conservation* 11:145-155.
- Corbane, C., S. Alleaume, and M. Deshayes. 2013. Mapping natural habitats using remote sensing and sparse partial least square discriminant analysis. *International Journal of Remote Sensing* 34:7625-7647.
- Corbane, C., S. Lang, K. Pipkins, S. Alleaume, M. Deshayes, V. E. G. Millán, T. Strasser, J. V. Borre, S. Toon, and F. Michael. 2015. Remote sensing for mapping natural habitats and their conservation status—New opportunities and challenges. *International Journal of Applied Earth Observation and Geoinformation* 37:7-16.
- Chavez Jr, P. S. 1988. Comparison of the spectral information content of Landsat Thematic Mapper and SPOT for three different sites in the Phoenix, Arizona region. *Photogrammetric engineering and remote sensing* 54:1699-1708.
- Delalieux, S., B. Somers, B. Haest, T. Spanhove, J. V. Borre, and C. Múcher. 2012. Heathland conservation status mapping through integration of hyperspectral mixture analysis and decision tree classifiers. *Remote Sensing of Environment* 126:222-231.
- Dennison, P. E., A. R. Brunelle, and V. A. Carter. 2010. Assessing canopy mortality during a mountain pine beetle outbreak using GeoEye-1 high spatial resolution satellite data. *Remote Sensing of Environment* 114:2431-2435.
- Eugenio, F., J. Martin, J. Marcello, and J. Bermejo. 2013. Worldview-2 high resolution remote sensing image processing for the monitoring of coastal areas. Pages 1-5 *in* Signal Processing Conference (EUSIPCO), 2013 Proceedings of the 21st European. IEEE.
- Förster, M., M. Zebisch, I. Wagner-Lücker, T. Schmidt, K. Renner, and M. Neubert. 2014. Remote sensing-based monitoring of potential climate-induced impacts on habitats. Pages 95-113 *Managing Protected Areas in Central and Eastern Europe Under Climate Change*. Springer.
- Friedl, M. A., D. K. McIver, J. C. Hodges, X. Y. Zhang, D. Muchoney, A. H. Strahler, C. E. Woodcock, S. Gopal, A. Schneider, and A. Cooper. 2002. Global land cover mapping from MODIS: algorithms and early results. *Remote Sensing of Environment* 83:287-302.
- Gao, F., M. C. Anderson, X. Zhang, Z. Yang, J. G. Alfieri, W. P. Kustas, R. Mueller, D. M. Johnson, and J. H. Prueger. 2017. Toward mapping crop progress at field scales through fusion of Landsat and MODIS imagery. *Remote Sensing of Environment* 188:9-25.
- Khare, S., and S. Ghosh. 2016. Satellite Remote Sensing Technologies for Biodiversity Monitoring and Its Conservation. *International Journal of Advanced Earth Science and Engineering* 5:pp. 375-389.

- Longbotham, N., C. Bleiler, C. Chaapel, C. Padwick, W. Emery, and F. Pacifici. 2011. Spatial classification of WorldView-2 multi-angle sequence. Pages 105-108 *in* Urban Remote Sensing Event (JURSE), 2011 Joint. IEEE.
- MacAlister, C., and M. Mahaxay. 2009. Mapping wetlands in the Lower Mekong Basin for wetland resource and conservation management using Landsat ETM images and field survey data. *Journal of Environmental Management* 90:2130-2137.
- Marcello, J., A. Medina, and F. Eugenio. 2013. Evaluation of spatial and spectral effectiveness of pixel-level fusion techniques. *Geoscience and Remote Sensing Letters, IEEE* 10:432-436.
- Medina, A., J. Marcello, A. Hernández Cordero, F. Eugenio, and J. Martín. 2018. Vegetation mapping of a vulnerable coastal-dune ecosystem using very high resolution satellite imagery.
- Mouginot, J., E. Rignot, B. Scheuchl, and R. Millan. 2017. Comprehensive annual ice sheet velocity mapping using Landsat-8, Sentinel-1, and RADARSAT-2 data. *Remote Sensing* 9:364.
- Mücher, C. A., L. Kooistra, M. Vermeulen, J. V. Borre, B. Haest, and R. Haveman. 2013. Quantifying structure of Natura 2000 heathland habitats using spectral mixture analysis and segmentation techniques on hyperspectral imagery. *Ecological Indicators* 33:71-81.
- Pagiola, S., K. Von Ritter, and J. Bishop. 2004. Assessing the economic value of ecosystem conservation. World Bank, Washington, DC. © World Bank. <https://www.openknowledge.worldbank.org/handle/10986/18391> License: CC BY 3.0 IGO.
- Reinke, K., and S. Jones. 2006. Integrating vegetation field surveys with remotely sensed data. *Ecological Management & Restoration* 7:S18-S23.
- Rocchini, D., N. Balkenhol, G. A. Carter, G. M. Foody, T. W. Gillespie, K. S. He, S. Kark, N. Levin, K. Lucas, and M. Luoto. 2010. Remotely sensed spectral heterogeneity as a proxy of species diversity: recent advances and open challenges. *Ecological Informatics* 5:318-329.
- Spanhove, T., J. V. Borre, S. Delalieux, B. Haest, and D. Paelinckx. 2012. Can remote sensing estimate fine-scale quality indicators of natural habitats? *Ecological Indicators* 18:403-412.
- Thomas, R. F., R. T. Kingsford, Y. Lu, and S. J. Hunter. 2011. Landsat mapping of annual inundation (1979–2006) of the Macquarie Marshes in semi-arid Australia. *International Journal of Remote Sensing* 32:4545-4569.
- Turner, W., S. Spector, N. Gardiner, M. Fladeland, E. Sterling, and M. Steininger. 2003. Remote sensing for biodiversity science and conservation. *Trends in ecology & evolution* 18:306-314.



- Wang, Z., W. Wei, S. Zhao, and X. Chen. 2004. Object-oriented classification and application in land use classification using SPOT-5 PAN imagery. Pages 3158-3160 in *Geoscience and Remote Sensing Symposium, 2004. IGARSS'04. Proceedings. 2004 IEEE International. IEEE.*
- Xiao, X., S. Boles, J. Liu, D. Zhuang, S. Froking, C. Li, W. Salas, and B. Moore III. 2005. Mapping paddy rice agriculture in southern China using multi-temporal MODIS images. *Remote Sensing of Environment* 95:480-492.
- Xie, Y., Z. Sha, and M. Yu. 2008. Remote sensing imagery in vegetation mapping: a review. *Journal of plant ecology* 1:9-23.



# CHAPTER 2. STUDY AREAS AND METHODOLOGY





## 2.1. STUDY AREAS AND ECOSYSTEMS DESCRIPTION

The Canary Islands are part of one of the most remarkable biodiversity hotspots on the Earth. These islands include 539 endemic vascular plants, almost 40% of the native flora and more than 25% of the total flora. Accordingly, vegetation communities have an important endemic element. Moreover, this endemic flora is highly vulnerable to environmental changes. For this reason, nearly 40% of the total archipelago area is protected, through a local network of 146 natural protected areas (Fig. 2.1), preserving this richness and floristic singularity (Garzón-Machado et al. 2011).

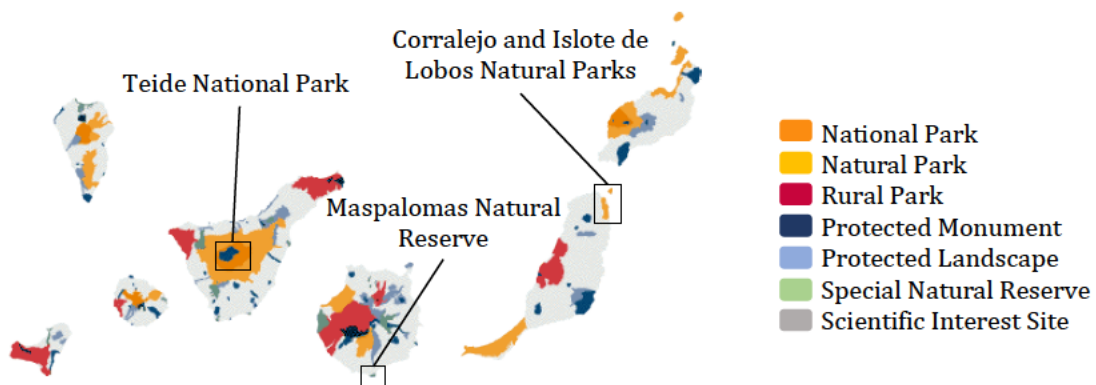


Figure 2.1. Protected Natural Spaces of the Canary Islands (Gobierno de Canarias).

The Thesis was mostly focused in the Teide National Park, located in Tenerife Island. However, in Chapter 3, additional sites were included in other protected areas of Canary Islands: Maspalomas Natural Reserve, south of Gran Canaria Island, and an area north of Fuerteventura, covering Corralejo and Isote de Lobos Natural Parks (Fig. 2.2). More information about these areas is given in Chapter 3, while Chapters 4, 6 and 7 are focused in the Teide National Park.

Finally, Chapter 5 uses a HS imagery acquired by INTA (Instituto Nacional de Técnica Aeroespacial), in Reborio (Asturias, Spain). Even though, the Thesis was not focused in this study area, it was used to assess different strategies for component selection, before having the final HS imagery from Teide National Park recorded by the same CASI (Compact Airborne Spectrographic Imager) HS instrument. Thus, this additional area is described in the corresponding article of Chapter 5.

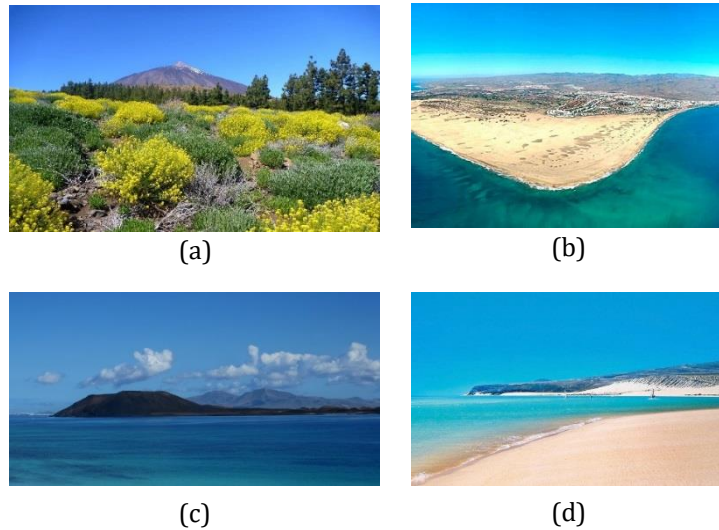


Figure 2.2. (a) Teide National Park, (b) Maspalomas Natural Reserve, (c) Islote de Lobos Natural Park and (d) Corralejo Natural Park.

### 2.1.1. Teide National Park

Teide National Park, located in Tenerife Island, is one of the most important natural areas of Canary Islands, in particular, and Spain, in general. It must be protected due to the high anthropogenic pressure which suffers, mainly caused by the tourism. It covers 18,990 ha and was declared National Park on 22th January 1954. It is made of a giant crater known as Las Cañadas del Teide, located in the center of the island, in one of the highest points of Tenerife Island (2000 m over the sea level), with an extension of 13,000 ha. The Teide peak, formed by several overlapping volcanoes, is the highest mountain in Spain (3718 m) (Wildpret de la Torre 2001, González-Lemus et al. 2009). The climate is mainly determined by the elevation and orientation respect to the Sun and Trade winds that, generally, blow from the NE direction. The annual mean temperature and precipitation are around  $11.4 \pm 0.93^{\circ}\text{C}$  and  $383.2 \pm 63.3$  mm from 2000 to 3000 m, and around  $10.8 \pm 0.9^{\circ}\text{C}$  and about  $409 \pm 59.6$  mm above this elevation to the Teide peak.

The ecosystem vegetation is a characteristic shrubland of the high Mediterranean mountain, but it incorporates elements of great physiognomic originality. The flora is vulnerable to environmental changes, thus, plants respond to thermic and hydric stress with a shrub physiognomy (Arozena-Concepción and Beltrán-Yanes 2006). The most characteristics species are *Pinus canariensis* (canarian pine), *Spartocytisus supranubius* (retama), *Descurainia bourgaeana* (hierba pajonera), *Pterocephalus lasiospermus* (rosalillo de cumbre), *Aenocarpus viscosus* (codeso), and *Echium wildpretii* and *Echium auberianum* (tajinaste) (Arozena-Concepción and Beltrán-Yanes 2006) (Fig 2.3).



(a)



(b)



(c)



(d)

Figure 2.3. (a) General view of the plant species of Teide National Park, (b) *P. lasiospermus*, (c) *S. supranubius* and (d) *D. bourgaeana*.

During last decades, the Teide National Park has suffered a decline in natural resources. Specifically, the European rabbit introduced by humans, as well as drought episodes, have led to a change in the vegetation structure. Teide managers have studied, with field-based traditional methods and in specific locations, how the two keystone vegetation species, *S. supranubius* and *P. lasiospermus*, changed their dynamics in this vulnerable and heterogenic ecosystem. While rabbits limited the expansion of *S. supranubius* by feeding on their seedlings and preventing their regeneration, they favored the expansion of *P. lasiospermus* because this plant is able to take advantage of the extra nutrients contribution from the latrines of the herbivore and it was less palatable than the brooms.

### 2.1.2. Maspalomas Special Natural Reserve

Maspalomas Special Natural Reserve is a dune field situated south of Gran Canaria with a total extension of 403.9 ha (Quevedo-Medina and Hernández-Calvento 2014). It was declared protected area in 1982 (Hernández-Calvento 2002, Gobierno de Canarias 2004). The northern limit is defined by an intense touristic resort occupation and the western limit is occupied by the Maspalomas lagoon. At the east limit appears 'El Inglés' beach. This beach is the main source of sand to the dune field, while Maspalomas beach is considered the sinking area (Alcántara-Carrió and Fontán 2009). The Natural Reserve presents interest at ecological, social and economic level. It has a great variety of natural systems (marine, eolic, lake and fluvial) giving high complexity to the Reserve. Moreover, the tourism and

urbanization development has conditioned the natural evolution of the system, interfering with the sand dynamics. Thus, the sedimentary deposition has a deficit since the 60's (Hernández et al. 2007, Pérez-Chacón-Espino et al. 2007).

The goal of the protection in this area is the maintenance of the essential ecological processes linked, both to the dune system and to the Maspalomas lagoon. It is important to protect this ecosystem due to the representative environment of the area, the presence of threaten habitats, the high ornithological interest, threaten flora, fauna endemic species, and to preserve the geomorphological structures (Gobierno de Canarias 2004).

### **2.1.3. Corralejo and Islote de Lobos Natural Parks**

Corralejo and Islote de Lobos Natural Parks were declared protected areas in Canary Islands in 1982 and Natural Parks in 1994.

Corralejo covers 2,668.7 ha. The dune system limits with urban edifications at north, with the coast in the east and, finally, the west and south are bordered by 'malpaís' landscape and volcanic structures. It is a mobile dune system that registers an important sediment deficit produced by a strong anthropic pressure since decades (Fernández-Cabrera et al. 2010). The dominant land vegetation and its abundance are determined by the sand mobility, the sea closeness and the weather conditions. Halophilic vegetation is located closer to the sea exposed to the tides action (Fernández Cabrera et al. 2012). One of the most important problems that appears in Corralejo is the sedimentary dynamic alteration by a consequence, in part, of the urban development in the northern area of the system, which affect as a wall to the sediment natural entrance from the sea. The multiple sand extractions are an adding problem to the sedimentary dynamic alteration (Fernández Cabrera et al. 2012).

Islote de Lobos, is a small island which covers 470 ha, situated north of Fuerteventura, northeast to Corralejo. It is one of the protected areas where the man has not settled down (Iglesias 2003). It has a high environmental value and it was declared ZEPA (Birds Special Protection Area), IBA (Birds Importance Area) and LIC (Community Interested Area). The volcanic structures, as well as its high biodiversity (more than 130 plant species) give to the island a high environmental importance. In Islote de Lobos, the dominant vegetation species are adapted to the high salinity of the area (Hernández-Calvento 2002).

Maspalomas Special Natural Reserve, as well as Corralejo and Islote de Lobos Natural Parks were only used to evaluate the different pansharpening algorithms in three different ecosystem types: land ecosystem as Teide National Park, coastal ecosystem as Corralejo and Islote de Lobos Natural Parks, and a mixed ecosystem corresponding to Maspalomas Special Natural Reserve.

## 2.2. DATASETS

### 2.2.1. Remote sensing data

The recent increase in Earth observing sensors has led to the availability of high resolution images of various types with different spatial, spectral and temporal resolutions (Alimuddin et al. 2012). They measure the electromagnetic waves reflected or emitted by distant objects present on the Earth surface. According to the source of illumination, two types of sensors can be considered: active and passive. Passive sensors, generally, use the Sun as an energy source. They record the radiation emitted by the Sun and reflected by the Earth's surface. For instance, MS which have 4-10 spectral bands, PAN has a single band covering a wider range of the spectrum with higher spatial resolution than the MS, and HS imagery, formed by hundreds of contiguous bands. Active sensors have their own energy source, emitting a signal that travels through the atmosphere, reflects on the Earth's surface and returns to the sensor, which measures the signal's travel time and strength, i.e. Radar and LiDAR (Khare and Ghosh 2016) (Fig. 2.4). Regarding medium and high spatial resolution passive sensors, some widely used are shown in Table 2.1.

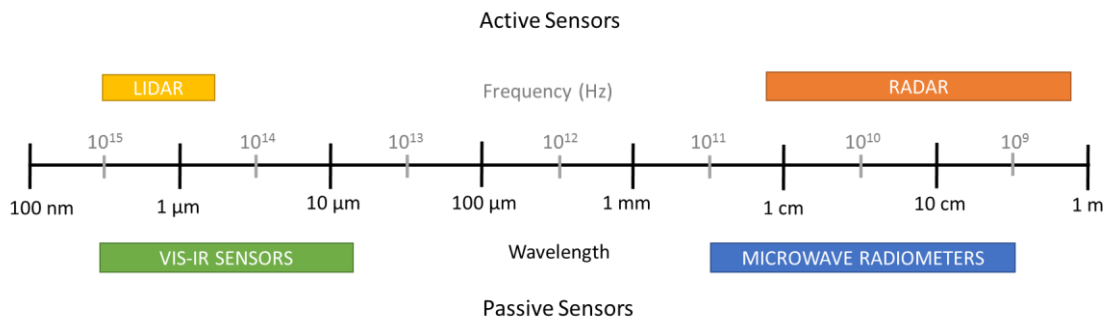


Figure 2.4. The frequency bands of the passive and active sensors (adapted from Lefeuvre and Tanzi, 2014).

Table 2.1. Common medium and high resolution passive sensors.

SATELLITES/ SENSORS	Spectral Resolution	Spatial Resolution	Comments
<b>Landsat TM/ETM+/OLI</b>	4 to 11 bands	Medium (30 m) to coarse resolution (60 m or 100 m in thermal bands)	Longest history and most used for land monitoring
<b>Sentinel-2</b>	13 bands	Medium resolution: 10 to 60 m	
<b>ASTER</b>	14 bands	Medium resolution: 15 - 90 m	
<b>SPOT-HRV</b>	3 and 4 bands	Medium spatial resolution (20 m to 2.5 m in PAN)	SPOT VGT with coarse resolution of 1 km
<b>IKONOS</b>	4 bands	VHSR: 1 m (PAN) - 4 m (MS)	
<b>Quickbird</b>	4 bands	VHSR: 0.6 m (PAN) - 2.4 m (MS)	
<b>Worldview-2</b>	8 bands	VHSR: 0.46 m (PAN) - 1.8 m (MS)	
<b>Hyperion</b>	220 bands	Medium resolution: 30 m	On board EO-1 satellite
<b>AVIRIS</b>	224 bands	Medium/coarse resolution: 20 m	Airborne HS sensor



In this context, regarding the different sensors, they all offer useful information for mapping habitats and their status. For instance, Corbane et al. 2015 reveal how MS imagery alone is often not enough for detailed forest type and grassland differentiation; however, more detailed analyses might be necessary when using high spatial resolution sensors. Moreover, the article adds that HS imagery enables the distinction of tree species based on the reflectance response.

This Thesis was focused in the use of VHRS MS imagery and HS imagery, which are explained in more detail in the next sub-sections.

### 2.2.2. Field data

Field data acquisition is essential for remote sensing processing techniques. It is needed to have knowledge of the study area and, therefore, field campaign observations are useful to acquire that information. Firstly, it is important to know the purpose of the study, and then, compile information of the study area regarding that purpose. That information acquired during the field camping is used during the pre-processing and processing steps, as well as to validate all the techniques.

For instance, to perform an accurate atmospheric correction in the imagery, it is necessary to know the atmospheric conditions the day that the imagery is acquired in order to validate the correction model. For georeferencing and orthorectification, a reference image can be used, but also some reference points obtained via global position system (GPS) during the field campaign are useful too. Besides, field data or samples are used to train supervised classifiers or unmixing models, in order to obtain accurate thematic maps. Finally, those samples are essential to validate all the results obtained.

During the Thesis, three field campaigns were carried out. Table 2.2 shows each field campaign, the area, the date and the data collected. All the field campaigns were carried out at the same date than the satellite and airborne imagery acquisition.

Table 2.2. Field campaigns carried out during the Thesis.

Field campaign	Area	Date	Data collected
Field campaign 1	Teide National Park Maspalomas Natural Reserve	June 2015	Atmospheric parameters and reflectance measurement using Spectroradiometry data (ASD-Field Spec)
Field campaign 2	Teide National Park Maspalomas Natural Reserve	May 2016	Training and testing samples
Field campaign 3	Teide National Park Maspalomas Natural Reserve	June 2017	Training and testing samples Spectroradiometry data (ASD-Field Spec)

### 2.2.3. Multispectral and panchromatic imagery

The level of details present in the images and the information associated with each object on the Earth's surface vary as the spatial resolution of sensors changes (Khare and Ghosh 2016). Normally, in remote sensing, high spatial resolution is also called fine spatial resolution, and it ranges from 0.5 to 10 m in the commercial domain for environmental studies. For instance, Worldview sensors (WV-2, WV-3 and WV-4), Pleiades, Quickbird, IKONOS and SPOT-5, are commonly high spatial resolution sensors (Baraldi et al. 2010, Mutanga et al. 2012). Specifically, WV-2 imagery was used in this Thesis as a VHSR data. The specific features of the sensor, spectral and spatial characteristics, as well as the acquisition time, is explained in Chapters 3 and 4. Moreover, Quickbird was used in Chapter 7 (Table 2.3).

Table 2.3. Specifications of the different imageries used in the Thesis.

SENSORS	TYPE OF IMAGERY	AREA OF COVERAGE	ADQUISITION DATE	CHAPTER
Quickbird	MS	Teide National Park	26 <sup>th</sup> May 2002	Chapter 7
Worldview-2	MS	Teide National Park	11 <sup>th</sup> May 2016	Chapters 3-7
		Maspalomas Natural Reserve	17 <sup>th</sup> January 2013	Chapter 3
		Corralejo and Islote de Lobos Natural Parks	20 <sup>th</sup> October 2010	Chapter 3
CASI	HS	Teide National Park	1 <sup>st</sup> June 2017	Chapters 6-7
		Reborio (Asturias)	22 <sup>nd</sup> May 2009	Chapter 5

### 2.2.4. Hyperspectral imagery

High resolution optical remote sensing has increased the number of acquired spectral bands, going from MS to HS imagery. HS sensors capture image data in hundreds of narrow and contiguous spectral bands covering a broad spectrum of wavelength range (typically, 0.4-2.5  $\mu\text{m}$ ), increasing the ability to classify and recognize different materials (Villa et al. 2009). This higher spectral accuracy is delivering more information, leading to a growing interest in HS remote sensing research and applications in a variety of fields, including geology, agriculture, forestry, coastal and inland water researching, environmental management or urban studies (Thenkabail et al. 1999, Dell'Acqua et al. 2004, Lawrence et al. 2006, Govender et al. 2007, Gao et al. 2009, Goodenough et al. 2012, Gupta 2017).

Compared to the MS remote sensing data, HS imagery not only has an extremely high spectral resolution that improves the detection capabilities of Earth observation, but also specific processing methods (Li et al. 2014). Besides, HS data can also be applied to record information of important plant properties (i.e. water content, leaf pigment and chemical composition), making possible to discriminate different vegetation species, as well as to assess of habitat degradation and stress, change detection in nitrogen, phosphorus and other foliage compounds level, which

are linked with several environmental factors (Khare and Ghosh 2016). So far, there are no high spatial resolution HS satellites; thus, sensors on board aerial platforms have been used in the research carried out in this Thesis.

In particular, the CASI 1550i (<http://www.itres.com/casi-1500/>) sensor was used to carry out the HS studies, which achieves the required spatial resolution to study the complex ecosystem of the Teide National Park (Table 2.3). More detailed information about the sensor and the type of imagery can be found in Chapters 5, 6 and 7.

## **2.3. PRE-PROCESSING TECHNIQUES**

Satellite data providers perform some preliminary pre-processing to the raw data received; however, it is necessary to apply additional processing techniques to correct and enhance the sensor data, to generate the final products. In particular, pre-processing algorithms are critical to improve the quality of the available information. Chapter 1, Section 1.3 shows every transformation and correction methods that were used in the original imagery. Moreover, Chapters from 3 to 7 explain this pre-processing in more detail.

In this section, every pre-processing step addressed in this Thesis (Fig. 1.4) is described. Since this document is produced as a compendium of articles, the detailed explanation of every technique is included in each article, which are individual chapters in the manuscript.

### **2.3.1. Radiometric calibration and atmospheric correction**

The identification of surface materials through remote sensing imagery is best achieved by deriving the reflectance of the materials. For studying surface properties using remote sensing data, accurate removal of atmospheric absorption and dispersion effects is required.

The atmosphere affects the radiance received at the sensor causing scattering, absorption, and refraction of the energy. Corrections for these effects, sensor gains and offsets, solar irradiance, and solar zenith angle, must be included in the radiometric calibration and atmospheric correction procedures that are used to convert sensor-recorded digital counts to ground reflectances (Fig. 2.5) (Martin et al. 2012, Pons et al. 2014, Marcello et al. 2016). In other words, the derivation of surface reflectance from image data requires radiometric calibration and atmospheric corrections of the measured top-of-atmosphere (TOA) radiance (Manakos et al. 2011). After the radiometric calibration to convert digital values recorded by the sensor to radiance values, atmospheric corrections are essential to convert radiance measured by the sensor to reflectances of the surface materials (Gao et al. 2009, Pons et al. 2014).

In land areas, atmospheric correction is essential for obtaining the real reflectance from the soil and vegetation in order to study the biophysical parameters or to achieve precise land use/land cover or vegetation maps (Martin et al. 2012, Marcello et al. 2016).

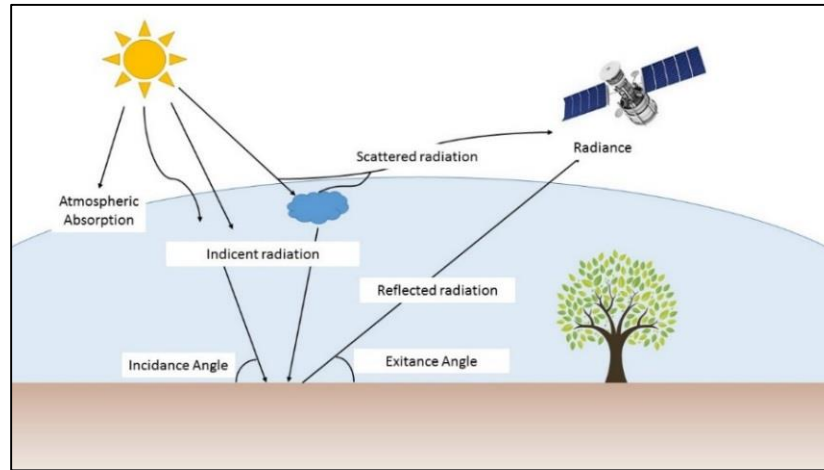


Figure 2.5. The radiance detected by the sensor includes the reflected radiation from the Earth's surface as well as radiation that is scattered in the atmosphere (adapted from: Humboldt State University, 2017).

The solar radiation on the sun-surface-sensor path is affected by dispersion and absorption. Accurate modeling of these effects is required in order to derive surface reflectance. The short wavelength region between 0.4-0.7 nm is strongly affected by molecular scattering (Rayleigh scattering). The radiances measured by a sensor from a satellite include atmospheric path radiance (due to Rayleigh and aerosol scattering) and surface-reflected solar radiance. These radiances are often converted to “apparent reflectances”, a measure of the reflectivity for the atmosphere and surface system. In real atmosphere, the scattering and absorption processes occur simultaneously and this coupling effects are small in regions where the atmospheric gaseous absorptions are weak and in regions where the scattering effects are small (Gao et al. 2009).

Since the mid-1980s, atmospheric correction algorithms have evolved from the earlier empirical line and flat field methods to more recent methods based on rigorous radiative transfer modeling approaches. Hence, approaches include, basically (Gao et al. 2009):

- (i) Scene-derived adjustments in which in-scene statistics are used. For example, Darkest Pixel Methods (Chavez Jr 1988, Wu et al. 2005, Hadjimitsis et al. 2010) or purely empirical methods in which ground-truth spectral data are required, i.e. the Empirical Line calibration (Staben et al. 2012).
- (ii) More complex and sophisticated atmospheric correction techniques that involve radiative transfer algorithms. For instance, the 6S (Second Simulation of

the Satellite Signal in the Solar Spectrum) code (Vermote et al. 1997) and the MODTRAN (MODerate spectral resolution atmospheric TRANsmittance) (Berk et al. 1998, Berk et al. 2005). These robust and high-spectral resolution methods retrieve the atmospheric properties by modeling the radiative transfer of the sunlight: the physical interaction with the gases and particles in the atmosphere; the interaction with the surface; and the transmission along a different path upward through the atmosphere to the sensor (Manakos et al. 2011). These models applied to remote sensing imagery often retrieve target reflectance with a relatively high accuracy. However, they require information about the atmosphere at the time of the sensor overflight, such as the optical thickness and the various atmospheric components. This information is sometimes difficult to get (Manakos et al. 2011, Martin et al. 2012).

Nowadays, there are several atmospheric corrections algorithms for retrieving surface reflectance. For instance, the Atmosphere CORrection Now (ACORN) (Kruse 2004), the Fast one-of-sight Atmospheric Analysis of Spectral Hypercubes (FLAASH) (Berk et al. 1998), a series of Atmospheric and Topographic Correction (ATCOR) codes (Richter 1996, 1998, Richter and Schläpfer 2002), 6S (Vermote et al. 1997) or Quick Atmospheric Correction (QUAC) (Bernstein et al. 2012).

In case of inhomogeneous horizontal surfaces, the radiances outside of the pixel can spill into the pixel being viewed by the sensor due to scattering of solar radiation by atmospheric molecules and aerosols. This effect is called the “atmospheric adjacency effect” (Tanré et al. 1979). Operational modelling and correction of the atmospheric adjacency effect are very difficult because of the requirement of accurate knowledge on aerosol optical properties and vertical distributions. Moreover, all models are based on a series of hypotheses to simplify them and, in this way, make their application suitable.

The performance of different atmospheric corrections methods are studied for many sensors like Landsat TM (Thematic Mapper) (Janzen et al. 2006, Hadjimitsis and Clayton 2008, Watmough et al. 2011), Quickbird (Wu et al. 2005, Richter 2008), Ikonos (Neubert and Meinel 2005), SPOT (Vaudour et al. 2008), Worldview-2 (Marcello et al. 2016), etc.

A previous study to the Thesis comparing 5 atmospheric correction algorithms (FLAASH, ATCOR, 6S, DOS and QUAC) was carried out, which revealed that 6S was the most suitable for the scenes regarding different settings (Marcello et al. 2016).

### **2.3.2. Sharpening**

Image fusion is the process of combining images from different sources to increase quality of the fused image as compared to the source images (Alimuddin et al. 2012). The extensive research on image fusion techniques in remote sensing

started in the 1980s (Schowengerdt 1980, Hallanda and Cox 1983). Generally, image fusion can be categorized into three levels: pixel level, feature level and knowledge or decision level (Ehlers et al. 2010, Zhang et al. 2011, Pohl 2014, Nikolakopoulos and Oikonomidis 2015). At pixel level, pansharpening data fusion techniques could be defined as the process of merging MS and PAN imagery to create a new MS image with higher spatial resolution than the original MS (Li et al. 2013b, Kpalma et al. 2014) (Fig. 2.6). It aims to obtain information of greater quality, integrating the spatial details of the PAN image and the spectral characteristics of the MS image into a single image.

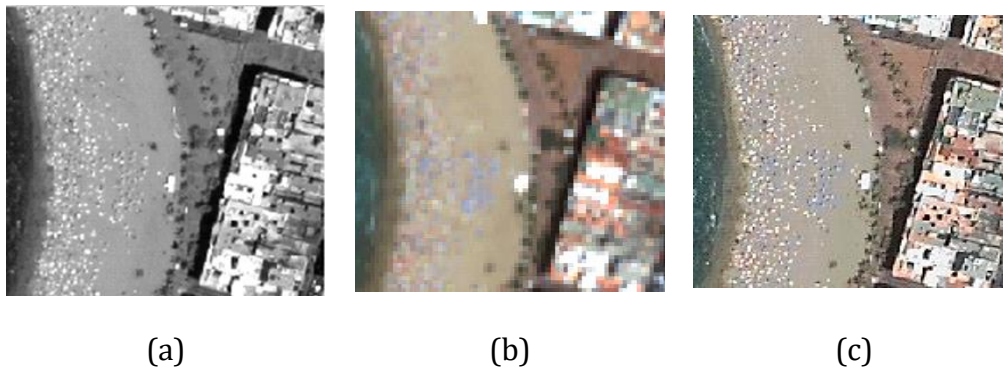


Figure 2.6. (a) Panchromatic (PAN) image, Color composite RGB (Red – Green – Blue) of the (b) Multispectral (MS) image and (c) of the Fused (FUS) image.

Many pansharpening techniques have appeared in the last decades, as a consequence of the launch of VHSR satellite sensors (Laben and Brower 2000, Tu et al. 2001, Amro et al. 2011, Fonseca et al. 2011, Palubinskas and Reinartz 2011, Li et al. 2012, Vivone et al. 2015). However, spatial and spectral resolutions are highly correlated factors with an inverse relation between them. Constraints on the signal to noise ratio impose that the spatial resolution must be lower if the requested spectral resolution is higher (González-Audícana et al. 2004, Lillo-Saavedra and Gonzalo 2006, Alimuddin et al. 2012, Li 2013, Li and Qi 2015).

### **Multispectral pansharpening**

Usually, VHSR satellite optical sensors provide a MS image with high spectral resolution and a PAN with high spatial resolution. In general, pansharpening algorithms disrupt the spectral information of the original MS image leading to a necessity of selecting the appropriate method for the considered application.

#### Pansharpening algorithms

It is difficult to find a universal classification for all the pansharpening methods and different authors have tried to categorize them in different ways (Alparone et al. 2007, Zhang 2010, Li et al. 2012, Li et al. 2013b, Palubinskas 2013, Pohl and van Genderen 2015, Vivone et al. 2015). A common classification is as follows:

1. *Component Substitution methods*: they are based on a linear transformation and the subsequent substitution for some components in the transformed domain. The MS image is transformed into another space, assuming that this transformation separates the spatial structure from the spectral information in different components. The transformed MS image can be enhanced by replacing its component containing most of the spatial detail with the spatial information of the PAN image. These methods are based on transformations as, Intensity-Hue-Saturation (IHS) (Carper 1990), Principal Component Analysis (PCA) (Hotelling 1933), Gram-Schmidt (GS) (Laben and Brower 2000) and Hyperspherical Color Sharpening (HCS) (Padwick et al. 2010).
2. *Relative Spectral Contribution methods*: they can be considered as a variant of the Component Substitution methods, when a linear combination instead of a substitution is applied. They include the Brovey Transform (BT) (Gillespie et al. 1987) and the Intensity Modulation (IM) methods (Cliche et al. 1985).
3. *High-Frequency Injection methods*: this methods extract the spatial details from the PAN image applying spatial filtering techniques, which are injected in the MS image or a filtered version on it. They include fusion techniques based on the application of filters in the Fourier Domain (Chavez et al. 1991, Lillo-Saavedra et al. 2005) as well as, High-Pass-Filtering (HPF) (Gillespie et al. 1987) and High-Pass-Modulation (HPM) (Schowengerdt 1980), which inject high frequency detail extracted by subtracting a low pass filtering PAN image from the original one.
4. *Statistics-based methods*: they include a set of methods that exploits the statistical characteristics of the MS and PAN imagery in the pansharpening process. They basically include Price's algorithm (Price 1987), Spatially Adaptive methods (Park and Kang 2004), Bayesian-based models and Super Resolution methods (Mascarenhas et al. 1996).
5. *Multiresolution methods*: these techniques are used to decompose MS and PAN imagery in different scales in order to extract the spatial details which are imported into finer scales of the MS images. They highlight the relationship between PAN and MS imagery in coarser scales and enhance spatial details. They mainly include Laplacian pyramids (Burt and Adelson 1983), Wavelet (Mallat 1989) and Contourlet methods (Da Cunha et al. 2006), as well as any combination of multiresolution analysis with methods of other categories (Aiazzi et al. 2002, Aiazzi et al. 2006, Alparone et al. 2007, Gonzalo-Martín and Lillo-Saavedra 2007, Lillo-Saavedra and Gonzalo 2007, Zhang 2010, Palubinskas and Reinartz 2011).

After a detailed review of the state-of-the-art in MS pansharpening techniques in the Thesis, a comprehensive assessment was performed selecting the following classic and new algorithms that could achieve good performance with WV-2 imagery:

- Gram-Schmidt (GS) (Laben and Brower 2000).
- Fast Intensity Hue Saturation (FIHS) (Tu et al. 2001).

- Hyperspherical Color Sharpening (HCS).
- Modulation Transfer Function (MTF) (Aiazzi et al. 2006, Vivone et al. 2015).
- Wavelet '*à trous*' (WAVE\_ATROUS) (Dutilleux et al. 1987).
- Weighted Wavelet '*à trous*' through Fractal Dimension Maps (WAT $\otimes$ FRAC) (Lillo-Saavedra and Gonzalo 2006).

All of them are explained in more detail in Chapters 3 and 4.

### Hyperspectral sharpening

Regarding the HS sharpening, the spatial and spectral compromise is more critical due to the necessity to capture energy in a greater number of narrow bands. Moreover, airborne sensors can achieve higher spatial resolution but there is still a trade-off between the number of bands and the spatial resolution to achieve an acceptable signal-to-noise ratio, especially when dealing with HS sensors. In order to solve this trade-off between both resolutions, HS sharpening is needed, using higher spatial resolution imagery obtained through other sensors, orthophotos, etc. (Loncan et al. 2015, Pohl and van Genderen 2015, Yokoya et al. 2017).

A preliminary study was carried out by a visual and quantitative comparison of fused images obtained through several HS sharpening algorithms to assess the HS fusion performance using 2 different approaches. First, semi-synthetic imagery was generated using CASI imagery. These datasets were used to carry out controlled experiments to check the robustness of each algorithm to different spatial resolution ratios and registration errors. Second, three real cases were assessed to analyze the algorithms on various fusion scenarios, with the aim to improve the spatial detail of the HS imagery (Table 2.4 and Figure 2.7).

Table 2.4. High spectral and spatial resolution images used in the three real cases' studies.

	Study Area	High Spectral Resolution Image	High Spatial Resolution Image
<b>Real Case 1</b>	Teide National Park	CASI (75 cm)	Drone (7.5 cm)
<b>Real Case 2</b>	Maspalomas Natural Reserve	CASI (50 cm)	Orthophoto (2.5cm)
<b>Real Case 3</b>	Maspalomas Natural Reserve	Hyperion (30 m)	Sentinel-2 (10 m)

The HS sharpening algorithms used in the analysis are different that the ones used in the MS study, due to the imagery features. They are named below (for more information see Loncan et al. 2015):

- Smoothing Filter-based Intensity Modulation (SFIM) (Liu 2000)
- Modulation Transfer Function (MTF) (Aiazzi et al. 2006, Vivone et al. 2015).



- Gram-Schmidt (GS) (Laben and Brower 2000).
- Gram-Schmidt Adaptive (GSA) (Aiazzi et al. 2007).
- Principal Component Analysis (PCA) (Hotelling 1933).
- Guided Filter PCA (GFPCA) (He et al. 2013).
- Coupled Nonnegative Matrix Factorization (CNMF) (Yokoya et al. 2012).
- Bayes Naïve (Hardie et al. 2004).
- Bayes Sparse (Wei et al. 2015).
- HySure (Bresson and Chan 2008).

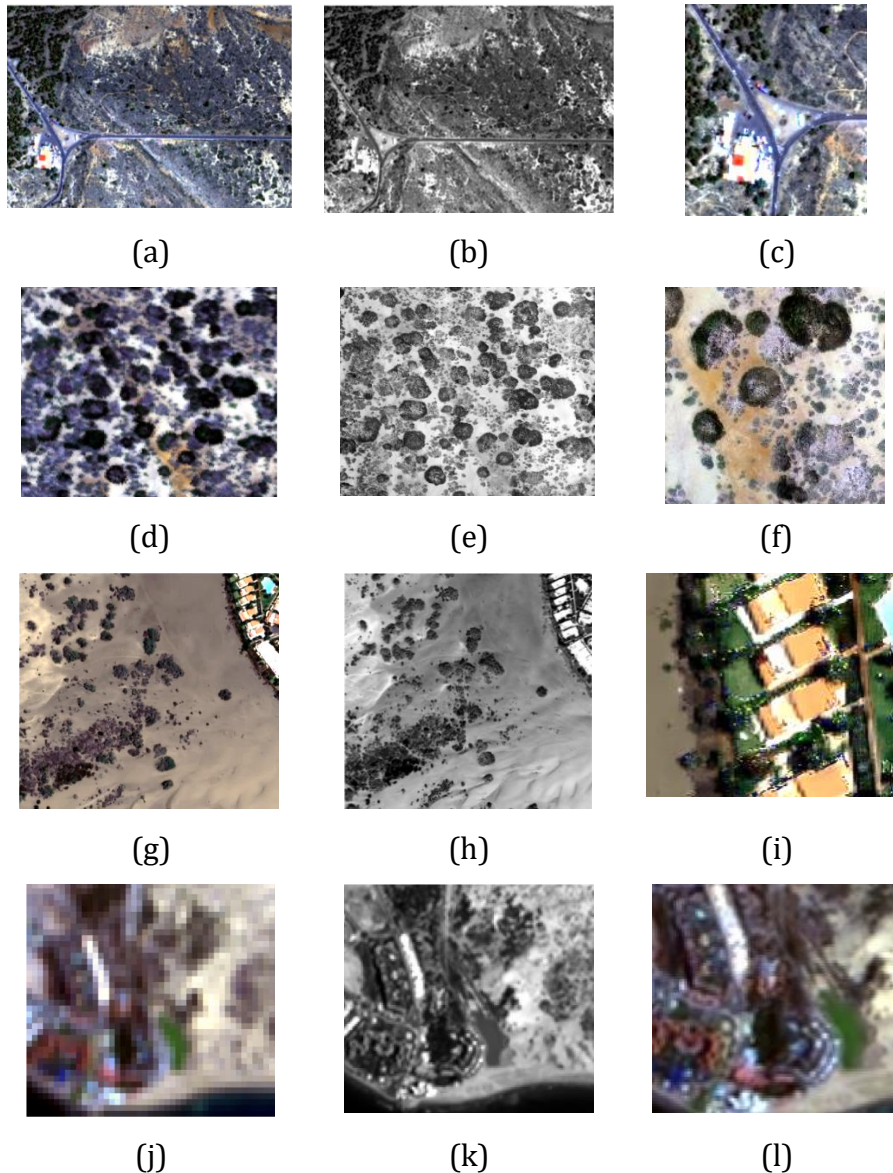


Figure 2.7. Datasets used in the HS sharpening assessment. Semi-synthetic data: (a) CASI HS, (b) CASI HS intensity image, (c) MTF\_GLP fused image. Real case 1: (d) CASI HS image, (e) Drone intensity image, (f) MTF\_GLP fused image. Real case 2: (g) CASI HS image, (h) orthophoto image, (i) MTF\_GLP fused image. Real case 3: (j) Hyperion-EO1 image, (k) ALI-(PAN)-EO1 intensity image, (l) MTF\_GLP fused image.

## Quality evaluation

Quality evaluation is a fundamental issue to assess the performance of different sharpening algorithms (Medina et al. 2012, Rodríguez-Esparragón 2015) and specifically, to assess the spectral and spatial quality of the fused images. There are two types of evaluation approaches commonly used: (1) qualitative analysis (visual analysis) and (2) quantitative analysis (quality indices).

Visual analysis is a powerful tool to capture the geometrical aspects and the main color disturbances (Alparone et al. 2007). According to Amro et al. 2011, some visual parameters are needed for testing the properties of the imagery, such as spectral preservation of features and the injection of the spatial information from the high spatial resolution imagery. On the other hand, quality indices measure the spectral and the spatial distortion due to the pansharpening process. Each fused image is compared to the high spectral or spatial image using one or more quality indices.

*Quality Indices:* As it was mentioned before, there are several types of Quality Indices. All of them are explained in Chapters 3 and 4. Alparone et al. 2008 categorized them in three main groups, (i) spectral quality indices, (ii) spatial quality indices and, finally, (iii) global quality indices. On the other hand, there exist some evaluation techniques with no reference requirement such as the Quality with No Reference (QNR) approach (Vivone et al. 2015).

- Spectral quality assessment: The spectral quality assessment measures the spectral distortion due to the pansharpening process. Each fused image was compared to the reference MS image. The metrics considered in the Thesis are:
  - *Correlation coefficient* (CC) (Wald et al. 1997)
  - *Spectral Angle Mapper* (SAM) (Kruse et al. 1993)
  - *ERGAS* (Spectral Relative Dimensionless Global Error) (Wald 2000).
- Spatial quality assessment: The spatial detail information of each fused band is compared with the spatial information of the reference PAN image. The metrics considered in the analysis are as follows:
  - *Spatial ERGAS* (Lillo-Saavedra et al. 2005).
  - *Frequency Comparison* (FC) (Rodríguez-Esparragón et al. 2014).
  - *Zhou* (Zhou et al. 1998).
- Global quality assessment:
  - *Q* index, which has been characterized to sensors with 5 bands (Q4) and 8 bands (Q8) (Wang and Bovik 2002).

Figure 2.8 shows the specific workflow of the MS pansharpening process carried out in the Thesis, and Figure 2.9 shows the workflow followed for the HS sharpening, which is not included as a chapter in the Thesis, but as future research.

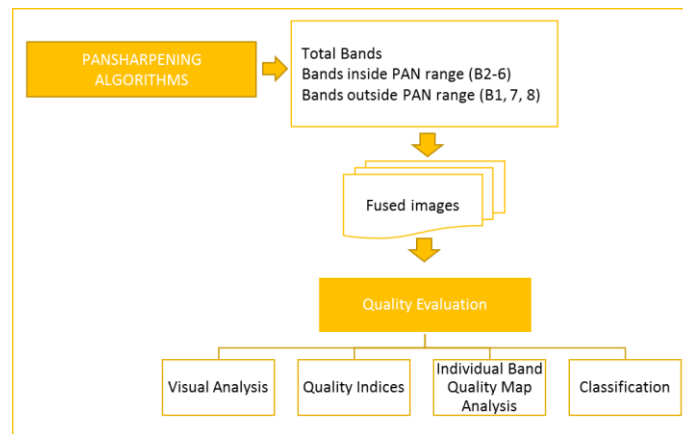


Figure 2.8. Multispectral pansharpening analysis workflow.

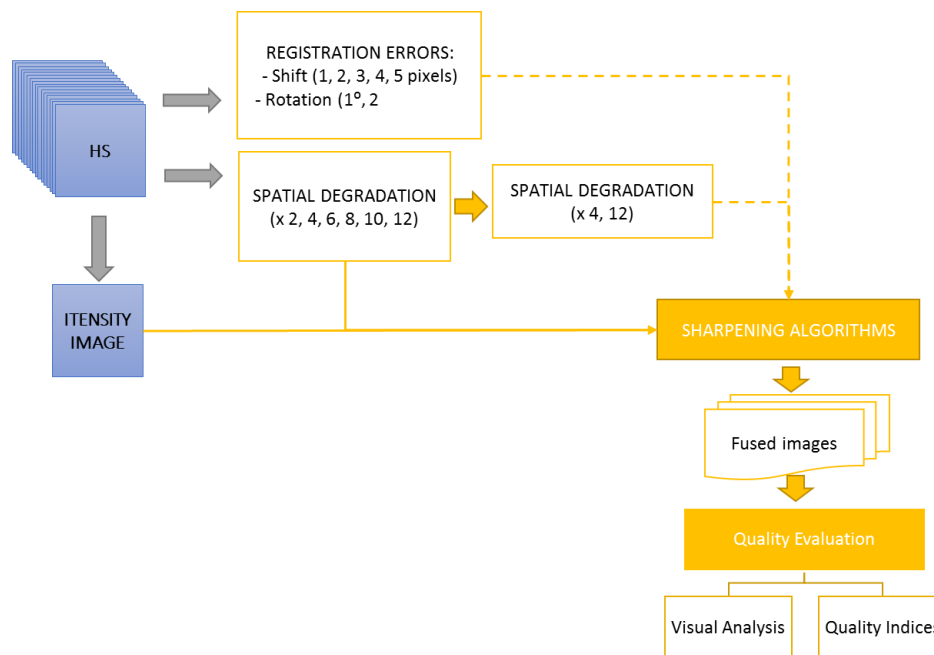


Figure 2.9. Hyperspectral sharpening analysis workflow.

### 2.3.3. Orthorectification

Orthorectification of remote sensing data is an important pre-processing step for mapping applications (i.e. image classification, adding georeferenced image data into Geographic Information Systems (GIS), etc.) and change detection studies. Specifically, multi-source data integration for these applications requires geometric processing adapted to the terrain and to the characteristics of the data, in order to keep the most suitable information from each image in the composite orthorectified products (Toutin 2004, Aguilar et al. 2013).

Each imagery acquisition system produces unique geometric distortions in the raw image leading to an incorrect geometry between the image and the terrain or the reference map projection. These distortions depend on different factors i.e. the platform (satellite, airborne, drone, etc.), the sensor, and the total field of view. In particular, some error sources could be the variation of the movement in the platform, variation in the sensor mechanics, the angle of view of the sensor, the time variations of the measuring instruments, Earth curvature and rotation, topographic effects, etc. Therefore, all these geometric distortions require models to perform the geometric corrections of the imagery, which cover the next steps (Toutin 2004):

- Acquisition of images and pre-processing of the metadata.
- Acquisition of the Ground Control Points (GCPs) with image coordinates and map coordinates.
- Computation of the unknown parameters of the geometric correction model.
- Image rectification with or without the Digital Elevation Model (DEM).

Thus, orthorectified images from VHRS satellite sensors (Quickbird, IKONOS, Worldview, Pleiades, etc.) are provided with nominal georeferencing computed from the satellite orbital positions and imaging geometry. In this context, highly accurate orthorectified images can be obtained using ancillary data such as DEMs and GCPs in very high resolution imagery (Schowengerdt 1980). The first step is the triangulation of the sensor orientation, whereas the final product is generated by removing the distorting effects of the terrain relief using a proper DEM (Grodecki and Dial 2003, McGlone 2004, Aguilar et al. 2013).

During last year several orthorectification studies have been carried out. For instance some authors have studied how to improve orthorectification models based on orthophotos as Habib et al. 2017 or based on improved algorithms as Geng et al. 2018. Moreover, improved or new orthorectification models in very high resolution imagery has been on trend lately (Marsetič et al. 2015, Zhang et al. 2016a, El Sagheer et al. 2017, Sidiropoulos et al. 2018).

In the Thesis, orthorectification has been performed using a RPC (Rational Polymodal Coefficients) model which replaces the rigorous sensor model with an approximation of the ground-to-image relationship using a DEM as ancillary data (ENVI 2004). More details about Orthorectification is given in Chapter 7.

#### **2.3.4. Co-registration**

An important application of remote sensing is the study of ecosystem changes occurring during a period of time. This topic will be explained in detail in Section 2.6. In this context, Earth surface changes can be determined by comparing pairs of remote sensing imagery acquired on different dates. Thus, precise image co-registration is essential. Difficulties in accurately co-registering imagery arise from

the non-ideal characteristics of the sensors, the changing attitude of the spacecraft during the image acquisition, DEM errors, and inaccurate resampling. Moreover, the accuracy of the measurements of the ground displacement depends on the performance of the correlation technique (Leprince et al. 2007).

Co-registration studies are usually carried out using data from only one imaging system and under restrictive conditions, i.e. similar viewing angles and satellite tracks (Van Puymbroeck et al. 2000, Michel and Avouac 2002, Avouac et al. 2006), or using external information from GPS measurements (Dominguez et al. 2003). Thus, remote sensed imagery needs to be projected and resampled into a common reference system, in order to be co-registered. Co-registering two images means to perform a spatial alignment between them, so they can be superimposable. One method consists in assuming one image as a reference image and the other as the image to be co-registered, which means to be projected and resampled into the reference image system. Another method is to project and resample each image into a common reference system that is independent of the sensor viewing geometry (Leprince et al. 2007). Nowadays, new image registration models have been developed. For instance, Ma et al. 2015 propose a flexible and general algorithm, called Locally Linear Transforming (LLT), for feature matching of remote sensing images. On the other hand, Wu et al. 2015 proposed a novel point-matching algorithm, which is an improved Random Sample Consensus (RANSAC) algorithm called Fast Sample Consensus (FSC).

In the Thesis, the geometric relationship between a warp image and a base image was obtained using a representative number of GCPs, in both image, and then, applying a geometrical transformation. This processing is more explained in Chapter 7.

### **2.3.5. Dimensionality reduction of hyperspectral imagery**

As it was explained, HS imagery is made by hundreds of spectral bands and, therefore, the following issues are found when using this type of imagery (De Backer et al. 2005):

- Neighboring bands in HS data are, generally, strongly correlated. Thus, it is possible that no information is added by increasing the spectral resolution.
- The high number of spectral bands increments the processing requirements and the computational times.
- When the ratio between the spectral bands and the number of training data samples used in a supervised classification is vastly different, high dimensional data suffers from the curse of dimensionality phenomenon or “Hughes” effect (Hughes 1968).

In this context, a reduction of the dimensionality is necessary in HS imagery, since the dependent variables provide no extra information about the classes, being noise for the predictor. This means that the total information content can be obtained from fewer unique features which contain maximum discrimination information about the classes of interest, which will be used for a future classification. Thus, by eliminating the dependent variables, the amount of data can be reduced which can lead to improvement in the classification performance (Chandrashekar and Sahin 2014). Reduction of dimensionality can be achieved by making a selection of few existing bands, using “feature selection” techniques, or generating new features by taking combinations of the original bands, using “feature extraction” techniques. A special case of feature extraction, where groups of consecutive bands are merged, can be referred as “band selection” (Du et al. 2003, De Backer et al. 2005, Fassnacht et al. 2014).

These assumptions do not mean that MS imagery is enough for most applications, as the required spectral bands should be specifically adapted to the applications (De Backer et al. 2005). Actually, significantly improved classification results with HS imagery over MS have been reported (Ustin et al. 2004, Buddenbaum et al. 2005, Gómez-Chova et al. 2015, Ballanti et al. 2016). Traditional dimensionality reduction techniques have been studied, compared and improved during last years. Chang et al. 1999 presented a new band selection method comprising a band prioritization and a band decorrelation technique. Lennon et al. 2001, Du et al. 2003, Wang and Chang 2006, Villa et al. 2009 and Li et al. 2014, show the Independent Component Analysis (ICA) algorithm as a technique for reducing the dimensionality. On the other hand, Cheriyyadat and Bruce 2003 doubt about PCA as a good method for feature extraction. Fassnacht et al. 2014 compare feature reduction techniques for classifying tree species, while Ren et al. 2014 show a review of both, feature extraction and data reduction methods. Moreover, Luo et al. 2016 compare Minimum Noise Fraction (MNF) and PCA techniques.

In summary, feature selection and extraction techniques help in understanding data, reducing computation requirement, reducing the effect of the curse of dimensionality and improving the classifier performance (Chandrashekar and Sahin 2014).

### **Feature selection algorithms**

This type of algorithms identify the subset of the original spectral bands that contains most of the information (Jia et al. 2012). They can be grouped into (Ladha and Deepa 2011, Fassnacht et al. 2014):

- *Wrapper methods*: they are search algorithms that continuously add (via forward selection) or drop (via backward selection) features based on a decision criteria, such as an accuracy measure of the applied statistical model.

However, they are computationally expensive and they have tendency to produce over-fitted models.

- *Filter methods*: they assess the importance of individual features outside of the modeling process itself. They are usually less computationally demanding than wrapper methods, but not directly targeting on the optimization of the classification or regression model, therefore, they might not deliver the desired accuracy.
- *Embedded methods*: they integrate the feature selection process within the training phase of the model, being directly embedded in the classification or regression method. They are computationally more demanding than filter methods, but less than wrapper methods.

### Feature extraction algorithms

They transform the original data onto a destination feature space through projections (Jia et al. 2012). Typical algorithms included would be PCA and its variations, as the Maximum-Variance PCA (MVP) (Chang et al. 1999), Kernel PCA (KPCA), Data Slicing PCA (SPCA) (Yang et al. 2004), MNF (Green et al. 1988) or ICA (Lennon et al. 2001).

Figure 2.10 shows the specific steps followed in the Thesis for carrying out the dimensionality reduction study in HSI imagery. PCA, MNF and ICA techniques were compared in HS imagery. Moreover, different component selection strategies were evaluated for selecting the suitable number of components in the transformed space, such as transformation statistics, texture measurements, transformed signatures and ROIs separability in the transformed space. SVM classification was used to evaluate the different features extraction techniques as well as the component selection strategies, taking different number of components.

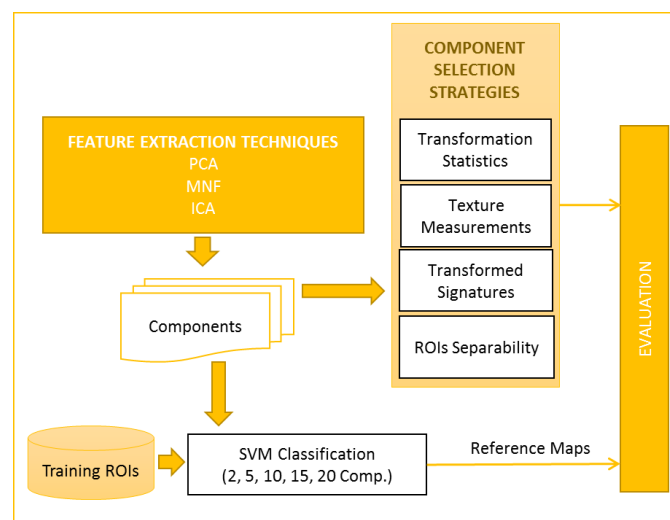


Figure 2.10. Dimensionality reduction pre-processing step workflow.

More information and details about Dimensionality Reduction methodology followed during the Thesis appear in Chapters 5 and 6.

## **2.4. SPECTRAL UNMIXING**

Following the scheme of Figure 1.2, next, the different spectral unmixing techniques are described.

An approach for vegetation mapping is the use of spectral mixture analysis techniques (Mücher et al. 2013). Collecting data in hundreds of spectral bands, HS sensor have demonstrated the capability of performing spectral unmixing. In HS imagery, mixed pixels are a mixture of more than one distinct cover. This is due to many factors: (i) the spatial resolution of a sensor is low enough that different materials can jointly occupy a single pixel, thus, the resulting spectral measurement will be some composite of the individual spectra and/or (ii) mixed pixels can result when distinct materials are combined into a homogeneous mixture. This circumstance can occur independent of the spatial resolution of the sensor (Keshava and Mustard 2002).

HS unmixing refers to a process that decomposes the pixel spectra into a collection of constituent spectra, or spectral signatures, called “endmembers”, and a set of corresponding fractions or “abundances”, that indicate the proportion of each endmember present in the pixel. Endmembers are generally assumed to represent the pure materials present in the image and the set of abundances at each pixel to represent the percentage of each endmember in the pixel. However, the notion of a pure material can be subjective and problem dependent. Thus, the definition of the endmembers can depend upon the application (Keshava and Mustard 2002, Bioucas-Dias et al. 2012).

### **2.4.1. Linear and Non-linear mixing models**

Most researches assume that abundance represents the percentage of material associated with an endmember present in the part of the scene imaged by a particular pixel. Hapke 2012 states that the abundances in a linear mixture represent the relative area of the corresponding endmember in an imaged region. However, in the non-linear case, the situation is not as straightforward. The reflectance is usually not a linear function of the mass of the material nor it is a linear function of the cross-sectional area of the material (Bioucas-Dias et al. 2012). As indicated, mixing models can be characterized as either linear or non-linear (Keshava and Mustard 2002).

#### **Linear mixing**

Linear mixing holds when the mixing scale is macroscopic and the incident light interacts with just one material. The mixing occurs within the instrument itself,



because the resolution of the instrument is not fine enough. The light from the materials, although almost completely separated, is mixed within the measuring instrument. Fig. 2.11 shows that the light scattered by three materials ( $m_1$ ,  $m_2$ ,  $m_3$ ) in a scene is incident on a detector that measures radiance in the sensor's bands. The measured spectrum,  $y$ , is a weighted average of the material spectra ( $m_i$ ). The relative amount of each material is represented by the associated weight ( $\alpha_i$ ) (Bioucas-Dias et al. 2012). If the total surface area is considered to be divided proportionally according to the fractional abundances of the endmembers, then the reflected radiation will convey the characteristics of the associated media with the same proportions (Keshava and Mustard 2002).

Linear mixing models have been improved during years, for instance Van der Meer and De Jong 2000 enhance the orthogonality of endmembers in order to improve the spectral unmixing results in Landsat imagery. Moreover, several authors have focused on including the spectral variability of endmembers in the spectral unmixing algorithms such as Bateson et al. 2000, García-Haro et al. 2005, Song 2005, Somers et al. 2011, Veganzones et al. 2014, Zare and Ho 2014, Drumetz et al. 2016, Thouvenin et al. 2016 or Drumetz et al. 2018.

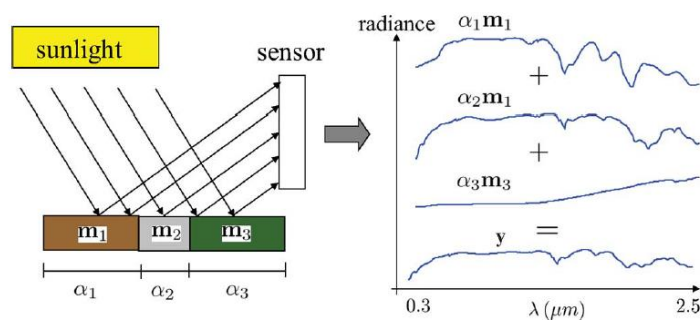


Figure 2.11. Linear mixing. The measured radiance at a pixel is a weighted average of the radiances of the materials present at the pixel in a linear model (Bioucas-Dias et al. 2012).

### Non-Linear mixing

Non-linear mixing is usually due to physical interactions between the light scattered by multiple materials in the scene. Light typically interacts with more than one component as it is multiply scattered and the mixing systematics between these different components are non-linear (Keshava and Mustard 2002). These interactions can be at “classical”, or “multilayered”, level or at “microscopic”, or “intimate”, level. Fig. 2.12 shows the two non-linear mixing scenarios (Bioucas-Dias et al. 2012).

- *Classical level mixing* occurs when light is scattered from one or more objects and is reflected off additional objects and, eventually, is measured by the HS imager. Generally, the first order terms are enough and this leads to the bilinear model.
- *Microscopic mixing* occurs when two materials are homogeneously mixed. In this case, the interactions consist of photons emitted from molecules of one material that are absorbed by molecules of another material, which may in turn emit more photons. The mixing is modeled by Hapke 2012 as occurring at the “albedo” level and not at the reflectance level. The apparent albedo of the mixture is a linear average of the albedos of the individual substances, but the reflectance is a non-linear function of albedo, leading to a different type of non-linear model.

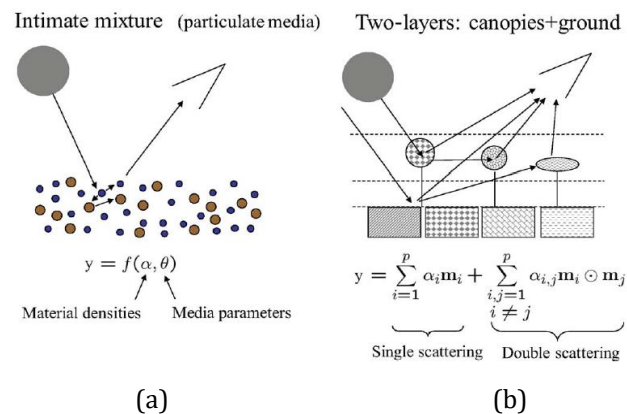


Figure 2.12. Two non-linear mixing scenarios. (a) intimate mixture: the materials are in close proximity; (b) multilayered scene: there are multiple interactions among the scatters at the different layers (Bioucas-Dias et al. 2012).

As it is explained in Keshava and Mustard 2002, the issue of whether linear or non-linear processes dominate the spectral signatures of mixed pixels is still unresolved (Heylen et al. 2014, Yu et al. 2017). It likely depends on a number of factors and conditions of the scene. The linear approach has been demonstrated in numerous applications to be a useful technique for interpreting the variability in remote sensing data and a powerful means for covering spectral information data products that can be related to the physical abundance of materials on the surface (Song 2005, Delalieux et al. 2012, Mùcher et al. 2013). However, it is only strictly valid for the situation where the endmembers are arranged in discrete, segregated patches on the surface. This condition is almost never met in nature, and many constituents of interest for Earth sciences exist in soils, or at smaller scales, in intimate association with one another (Borel and Gerstl 1994). However, non-linear methods are complex and still under study.

Figure 2.13 shows the diagram of the spectral unmixing processing steps followed in the Thesis. A linear mixing model was used but the spectral variability

of the endmembers produced by topographic changes and radiometric bands changes in each airborne pass, are considered. Thus, specific spectral unmixing algorithms which consider this spectral variability were analyzed, i.e. Scaled Constrained Least Squares Unmixing (SCLSU), Extended Linear Mixing Model (ELMM) and Robust ELMM (RELMM). Classification maps taking the abundances maps as inputs were obtained. More detailed information about the linear mixing models used in the Thesis is given in Chapter 6.

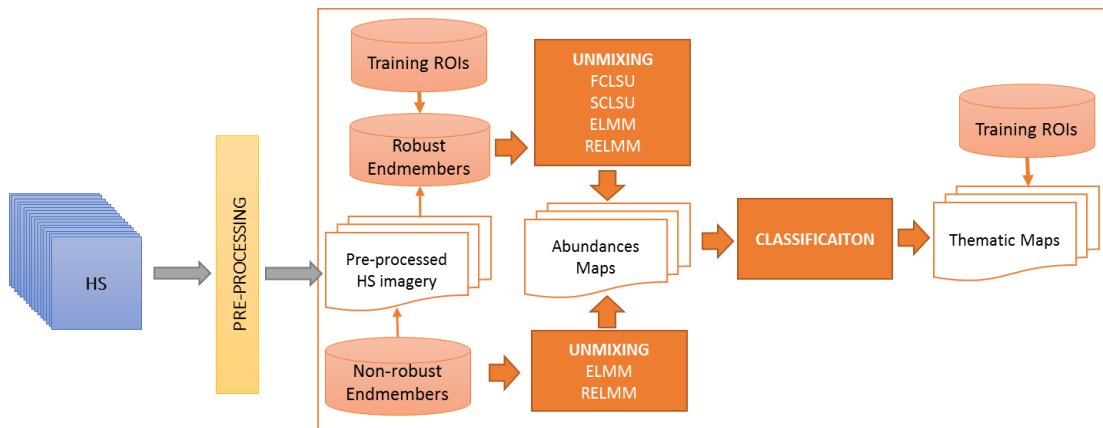


Figure 2.13. Specific workflow of the spectral unmixing processing.

## 2.5. CLASSIFICATION TECHNIQUES

Remote sensing research focusing on image classification has long attracted the attention of the remote sensing community because classification results are the basis for many environmental and socioeconomic applications. In this context, classification involves the association of features within the remotely sensed imagery with specific land cover classes and results in the production of land cover maps (Aplin 2004). However, classifying remotely sensed data into a thematic map remains a challenge because many factors. For instance, mapping in less complex habitats is relatively straightforward, but becomes more challenging when landscapes are more heterogeneous and when the variations between habitats are more continuous (Corbane et al. 2015). Another challenge is the selection of training and testing data, in which the quality and quantity of training sample data are crucial to produce accurate classification results. Moreover, the image pre-processing, as well as the classification approaches considered, may affect the success of a classification (Lu and Weng 2007). Additionally, the user's need, scale of the study area, economic condition, and analyst's skills are important factors that influence the selection of remotely sensed data, the design of the classification procedure, and the quality of the classification results (Lu and Weng 2007).

Classification techniques can be grouped between unsupervised and supervised classification methods. Another division is regarding the approach followed, where pixel-based or object-based approaches can be distinguished.

### 2.5.1. Unsupervised and Supervised classification

Unsupervised classification methods are purely relying on spectral pixel-based statistic and incorporate *no priori* knowledge of the characteristics of the covers being studied. The benefit of applying unsupervised classification methods is to automatically convert raw image data into useful information (Xie et al. 2008). Duda and Canty 2002 investigated and compared unsupervised classification algorithms with regard their abilities to reproduce ground data in a complex area. A disadvantage is that classes have to be assigned to real covers and the classification process must be repeated if new data (samples) are added. Typical unsupervised classification algorithms are K-Means and ISODATA (Congalton 1991, Richards 1999).

Supervised classification methods establish classification by learning from a training dataset, which contains the predictor variables measured in each sampling unit and assigns prior classes of interest to the sampling's units. Hence, supervised classification consists on assigning new sampling units to the *priori* classes (Xie et al. 2008). Maximum Likelihood classification, Minimum Distance, Support Vector Machine (SVM) are the most common supervised classifiers (Tuia et al. 2011, Huang and Zhang 2013). Other classifiers have been studied as well, such as Artificial Neural Networks (ANN) (Civco 1993) and Fuzzy Logic approaches (Filippi and Jensen 2006). Belgiu and Drăguț 2016 give a review of Random Forest classification in remote sensing. Shao and Lunetta 2012 show the good performance of SVM versus ANN and Classification and Regression Trees (CART) algorithms in land-cover classification (Benediktsson and Ghamisi 2015).

On the other hand, deep learning algorithms learn the representative and discriminative features in a hierarchical manner from the data. They have become a hotspot in the machine-learning area and being introduced into the geoscience and remote sensing community for remote sensing big data analysis. Deep learning provides an alternative way to automatically learn features from the training samples or unsupervised feature learning from very large raw images. It can represent hierarchically the information to express complex relationships between data with very deep neural networks, leading to a more efficient and robust image classification. Deep learning methods have proven to be efficient for processing both optical (HS and MS imagery) and radar images, in extracting different land cover types. However, deep learning cannot be directly used in many remote sensing tasks, due to the amount of training data required and the large numbers of bands (Chen et al. 2014, Zhao et al. 2015, Zhang et al. 2016b, Kussul et al. 2017). Some basic deep learning algorithms such as Deep Belief Networks (DBNs) (Hinton et al. 2006),

Restricted Boltzmann Machines (RBMs) (Freund and Haussler 1992), Autoencoder (AE) based algorithms (Bengio et al. 2007, Vincent et al. 2010), Convolutional Neural Networks (CNN) (Fukushima and Miyake 1982), allow to learn highly abstract feature detectors and to map the input features into representations clearly boosting the performance of the subsequent classifiers (Chen et al. 2014, Zhang et al. 2016b). Recent studies have been worked in proposing new deep learning approaches for classification such as Chen et al. 2014, Zhao et al. 2015, Zou et al., 2015, Garcia-Pedrero et al., 2017 and Kussul et al. 2017. However, as indicated, they are complex and difficult to apply in remote sensing scenarios.

On the other hand, authors include vegetation indices and texture to improve the results of these classifiers. For instance, Wang and Tenhunen 2004 use NDVI (Normalized Difference Vegetation Index) to offer valuable information of the dynamic changes of specific vegetation species using multi-temporal images. Ozdemir and Karnieli 2011 predicts forest structural parameters using Gray Level Co-occurrence Matrix (GLCM) in WV-2 imagery.

Regarding HS classification, several techniques have been successfully used, particularly supervised techniques as kernel methods, which can deal effectively with the “Hughes” phenomenon, already explained in Section 2.3.5. SVM shows accurate results in several HS remote sensing applications, as it is shown in Pal and Mather 2004, Camps-Valls and Bruzzone 2009, Li et al. 2013a, Ballanti et al. 2016.

Several authors have combined HS data with ancillary data, such as LiDAR, in order to obtain accurate classification results (Ghamisi et al. 2015), combining with MS imagery, such as Goodenough et al. 2003 for forest classification and Belluco et al. 2006 that used K-Means classifier as well as Spectral Angle Mapper (SAM) and Maximum Likelihood as supervised methods. Fauvel et al. 2013 made a review of the spectral-spatial classification of HS imagery and Ghamisi et al. 2017 updated it, focusing only in advanced spectral classifiers.

Besides, the training data are generally difficult and expensive to obtain. Thus, semi-supervised techniques are able to exploit unlabeled training samples that can be obtained from a limited set of labeled samples without significant effort/cost. For instance, a semi-supervised method when HS imagery is available, consist on performing spectral unmixing and then, obtaining classification maps from the abundances maps (Delalieux et al. 2012, García-Dópido 2013).

### **2.5.2. Pixel and Object-based classification approaches**

As it was mentioned, two approaches are presented for the classification and monitoring of ecosystems with remote sensing data: pixel-based approach and object-based approach.

In the conventional pixel-based methodology, pixels are individually classified according to their digital values, but spatial concepts or contextual information are not, generally, incorporated (Peña-Barragán et al. 2011). The processing on very high resolution imagery represents a restraint for traditional pixel-based approaches due to: (1) the high spectral variability within natural and semi-natural covers that produces a low classification accuracy, and (2) the pixel is only a consequence of the discrete representation of an image and, therefore, it lacks of semantic meaning in the real world being pointless for end users (Garcia-Pedrero et al. 2015).

Burnett and Blaschke 2003 states that natural complexity can be best explored using spatial analysis tools based on concepts of ecosystems or landscapes that can be partially decomposed into objects or patches.

Object-based image analysis (OBIA) has been proposed as a strong approach to identify, delineate, describe and label the required patches in a consistent way (Bock 2003, Múcher et al. 2013). The preliminary step of OBIA is the segmentation of the image and the construction of a hierarchical network of homogeneous objects. Segmentation is the process in which the image is subdivided into homogeneous regions, segments, according to several parameters. Hence, segments are groups of pixels representing patches, entities or their elements (primitives) which, subsequently can be classified into categories. Then, after segmentation, in the classification process, all pixels in the entire object are assigned to the same class and therefore, removing the problem of spectral variability and mixed pixels (Blaschke 2010, Peña-Barragán et al. 2011).

Langanke et al. 2007 assessed the mire conservation status of a raised bog site using object-based monitoring and structural analysis, and Strasser et al. 2014 developed multiscale object feature library for habitat quality monitoring in riparian forest using WV-2 and SPOT-5 imagery. Object-based analysis allows incorporating textural, geometric and contextual features defined at the level of object unit. Peña-Barragán et al. 2011 implemented this methodology for crop identification, while Dronova 2015 reviewed the OBIA analysis in wetlands. During the last two decades, many object-oriented approaches in remote sensing image analysis have been presented to overcome the traditional pixel-based problems, e.g. mixed pixels and object spectral variability. For instance, Oruc et al. 2014 and Agarwal et al. 2013 compared pixel-based and object-based approaches in classification processes.

Figure 2.14 shows the classification workflow followed in the Thesis. As it was mentioned before, the Teide National Park is a vulnerable and heterogeneous mountain ecosystem with small and mixed vegetation species. This fact leads to use VHRS MS and HS imagery. A thorough analysis was conducted and, finally, the classification was carried out using the optimal classifier adding different features

(textures, abundances, vegetation indices, etc.) to the classification model in order to obtain the most accurate thematic map.

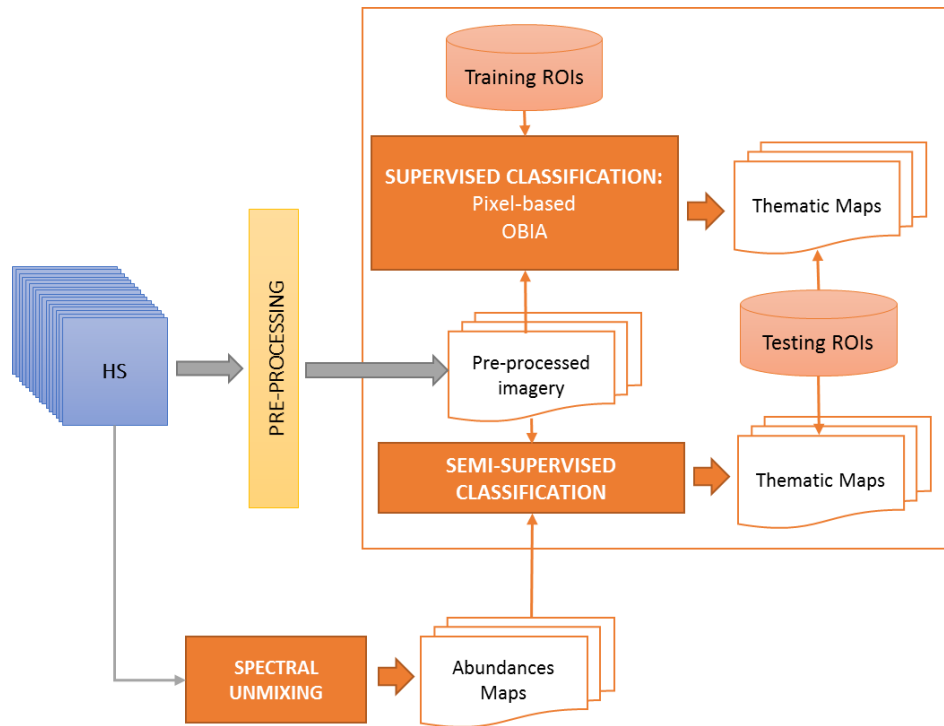


Figure 2.14. Classification workflow followed in the Thesis.

More information about the classification models carried out in the Thesis is given in Chapters 4, 6 and 7.

## 2.6. APPLICATIONS OF REMOTE SENSING

Remote sensing has been successfully used for many ecological applications, such as detecting land changes, monitoring deforestation, estimating carbon sequestration, vegetation stress, etc. Specifically, land-use and land-cover mapping and monitoring, biodiversity characterization and assessment, as well as forest degradation and species invasion, are important applications of remote sensing in biodiversity monitoring (Kerr and Ostrovsky 2003, Aplin 2005, Xie et al. 2008, Horning et al. 2010, Wang et al. 2010, Khare and Ghosh 2016). For instance, remote sensing may have a major role to play in helping to prioritize candidate locations for new reserves. Methods to identify priority areas for conservation have generally focused on habitat structures, presence of typical species in the habitat, abiotic factors and pressures on or disturbances of the habitat type. Frequently, quick and rigorous methods are required in conservation assessments to identify where human-induced threats and high biodiversity areas coincide. Remote sensing offers a repeatable, systematic, and spatially exhaustive source of information on key variables such as productivity, disturbance, and land-cover than impact

biodiversity. Besides, the spatial coverage provided by remote sensing offers the potential to monitor the effectiveness of protected areas, allowing comparisons of changes inside and outside of reserves to be evaluated (Gillespie et al. 2008, Corbane et al. 2015).

Regarding very high resolution imagery, the identification of certain species and species assemblages is feasible. Remote sensing of phenological change is possible as well as a method for the detection of vegetation types down to the species level (Hufkens et al. 2012, Schmidt et al. 2015). In case of HS data, it can be measured the leaf-surface attributes during different season, leading to a useful information about ecosystem functioning, evolution and change (Garcia and Ustin 2001, Zarco-Tejada et al. 2016). Moreover, indirect detection of species diversity through remote sensing on environmental parameters can be used for discerning patterns of species diversity. Although not single factor drives biodiversity patters (e.g. latitudinal gradient in species richness) (Turner et al. 2003), researchers have considered primary productivity, climate and habitat structure as important in determining species richness and distribution patters (Lee et al. 2015, Frohn and Lopez 2017). In this Thesis, we focused in change detection application.

Generally, classification maps provide a snapshot of the distribution of land cover at a given time. However, ecosystems are dynamics, being useful their temporal monitoring (Aplin 2004).

Change detection is the process of identifying differences in the state of an object or phenomenon by observing it at different times (Singh 1989). Timely and accurate change detection of Earth's surface features provides the foundation for better understanding relationships and interactions between human and natural phenomena to better manage and use resources (Lu et al. 2004).

The main challenges facing ecosystem change monitoring are: (i) detect modification in addition to conversions; (ii) monitor rapid and abrupt changes in addition to the progressive and incremental changes; (iii) separate inter-annual variability from secular trends; (iv) understand the scale dependence of statistical estimates in change derived from remote sensing data at different spatial resolutions; and (v) match the temporal sampling rates of observations of processes to the intrinsic scales of these processes (Coppin et al. 2004).

Regarding Lu et al. 2004, change detection methods are divided into the following groups:

- *Algebraic methods*: they includes different techniques as image differencing, image regression, image rationing, vegetation index differencing, Change Vector Analysis (CVA) and background subtraction. These algorithms select thresholds to determine the changed areas. They are relatively simple from a conceptual



point of view, straightforward, and easy to implement and interpret. However, it is difficult to set the suitable threshold to provide detailed change information.

- *Based on transformation*: this category includes PCA, Kauth-Thomas (KT) or Tasseled Cap Transformation, GS and Chi-square transformations. These methods reduce the data redundancy between bands and emphasize changes on the derived components. A disadvantage is that they are difficult to interpret and label the change information on the transformed images.
- *Based on classification*: they are based on the classified images on different dates. They include post-classification comparison, spectral-temporal combined analysis, Expectation-Maximization algorithm (EM) change detection, unsupervised change detection, hybrid change detection, and ANN. The major advantage is the capability of providing a matrix of change information and reducing external impact from atmosphere and environmental differences between the multi-temporal images. However, selecting high-quality and enough training samples is often difficult.
- *GIS approaches*: the advantage to use GIS is the ability to incorporate different source data into change detection applications. However, different source data associated with diverse data accuracies and formats often affect the change detection results. Alqurashi and Kumar 2013 reviewed the use of remote sensing and GIS techniques to detect land-use and land-cover changes.
- *Visual Analysis*: it is a visual interpretation of multi-temporal image composite and on-screen digitizing of changed areas. This method can make full use of an analyst's experience and knowledge, but it is time consuming for a large-area application and it is hard to update the change detection results. It is difficult to provide detailed change trajectories.
- *Advanced models*: this group includes the Li-Strahler reflectance model (Wanner et al. 1995), spectral mixture models (Wu and Murray 2003), and biophysical parameter estimation models (Sexton et al. 2015). The main disadvantage is the time-consuming and difficult process of developing suitable models for conversion of image reflectance values to biophysical parameters.

On the other hand, Jianya et al. 2008 characterized, the change detection approaches, into two broad groups: (1) bi-temporal change detection, which measures changes by comparing two dates; and (2) temporal trajectory that analyses the changes based on a 'continuous' timescale.

In this context, Key et al. 2001 compare multi-temporal information on high spatial resolution imagery to classify individual tree species, while Lucas et al. 2007 applied a rule-based classification of multi-temporal Landsat imagery for mapping a semi-natural habitats and agricultural land cover. Camps-Valls et al. 2008 used a kernel-based method for multi-temporal classification and developed a non-linear kernel classifier for the well-known difference and rationing changes detection methods. Other studies using multi-source and multi-temporal data are Xu et al.

2009, Wen 2011, Corcoran et al. 2013 and Zhan et al. 2018. Moreover, Lu et al. 2014 reviewed the current situation of change detection techniques, indicating the need to develop new techniques to solve the mixed pixel problem and Gong et al. 2016 designed a Coupled Dictionary Learning (CDL) to explore the intrinsic difference of multi-source data for change detection.

In the Thesis a framework was proposed to monitor and analyze the changes produced in the Teide National Park, at species level, using vegetation maps derived from MS and HS remote sensing imagery from 2002 until 2017. The change detection framework followed in the Thesis is explained in Chapter 7.

## 2.7. REFERENCES

- Agarwal, S., L. S. Vailshery, M. Jaganmohan, and H. Nagendra. 2013. Mapping urban tree species using very high resolution satellite imagery: comparing pixel-based and object-based approaches. *ISPRS International Journal of Geo-Information* 2:220-236.
- Aguilar, M. A., M. del Mar Saldana, and F. J. Aguilar. 2013. Assessing geometric accuracy of the orthorectification process from GeoEye-1 and WorldView-2 panchromatic images. *International Journal of Applied Earth Observation and Geoinformation* 21:427-435.
- Aiazzi, B., L. Alparone, S. Baronti, and A. Garzelli. 2002. Context-driven fusion of high spatial and spectral resolution images based on oversampled multiresolution analysis. *IEEE Transactions on Geoscience and Remote Sensing* 40:2300-2312.
- Aiazzi, B., L. Alparone, S. Baronti, A. Garzelli, and M. Selva. 2006. MTF-tailored multiscale fusion of high-resolution MS and Pan imagery. *Photogrammetric Engineering & Remote Sensing* 72:591-596.
- Aiazzi, B., S. Baronti, and M. Selva. 2007. Improving component substitution pansharpening through multivariate regression of MS + Pan data. *IEEE Transactions on Geoscience and Remote Sensing* 45:3230-3239.
- Alcántara-Carrió, J., and A. Fontán. 2009. Factors controlling the morphodynamics and geomorphologic evolution of a cusped foreland in a volcanic intraplate island (Maspalomas, Canary Islands). *Journal of Coastal Research* 56:683-687.
- Alimuddin, I., J. T. S. Sumantyo, and H. Kuze. 2012. Assessment of pan-sharpening methods applied to image fusion of remotely sensed multi-band data. *International Journal of Applied Earth Observation and Geoinformation* 18:165-175.
- Alparone, L., B. Aiazzi, S. Baronti, A. Garzelli, F. Nencini, and M. Selva. 2008. Multispectral and panchromatic data fusion assessment without reference. *Photogrammetric Engineering & Remote Sensing* 74:193-200.
- Alparone, L., L. Wald, J. Chanussot, C. Thomas, P. Gamba, and L. M. Bruce. 2007. Comparison of pansharpening algorithms: Outcome of the 2006 GRS-S data-fusion contest. *IEEE Transactions on Geoscience and Remote Sensing* 45:3012-3021.

- Alqurashi, A. F., and L. Kumar. 2013. Investigating the use of remote sensing and GIS techniques to detect land use and land cover change: A review. *Advances in Remote Sensing* 2:193.
- Amro, I., J. Mateos, M. Vega, R. Molina, and A. K. Katsaggelos. 2011. A survey of classical methods and new trends in pansharpening of multispectral images. *EURASIP J. Adv. Sig. Proc.*:79.
- Aplin, P. 2004. Remote sensing: land cover. *Progress in Physical Geography* 28:283-293.
- Aplin, P. 2005. Remote sensing: ecology. *Progress in Physical Geography* 29:104-113.
- Arozena-Concepción, M., and E. Beltrán-Yanes. 2006. Geografía de la vegetación de las coladas domáticas del atrio de las Cañadas del Teide (Tenerife. I. Canarias). *Serie Geográfica - Biogeografía: Distribuciones, Dinámicas y Diversidad* 13:43-64.
- Avouac, J.-P., F. Ayoub, S. Leprince, O. Konca, and D. V. Helmberger. 2006. The 2005, Mw 7.6 Kashmir earthquake: Sub-pixel correlation of ASTER images and seismic waveforms analysis. *Earth and Planetary Science Letters* 249:514-528.
- Ballanti, L., L. Blesius, E. Hines, and B. Kruse. 2016. Tree species classification using hyperspectral imagery: A comparison of two classifiers. *Remote Sensing* 8:445.
- Baraldi, A., L. Durieux, D. Simonetti, G. Conchedda, F. Holecz, and P. Blonda. 2010. Automatic spectral-rule-based preliminary classification of radiometrically calibrated SPOT-4/-5/IRS, AVHRR/MSG, AATSR, IKONOS/QuickBird/OrbView/GeoEye, and DMC/SPOT-1/-2 imagery—Part I: System design and implementation. *IEEE Transactions on Geoscience and Remote Sensing* 48:1299-1325.
- Bateson, C. A., G. P. Asner, and C. A. Wessman. 2000. Endmember bundles: A new approach to incorporating endmember variability into spectral mixture analysis. *IEEE Transactions on Geoscience and Remote Sensing* 38:1083-1094.
- Belgiu, M., and L. Drăguț. 2016. Random forest in remote sensing: A review of applications and future directions. *ISPRS Journal of Photogrammetry and Remote Sensing* 114:24-31.
- Belluco, E., M. Camuffo, S. Ferrari, L. Modenese, S. Silvestri, A. Marani, and M. Marani. 2006. Mapping salt-marsh vegetation by multispectral and hyperspectral remote sensing. *Remote Sensing of Environment* 105:54-67.
- Benediktsson, J. A., and P. Ghamisi. 2015. *Spectral-Spatial Classification of Hyperspectral Remote Sensing Images*. Artech House.
- Bengio, Y., P. Lamblin, D. Popovici, and H. Larochelle. 2007. Greedy layer-wise training of deep networks. Pages 153-160 *in* *Advances in neural information processing systems*.
- Berk, A., G. P. Anderson, P. K. Acharya, L. S. Bernstein, L. Muratov, J. Lee, M. Fox, S. M. Adler-Golden, J. H. Chetwynd, and M. L. Hoke. 2005. MODTRAN 5: a reformulated atmospheric band model with auxiliary species and practical multiple scattering options: update. Pages 662-668 *in* *Algorithms and technologies for multispectral,*

- hyperspectral, and ultraspectral imagery XI. International Society for Optics and Photonics.
- Berk, A., L. Bernstein, G. Anderson, P. Acharya, D. Robertson, J. Chetwynd, and S. Adler-Golden. 1998. MODTRAN cloud and multiple scattering upgrades with application to AVIRIS. *Remote Sensing of Environment* 65:367-375.
- Bernstein, L. S., S. M. Adler-Golden, X. Jin, B. Gregor, and R. L. Sundberg. 2012. Quick atmospheric correction (QUAC) code for VNIR-SWIR spectral imagery: Algorithm details. Pages 1-4 in *Hyperspectral Image and Signal Processing (WHISPERS)*, 2012 4th Workshop on. IEEE.
- Bioucas-Dias, J. M., A. Plaza, N. Dobigeon, M. Parente, Q. Du, P. Gader, and J. Chanussot. 2012. Hyperspectral unmixing overview: Geometrical, statistical, and sparse regression-based approaches. *IEEE Journal of Selected Topics in Applied Earth Observations and Remote Sensing* 5:354-379.
- Blaschke, T. 2010. Object based image analysis for remote sensing. *ISPRS Journal of Photogrammetry and Remote Sensing* 65:2-16.
- Bock, M. 2003. Remote sensing and GIS-based techniques for the classification and monitoring of biotopes: Case examples for a wet grass-and moor land area in Northern Germany. *Journal for Nature Conservation* 11:145-155.
- Borel, C. C., and S. A. Gerstl. 1994. Nonlinear spectral mixing models for vegetative and soil surfaces. *Remote Sensing of Environment* 47:403-416.
- Bresson, X., and T. F. Chan. 2008. Fast dual minimization of the vectorial total variation norm and applications to color image processing. *Inverse problems and imaging* 2:455-484.
- Buddenbaum, H., M. Schlerf, and J. Hill. 2005. Classification of coniferous tree species and age classes using hyperspectral data and geostatistical methods. *International Journal of Remote Sensing* 26:5453-5465.
- Burnett, C., and T. Blaschke. 2003. A multi-scale segmentation/object relationship modelling methodology for landscape analysis. *Ecological modelling* 168:233-249.
- Burt, P. J., and E. H. Adelson. 1983. The Laplacian pyramid as a compact image code. *IEEE Transactions on Communications* 31:532-540.
- Camps-Valls, G., and L. Bruzzone. 2009. *Kernel methods for remote sensing data analysis*. John Wiley & Sons.
- Camps-Valls, G., L. Gómez-Chova, J. Muñoz-Marí, J. L. Rojo-Álvarez, and M. Martínez-Ramón. 2008. Kernel-based framework for multitemporal and multisource remote sensing data classification and change detection. *IEEE Transactions on Geoscience and Remote Sensing* 46:1822-1835.
- Carper, W. J., Lillesand, T.M, Kiefer, R.W. 1990. The used of intensity-hue-saturation transformations ofr merging SPOT panchromatic and multispectral image data. *Photogramm. Eng. Remote Sens.* 59:295-303.

- Civco, D. L. 1993. Artificial neural networks for land-cover classification and mapping. *International Journal of Geographical Information Science* 7:173-186.
- Cliche, G., F. Bonn, and P. Teillet. 1985. Integration of the SPOT panchromatic channel into its multispectral mode for image sharpness enhancement. *Photogrammetric engineering and remote sensing* 51:311-316.
- Congalton, R. G. 1991. A review of assessing the accuracy of classifications of remotely sensed data. *Remote Sensing of Environment* 37:35-46.
- Coppin, P., I. Jonckheere, K. Nackaerts, and B. Muys. 2004. Digital Change Detection Methods in Ecosystem Monitoring: a review. *International Journal of Remote Sensing* 25:1565-1596.
- Corbane, C., S. Lang, K. Pipkins, S. Alleaume, M. Deshayes, V. E. G. Millán, T. Strasser, J. V. Borre, S. Toon, and F. Michael. 2015. Remote sensing for mapping natural habitats and their conservation status—New opportunities and challenges. *International Journal of Applied Earth Observation and Geoinformation* 37:7-16.
- Corcoran, J. M., J. F. Knight, and A. L. Gallant. 2013. Influence of multi-source and multi-temporal remotely sensed and ancillary data on the accuracy of random forest classification of wetlands in Northern Minnesota. *Remote Sensing* 5:3212-3238.
- Chandrashekar, G., and F. Sahin. 2014. A survey on feature selection methods. *Computers & Electrical Engineering* 40:16-28.
- Chang, C.-I., Q. Du, T.-L. Sun, and M. L. Althouse. 1999. A joint band prioritization and band-decorrelation approach to band selection for hyperspectral image classification. *IEEE Transactions on Geoscience and Remote Sensing* 37:2631-2641.
- Chavez Jr, P. S. 1988. An improved dark-object subtraction technique for atmospheric scattering correction of multispectral data. *Remote Sensing of Environment* 24:459-479.
- Chavez, P., S. C. Sides, and J. A. Anderson. 1991. Comparison of three different methods to merge multiresolution and multispectral data- Landsat TM and SPOT panchromatic. *Photogrammetric engineering and remote sensing* 57:295-303.
- Chen, Y., Z. Lin, X. Zhao, G. Wang, and Y. Gu. 2014. Deep learning-based classification of hyperspectral data. *IEEE Journal of Selected Topics in Applied Earth Observations and Remote Sensing* 7:2094-2107.
- Cheriyadat, A., and L. M. Bruce. 2003. Why principal component analysis is not an appropriate feature extraction method for hyperspectral data. Pages 3420-3422 *in* *Geoscience and Remote Sensing Symposium, 2003. IGARSS'03. Proceedings. 2003 IEEE International. IEEE.*
- Da Cunha, A. L., J. Zhou, and M. N. Do. 2006. The nonsubsampling contourlet transform: theory, design, and applications. *IEEE Transactions on Image Processing* 15:3089-3101.

- De Backer, S., P. Kempeneers, W. Debruyne, and P. Scheunders. 2005. A band selection technique for spectral classification. *IEEE Geoscience and Remote Sensing Letters* 2:319-323.
- Delalieux, S., B. Somers, B. Haest, T. Spanhove, J. V. Borre, and C. Múcher. 2012. Heathland conservation status mapping through integration of hyperspectral mixture analysis and decision tree classifiers. *Remote Sensing of Environment* 126:222-231.
- Dell'Acqua, F., P. Gamba, A. Ferrari, J. A. Palmason, J. A. Benediktsson, and K. Árnason. 2004. Exploiting spectral and spatial information in hyperspectral urban data with high resolution. *IEEE Geoscience and Remote Sensing Letters* 1:322-326.
- Dominguez, S., J. P. Avouac, and R. Michel. 2003. Horizontal coseismic deformation of the 1999 Chi-Chi earthquake measured from SPOT satellite images: Implications for the seismic cycle along the western foothills of central Taiwan. *Journal of Geophysical Research: Solid Earth* 108.
- Dronova, I. 2015. Object-based image analysis in wetland research: A review. *Remote Sensing* 7:6380-6413.
- Drumetz, L. 2016. Endmember variability in hyperspectral image unmixing. *Université de Grenoble Alpes*.
- Drumetz, L., J. Chanussot, and A. Iwasaki. 2018. Endmembers as directional data for robust material variability retrieval in hyperspectral image unmixing. *IEEE International Conference on Acoustics, Speech and Signal Processing (ICASSP)*:1-5.
- Drumetz, L., J. Chanussot, and C. Jutten. 2016a. Variability of the endmembers in spectral unmixing: recent advances. *in 8th IEEE Workshop on Hyperspectral Image and Signal Processing: Evolution in Remote Sensing*.
- Drumetz, L., M.-A. Veganzones, S. Henrot, R. Phlypo, J. Chanussot, and C. Jutten. 2016b. Blind hyperspectral unmixing using an Extended Linear Mixing Model to address spectral variability. *IEEE Transactions on Image Processing* 25:3890-3905.
- Du, H., H. Qi, X. Wang, R. Ramanath, and W. E. Snyder. 2003. Band selection using independent component analysis for hyperspectral image processing. Pages 93-98 *in Applied Imagery Pattern Recognition Workshop, 2003. Proceedings. 32nd. IEEE*.
- Duda, T., and M. Canty. 2002. Unsupervised classification of satellite imagery: choosing a good algorithm. *International Journal of Remote Sensing* 23:2193-2212.
- Dutilleul, P., C. Aiguier, and R. Joliot. 1987. An implementation of the 'algorithm a trous' to compute the wavelet transform: in Combes, J.M., Grossman, A., and Tchamitchian, Ph. Ed. s, 1990, *Wavelets: Time-Frequency Methods and Phase Space*, Second Edition, Springer-Verlag, New York.
- Ehlers, M., S. Klonus, P. Johan Åstrand, and P. Rosso. 2010. Multi-sensor image fusion for pansharpening in remote sensing. *International Journal of Image and Data Fusion* 1:25-45.
- El Sagheer, A. A., K. M. Zaki, M. S. Gomaa, and A. M. Marrei. 2017. Rigorous Versus Generalized Sensor Models: Assessment of Different Height Sources for

- Orthorectification of High-Resolution Satellite Imagery. *Surveying and Land Information Science* 76:49-57.
- ENVI. 2004. ENVI User's Guide. Research System Inc.
- Fassnacht, F. E., C. Neumann, M. Förster, H. Buddenbaum, A. Ghosh, A. Clasen, P. K. Joshi, and B. Koch. 2014. Comparison of feature reduction algorithms for classifying tree species with hyperspectral data on three central European test sites. *IEEE Journal of Selected Topics in Applied Earth Observations and Remote Sensing* 7:2547-2561.
- Fauvel, M., Y. Tarabalka, J. A. Benediktsson, J. Chanussot, and J. C. Tilton. 2013. Advances in spectral-spatial classification of hyperspectral images. *Proceedings of the IEEE* 101:652-675.
- Fernández-Cabrera, E., E. Roca-Bosch, M. Villares-Junyent, E. Pérez-Chacón-Espino, and L. Hernández-Calvento. 2010. Propuesta metodológica para la integración en SIG de métodos de participación social para la planificación y gestión de sistemas de dunas litorales. El ejemplo del Parque Natural de Corralejo (Fuerteventura, Islas Canarias). Pages 803-817 *in* La información geográfica al servicio de los ciudadanos: de lo global a lo local. Secretariado de Publicaciones.
- Fernández Cabrera, E., E. Roca Bosch, L. Cabrera, L. Hernández-Calvento, and E. Pérez-Chacon. 2012. Estudio de la percepción social en el entorno del Parque Natural de las Dunas de Corralejo (Fuerteventura, Islas Canarias): aplicaciones para la gestión integrada de zonas costeras. *in* I Congreso Iberoamericano de Gestión Integrada de Áreas Litorales.
- Filippi, A. M., and J. R. Jensen. 2006. Fuzzy learning vector quantization for hyperspectral coastal vegetation classification. *Remote Sensing of Environment* 100:512-530.
- Fonseca, L., L. Namikawa, E. Castejon, L. Carvalho, C. Pinho, and A. Pagamisse. 2011. Image Fusion for Remote Sensing Applications. *Image Fusion and Its Applications* [www.intechopen.com](http://www.intechopen.com).
- Freund, Y., and D. Haussler. 1992. Unsupervised learning of distributions on binary vectors using two layer networks. Pages 912-919 *in* Advances in neural information processing systems.
- Frohn, R. C., and R. D. Lopez. 2017. Remote Sensing for Landscape Ecology: New Metric Indicators: Monitoring, Modeling, and Assessment of Ecosystems. CRC Press.
- Fukushima, K., and S. Miyake. 1982. Neocognitron: A self-organizing neural network model for a mechanism of visual pattern recognition. Pages 267-285 *Competition and cooperation in neural nets*. Springer.
- Gao, B.-C., M. J. Montes, C. O. Davis, and A. F. Goetz. 2009. Atmospheric correction algorithms for hyperspectral remote sensing data of land and ocean. *Remote Sensing of Environment* 113:S17-S24.
- García-Dópido, I. 2013. New Techniques for Hyperspectral Image Classification. Universidad de Extremadura.

- García-Pedrero, A., C. Gonzalo-Martín, D. Fonseca-Luengo, and M. Lillo-Saavedra. 2015. A GEOBIA Methodology for Fragmented Agricultural Landscapes. *Remote Sensing* 7:767-787.
- García-Pedrero, A., C. Gonzalo-Martín, and M. Lillo-Saavedra. 2017. A machine learning approach for agricultural parcel delineation through agglomerative segmentation. *International Journal of Remote Sensing* 38:1809-1819.
- García-Haro, F., S. Sommer, and T. Kemper. 2005. A new tool for variable multiple endmember spectral mixture analysis (VMESMA). *International Journal of Remote Sensing* 26:2135-2162.
- García, M., and S. L. Ustin. 2001. Detection of interannual vegetation responses to climatic variability using AVIRIS data in a coastal savanna in California. *IEEE Transactions on Geoscience and Remote Sensing* 39:1480-1490.
- Garzón-Machado, V., M. J. del Arco-Aguilar, and P. L. Pérez-de-Paz. 2011. A tool set for description and mapping vegetation on protected natural areas: an example from the Canary Islands. *Biodiversity and Conservation* 20:3605-3625.
- Geng, X., Q. Xu, C. Lan, S. Xing, Y. Hou, and L. Lyu. 2018. Orthorectification of Planetary Linear Pushbroom Images Based on an Improved Back-Projection Algorithm. *IEEE Geoscience and Remote Sensing Letters*.
- Ghamisi, P., J. A. Benediktsson, and S. Phinn. 2015. Land-cover classification using both hyperspectral and LiDAR data. *International Journal of Image and Data Fusion* 6:189-215.
- Gillespie, A. R., A. B. Kahle, and R. E. Walker. 1987. Color enhancement of highly correlated images. II. Channel ratio and "chromaticity" transformation techniques. *Remote Sensing of Environment* 22:343-365.
- Gillespie, T. W., G. M. Foody, D. Rocchini, A. P. Giorgi, and S. Saatchi. 2008. Measuring and modelling biodiversity from space. *Progress in Physical Geography* 32:203-221.
- Gobierno de Canarias, C. 2004. Plan Director Reserva Natural Especial de Las Dunas de Maspalomas. Gobierno de Canarias. Consejería de Medio Ambiente y Ordenación Territorial. Videconsejería de Ordenación Territorial. Dirección General de Ordenación al Territorio.
- Gómez-Chova, L., D. Tuia, G. Moser, and G. Camps-Valls. 2015. Multimodal classification of remote sensing images: A review and future directions. *Proceedings of the IEEE* 103:1560-1584.
- Gong, M., P. Zhang, L. Su, and J. Liu. 2016. Coupled dictionary learning for change detection from multisource data. *IEEE Transactions on Geoscience and Remote Sensing* 54:7077-7091.
- González-Audícana, M., J. L. Saleta, R. G. Catalán, and R. García. 2004. Fusion of multispectral and panchromatic images using improved IHS and PCA mergers based on wavelet decomposition. *IEEE Transactions on Geoscience and Remote Sensing* 42:1291-1299.



- González-Lemus, N., J. C. Carracedo-Gómez, and M. Durbán-Villonga. 2009. El Parque Nacional del Teide: patrimonio mundial de la UNESCO. *Anuario de Estudios Atlánticos* 1:519-568.
- Gonzalo-Martín, C., and M. Lillo-Saavedra. 2007. Fusión de Imágenes QuickBird Mediante una Representación Conjunta Multirresolución-Multidireccional. *IEEE Latin America Transactions*. 5:32-37.
- Goodenough, D. G., H. Chen, P. Gordon, K. O. Niemann, and G. Quinn. 2012. Forest applications with hyperspectral imaging. Pages 7309-7312 in *Geoscience and Remote Sensing Symposium (IGARSS), 2012 IEEE International*. IEEE.
- Goodenough, D. G., A. Dyk, K. O. Niemann, J. S. Pearlman, H. Chen, T. Han, M. Murdoch, and C. West. 2003. Processing Hyperion and ALI for forest classification. *IEEE Transactions on Geoscience and Remote Sensing* 41:1321-1331.
- Govender, M., K. Chetty, and H. Bulcock. 2007. A review of hyperspectral remote sensing and its application in vegetation and water resource studies. *Water Sa* 33.
- Green, A. A., M. Berman, P. Switzer, and M. D. Craig. 1988. A transformation for ordering multispectral data in terms of image quality with implications for noise removal. *IEEE Transactions on Geoscience and Remote Sensing* 26:65-74.
- Grodecki, J., and G. Dial. 2003. Block adjustment of high-resolution satellite images described by rational polynomials. *Photogrammetric Engineering & Remote Sensing* 69:59-68.
- Gupta, R. P. 2017. *Remote sensing geology*. Springer.
- Habib, A., W. Xiong, F. He, H. L. Yang, and M. Crawford. 2017. Improving orthorectification of UAV-based push-broom scanner imagery using derived orthophotos from frame cameras. *IEEE Journal of Selected Topics in Applied Earth Observations and Remote Sensing* 10:262-276.
- Hadjimitsis, D. G., and C. R. Clayton. 2008. The use of an improved atmospheric correction algorithm for removing atmospheric effects from remotely sensed images using an atmosphere-surface simulation and meteorological data. *Meteorological applications* 15:381-387.
- Hadjimitsis, D. G., G. Papadavid, A. Agapiou, K. Themistocleous, M. Hadjimitsis, A. Retalis, S. Michaelides, N. Chrysoulakis, L. Toullos, and C. Clayton. 2010. Atmospheric correction for satellite remotely sensed data intended for agricultural applications: impact on vegetation indices. *Natural Hazards and Earth System Sciences* 10:89-95.
- Hallanda, W. A., and S. Cox. 1983. Image sharpening for mixed spatial and spectral resolution satellite systems. In: *Proc. of 17th International Symposium of Remote Sensing of Environment*. University of Michigan, Ann Arbor, MI:1023-1032.
- Hapke, B. 2012. *Theory of reflectance and emittance spectroscopy*. Cambridge university press.

- Hardie, R. C., M. T. Eismann, and G. L. Wilson. 2004. MAP estimation for hyperspectral image resolution enhancement using an auxiliary sensor. *IEEE Transactions on Image Processing* 13:1174-1184.
- He, K., J. Sun, and X. Tang. 2013. Guided image filtering. *IEEE transactions on pattern analysis & machine intelligence*:1397-1409.
- Hernández-Calvento, L. 2002. Análisis de la evolución del sistema de dunas de Maspalomas, Gran Canaria, Islas Canarias (1960-2000). Universidad de Las Palmas de Gran Canaria.
- Hernández, L., J. Ojeda, N. Sánchez, and P. Máyer. 2007. Aproximación al análisis del desplazamiento de las dunas de Maspalomas (Gran Canaria, Islas Canarias). *Investigaciones recientes (2005–2007) en Geomorfología Litoral*. Palma de Mallorca, Spain:113-118.
- Heylen, R., M. Parente, and P. Gader. 2014. A review of nonlinear hyperspectral unmixing methods. *IEEE Journal of Selected Topics in Applied Earth Observations and Remote Sensing* 7:1844-1868.
- Hinton, G. E., S. Osindero, and Y.-W. Teh. 2006. A fast learning algorithm for deep belief nets. *Neural computation* 18:1527-1554.
- Horning, N., J. A. Robinson, E. J. Sterling, W. Turner, and S. Spector. 2010. *Remote sensing for ecology and conservation: a handbook of techniques*. Oxford University Press.
- Hotelling, H. 1933. Analysis of a complex of statistical variables into principal components. *Journal of educational psychology* 24:417.
- Huang, X., and L. Zhang. 2013. An SVM ensemble approach combining spectral, structural, and semantic features for the classification of high-resolution remotely sensed imagery. *Geoscience and Remote Sensing, IEEE Transactions on* 51:257-272.
- Hufkens, K., M. Friedl, O. Sonnentag, B. H. Braswell, T. Milliman, and A. D. Richardson. 2012. Linking near-surface and satellite remote sensing measurements of deciduous broadleaf forest phenology. *Remote Sensing of Environment* 117:307-321.
- Hughes, G. 1968. On the mean accuracy of statistical pattern recognizers. *IEEE transactions on information theory* 14:55-63.
- Iglesias, J. R. 2003. Salvaje y desconocido: Parque Natural del Islote de Lobos. *Ambienta: La revista del Ministerio de Medio Ambiente* 25:49-53.
- Janzen, D. T., A. L. Fredeen, and R. D. Wheate. 2006. Radiometric correction techniques and accuracy assessment for Landsat TM data in remote forested regions. *Canadian Journal of Remote Sensing* 32:330-340.
- Jia, S., Z. Ji, Y. Qian, and L. Shen. 2012. Unsupervised band selection for hyperspectral imagery classification without manual band removal. *IEEE Journal of Selected Topics in Applied Earth Observations and Remote Sensing* 5:531-543.

- Jianya, G., S. Haigang, M. Guorui, and Z. Qiming. 2008. A review of multi-temporal remote sensing data change detection algorithms. *The International Archives of the Photogrammetry, Remote Sensing and Spatial Information Sciences* 37:757-762.
- Kerr, J. T., and M. Ostrovsky. 2003. From space to species: ecological applications for remote sensing. *Trends in ecology & evolution* 18:299-305.
- Keshava, N., and J. F. Mustard. 2002. Spectral unmixing. *IEEE Signal Processing Magazine* 19:44-57.
- Key, T., T. A. Warner, J. B. McGraw, and M. A. Fajvan. 2001. A comparison of multispectral and multitemporal information in high spatial resolution imagery for classification of individual tree species in a temperate hardwood forest. *Remote Sensing of Environment* 75:100-112.
- Khare, S., and S. Ghosh. 2016. Satellite Remote Sensing Technologies for Biodiversity Monitoring and Its Conservation. *International Journal of Advanced Earth Science and Engineering* 5:pp. 375-389.
- Kpalma, K., M. C. El-Mezouar, and N. Taleb. 2014. Recent Trends in Satellite Image Pan-sharpening techniques. *in* 1st International Conference on Electrical, Electronic and Computing Engineering.
- Kruse, F. 2004. Comparison of ATREM, ACORN, and FLAASH atmospheric corrections using low-altitude AVIRIS data of Boulder, CO. *in* Summaries of 13th JPL Airborne Geoscience Workshop, Jet Propulsion Lab, Pasadena, CA.
- Kruse, F., A. Lefkoff, J. Boardman, K. Heidebrecht, A. Shapiro, P. Barloon, and A. Goetz. 1993. The spectral image processing system (SIPS)—interactive visualization and analysis of imaging spectrometer data. *Remote Sensing of Environment* 44:145-163.
- Kussul, N., M. Lavreniuk, S. Skakun, and A. Shelestov. 2017. Deep learning classification of land cover and crop types using remote sensing data. *IEEE Geoscience and Remote Sensing Letters* 14:778-782.
- Laben, C. A., and B. V. Brower. 2000. Process for enhancing the spatial resolution of multispectral imagery using pan-sharpening. Google Patents.
- Ladha, L., and T. Deepa. 2011. Feature selection methods and algorithms. *International journal on computer science and engineering* 3:1787-1797.
- Langanke, T., C. Burnett, and S. Lang. 2007. Assessing the mire conservation status of a raised bog site in Salzburg using object-based monitoring and structural analysis. *Landscape and Urban Planning* 79:160-169.
- Lawrence, R. L., S. D. Wood, and R. L. Sheley. 2006. Mapping invasive plants using hyperspectral imagery and Breiman Cutler classifications (RandomForest). *Remote Sensing of Environment* 100:356-362.
- Lee, Z., J. Marra, M. J. Perry, and M. Kahru. 2015. Estimating oceanic primary productivity from ocean color remote sensing: A strategic assessment. *Journal of Marine Systems* 149:50-59.

- Lefeuvre, F., and T. J. Tanzi. 2014. Radio science's contribution to disaster emergencies. *URSI Radio Science Bulletin* 87:37-46.
- Lennon, M., G. Mercier, M. Mouchot, and L. Hubert-Moy. 2001. Independent component analysis as a tool for the dimensionality reduction and the representation of hyperspectral images. Pages 2893-2895 *in* *Geoscience and Remote Sensing Symposium, 2001. IGARSS'01. IEEE 2001 International*. IEEE.
- Leprince, S., S. Barbot, F. Ayoub, and J.-P. Avouac. 2007. Automatic and precise orthorectification, coregistration, and subpixel correlation of satellite images, application to ground deformation measurements. *IEEE Transactions on Geoscience and Remote Sensing* 45:1529-1558.
- Li, C., J. Yin, and J. Zhao. 2014. Using Improved ICA Method for Hyperspectral Data Classification. *Arabian Journal for Science & Engineering (Springer Science & Business Media BV)* 39.
- Li, J., P. R. Marpu, A. Plaza, J. M. Bioucas-Dias, and J. A. Benediktsson. 2013a. Generalized composite kernel framework for hyperspectral image classification. *IEEE Transactions on Geoscience and Remote Sensing* 51:4816-4829.
- Li, X. 2013. Band grouping pansharpening for WorldView-2 satellite images, *Information Systems and Computing Technology*.
- Li, X., M. He, and L. Zhang. 2013b. Hyperspherical Color Transform Based Pansharpening Method for WorldView-2 Satellite Images, *Proceedings of the 2013 IEEE 8th Conference on Industrial Electronics and Applications*.
- Li, X., L. Li, and M. He. 2012. A Novel Pansharpening Algorithm for WorldView-2 Satellite Images. *in* *International Conference on Industrial and Intelligent Information (ICIII 2012)*.
- Li, X., and W. Qi. 2015. An effective pansharpening method for WorldView-2 satellite images. *in* *International Conference on Estimation, Detection and Information Fusion (ICEDIF)*. IEEE.
- Lillo-Saavedra, M., and C. Gonzalo. 2006. Spectral or spatial quality for fused satellite imagery. A trade-off solution using the wavelet à trous algorithm. *International Journal of Remote Sensing* 27:1453-1464.
- Lillo-Saavedra, M., and C. Gonzalo. 2007. Multispectral images fusion by a joint multidirectional and multiresolution representation. *International Journal of Remote Sensing* 28:4065-4079.
- Lillo-Saavedra, M., C. Gonzalo, A. Arquero, and E. Martinez. 2005. Fusion of multispectral and panchromatic satellite sensor imagery based on tailored filtering in the Fourier domain. *International Journal of Remote Sensing* 26:1263-1268.
- Liu, J. 2000. Smoothing filter-based intensity modulation: A spectral preserve image fusion technique for improving spatial details. *International Journal of Remote Sensing* 21:3461-3472.

- Loncan, L., L. B. Almeida, J. M. Bioucas-Dias, X. Briottet, J. Chanussot, N. Dobigeon, S. Fabre, W. Liao, G. A. Licciardi, and M. Simoes. 2015. Hyperspectral pansharpening: A review. arXiv preprint arXiv:1504.04531.
- Lu, D., G. Li, and E. Moran. 2014. Current situation and needs of change detection techniques. *International Journal of Image and Data Fusion* 5:13-38.
- Lu, D., P. Mausel, E. Brondizio, and E. Moran. 2004. Change detection techniques. *International Journal of Remote Sensing* 25:2365-2401.
- Lu, D., and Q. Weng. 2007. A survey of image classification methods and techniques for improving classification performance. *International Journal of Remote Sensing* 28:823-870.
- Luo, G., G. Chen, L. Tian, K. Qin, and S.-E. Qian. 2016. Minimum noise fraction versus principal component analysis as a preprocessing step for hyperspectral imagery denoising. *Canadian Journal of Remote Sensing* 42:106-116.
- Ma, J., H. Zhou, J. Zhao, Y. Gao, J. Jiang, and J. Tian. 2015. Robust feature matching for remote sensing image registration via locally linear transforming. *IEEE Transactions on Geoscience and Remote Sensing* 53:6469-6481.
- Mallat, S. G. 1989. A theory for multiresolution signal decomposition: the wavelet representation. *IEEE Transactions on Pattern Analysis and Machine Intelligence* 11:674-693.
- Manakos, I., K. Manevski, C. Kalaitzidis, and D. Edler. 2011. Comparison between Atmospheric Correction Modules on the Basis of Worldview-2 Imagery and in situ Spectroradiometric Measurements Pages 11-13 *in* 7th EARSEL SIG Imaging Spectroscopy workshop, Edinburgh.
- Marcello, J., F. Eugenio, U. Perdomo, and A. Medina. 2016. Assessment of Atmospheric Algorithms to Retrieve Vegetation in Natural Protected Areas Using Multispectral High Resolution Imagery. *Sensors* 16:1624.
- Marsetič, A., K. Oštir, and M. K. Fras. 2015. Automatic orthorectification of high-resolution optical satellite images using vector roads. *IEEE Transactions on Geoscience and Remote Sensing* 53:6035-6047.
- Martin, J., F. Eugenio, J. Marcello, A. Medina, J. A. Bermejo, and M. Arbelo. 2012. Atmospheric correction models for high resolution WorldView-2 multispectral imagery: a case study in Canary Islands, Spain. Pages 853400-853400-85310 *in* SPIE Remote Sensing. International Society for Optics and Photonics.
- Mascarenhas, N. D. A., G. J. F. Banon, and A. L. B. Candeias. 1996. Multispectral image data fusion under a Bayesian approach. *International Journal of Remote Sensing* 17:1457-1471.
- McGlone, J. 2004. *Manual of Photogrammetry Fifth Edition*, the American Society for Photogrammetry and Remote Sensing.

- Medina, A., J. Marcello, D. Rodriguez, F. Eugenio, and J. Martín. 2012. Quality evaluation of pansharpening techniques on different land cover types. Pages 5442-5445 *in* Geoscience and Remote Sensing Symposium (IGARSS). IEEE International. IEEE.
- Michel, R., and J. P. Avouac. 2002. Deformation due to the 17 August 1999 Izmit, Turkey, earthquake measured from SPOT images. *Journal of Geophysical Research: Solid Earth* 107:ETG 2-1-ETG 2-6.
- Mücher, C. A., L. Kooistra, M. Vermeulen, J. V. Borre, B. Haest, and R. Haveman. 2013. Quantifying structure of Natura 2000 heathland habitats using spectral mixture analysis and segmentation techniques on hyperspectral imagery. *Ecological Indicators* 33:71-81.
- Mutanga, O., E. Adam, and M. A. Cho. 2012. High density biomass estimation for wetland vegetation using WorldView-2 imagery and random forest regression algorithm. *International Journal of Applied Earth Observation and Geoinformation* 18:399-406.
- Neubert, M., and G. Meinel. 2005. Atmospheric and terrain correction of IKONOS imagery using ATCOR3. *in* Proc. ISPRS Hanover Workshop.
- Nikolakopoulos, K., and D. Oikonomidis. 2015. Quality assessment of ten fusion techniques applied on Worldview-2. *European Journal of Remote Sensing* 48:141-167.
- Oruc, M., A. Marangoz, and G. Buyuksalih. 2004. Comparison of pixel-based and object-oriented classification approaches using Landsat-7 ETM spectral bands. Page 5 *in* Proceedings of XX ISPRS Congress.
- Ozdemir, I., and A. Karnieli. 2011. Predicting forest structural parameters using the image texture derived from WorldView-2 multispectral imagery in a dryland forest, Israel. *International Journal of Applied Earth Observation and Geoinformation* 13:701-710.
- Padwick, C., M. Deskevich, F. Pacifici, and S. Smallwood. 2010. WorldView-2 pansharpening. *in* American Society for Photogrammetry and Remote Sensing.
- Pal, M., and P. M. Mather. 2004. Assessment of the effectiveness of support vector machines for hyperspectral data. *Future Generation Computer Systems* 20:1215-1225.
- Palubinskas, G. 2013. Fast, simple, and good pan-sharpening method. *Journal of Applied Remote Sensing* 7:073526-073526.
- Palubinskas, G., and P. Reinartz. 2011. Multi-resolution, multi-sensor image fusion: general fusion framework. Pages 313-316 *in* IEEE Urban Remote Sensing Event (JURSE), 2011 Joint.
- Park, J. H., and M. G. Kang. 2004. Spatially adaptive multi-resolution multispectral image fusion. *International Journal of Remote Sensing* 25:5491-5508.
- Peña-Barragán, J. M., M. K. Ngugi, R. E. Plant, and J. Six. 2011. Object-based crop identification using multiple vegetation indices, textural features and crop phenology. *Remote Sensing of Environment* 115:1301-1316.

- Pérez-Chacón-Espino, E., A. Hernández-Calvento, P. Máyer-Suárez, L. Romero-Martín, I. Alonso-Bilbao, J. Mangas-Viñuelo, I. Menéndez-Gonzales, I. Sánchez-Pérez, J. Ojeda-Zújar, R. Ruiz-Flaño, and J. Alcántara-Carrió. 2007. *Maspalomas: Claves Científicas para el Análisis de su Problemática Ambiental*. Universidad Las Palmas de Gran Canaria.
- Pohl, C. 2014. Challenges of Remote Sensing Image Fusion to Optimize Earth Observation Data Exploitation. *European Scientific Journal* 9:355-365.
- Pohl, C., and J. van Genderen. 2015. Structuring contemporary remote sensing image fusion. *International Journal of Image and Data Fusion* 6:3-21.
- Pons, X., L. Pesquer, J. Cristóbal, and O. González-Guerrero. 2014. Automatic and improved radiometric correction of Landsat imagery using reference values from MODIS surface reflectance images. *International Journal of Applied Earth Observation and Geoinformation* 33:243-254.
- Price, J. C. 1987. Combining panchromatic and multispectral imagery from dual resolution satellite instruments. *Remote Sensing of Environment* 21:119-128.
- Quevedo-Medina, U., and L. Hernández-Calvento. 2014. Evolución reciente de la línea de costa en un sistema playa-dunas deficitario (Maspalomas, Gran Canaria). *in XVI Congreso Nacional de Tecnologías de Información Geográfica*.
- Ren, J., J. Zabalza, S. Marshall, and J. Zheng. 2014. Effective feature extraction and data reduction in remote sensing using hyperspectral imaging [applications corner]. *IEEE Signal Processing Magazine* 31:149-154.
- Richards, J. A. 1999. *Remote sensing digital image analysis*. Springer.
- Richter, R. 1996. Atmospheric correction of DAIS hyperspectral image data. Pages 390-400 *in Algorithms for Multispectral and Hyperspectral Imagery II*. International Society for Optics and Photonics.
- Richter, R. 1998. Correction of satellite imagery over mountainous terrain. *Applied optics* 37:4004-4015.
- Richter, R. 2008. Classification metrics for improved atmospheric correction of multispectral VNIR imagery. *Sensors* 8:6999-7011.
- Richter, R., and D. Schläpfer. 2002. Geo-atmospheric processing of airborne imaging spectrometry data. Part 2: atmospheric/topographic correction. *International Journal of Remote Sensing* 23:2631-2649.
- Rodríguez-Esparragón, D. 2015. Evaluación y desarrollo de métricas de calidad espacial y espectral para aplicaciones de fusión de imágenes multiespectrales de teledetección de alta resolución. Universidad Las Palmas de Gran Canaria.
- Rodríguez-Esparragón, D., J. Marcello-Ruiz, A. Medina-Machín, F. Eugenio-González, C. Gonzalo-Martín, and A. García-Pedrero. 2014. Evaluation of the performance of the spatial assessment of pansharpened images. *IGARS. IEEE*:4.

- Schmidt, M., R. Lucas, P. Bunting, J. Verbesselt, and J. Armston. 2015. Multi-resolution time series imagery for forest disturbance and regrowth monitoring in Queensland, Australia. *Remote Sensing of Environment* 158:156-168.
- Schowengerdt, R. A. 1980. Reconstruction of multispatial, multispectral image data using spatial frequency content. *Photogramm. Eng. Remote Sens.* 46:13525-11334.
- Sexton, J. O., P. Noojipady, A. Anand, X.-P. Song, S. McMahon, C. Huang, M. Feng, S. Channan, and J. R. Townshend. 2015. A model for the propagation of uncertainty from continuous estimates of tree cover to categorical forest cover and change. *Remote Sensing of Environment* 156:418-425.
- Shao, Y., and R. S. Lunetta. 2012. Comparison of support vector machine, neural network, and CART algorithms for the land-cover classification using limited training data points. *ISPRS Journal of Photogrammetry and Remote Sensing* 70:78-87.
- Sidiropoulos, P., J.-P. Muller, G. Watson, G. Michael, and S. Walter. 2018. Automatic Coregistration and orthorectification (ACRO) and subsequent mosaicing of NASA high-resolution imagery over the Mars MC11 quadrangle, using HRSC as a baseline. *Planetary and Space Science* 151:33-42.
- Singh, A. 1989. Review article digital change detection techniques using remotely-sensed data. *International Journal of Remote Sensing* 10:989-1003.
- Somers, B., G. P. Asner, L. Tits, and P. Coppin. 2011. Endmember variability in spectral mixture analysis: A review. *Remote Sensing of Environment* 115:1603-1616.
- Song, C. 2005. Spectral mixture analysis for subpixel vegetation fractions in the urban environment: How to incorporate endmember variability? *Remote Sensing of Environment* 95:248-263.
- Staben, G. W., K. Pfitzner, R. Bartolo, and A. Lucieer. 2012. Empirical line calibration of WorldView-2 satellite imagery to reflectance data: Using quadratic prediction equations. *Remote sensing letters* 3:521-530.
- Strasser, T., S. Lang, B. Riedler, L. Pernkopf, and K. Paccagnel. 2014. Multiscale object feature library for habitat quality monitoring in riparian forests. *IEEE Geoscience and Remote Sensing Letters* 11:559-563.
- Tanré, D., M. Herman, P. Deschamps, and A. De Lefte. 1979. Atmospheric modeling for space measurements of ground reflectances, including bidirectional properties. *Applied optics* 18:3587-3594.
- Thenkabail, P. S., R. B. Smith, and E. De Pauw. 1999. Hyperspectral vegetation indices for determining agricultural crop characteristics. Yale University, Center for Earth Observation.
- Thouvenin, P.-A., N. Dobigeon, and J.-Y. Tourneret. 2016. Hyperspectral unmixing with spectral variability using a perturbed linear mixing model. *IEEE Transactions on Signal Processing* 64:525-538.
- Toutin, T. 2004. Geometric processing of remote sensing images: models, algorithms and methods. *International Journal of Remote Sensing* 25:1893-1924.




- Tu, T. M., S. C. Su, H. C. Shyu, and P. S. Huang. 2001. A new look at IHS-like image fusion methods. *Information fusion* 2:177-186.
- Tuia, D., M. Volpi, L. Copa, M. Kanevski, and J. Muñoz-Marí. 2011. A survey of active learning algorithms for supervised remote sensing image classification. *IEEE Journal of Selected Topics in Signal Processing* 5:606-617.
- Turner, W., S. Spector, N. Gardiner, M. Fladeland, E. Sterling, and M. Steininger. 2003. Remote sensing for biodiversity science and conservation. *Trends in ecology & evolution* 18:306-314.
- University, H. S. 2017. Introduction to Remote Sensing Course. Humboldt State University, GSP 2016, [http://gsp.humboldt.edu/OLM/Courses/GSP\\_216\\_Online/lesson4-1/radiometric.html](http://gsp.humboldt.edu/OLM/Courses/GSP_216_Online/lesson4-1/radiometric.html).
- Ustin, S. L., D. A. Roberts, J. A. Gamon, G. P. Asner, and R. O. Green. 2004. Using imaging spectroscopy to study ecosystem processes and properties. *AIBS Bulletin* 54:523-534.
- Van der Meer, F., and S. De Jong. 2000. Improving the results of spectral unmixing of Landsat Thematic Mapper imagery by enhancing the orthogonality of end-members. *International Journal of Remote Sensing* 21:2781-2797.
- Van Puymbroeck, N., R. Michel, R. Binet, J.-P. Avouac, and J. Taboury. 2000. Measuring earthquakes from optical satellite images. *Applied optics* 39:3486-3494.
- Vaudour, E., J. Moeys, J.-M. Gilliot, and Y. Coquet. 2008. Spatial retrieval of soil reflectance from SPOT multispectral data using the empirical line method. *International Journal of Remote Sensing* 29:5571-5584.
- Veganzones, M. A., L. Drumetz, G. Tochon, M. Dalla Mura, A. Plaza, J. M. Bioucas-Dias, and J. Chanussot. 2014. A new extended linear mixing model to address spectral variability. *in IEEE Workshop on Hyperspectral Image and Signal Processing: Evolution in Remote Sensing (WHISPERS 2014)*.
- Vermote, E. F., D. Tanré, J. L. Deuze, M. Herman, and J. J. Morcette. 1997. Second simulation of the satellite signal in the solar spectrum, 6S: An overview. *IEEE transactions on geoscience and remote sensing* 35:675-686.
- Villa, A., J. Chanussot, C. Jutten, J. A. Benediktsson, and S. Moussaoui. 2009. On the use of ICA for hyperspectral image analysis. Pages IV-97-IV-100 *in Geoscience and Remote Sensing Symposium, 2009 IEEE International, IGARSS 2009*. IEEE.
- Vincent, P., H. Larochelle, I. Lajoie, Y. Bengio, and P.-A. Manzagol. 2010. Stacked denoising autoencoders: Learning useful representations in a deep network with a local denoising criterion. *Journal of machine learning research* 11:3371-3408.
- Vivone, G., L. Alparone, J. Chanussot, M. Dalla Mura, A. Garzelli, G. Licciardi, R. Restaino, and L. Wald. 2015. A Critical Comparison Among Pansharpening Algorithms. *IEEE Transactions on Geoscience and Remote Sensing* 53:2565-2586.

- Wald, L. 2000. Quality of high resolution synthesised images: Is there a simple criterion? Pages 99-103 in "Third conference" Fusion of Earth data: merging point measurements, raster maps and remotely sensed images". SEE/URISCA.
- Wald, L., T. Ranchin, and M. Mangolini. 1997. Fusion of satellite images of different spatial resolutions: assessing the quality of resulting images. *Photogrammetric engineering and remote sensing* 63:691-699.
- Wang, J., and C.-I. Chang. 2006. Independent component analysis-based dimensionality reduction with applications in hyperspectral image analysis. *IEEE Transactions on Geoscience and Remote Sensing* 44:1586-1600.
- Wang, K., S. E. Franklin, X. Guo, and M. Cattet. 2010. Remote sensing of ecology, biodiversity and conservation: a review from the perspective of remote sensing specialists. *Sensors* 10:9647-9667.
- Wang, Q., and J. D. Tenhunen. 2004. Vegetation mapping with multitemporal NDVI in North Eastern China transect (NECT). *International Journal of Applied Earth Observation and Geoinformation* 6:17-31.
- Wang, Z., and A. C. Bovik. 2002. A universal image quality index. *IEEE Signal Letter* 9:4.
- Wanner, W., X. Li, and A. Strahler. 1995. On the derivation of kernels for kernel-driven models of bidirectional reflectance. *Journal of Geophysical Research: Atmospheres* 100:21077-21089.
- Watmough, G. R., P. M. Atkinson, and C. W. Hutton. 2011. A combined spectral and object-based approach to transparent cloud removal in an operational setting for Landsat ETM+. *International Journal of Applied Earth Observation and Geoinformation* 13:220-227.
- Wei, Q., N. Dobigeon, and J.-Y. Tournet. 2015. Bayesian fusion of multi-band images. *IEEE Journal of Selected Topics in Signal Processing* 9:1117-1127.
- Wen, Y. 2011. Data application of multi-temporal and multi-source data for land cover change detection in Guam, USA. Pages 1-4 in *Geoinformatics, 2011 19th International Conference on*. IEEE.
- Wildpret de la Torre, W. 2001. Consideraciones sobre la fitobiodiversidad de las cañadas del Teide. Curso de acreditación de conocimientos para ejercer de guía en el Parque Nacional del Teide. Departamento de Biología Vegetal, Universidad de La Laguna.
- Wu, C., and A. T. Murray. 2003. Estimating impervious surface distribution by spectral mixture analysis. *Remote Sensing of Environment* 84:493-505.
- Wu, J., D. Wang, and M. E. Bauer. 2005. Image-based atmospheric correction of QuickBird imagery of Minnesota cropland. *Remote Sensing of Environment* 99:315-325.
- Wu, Y., W. Ma, M. Gong, L. Su, and L. Jiao. 2015. A Novel Point-Matching Algorithm Based on Fast Sample Consensus for Image Registration. *IEEE Geosci. Remote Sensing Lett.* 12:43-47.


- Xie, Y., Z. Sha, and M. Yu. 2008. Remote sensing imagery in vegetation mapping: a review. *Journal of plant ecology* 1:9-23.
- Xu, M., C. Cao, H. Zhang, Y. Xue, Y. Li, J. Guo, C. Chang, Q. He, M. Gao, and X. Li. 2009. Change detection of the Tangjiashan barrier lake based on multi-source remote sensing data. Pages IV-303-IV-306 in *Geoscience and Remote Sensing Symposium, 2009 IEEE International, IGARSS 2009*. Ieee.
- Yang, J., D. Zhang, A. F. Frangi, and J.-y. Yang. 2004. Two-dimensional PCA: a new approach to appearance-based face representation and recognition. *IEEE Transactions on Pattern Analysis and Machine Intelligence* 26:131-137.
- Yokoya, N., C. Grohnfeldt, and J. Chanussot. 2017. Hyperspectral and multispectral data fusion: A comparative review of the recent literature. *IEEE Geoscience and remote sensing magazine* 5:29-56.
- Yokoya, N., T. Yairi, and A. Iwasaki. 2012. Coupled nonnegative matrix factorization unmixing for hyperspectral and multispectral data fusion. *IEEE Transactions on Geoscience and Remote Sensing* 50:528-537.
- Yu, J., D. Chen, Y. Lin, and S. Ye. 2017. Comparison of linear and nonlinear spectral unmixing approaches: a case study with multispectral TM imagery. *International Journal of Remote Sensing* 38:773-795.
- Zarco-Tejada, P. J., M. González-Dugo, and E. Fereres. 2016. Seasonal stability of chlorophyll fluorescence quantified from airborne hyperspectral imagery as an indicator of net photosynthesis in the context of precision agriculture. *Remote Sensing of Environment* 179:89-103.
- Zare, A., and K. Ho. 2014. Endmember variability in hyperspectral analysis: Addressing spectral variability during spectral unmixing. *IEEE Signal Processing Magazine* 31:95-104.
- Zhan, T., M. Gong, J. Liu, and P. Zhang. 2018. Iterative feature mapping network for detecting multiple changes in multi-source remote sensing images. *ISPRS Journal of Photogrammetry and Remote Sensing* 146:38-51.
- Zhang, H., R. Pu, and X. Liu. 2016a. A new image processing procedure integrating PCI-RPC and ArcGIS-Spline tools to improve the orthorectification accuracy of high-resolution satellite imagery. *Remote Sensing* 8:827.
- Zhang, J. 2010. Multi-source remote sensing data fusion: status and trends. *International Journal of Image and Data Fusion* 1:5-24.
- Zhang, L., L. Zhang, and B. Du. 2016b. Deep learning for remote sensing data: A technical tutorial on the state of the art. *IEEE Geoscience and remote sensing magazine* 4:22-40.
- Zhang, X., Y. Jia, X. Chen, D. Pan, J. Chen, and Z. Hao. 2011. Application of modulation transfer function in high-resolution image fusion. Pages 818005-818005-818008 in *SPIE Remote Sensing*. International Society for Optics and Photonics.

- Zhao, W., Z. Guo, J. Yue, X. Zhang, and L. Luo. 2015. On combining multiscale deep learning features for the classification of hyperspectral remote sensing imagery. *International Journal of Remote Sensing* 36:3368-3379.
- Zhou, J., D. Civco, and J. Silander. 1998. A wavelet transform method to merge Landsat TM and SPOT panchromatic data. *International Journal of Remote Sensing* 19:743-757.
- Zou, Q., L. Ni, T. Zhang, and Q. Wang. 2015. Deep Learning Based Feature Selection for Remote Sensing Scene Classification. *IEEE Geosci. Remote Sensing Lett.* 12:2321-2325.





CHAPTER 3. FUSION OF  
HIGH RESOLUTION  
MULTISPECTRAL IMAGERY  
IN VULNERABLE COASTAL  
AND LAND ECOSYSTEMS





This chapter includes the following published article: E. Ibarrola-Ulzurrun, C. Gonzalo-Martín, J. Marcello-Ruiz, García-Pedrero, A., Rodríguez-Esparragón, D. *Fusion of High Resolution Multispectral images in vulnerable coastal and land ecosystems*. *Sensors* 2017, 17(2), pp. 228.

This work addresses an important pre-processing methodology applied to the high resolution WV-2 multispectral imagery. The article analyses and evaluates different pansharpener techniques in three different types of ecosystems: land, mixed and coastal ecosystems to allow the study be applicable to other ecosystems around the Earth. Specifically, the ecosystems belong to three protected areas of Canary Islands (Spain): Teide National Park, Maspalomas Natural Reserve and, Corralejo and Islote de Lobos Natural Parks, already described in Chapter 2.

The paper, basically, performs a preliminary evaluation of twelve classic and novel pansharpener algorithms applied to an 8-band MS sensor and then, a total of four algorithms were used in the final study. The main objective of the paper was to select the most suitable pansharpener algorithm which provides a fused image with the best trade-off between spatial and spectral quality in different real ecosystems. The comprehensive evaluation was implemented, not only for the whole set of MS bands, but also in the spectral channels located inside and outside the range of the PAN band using six quality indices. In addition, analysis of quality maps was performed to evaluate the fusion results in each band at local level. It was concluded that coastal ecosystems require simpler algorithms, i.e. FIHS, while more complex areas as, Teide National Park and Maspalomas Natural Reserve, need advanced algorithms i.e. WAT $\otimes$ FRAC. The most suitable pansharpener technique for each study area was identified and applied. Therefore it was possible to obtain high spatial resolution products.

The main contributions of this paper are:

- A novel analysis was applied using VHR imagery in shallow water areas, as pansharpener could be useful for the mapping of seabed species, such as seagrasses and coral reefs.
- The best fused image using an eight-band sensor (WorldView-2) was obtained in the study, instead of considering a four-band sensor, as usually in the literature.
- A user's guide is provided to choose the most suitable algorithm in accordance with the ecosystem type and the information to be preserved.
- An analysis of the behavior of each algorithm when applied to the complete set of MS bands and on bands covered by and outside of the PAN range was performed.
- A local study was carried out to identify the distortion introduced in each single band by the best fused algorithms chosen for each ecosystem type.



- The use of heterogenic regions with sparse vegetation mainly made up of small and mixed shrubs and with low radiance absorption in complex and dynamic coastal ecosystems. Hence, the analysis was not performed in urban and homogeneous land areas, as other studies.

Article

# Fusion of High Resolution Multispectral Imagery in Vulnerable Coastal and Land Ecosystems

Edurne Ibarrola-Ulzurrun <sup>1,2,\*</sup>, Consuelo Gonzalo-Martin <sup>2</sup>, Javier Marcello-Ruiz <sup>1</sup>, Angel Garcia-Pedrero <sup>2</sup> and Dionisio Rodriguez-Esparragon <sup>1</sup>

<sup>1</sup> Instituto de Oceanografía y Cambio Global, IOCAG, Universidad Las Palmas de Gran Canaria (ULPGC), Parque Científico Tecnológico Marino de Taliarte, 35214 Telde, Spain; javier.marcello@ulpgc.es (J.M.-R.); dionisio.rodriguez@ulpgc.es (D.R.-E.)

<sup>2</sup> Centro de Tecnología Biomédica, Universidad Politécnica de Madrid (UPM), Campus de Montegancedo, 28223 Pozuelo de Alarcón, Spain; chelo@fi.upm.es (C.G.-M.); am.garcia@alumnos.upm.es (A.G.-P.)

\* Correspondence: edurne.ibarrola101@alu.ulpgc.es; Tel.: +34-928-457-365

Academic Editor: Alistair M. S. Smith

Received: 4 October 2016; Accepted: 17 January 2017; Published: 25 January 2017

**Abstract:** Ecosystems provide a wide variety of useful resources that enhance human welfare, but these resources are declining due to climate change and anthropogenic pressure. In this work, three vulnerable ecosystems, including shrublands, coastal areas with dunes systems and areas of shallow water, are studied. As far as these resources' reduction is concerned, remote sensing and image processing techniques could contribute to the management of these natural resources in a practical and cost-effective way, although some improvements are needed for obtaining a higher quality of the information available. An important quality improvement is the fusion at the pixel level. Hence, the objective of this work is to assess which pansharpening technique provides the best fused image for the different types of ecosystems. After a preliminary evaluation of twelve classic and novel fusion algorithms, a total of four pansharpening algorithms was analyzed using six quality indices. The quality assessment was implemented not only for the whole set of multispectral bands, but also for the subset of spectral bands covered by the wavelength range of the panchromatic image and outside of it. A better quality result is observed in the fused image using only the bands covered by the panchromatic band range. It is important to highlight the use of these techniques not only in land and urban areas, but a novel analysis in areas of shallow water ecosystems. Although the algorithms do not show a high difference in land and coastal areas, coastal ecosystems require simpler algorithms, such as fast intensity hue saturation, whereas more heterogeneous ecosystems need advanced algorithms, as weighted wavelet 'à trous' through fractal dimension maps for shrublands and mixed ecosystems. Moreover, quality map analysis was carried out in order to study the fusion result in each band at the local level. Finally, to demonstrate the performance of these pansharpening techniques, advanced Object-Based (OBIA) support vector machine classification was applied, and a thematic map for the shrubland ecosystem was obtained, which corroborates wavelet 'à trous' through fractal dimension maps as the best fusion algorithm for this ecosystem.

**Keywords:** pansharpening; high resolution satellite images; WorldView-2; ecosystem management; classification

## 1. Introduction

Natural ecosystems provide a wide variety of useful resources that enhance human welfare. However, in recent decades, there has been a decline in these ecosystem services, as well as their biodiversity [1]. In particular, coastal ecosystems are the most complex, dynamic and productive systems in the world [2]. This creates a demand to preserve environmental resources; hence, it is of

great importance to develop reliable methodologies, applied to new high resolution satellite imagery. Thus, the analysis, conservation and management of these environments could be studied, in a continuous, reliable and economic way, and at the suitable spatial, spectral and temporal resolution. However, some processing tasks need to be improved; for instance, the weaknesses in the classification and analysis of land and coastal ecosystems on the basis of remote sensing data, as well as the lack of reliability of the maps; particularly, the extreme difficulty to monitor the coastal ecosystems from remote sensing imagery due to the low reflectivity of these areas covered by water.

The framework in which the study has been developed is the analysis of both coastal and land ecosystems through very high resolution (VHR) remote sensing imagery in order to obtain high quality products that will allow the comprehensive analysis of natural resources. In this context, remote sensing imagery offers practical and cost-effective means for a good environmental management, especially when large areas have to be monitored [3] or periodic information is needed. Most VHR optical sensors provide a multispectral image (MS) and a panchromatic image (PAN), which require a number of corrections and enhancements. Image fusion or pansharpening algorithms are important for improving the spatial quality of information available. The pansharpening data fusion technique could be defined as the process of merging MS and PAN images to create new multispectral images with a high spatial resolution [4,5]. This fusion stage is important in the analysis of such vulnerable ecosystems, mainly characterized by heterogeneous and mixed vegetation shrubs, with small shrubs in the case of terrestrial ecosystems and the complexity of seagrass meadows or algae distribution in shallow water ecosystems.

Image fusion techniques combine sensor data from different sources with the aim of providing more detailed and reliable information. The extensive research into image fusion techniques in remote sensing started in the 1980s [6,7]. Generally, image fusion can be categorized into three levels: pixel level, feature level and knowledge or decision level [8,9], and pansharpening is performed at the pixel level.

Many pansharpening techniques have appeared in recent decades, as a consequence of the launch of very high resolution sensors [10–14]. An ideal pansharpening algorithm should have two main attributes: (i) enhancing high spatial resolution; and (ii) reducing spectral distortion [15]. The simplest pansharpening methods, at the conceptual and computational level, are intensity-hue-saturation (IHS), principal component analysis (PCA) and Brovey transforms (BT). However, these techniques have problems because the radiometry on the spectral channels is distorted after fusion. New approaches, such as wavelet transformations and high pass filtering (HPF) [4,8,16–18], have been proposed to address particular problems with the traditional techniques.

On the other hand, quality evaluation is a fundamental issue to benchmark and optimize different pansharpening algorithms [18,19], as there is the necessity to assess the spectral and spatial quality of the fused images. There are two types of evaluation approaches commonly used: (1) qualitative analysis (visual assessment); and (2) quantitative analysis (quality indices). Visual analysis is a powerful tool for capturing the geometrical aspect [20] and the main color disturbances. According to [10], some visual parameters are necessary for testing the properties of the image, such as the spectral preservation of features, multispectral synthesis in fused images and the synthesis of images close to actual images at high resolution. On the other hand, quality indices measure the spectral and the spatial distortion produced due to the pansharpening process by comparing each fused image to the reference MS or PAN image. The work in [21] categorized them into three main groups: (i) spectral quality indices such as the spectral angle mapper (SAM) [22] and the spectral relative dimensionless global error, in French '*erreur relative globale adimensionnelle de synthèse*' (ERGAS) [23]; (ii) spatial quality indices, i.e., the spatial ERGAS [24], the frequency comparison index (FC) [25] and the Zhou index [26]; and (iii) global quality indices, such as the 8-band image quality index (Q8) [27]. On the other hand, there are several evaluation techniques with no reference requirement, such as the quality with no reference (QNR) approach [28].

In this study, the main goal is to assess which pansharpener technique, using Worldview-2 VHR imagery with eight MS bands, provides a better fused image. Future research will be focused on the classification of the vulnerable ecosystems, in order to obtain specific products for the management of coastal and land resources, in contrast to several studies assessing and reviewing pansharpener techniques [11,16,20,29–34]. Further specific goals in this paper are: (i) the study of the spatial and spectral quality of pansharpener bands covered by and outside the PAN wavelength range; (ii) analysis of pansharpener algorithms' behavior in vulnerable natural ecosystems, unlike the majority of previous studies, which apply the pansharpener techniques in urban areas or on other land cover types; and (iii) novel assessment in VHR image fusion in shallow coastal waters, whilst being aware of the pansharpener difficulty of these ecosystems. Although other authors apply fusion in water areas, such as [35,36], they use Landsat imagery, not VHR imagery. The aim of the last point is to identify which techniques were more suitable for shallow water areas and the improvement achieved. This information can lead to obtaining more accurate seafloor segmentation or mapping of coastal zones [37]; hence, studies on the state of conservation of natural resources could be conducted.

Finally, in order to strengthen the study, a final thematic map of the shrubland area was carried out. Thus, it will analyze the influence of the fusion on the classification results which serve to obtain accurate information for the conservation of natural resources. This study can be found in more detail in [38].

The paper is structured as follows: Section 2 includes the description of the study area, datasets, the image fusion methods used in the analysis and the evaluation methodology. The visual and quantitative evaluation of the different algorithms, as well as map analysis are presented in Section 3. Finally, Section 4 summarizes the main outcomes and contributions.

## 2. Materials and Methods

### 2.1. Study Area

This study focuses on three types of vulnerable ecosystems found in different islands of the Macaronesia region. Macaronesia is considered a geological and a biodiversity hotspot due to the volcanic origin and due to the high degree of vulnerability that insular ecosystems are subjected to, mainly as a consequence of climate change and anthropogenic pressure. The ecosystems selected from the Canary Islands were: the shrubland ecosystem, the coastal ecosystem and, finally, a mixed ecosystem surrounded by a touristic area and a lagoon, as a transitional system within the coastal and land ecosystems. The Canary Islands are one of the most remarkable biodiversity areas on the planet [39], and they are chosen as a representative sample of these ecosystems because of the availability of VHR remote sensing imagery and simultaneous field data. Figure 1 displays the 3 protected areas considered in the analysis.

As regards shrubland ecosystems, it is important to highlight the large concentration of vascular plants, which are highly vulnerable to environmental changes. In coastal areas, an intensive natural fragility also appears due to the interaction of a great variety of environmental factors. Moreover, the coastal occupation of urban areas and the development of tourism increase this fragility and vulnerability. In particular, dune systems are affected by this urban-touristic expansion [40–43]. Furthermore, many coastal ecosystems contain seagrass meadows [44]. The importance of these particular meadows is related to the ocean productivity as they are one of the most valuable ecosystems in the world. In addition, these meadows are part of the solution to climate change, not only producing oxygen, but storing up to twice as much carbon per unit area as the world's temperate and tropical forests [45]. As indicated, three sensible and heterogenic protected areas of the Canary Islands have been selected (Figure 1) as representative examples of more general ecosystems: the Teide National Park (Tenerife Island), as an example of shrubland ecosystems, the Corralejo Natural Park and Isote de Lobos (Fuerteventura), representing coastal ecosystems, and the Maspalomas Natural Reserve (Gran Canaria Island), an important coastal-dune ecosystem with significant tourism pressure, called the mixed ecosystem in this paper, not only because it is the transitional region within the coastal and land ecosystem, but also due to the inner water ecosystem, known as the Maspalomas lagoon.

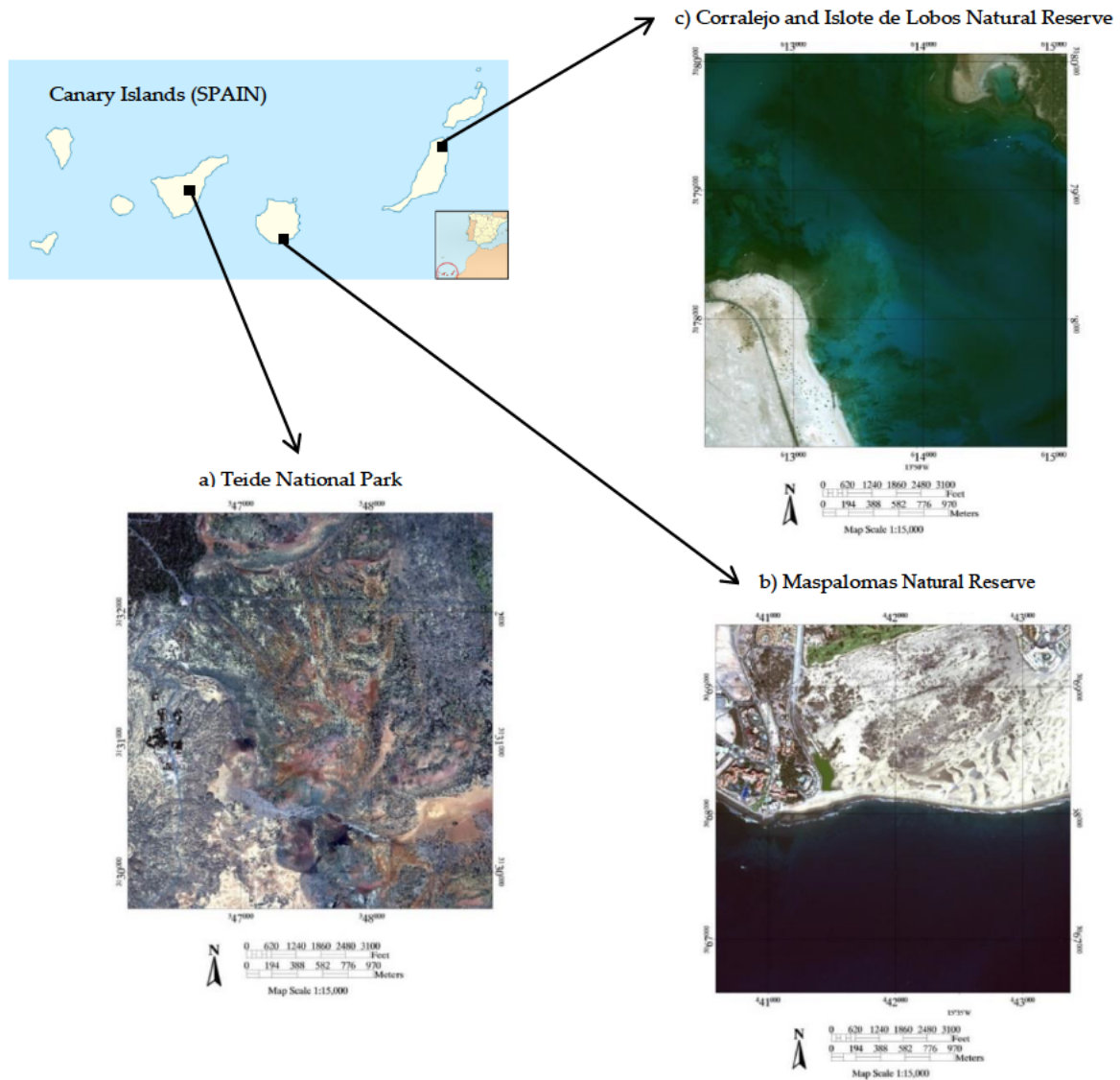


**Figure 1.** Study areas from the Canary Islands: (a) Teide National Park; (b) Corralejo and Isote de Lobos Natural Park; and (c) Maspalomas Natural Reserve.

Other similar shrubland ecosystems can be identified around the world, for example: Pico do Pico in the Azores, Mt. Halla in South Korea and Hawaii or the Galapagos. Corralejo and Maspalomas are important coastal sand dune systems in Europe, as they contain a large degree of biodiversity [46]. The importance of studying these ecosystems is their similarity with other Mediterranean, temperate or tropical parts of the world: Tuscany (Italy), Doñana National Park (Spain), as well as other parts of the world, such as Parangtritis (Java, Indonesia), Malaysia, Philippines, Vietnam, NE Queensland, the tropical coast of Brazil, the West African coast, Cuba, the Galapagos islands, the West Indies, Cox's Bazaar (Bangladesh), Hawaii, Ghana, the coast of India or Christmas Island [47].

## 2.2. Datasets

The WorldView-2 (WV-2) satellite, launched by Digital Globe on 8 October 2009, was the first commercial satellite to provide a VHR sensor with one PAN and eight MS bands (Table 1). WV-2 ortho-ready imagery of the three representative ecosystems were used in the study. Images of the Canary Islands and the central locations of the corresponding three study areas are detailed in Table 2. In order to reduce the computation times in the multiple analyses,  $512 \times 512$  MS pixel scenes were used. Figure 2 displays the PAN band and the corresponding resized MS image (RGB composite). They were selected for their spectral and spatial richness and the content of land and coastal areas. In addition, the scenes include different coverages, basically predominating coastal areas, shallow waters, vegetation and urban regions, and they contain features with different shapes and edges.

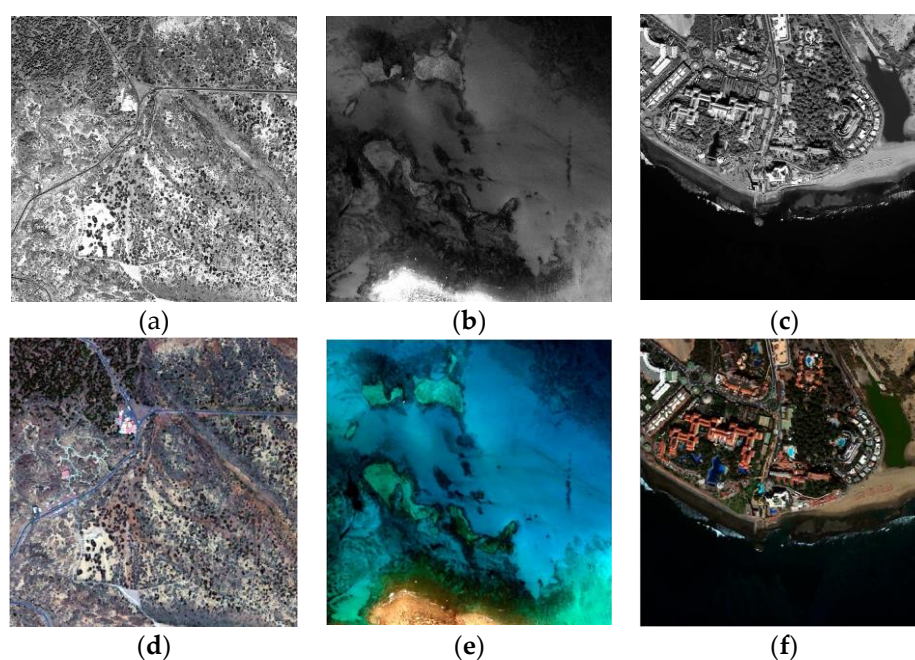


**Figure 2.** PAN and MS scenes of WorldView-2 images ( $512 \times 512$  pixels for the MS image): (a, d) shrub land ecosystem; (b, e) coastal ecosystem; (c, f) mixed ecosystem with urban area and inner water lagoon.

**Table 1.** WorldView-2 sensor technical specifications.

Imaging Mode	Panchromatic	Multispectral
Spatial Resolution	0.46 meter	1.84 meters
Spectral Range	450–800 nm	400–450 nm (coastal) 450–510 nm (blue) 510–580 nm (green) 585–625 nm (yellow) 630–690 nm (red) 705–745 nm (red edge) 770–895 nm (near IR-1) 860–1040 nm (near IR-2)

**Table 2.** Location and acquisition date of the three images selected from the Canary Islands.

Worldview-2 Image	Coordinates	Acquisition Date
Teide National Park	28° 18'16" N, 16° 33'50" W	16 May 2011
Maspalomas Natural Reserve	27° 44'12" N, 15° 35'52" W	17 January 2013
Corralejo and Isote de Lobos Natural Park	28° 43'52" N, 13° 50'37" W	28 October 2010

2.3. Image Fusion Methodology

In the flow shown in Figure 3, every step of the methodology for assessing which algorithm gives the best fused image for each area is presented.

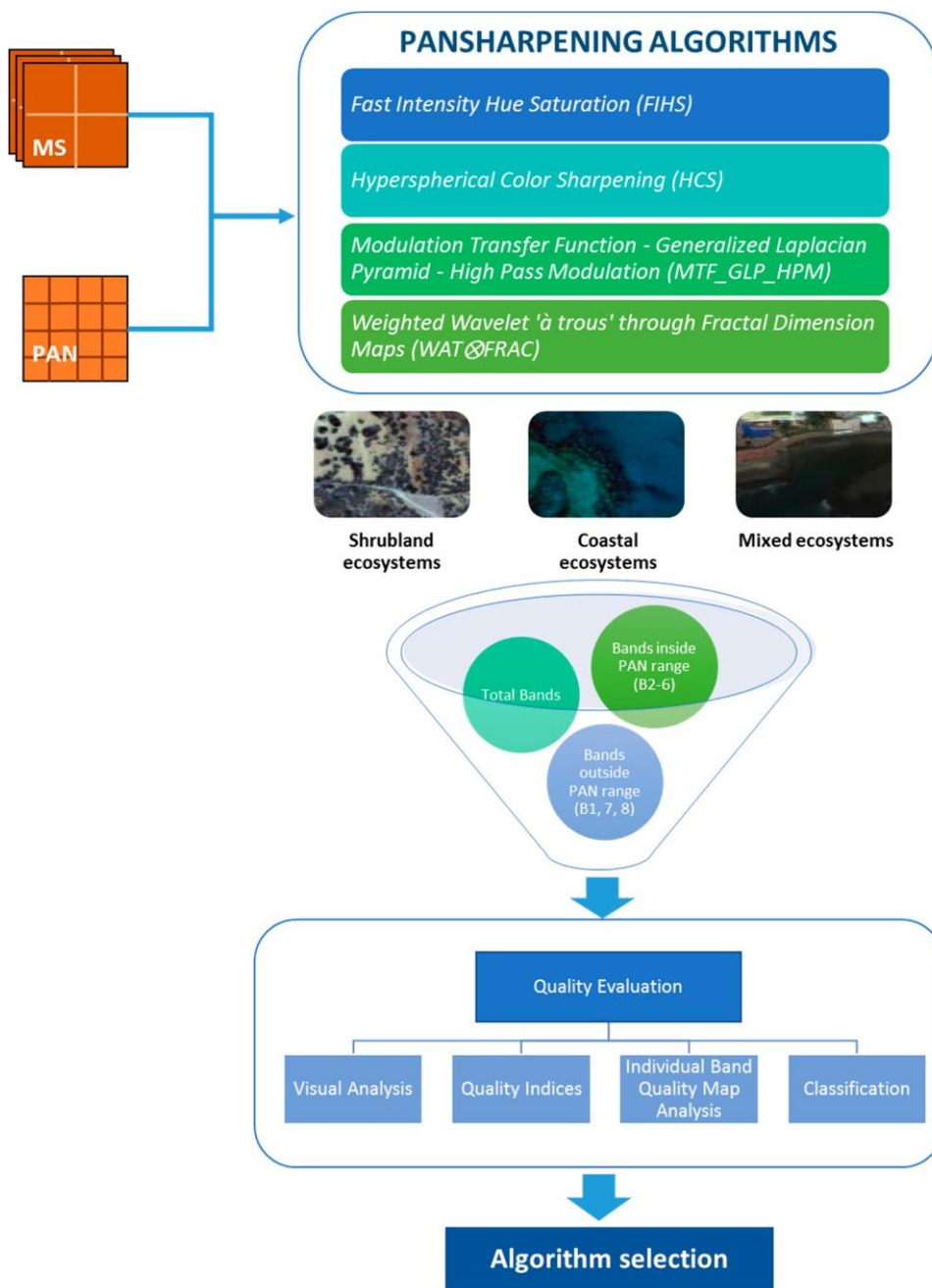


**Figure 3.** The flow diagram followed in the study for each scenario.

The first four pansharpening techniques were implemented in the three different vulnerable ecosystems; afterwards, a visual and quantitative assessment was undertaken in order to evaluate the pansharpening results in the different fused images. The quality assessment was carried out for the whole set of MS bands, as well as for those MS bands covering the range of the PAN channel (Bands 2–6) and those outside this range (Bands 1, 7 and 8). Furthermore, an individual band quality map analysis was carried out in the best fused images according to each ecosystem type. Finally, a classification map is obtained in the different fused images, to analyze the influence of the pansharpening in the classification result.

### 2.3.1. Image Fusion Methods

After a review of the state-of-the-art in pansharpening techniques, at the pixel level, a preliminary assessment was carried out selecting classic and new algorithms that could achieve good performance with WV-2 imagery. Some algorithms specifically adapted to the WorldView-2 sensor have been chosen. An initial visual and quantitative assessment was carried out using a total of 12 different pansharpening techniques in these data, but only the best algorithms were selected for this study. The final election of these four algorithms was carried out with the same methodology explained in this paper. Thus, a visual and quantitative evaluation was performed to assess the spectral and the spatial quality of each algorithm, taking into account the compromise between both qualities in each fused image, depending on each ecosystem type. Thus, after obtaining an objective ranking of the 12 algorithms selected using the Borda count method, explained in Section 2.3.2, the final best four pansharpening algorithms were selected, in order to obtain the most suitable fused image for each ecosystem. Next, a brief overview of each family of the algorithms selected in the study is presented. Any formula or block diagram is omitted (for detailed information, see the references).

- Fast intensity hue saturation (FIHS) [48]: It uses the spectral bands to estimate the new component  $I$ . The spatial detail is extracted, computing the difference between the PAN band and the new component  $I$ . The spatial detail is injected into any number of bands.
- Hyperspherical color sharpening (HCS): This pansharpening algorithm is designed specifically for WV-2 by [49] based on the transformation between any native color space and the hyperspherical color space. Once transformed into HCS, the intensity can be scaled without changing the color, essential for the HCS pansharpening algorithm [15,50]. The transformation to HCS can be made from any native color space.
- Based on modulation transfer function: The modulation transfer function (MTF) is a function of the sensor spatial frequency response, describing the resolution of an imaging system [28]. Generalized Laplacian Pyramid (GLP) is an extension of the Laplacian pyramid where a scale factor different from two is used [10]. Finally, in high pass modulation (HPM), the PAN image is multiplied by each band of the original MS image and normalized by a low pass filtered version of the PAN image in order to estimate the enhanced MS image bands.
- Weighted wavelet ‘à trous’ method through fractal dimension maps (WAT@FRAC) [14]: This method is based on the wavelet ‘à trous’ algorithm. A mechanism that controls the trade-off between the spatial and spectral quality by introducing a weighting factor ( $\alpha_i$ ) for the PAN wavelet coefficients is established. However, this factor only discriminates between different spectral bands, but not between different land covers; therefore, the authors proposed a new approach [51], defining a different weight factor  $\alpha_i(x, y)$  for each point of each band.  $\alpha_i(x, y)$  was defined as a fractal dimension map (FDM) with the same size as the original image. A preliminary analysis was carried out using three different window sizes for the windowing process: 7, 15 and 27.



### 2.3.2. Quality Evaluation Methodology

#### (a) Visual quality:

A visual analysis was the first step in the quality assessment. Through this approach, the main errors on an overall scale were observed, and then, local artefacts were analyzed closely. For the visual spectral assessment, fused true color images were compared to their original MS image, used as the reference, and its spectral features compared with the original MS image. Firstly, several aspects of the image features were taken into account in the spectral assessment, such as the tone, contrast, saturation, sharpness and texture. Furthermore, we paid attention to color disturbances. False color composites were produced in order to evaluate the fused NIR bands, where we focused on the same aspects as mentioned above. Finally, we concentrated on linear features, specific objects, surfaces or edges of buildings in order to observe spatial disturbances using the PAN as a reference.

#### (b) Quality indices

There is no current consensus in the literature on the best quality index for pansharpening images [52]. The quantitative quality evaluation of fused images is a debated issue since no reference image exists at the pansharpened resolution [4,20]. A number of statistical evaluation indices were used to measure the quality of the fused images. Each fused image is compared to the reference MS image.

The spectral quality assessment measures the spectral distortion brought by the pansharpening process. The metrics considered in the analysis are as follows:

- The spectral angle mapper (SAM) was designed to determine the spectral similarity in a multidimensional space [22] (Equation (1) in Table 3).
- The spectral ERGAS (relative dimensionless global error) is an overall quality index sensitive to mean shifting and dynamic range change (Table 2, Equation (3)). The  $rmse_i$  (root mean square error) is calculated by its standard definition [23].

The correlation coefficient was not selected as spectral index due to its low capability in techniques with low quality differences.

On the other hand, the spatial detail information of each fused band is compared with the spatial information of the reference PAN image. The metrics considered in the analysis are as follows:

- The spatial ERGAS was proposed by [24]. It is a new spatial index considering the PAN band as a reference (Table 3, Equation (3)).
- The frequency comparison index (FC) is proposed by [25]. It is based on the discrete cosine transform ( $dct$ ) for the spatial assessment (Table 3, Equation (4)).
- The Zhou index (Table 3, Equation (5)) measures the spatial quality computing correlation between the high pass filtered fused image ( $FUS_i^{high\_pass}$ ) and PAN ( $PAN^{high\_pass}$ ).

Finally, as the global quality assessment:

- The Q8 index is a generalization to eight-band images of the Q index [27]. It is based on the different statistical properties of the fused and MS images (Table 3, Equation (6)).

**Table 3.** Indices for the quality assessment of the fused image.

Quality Indices	Equation	Reference	Eq.
Spectral Angle Mapper	$\cos^{-1} \frac{\sum_{i=1}^{nband} FUS_i MS_i}{\sqrt{\sum_{i=1}^{nband} FUS_i^2} \sqrt{\sum_{i=1}^{nband} MS_i^2}}$	[22]	(1)
Spectral ERGAS	$100 * \frac{h}{l} \sqrt{\frac{1}{nband} \sum_{i=1}^{nband} \left( \frac{rmse_i(MS)}{MS_i} \right)^2}$	[23]	(2)
Spatial ERGAS	$100 * \frac{h}{l} \sqrt{\frac{1}{nband} \sum_{i=1}^{nband} \left( \frac{rmse_i(PAN)}{PAN_i} \right)^2}$	[24]	(3)
Frequency Comparison	$\frac{1}{nband} \sum_{i=1}^{nband} corr_i(dct_{n \times n}^{AC}(PAN), dct_{n \times n}^{AC}(FUS_i))$	[25]	(4)
Zhou	$\frac{1}{nband} \sum_{i=1}^{nband} corr_i(PAN^{high\_pass}, FUS_i^{high\_pass})$	[26]	(5)
Q8	$\sum_{i=1}^8 \frac{8\sigma_{MS,FUS} mean_{MS} mean_{FUS}}{(\sigma_{MS}^2 + \sigma_{FUS}^2) + [(mean_{MS})^2 + (mean_{FUS})^2]}$	[27]	(6)

Note:  $nband$  is the number of bands;  $FUS_i$  represents the fused image;  $MS_i$  is the  $i$ th band of the MS image;  $PAN_i$  is the PAN image;  $h$  and  $l$  represent the spatial resolution of the PAN and MS images respectively;  $dct_{n \times n}^{AC}$  is the discrete cosine transform computed in blocks of  $n \times n$  pixels and  $corr_i$  defines the cross-correlation of  $i$ th band;  $FUS_i^{high\_pass}$  is high pass filtered fused image and  $PAN^{high\_pass}$  is the high pass filtered of the PAN image;  $\sigma$  is the variance of the MS and FUS image.

In order to identify, in an objective way, the best fused image for each ecosystem, the best algorithms at the spectral, spatial and global level for each scene have been established by the Borda count rank aggregation method (Equation (7)) [53]. Consider  $U$  a set of items  $i$ , called the universe, and  $R$  a set of the rank list, where  $\tau$  is an item of the rank list. The method is equivalent to: for each  $i \in U$ , a rank list  $\tau \in R$ , and considering Borda normalized weight  $\omega^\tau(i)$ , the fused rank list  $\hat{\tau}$  is ordered with respect to the Borda score  $s^{\hat{\tau}}$ , where the Borda score of an item  $i \in U$  in  $\hat{\tau}$  is defined as:

$$s^{\hat{\tau}}(i) = \sum_{\tau \in R} \omega^\tau(i) \quad (7)$$

#### 2.4. Classification Maps

A supervised classification technique was applied only in the shrubland ecosystem scene in order to analyze the influence of the different pansharpening techniques in the generation of thematic maps [38]. The first step was to determine the classes appearing in the image and obtain a sufficient number of training samples. The classes chosen for this ecosystem were selected by experts of the Teide National Park, the vegetation classes being: *Spartocytisus supranubius* (Teide broom), *Pteroccephalus lasiospermus* (rosalillo de cumbre), *Descurainia bourgaeana* (hierba pajonera) and *Pinus canariensis* (Canarian pine). Urban, road and bare soil classes were also included. In the second step, the OBIA process starts with a segmentation of the input images into local groups of pixels, i.e., objects that become spatial units in the later analysis, classifications and accuracy assessment. Object shape, size and spectral properties depend on both the segmentation approach and the research goals. The image was segmented using the multiresolution segmentation followed by the spectral difference segmentation, in order to preserve the small objects of interest to classify. Once the objects are obtained from the segmentation techniques, classification algorithms can be applied. The last step was to determine the classification algorithm; in our case, we applied the novel object-based or OBIA classification approach [54], using support vector machine (SVM) as the supervised classifier [55]. SVM is a related supervised learning method that analyzes data and recognizes patterns, used for classification and regression analysis. The standard SVM takes a set of input data and predicts, for each given input, which of the different possible classes the input is a member. Given a set of training examples, each marked as belonging to the categories, an SVM training algorithm builds a model that assigns new examples into one category [56]. Thematic maps were obtained after implementing the SVM classifier in each fused image. Afterwards, the accuracy of the classification must be measured;

in this case, testing samples were collected. The statistical accuracy assessment technique used was the overall accuracy and the kappa coefficient.

### 3. Results

This section is divided into three main blocks: (i) the visual assessment; (ii) the quantitative evaluation based on the quality indices; and (iii) the thematic maps resulting from the OBIA classification in the shrubland ecosystem.

#### 3.1. Visual Evaluation

For the visual analysis, both color and edge preservation are the most important criteria to evaluate the performance of image fusion techniques in order to identify the fusion technique that provides the fused image with the highest spectral and spatial quality. To facilitate the visual inspection and for a more detailed spatial analysis, a zoom of the previous scenes is shown in Figures 4–6. It is important to highlight that, after the preliminary assessment, robust pansharpening algorithms have been selected, so all fusion results are satisfactory, and the spectral differences are difficult to appreciate visually, except in some specific areas. We want to underline that, to the best of our knowledge, this is the first time pansharpening algorithms have been assessed in coastal ecosystems using VHR imagery. This improvement in the spatial quality due to the application of fusion techniques could be useful to improve seafloor or benthic classification of shallow waters (i.e., coral reefs or seagrass meadows).

The visual interpretation at the spectral level in the shrubland region (Figure 4) indicates that every algorithm, except for WAT $\otimes$ FRAC, produces a slight color distortion over the entire fused image. On the other hand, in the preliminary analysis, WAT $\otimes$ FRAC with a window size of seven pixels provides the best fused image from among the WAT $\otimes$ FRAC algorithms, although the differences are minimal.

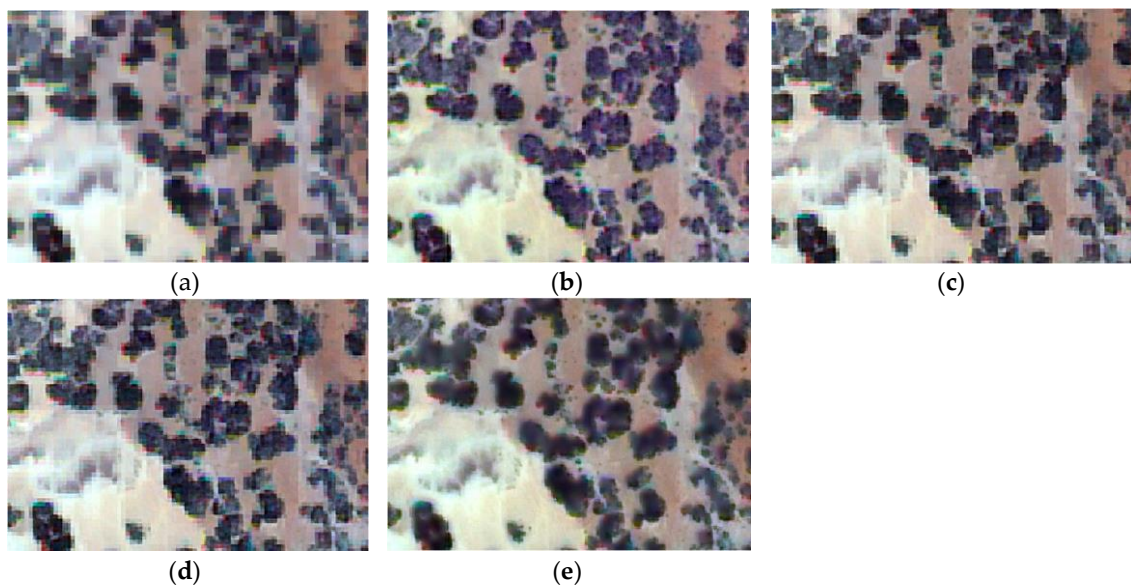


**Figure 4.** True color fused images of the shrubland region: (a) original MS; (b) FIHS; (c) HCS; (d) MTF\_GLP\_HPM; (e) WAT $\otimes$ FRAC with a window size of seven.

Observing the coastal region (Figure 5), differences among the techniques are basically undetectable at the spectral level. The WAT $\otimes$ FRAC window size, which gives a slightly better result in this image, is 27.

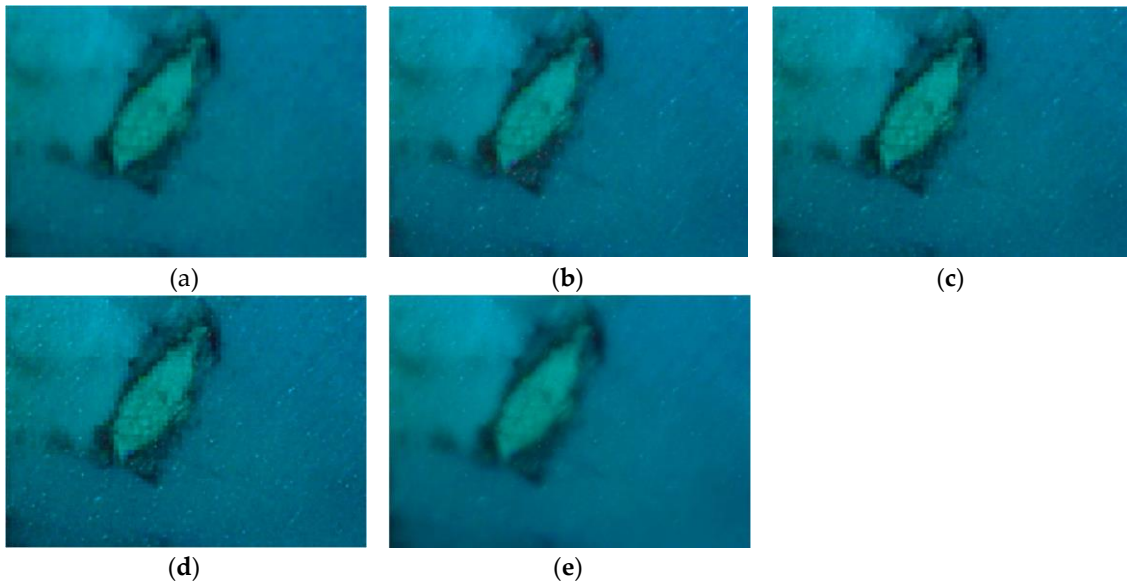


**Figure 5.** True color fused images of the coastal region: (a) original MS; (b) FIHS; (c) HCS; (d) MTF\_GLP\_HPM; (e) WAT $\otimes$ FRAC with a window size of 27.

Visual results similar to those of the shrubland region appear in the mixed ecosystem (Figure 6), where the FIHS, HCS and MTF algorithms show a more perceptible color distortion in the sea than in buildings. The WAT $\otimes$ FRAC window size chosen for this scene is 15.

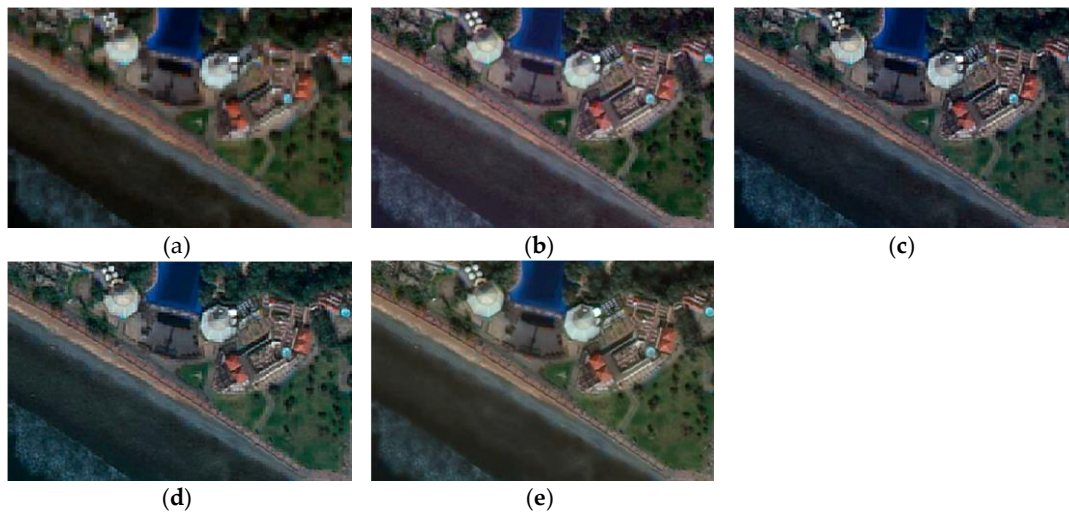


**Figure 6.** True color fused images of the mixed ecosystem with an urban region: (a) original MS; (b) FIHS; (c) HCS; (d) MTF\_GLP\_HPM; (e) WAT $\otimes$ FRAC with a window size of 15.

Spatially, the differences are clearer than spectrally. In the case of the HCS and MTF\_GLP\_HPM techniques, although they maintain the spectral information well, the spatial details are not satisfactorily injected, thus not achieving a good spatial enhancement. Furthermore, the blurred aspect found in the WAT $\otimes$ FRAC algorithm is because the algorithm makes uniform the homogenous areas found in the multispectral image, which appear as heterogeneous areas in the panchromatic image. Thus, the ‘salt and pepper’ effect is avoided with it, obtaining a better classification and more accurate thematic maps, as demonstrated in Section 3.3.

Finally, Figure 7 shows an example of the false color composite using bands outside the PAN range (Bands (B) 8, 7 and 1).

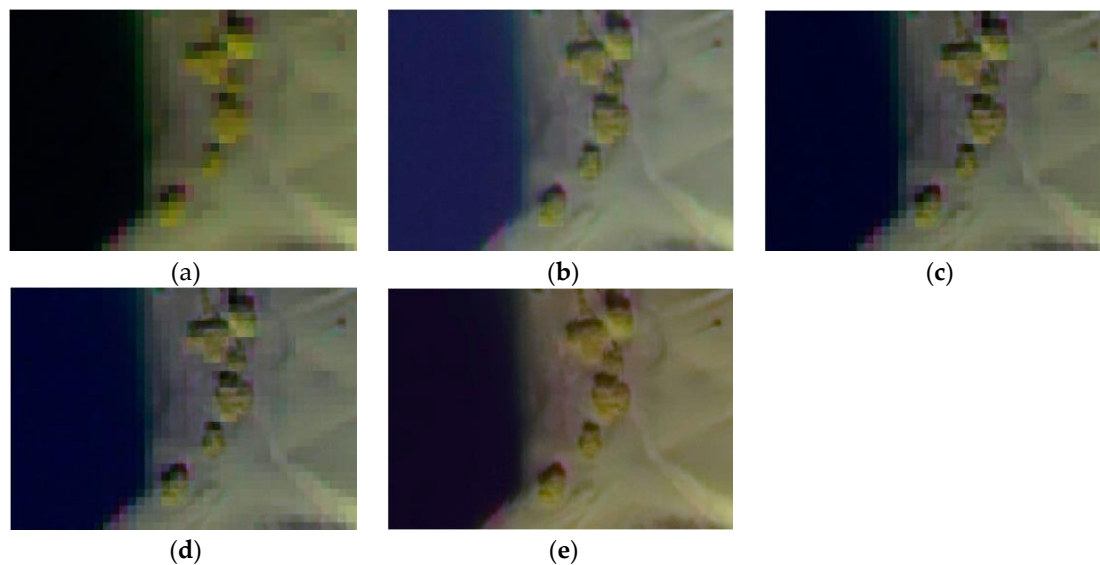


**Figure 7.** False color fused images using Bands 8, 7 and 1 color composition (bands outside the PAN range): (a) original MS; (b) FIHS; (c) HCS; (d) MTF\_GLP\_HPM; (e) WAT⊗FRAC.

In this case, a region with soil, vegetation and water is chosen in order to analyze the behavior of the different techniques. Spectrally, algorithms show a more significant color distortion in the water area. At the spatial level, pansharpening algorithms demonstrate the same behavior as in the true color composite, with WAT⊗FRAC achieving an optimum result.

### 3.2. Quantitative Evaluation of Pansharpened Images

As was mentioned in Section 2.4, in order to perform an objective evaluation of the pansharpening techniques, six spectral and spatial quality indices have been computed on the complete scenes of Figure 2. First, quantitative indices were calculated for all of the bands in the MS image in the three ecosystems. Second, the pansharpening performance for bands covered by and outside of the PAN range was assessed. Finally, an individual band quality map analysis was carried out (Figure 3).

#### 3.2.1. Shrubland Ecosystems

The quality analysis of all multispectral bands can be appreciated in Table 4. SAM, spectral ERGAS and Q8 confirm that the MTF method and the HCS algorithm provide better spectral performance, while FIHS and WAT⊗FRAC get the lowest result, even though there is not a large difference between the highest and the lowest value. As regards the spatial performance, WAT⊗FRAC is confirmed as the best spatial quality method, while HCS shows the worst values. Furthermore, these results confirm the compromise between the spectral and spatial quality, in which the best fused image considered in this study would be the one that provides the best compromise between them. Hence, the Borda count method is used a posteriori to observe this compromise.

The Borda count method has allowed analyzing the balance between the spectral and spatial quality in the pansharpening algorithms to be distinguished to avoid any bias in the global result (Table 4). The results obtained by the Borda count method including the respective spectral and spatial quality indices appear in the 'spectral' and 'spatial' columns. On the other hand, the 'global' column shows the results using the Borda count method in every algorithm considering all of the quality indices.

Analyzing Table 4, WAT⊗FRAC generates the best fused image, not only in the overall evaluation, but also at the spatial level.

**Table 4.** Quality results for the complete WV-2 bands and the shrubland ecosystem (best results in bold). SAM: spectral angle mapper; FC: frequency comparison; Spec.: spectral; Spat.: spatial.

	Spectral Quality		Spatial Quality			Global Quality	Borda Count Rank		
	SAM	Spectral ERGAS	Spatial ERGAS	FC	Zhou	Q8	Global	Spec.	Spat.
FIHS	3.78	1.68	0.89	0.84	0.72	0.90	13	4	6
HCS	3.52	0.39	0.91	0.77	0.67	0.93	14	7	2
MTF_GLP_HPM	3.87	0.33	0.89	0.81	0.71	0.92	16	6	4
WAT@FRAC	4.19	1.44	0.82	0.86	0.89	0.90	17	3	8

As regards the band analysis based on the PAN range, the behavior of the quality index is analyzed with respect to the MS fused bands. Thus, Figure 8 shows the quantitative values obtained for the pansharpened bands within the PAN spectral range (B 2–6) and outside of this range (B 1, 7 and 8). The results for the complete set of bands are included as a reference.

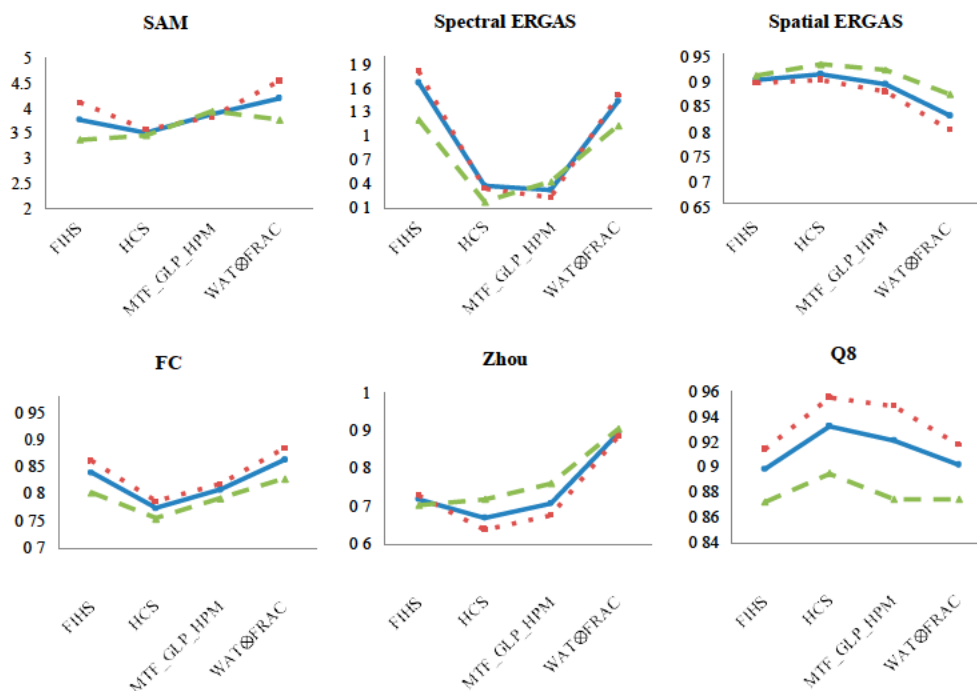


**Figure 8.** Results of the quality indices for the shrubland ecosystem fused image considering the three different MS band combinations (blue: total bands; red: Bands 2–6; green: Bands 1, 7 and 8). X-axis: pansharpening algorithms and Y-axis: range values of each quality indices (SAM: better value closer to 0; Spectral and Spatial ERGAS: better values closer to 0; FC: values between 0 and 1, better closer to 1; Zhou: values between 0 and 1, better closer to 1; Q8: values between 0 and 1, better closer to 1).

SAM and spectral ERGAS indices provide similar results, where fused bands outside of the PAN range have better quality than the bands within the PAN range, the results for the complete set of bands being an average of them. There is an exception with MTF\_GLP\_HPM, providing similar results irrespective of the bands that are used for their estimation. While the analysis of the spatial indices, in general, shows that bands inside the PAN range achieve better spatial quality.

### 3.2.2. Coastal Ecosystems

Table 5 includes the values of the quality indices for all bands obtained when applying the different fusion methods in the coastal ecosystem scenario. It is important to point out that most of the scene is covered by shallow water. The SAM index shows as the best fused images the ones obtained by MTF\_GLP\_HPM and FIHS; however, it does not demonstrate a large variability in the results, just like that of Q8. In the case of spectral ERGAS, MTF\_GLP\_HPM shows the best fused image. Spatial

indices also show some variability, where spatial ERGAS and FC identify FIHS as the best method, while the WAT@FRAC algorithm gets the best quality result in Zhou. All spatial indices agree that the lowest quality image is achieved by the MTF\_GLP\_HPM and HCS methods.

**Table 5.** Quality results for the complete WV-2 bands and the coastal ecosystem (best results in bold).

SAM: spectral angle mapper; FC: frequency comparison; Spec.: spectral; Spat.: spatial.

	Spectral Quality		Spatial Quality			Global Quality	Borda Count Rank		
	SAM	Spectral ERGAS	Spatial ERGAS	FC	Zhou	Q8	Global	Spec.	Spat.
FIHS	1.77	2.91	2.36	0.85	0.83	0.98	19	8	7
HCS	1.81	1.73	2.64	0.64	0.71	0.98	10	15	2
MTF_GLP_HPM	1.64	1.22	2.61	0.72	0.73	0.98	17	18	4
WAT@FRAC	1.93	2.63	2.54	0.78	<b>0.88</b>	0.98	14	15	7

According to the Borda count method, the best algorithm for getting a good fusion in coastal ecosystems is FIHS, which achieves a good balance between the spectral and the spatial quality.

With respect to the band analysis based on the PAN range (Figure 9), from the spectral point of view, SAM provides similar values between the fusion algorithms, and the spectral ERGAS shows better quality images for the MS bands covered by the PAN range, as expected, except in FIHS. Concerning the spatial indices, the Spatial ERGAS and FC metrics achieve a superior spatial quality for Bands 2–6, while Zhou shows very similar results. The Q8 index also gives higher values to the bands covered by the PAN.

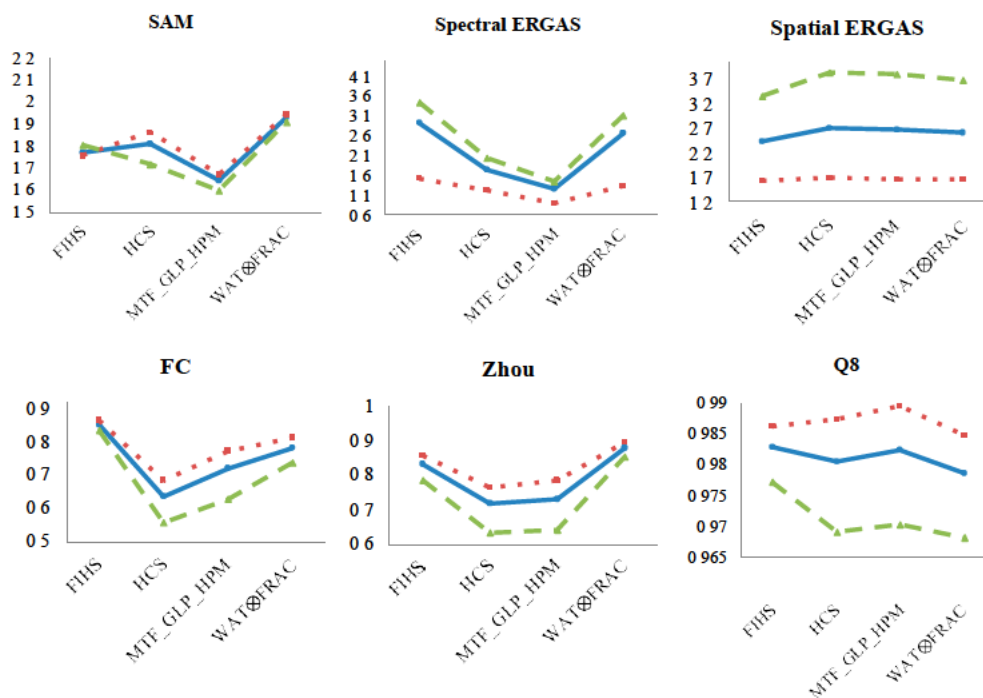


**Figure 9.** Results of the quality indices for the coastal ecosystem fused image considering the three different MS band combinations (blue: total bands; red: Bands 2–6; green: Bands 1, 7 and 8). X-axis: panharpening algorithms and Y-axis: range values of each quality indices (SAM: better value closer to 0; Spectral and Spatial ERGAS: better values closer to 0; FC: values between 0 and 1, better closer to 1; Zhou: values between 0 and 1, better closer to 1; Q8: values between 0 and 1, better closer to 1).

### 3.2.3. Mixed Ecosystems

The quantitative evaluation in all bands for the mixed ecosystem is shown in Table 6. According to the spectral and spatial quality indices, the results are similar to those of shrubland ecosystems.

The MTF\_GLP\_HPM technique provides the best result at the spectral level, while the WAT@FRAC algorithm does so at the spatial level.

**Table 6.** Quality results for the complete WV-2 bands and the mixed ecosystem (best results in bold). SAM: spectral angle mapper; FC: frequency comparison; Spec.: spectral; Spat.: spatial.

	Spectral Quality		Spatial Quality		Global Quality		Borda Count Rank		
	SAM	Spectral ERGAS	Spatial ERGAS	FC	Zhou	Q8	Global	Spec.	Spat.
FIHS	7.11	2.98	2.08	0.89	0.73	0.93	12	2	6
HCS	5.66	1.73	2.23	0.80	0.61	<b>0.96</b>	13	6	2
MTF_GLP_HPM	5.62	1.72	2.23	0.81	0.61	<b>0.96</b>	17	8	4
WAT@FRAC	6.88	2.85	2.05	0.93	0.98	0.95	18	4	8

Looking at the spectral quality indices in the mixed ecosystem scene (Figure 10), the same behavior is found for the Spectral ERGAS, which obtains the worst fused image using MS bands outside of the PAN range for the fusion, while in SAM, the values are, in general, very similar between them. With respect to the spatial quality, the bands inside the PAN range obtain better quality values. Finally, Q8 obtains worse quality results for the MS bands outside of the PAN range, as expected.

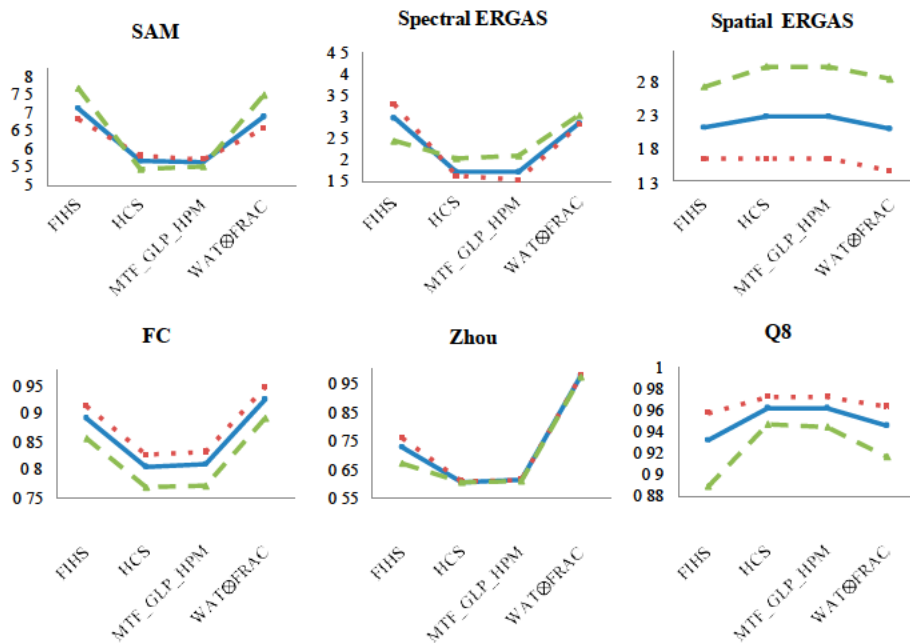


**Figure 10.** Results of the quality indices for the mixed ecosystem fused image considering the three different MS band combinations (blue: total bands; red: Bands 2–6; green: Bands 1, 7 and 8). X-axis: panharpening algorithms and Y-axis: range values of each quality indices (SAM: better value closer to 0; Spectral and Spatial ERGAS: better values closer to 0; FC: values between 0 and 1, better closer to 1; Zhou: values between 0 and 1, better closer to 1; Q8: values between 0 and 1, better closer to 1).

In this case, the WAT@FRAC algorithm also achieves the best score in the Borda count rank, making it the most reliable algorithm for this kind of ecosystem.

### 3.2.4. Individual Band Quality Map Analysis

Quality values for each individual band in each scene are included in Table 7. The Q8 overall index does not show the variability at the local level; thus, quality map analyses were carried out using the Q8 metric with a block size of 64 in order to examine the quality at local level in each band using the best algorithms for each area. The maximum quality index is achieved if a window is not used. This block size of 64 was chosen because increasing the block size increases the index values, and thus,



the values obtained in the quality maps could be comparable to the values obtained for the overall Q8. In each quality map, a blue scale has been used with white indicating a higher similarity (Q8 metric) between the original and the fused MS band.

**Table 7.** Quality results for Bands 1–8 using the best algorithms for each scene. Best results are in bold.

	Shrubland ecosystem	Coastal ecosystem	Mixed ecosystem
Q8, BlockSize: 64	Q8 value for WAT $\otimes$ FRAC_w7	Q8 value for FIHS	Q8 value for WAT $\otimes$ FRAC_15
B1 (Coastal Blue)	0.696	0.764	0.695
B2 (Blue)	0.736	0.889	0.842
B3 (Green)	0.878	<b>0.936</b>	<b>0.905</b>
B4 (Yellow)	<b>0.904</b>	0.647	0.890
B5 (Red)	0.872	0.410	0.851
B6 (Red Edge)	0.897	0.395	0.857
B7 (NIR 1)	0.841	0.318	0.845
B8 (NIR 2)	0.881	0.239	0.832

As indicated, the WAT $\otimes$ FRAC algorithm was selected as the best compromise to fuse images in a shrubland ecosystem scenario. Quality maps of WAT $\otimes$ FRAC (window size of seven) are presented in Figure 11. Better results can be appreciated for Bands 3–8, with Band 4 achieving the best fusion. On the other hand, Bands 1 and 2 (coastal blue and blue) do not show good quality in some areas, with a greater concentration of dark blue pixels, in accordance with the lowest quality results of Table 7.

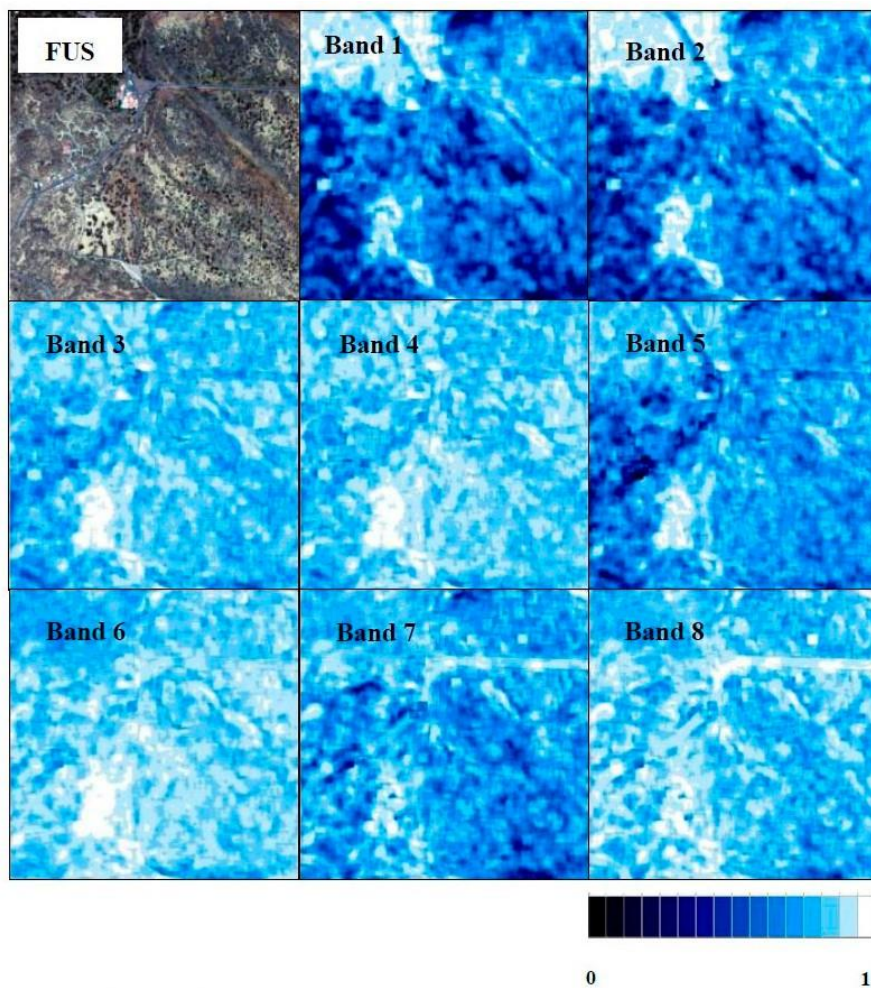


**Figure 11.** Fused image with the WAT $\otimes$ FRAC of the shrubland ecosystem and its quality maps for each band (scale from 0–1, zero being less fusion quality and one the highest fusion quality).

As regards the coastal ecosystem, in the individual band quality maps of FIHS (Table 7 and Figure 12), the higher quality is achieved in Bands 2 and 3, with values over 0.88. For Band 1 (0.764), a light blue aspect (medium quality) in the sea area is clear, whereas, in the land area, both bands get dark blue pixels in the quality maps with this algorithm. From Bands 4–8, the quality increases in land areas, showing mostly dark blue pixels; however, the quality in sea areas decreases considerably. Band 8 gets a quality value of 0.239, while Bands 5–7 show values around 0.3–0.4. Regardless of the fact that the FIHS algorithm gets the best fusion for this scenario, the quality maps are not very satisfactory for longer wavelengths, but this portion of the spectrum is of minimum interest in seafloor mapping applications due to the low capability of light to penetrate the water.

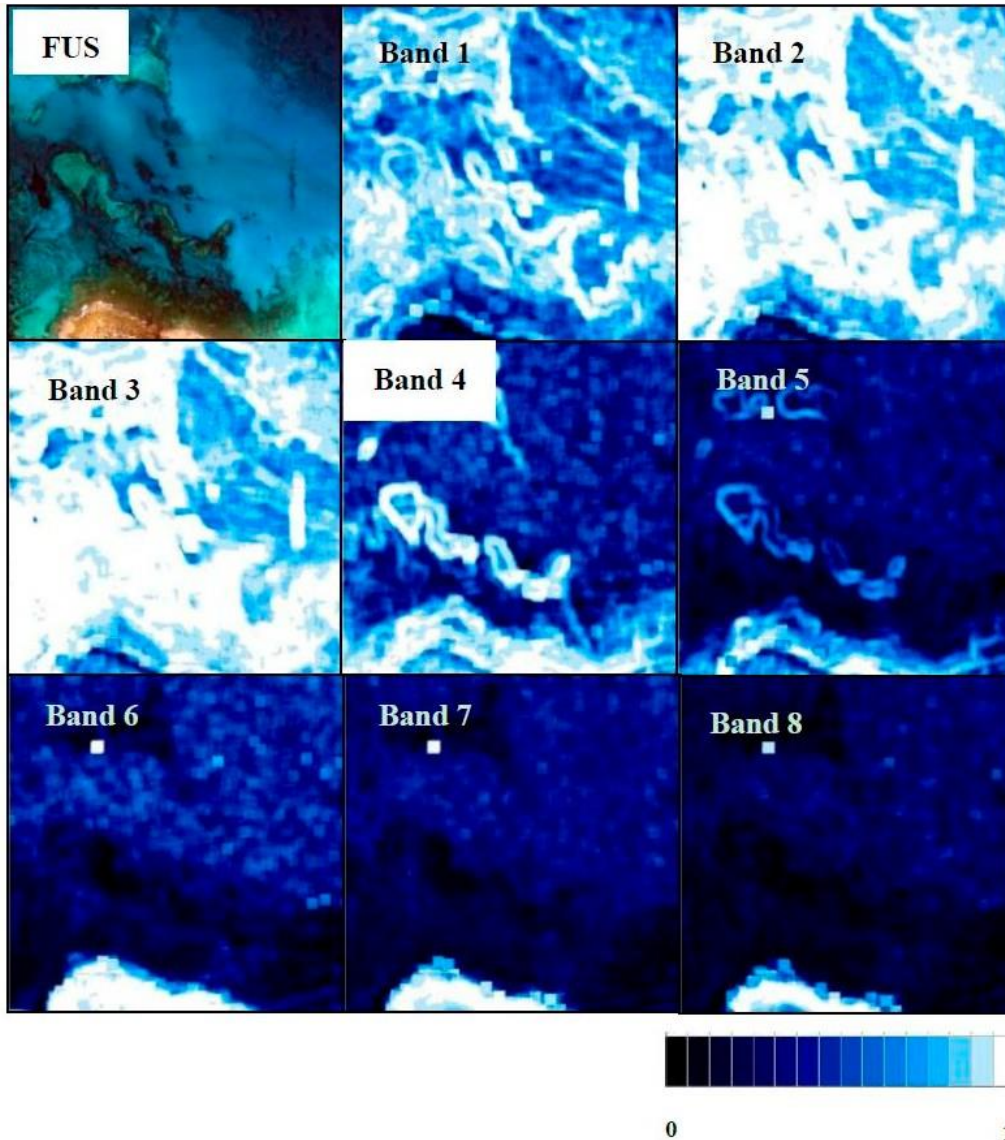


**Figure 12.** Fused image with FIHS of the coastal ecosystem and its quality maps for each band (scale from 0–1, zero being less fusion quality and one the higher fusion quality).

Concerning the quality maps of the WAT $\otimes$ FRAC algorithm in mixed ecosystems (Figure 13), they present a similar behavior to that of shrubland areas. Specifically, Bands 3 and 4 have the highest quality values (0.905 and 0.890, respectively, as presented in Table 7), while Bands 1 and 2 show lower quality (0.695 for Band 1 and 0.842 for Band 2). On the other hand, water areas have, in general, worse quality as the band number increases.

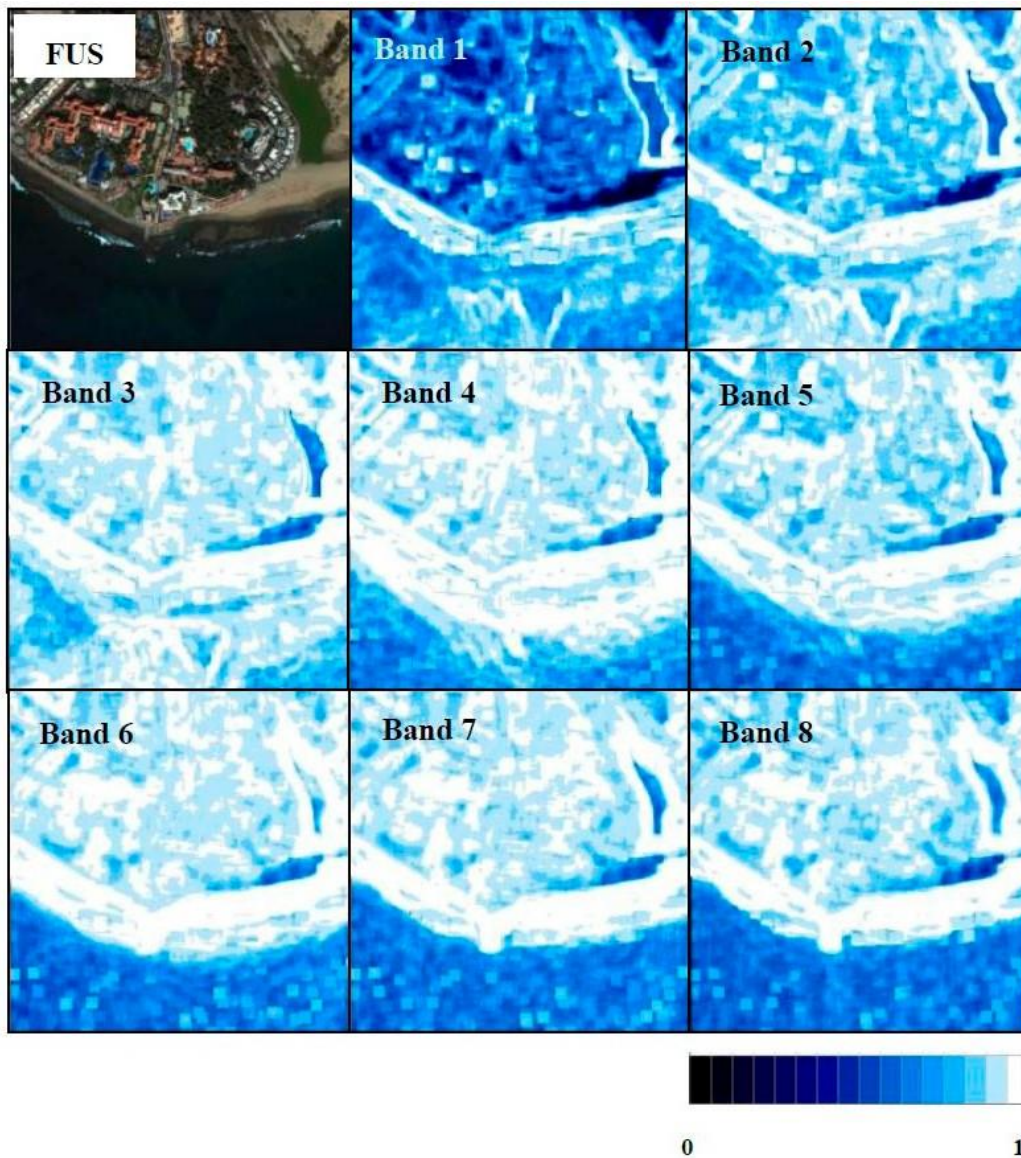


**Figure 13.** Fused image with WAT $\otimes$ FRAC of the mixed ecosystem and its quality maps for each band. Scale from 0–1, zero being less fusion quality and one the higher fusion quality.

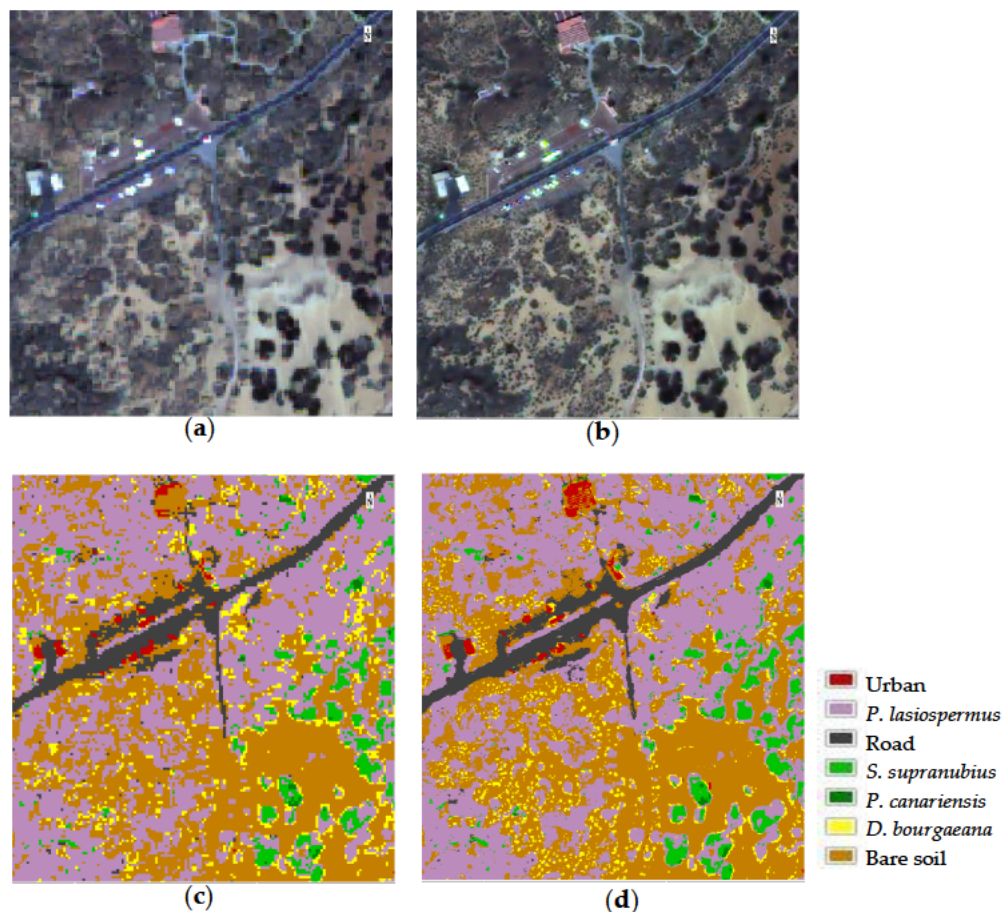
### 3.3. Thematic Maps of Shrubland Ecosystems

Table 8 shows the overall accuracy and the kappa coefficient for the SVM object-based classification applied to each fused image. The best result is obtained in the WAT $\otimes$ FRAC fused image, corroborating the results achieved in the Quantitative Evaluation section, where WAT $\otimes$ FRAC shows the best fusion result.

**Table 8.** Segmentation parameters used for the images and classification accuracy.

Classification Techniques	Support Vector Machine	
Pansharpining Algorithms	Overall Accuracy	Kappa
MS	80.61%	0.72
FIHS	83.72%	0.76
HCS	82.72%	0.75
MTF_GLP_HPM	83.18%	0.75
WAT $\otimes$ FRAC	89.39%	0.85

Finally, Figure 14 presents the thematic map from the shrubland ecosystem obtained in the original MS image and in the WAT@FRAC fused image by SVM classification. It is observed how the fusion is a fundamental preprocessing in these complex ecosystems because some classes of interest are not well delimited in the original multispectral thematic maps. On the other hand, buildings (red) are erroneously classified as bare soil (brown) in the original multispectral image, and road limits (grey) and vegetation contours seem to be stepped, due to the pixel size in the original image. The results were analyzed by the experts of the national park, confirming a good agreement with respect the real vegetation of the area.



**Figure 14.** Zoom of the original MS (a) and WAT@FRAC fused image (b) of the thematic maps obtained by the OBIA-SVM classifier applied to the multispectral image (c) and WAT@FRAC fused image (d) in the shrubland ecosystem.

#### 4. Conclusions

As indicated, the main objective of this work was to select the pansharpening algorithm that provides the image with the best spatial and spectral quality for land and coastal ecosystems. Due to this reason, the most efficient pansharpening techniques developed in recent years have been applied, in order to achieve the highest spatial resolution of the MS bands while preserving the original spectral information, and assessed. As not a single pansharpening algorithm has exhibited a superior performance, the best techniques have been evaluated in three different types of ecosystems, i.e., heterogenic shrubland ecosystems, coastal systems and coastal-land transitional zones with inland water and an urban area. Fusion methods have frequently been applied to land and urban areas; however, a novel analysis has been conducted covering their evaluation in areas of shallow water using VHR imagery, as well, as they could be useful for the mapping of seabed species, such as seagrasses and coral reefs.

After a preliminary assessment of twelve pansharpening techniques, a total of four algorithms was selected for the study. In the literature, four band sensors are mostly selected to carry out this kind

of study (Ikonos, GeoEye, QuickBird, etc.); however, we have tried to find the best fused image using an eight-band sensor (WorldView-2).

Both the visual evaluation and the quantitative analysis were achieved using six quality indices at the overall, spectral and spatial level. The best algorithms at the spectral and spatial levels were obtained for each type of ecosystem. Finally, the best fused technique with a compromise between the spectral and spatial quality was identified following the Borda count method. Thus, we provide guidance to users in order to choose the best algorithm that would be more suitable in accordance with the type of ecosystem and the information to be preserved.

It is interesting to observe that, for land regions, the MTF algorithm performs better at preserving the spectral quality, while the weighted wavelet 'à trous' method through the fractal dimension maps algorithm demonstrates better results considering the spatial detail of the fused imagery. Balancing the spectral and spatial quality, the most appropriate pansharpening algorithm for shrubland and mixed ecosystems is the WAT $\otimes$ FRAC technique, while FIHS is selected for the coastal ecosystems. Note that to date, the WAT $\otimes$ FRAC algorithm has only been used in agricultural areas; however, we have applied this algorithm in natural vulnerable ecosystems, where a successful result has been obtained. Moreover, we can conclude that the more heterogenic the area to be fused, the smaller the window size in WAT $\otimes$ FRAC. FIHS provides the best overall fused image in the simplest scenario. Thus, even though there is no remarkable difference in the way the algorithms perform with respect to land and water areas, we have concluded that images with low variability, such as a coastal scenario, covered mostly by water, require simpler algorithms, rather than more complex and heterogeneous images (i.e., shrubland and mixed ecosystems), which need more advanced algorithms in order to obtain good fused imagery.

Moreover, we have studied the behavior of each algorithm when applied to the complete set of MS bands and on bands covered by and outside of the PAN range. In general, Bands 2–6 mainly have better spatial and spectral quality, but the quality of the remaining bands is acceptable. Analyzing the results, there is a difference in how the same algorithm works on land and coastal areas. The fusion might have higher quality on land, while a lower quality appears in bodies of water.

Additionally, a local study was carried out to identify the distortion introduced in each single band by the best fused algorithms chosen for each scenario. In general, Bands 3–8 attained higher quality for land areas, while in water areas, red and near-infrared bands (5, 7 and 8) experience high spectral distortion. However, these bands are not usually used in seabed mapping applications due to their low penetration capability in water.

Finally, it is important to recall the need to obtain the best fused image in the analyzed ecosystems, as they are heterogenic regions with sparse vegetation mainly made up of small and mixed shrubs with reduced leaf area in the case of shrubland ecosystems and with low radiance absorption in complex and dynamic coastal ecosystems. In this context, thematic maps were obtained using the SVM classifier in the original MS image and in the WAT $\otimes$ FRAC fused image. This corroborates the best performance of the WAT $\otimes$ FRAC algorithm to generate accurate thematic maps in the shrubland ecosystem. The excellent results provided by these studies are being applied to the generation of challenging thematic maps of coastal and land protected areas, and studies of the state of conservation of natural resources will be performed.

**Acknowledgments:** This research has been supported by the ARTEMISAT (*Análisis de recursos marinos y terrestres mediante el procesamiento de imágenes de alta resolución*) (CGL2013-46674-R) project, funded by the Spanish Ministerio de Economía y Competitividad. This work was completed while E. I-U was a Ph.D. student in the IOGAG Doctoral Program in Oceanography and Global Change (ULPGC).

**Author Contributions:** All of these authors contributed extensively to the work. Edurne Ibarrola-Ulzurrun, Consuelo Gonzalo-Martin and Javier Marcello-Ruiz developed the methodology and analyzed the results. Ángel García-Pedrero contributed with the implementation of the pansharpening algorithms, and Dionisio Rodríguez-Esparragon contributed with the quality evaluation indices. Edurne Ibarrola-Ulzurrun processed the WorldView-2 data and carried out the image fusions and their quality evaluation, supervised by Consuelo Gonzalo-Martin and Javier Marcello-Ruiz. Finally, Edurne Ibarrola-Ulzurrun wrote the overall paper under the supervision of Consuelo Gonzalo-Martin and Javier Marcello-Ruiz, who were also involved in the manuscript's discussion and revision.

**Conflicts of Interest:** The authors declare no conflicts of interest. The founding sponsors had no role in the design of the study; in the collection, analyses or interpretation of data; in the writing of the manuscript; nor in the decision to publish the results.

## References

- Pagiola, S.; Von Ritter, K.; Bishop, J. *Assessing the Economic Value of Ecosystem Conservation*; World Bank: Washington, DC, USA, 2004.
- Barange, M.; Harris, R.P. *Marine Ecosystems and Global Change*; Oxford University Press: Oxford, UK, 2010.
- Reinke, K.; Jones, S. Integrating vegetation field surveys with remotely sensed data. *Ecol. Manag. Restor.* **2006**, *7*, S18–S23. [[CrossRef](#)]
- Kpalma, K.; El-Mezouar, M.C.; Taleb, N. Recent trends in satellite image pan-sharpening techniques. In Proceedings of the 1st International Conference on Electrical, Electronic and Computing Engineering, Vrnjacka Banja, Serbia, 2–5 June 2014.
- Li, X.; He, M.; Zhang, L. Hyperspherical color transform based pansharpening method for worldview-2 satellite images. In Proceedings of the 2013 IEEE 8th Conference on Industrial Electronics and Applications, Melbourne, Australia, 19–21 June 2013.
- Hallanda, W.A.; Cox, S. Image sharpening for mixed spatial and spectral resolution satellite systems. In Proceedings of the 17th International Symposium of Remote Sensing of Environment, University of Michigan, Ann Arbor, MI, USA, 9–13 May 1983.
- Schowengerdt, R.A. Reconstruction of multispatial, multispectral image data using spatial frequency content. *Photogramm. Eng. Remote Sens.* **1980**, *46*, 1325–1334.
- Pohl, C. Challenges of remote sensing image fusion to optimize earth observation data exploitation. *Eur. Sci. J.* **2014**, *9*, 355–365.
- Zhang, J. Multi-source remote sensing data fusion: Status and trends. *Int. J. Image Data Fusion* **2010**, *1*, 5–24. [[CrossRef](#)]
- Amro, I.; Mateos, J.; Vega, M.; Molina, R.; Katsaggelos, A.K. A survey of classical methods and new trends in pansharpening of multispectral images. *EURASIP J. Adv. Sig. Proc.* **2011**, *2011*, 1–22. [[CrossRef](#)]
- Fonseca, L.; Namikawa, L.; Castejon, E.; Carvalho, L.; Pinho, C.; Pagamisse, A. Image fusion for remote sensing applications. In *Image Fusion and Its Applications*; InTech: Rijeka, Croatia, 2011.
- Laben, C.A.; Brower, B.V. Process for Enhancing the Spatial Resolution of multispectral Imagery Using Pan-Sharpening. U.S. Patent 6011875 A, 4 January 2000.
- Li, X.; Qi, W. An effective pansharpening method for worldview-2 satellite images. In Proceedings of the International Conference on Estimation, Detection and Information Fusion (ICEDIF), Harbin, China, 10–11 January 2015.
- Lillo-Saavedra, M.; Gonzalo, C. Spectral or spatial quality for fused satellite imagery? A trade-off solution using the wavelet à trous algorithm. *Int. J. Remote Sens.* **2006**, *27*, 1453–1464. [[CrossRef](#)]
- Li, X.; Li, L.; He, M. A novel pansharpening algorithm for worldview-2 satellite images. In Proceedings of the International Conference on Industrial and Intelligent Information (ICIII 2012), Singapore, 17–18 March 2012.
- Alimuddin, I.; Sumantyo, J.T.S.; Kuze, H. Assessment of pan-sharpening methods applied to image fusion of remotely sensed multi-band data. *Int. J. Appl. Earth Observ. Geoinf.* **2012**, *18*, 165–175.
- González-Audicana, M.; Saleta, J.L.; Catalán, R.G.; García, R. Fusion of multispectral and panchromatic images using improved ihs and pca mergers based on wavelet decomposition. *IEEE Trans. Geosci. Remote Sens.* **2004**, *42*, 1291–1299. [[CrossRef](#)]
- Marcello, J.; Medina, A.; Eugenio, F. Evaluation of spatial and spectral effectiveness of pixel-level fusion techniques. *IEEE Geosci. Remote Sens. Lett.* **2013**, *10*, 432–436. [[CrossRef](#)]
- Rodríguez-Esparragón, D. *Evaluación y Desarrollo de Métricas de Calidad Espacial y Espectral Para Aplicaciones de Fusión de Imágenes Multiespectrales de Teledetección de Alta Resolución*; Universidad Las Palmas de Gran Canaria: Palmas, Spain, 2015.
- Alparone, L.; Wald, L.; Chanussot, J.; Thomas, C.; Gamba, P.; Bruce, L.M. Comparison of pansharpening algorithms: Outcome of the 2006 grs-s data-fusion contest. *IEEE Trans. Geosci. Remote Sens.* **2007**, *45*, 3012–3021. [[CrossRef](#)]
- Alparone, L.; Aiazzi, B.; Baronti, S.; Garzelli, A.; Nencini, F.; Selva, M. Multispectral and panchromatic data fusion assessment without reference. *Photogramm. Eng. Remote Sens.* **2008**, *74*, 193–200. [[CrossRef](#)]

22. Kruse, F.; Lefkoff, A.; Boardman, J.; Heidebrecht, K.; Shapiro, A.; Barloon, P.; Goetz, A. The spectral image processing system (sips) – Interactive visualization and analysis of imaging spectrometer data. *Remote Sens. Environ.* **1993**, *44*, 145–163. [[CrossRef](#)]
23. Wald, L. Quality of high resolution synthesised images: Is there a simple criterion? In Proceedings of the Third Conference: Fusion of Earth Data: Merging Point Measurements, Raster Maps And Remotely Sensed Images, Sophia Antipolis, France, 26–28 January 2000.
24. Lillo-Saavedra, M.; Gonzalo, C.; Arquero, A.; Martinez, E. Fusion of multispectral and panchromatic satellite sensor imagery based on tailored filtering in the fourier domain. *Int. J. Remote Sens.* **2005**, *26*, 1263–1268. [[CrossRef](#)]
25. Rodríguez-Esparragón, D.; Marcello-Ruiz, J.; Medina-Machín, A.; Eugenio-González, F.; Gonzalo-Martín, C.; García-Pedrero, A. Evaluation of the performance of the spatial assessment of pansharpened images. In Proceedings of the 2014 IEEE International Geoscience and Remote Sensing Symposium, Quebec City, QC, Canada, 13–18 July 2014.
26. Zhou, J.; Civco, D.; Silander, J. A wavelet transform method to merge landsat TM and SPOT panchromatic data. *Int. J. Remote Sens.* **1998**, *19*, 743–757. [[CrossRef](#)]
27. Wang, Z.; Bovik, A.C. A universal image quality index. *IEEE Signal Lett.* **2002**, *9*, 81–84. [[CrossRef](#)]
28. Vivone, G.; Alparone, L.; Chanussot, J.; Dalla Mura, M.; Garzelli, A.; Licciardi, G.; Restaino, R.; Wald, L. A critical comparison among pansharpening algorithms. *IEEE Trans. Geosci. Remote Sens.* **2015**, *53*, 2565–2586. [[CrossRef](#)]
29. Amolins, K.; Zhang, Y.; Dare, P. Wavelet based image fusion techniques – An introduction, review and comparison. *ISPRS J. Photogramm. Remote Sens.* **2007**, *62*, 249–263. [[CrossRef](#)]
30. Ehlers, M.; Klonus, S.; Johan Åstrand, P.; Rosso, P. Multi-sensor image fusion for pansharpening in remote sensing. *Int. J. Image Data Fusion* **2010**, *1*, 25–45. [[CrossRef](#)]
31. Ozdemir, I.; Karnieli, A. Predicting forest structural parameters using the image texture derived from worldview-2 multispectral imagery in a dryland forest, israel. *Int. J. Appl. Earth Observ. Geoinf.* **2011**, *13*, 701–710. [[CrossRef](#)]
32. Witharana, C.; Civco, D.L.; Meyer, T.H. Evaluation of pansharpening algorithms in support of earth observation based rapid-mapping workflows. *Appl. Geogr.* **2013**, *37*, 63–87. [[CrossRef](#)]
33. Hasanlou, M.; Saradjian, M.R. Quality assessment of pan-sharpening methods in high-resolution satellite images using radiometric and geometric index. *Arab. J. Geosci.* **2016**, *9*, 1–10. [[CrossRef](#)]
34. Jawak, S.D.; Luis, A.J. A semiautomatic extraction of antarctic lake features using worldview-2 imagery. *Photogramm. Eng. Remote Sens.* **2014**, *80*, 939–952. [[CrossRef](#)]
35. Gungor, O.; Boz, Y.; Gokalp, E.; Comert, C.; Akar, A. Fusion of low and high resolution satellite images to monitor changes on costal zones. *Sci. Res. Essays* **2010**, *5*, 654–662.
36. Embabi, N.S.; Moawad, M.B. A semi-automated approach for mapping geomorphology of el bardawil lake, northern sinai, egypt, using integrated remote sensing and gis techniques. *Egypt. J. Remote Sens. Space Sci.* **2014**, *17*, 41–60. [[CrossRef](#)]
37. Eugenio, F.; Marcello, J.; Martin, J. High-resolution maps of bathymetry and benthic habitats in shallow-water environments using multispectral remote sensing imagery. *IEEE Trans. Geosci. Remote Sens.* **2015**, *53*, 3539–3549. [[CrossRef](#)]
38. Ibarrola-Ulzurrun, E.; Gonzalo-Martín, C.; Marcello-Ruiz, J. Influence of pansharpening techniques in obtaining accurate vegetation thematic maps. In Proceedings of the Earth Resources and Environmental Remote Sensing/GIS Applications, Edinburgh, UK, 26–29 September 2016.
39. Mayer-Suárez, P.; Romero-Martín, L.E. La Naturaleza Desértica de Fuerteventura y la Erosionabilidad de sus Precipitaciones. Available online: <http://catalogo.museosdetenerife.org/cdm/singleitem/collection/Arca/id/4130/rec/14> (accessed on 14 December 2016).
40. Fernández-Cabrera, E.; Pérez-Chacón, E.; Cruz Avero, N.; Hernández Cordero, A.; Hernández Calvento, L. Consecuencias ambientales del crecimiento urbano-turístico en el sistema de dunas de corralejo (fuerteventura-islas canarias). In *Urbanismo Expansivo de la Utopía a la Realidad. Asociación de Geógrafos Españoles*; Colegio de Geógrafos de España y Universidad de Alicante: Alicante, Spain, 2011; pp. 241–252.


41. Fernández Cabrera, E.; Roca Bosch, E.; Cabrera, L.; Hernández-Calvento, L.; Pérez-Chacon, E. Estudio de la Percepción Social en el Entorno del Parque Natural de Las Dunas de Corralejo (Fuerteventura, Islas Canarias): Aplicaciones Para la Gestión Integrada de Zonas Costeras. Available online: <http://upcommons.upc.edu/handle/2117/18108> (accessed on 14 December 2016).
42. Garzón-Machado, V.; del Arco-Aguilar, M.J.; Pérez-de-Paz, P.L. A tool set for description and mapping vegetation on protected natural areas: An example from the canary islands. *Biodivers. Conserv.* **2011**, *20*, 3605–3625. [[CrossRef](#)]
43. Hernández-Cordero, A.; Pérez-Chacón, E.; Hernández-Calvento, L. Aplicación de tecnologías de la información geográfica al estudio de la vegetación en sistemas de dunas litorales. Resultados preliminares en el campo de dunas de maspalomas (gran canaria, islas canarias). In *Tecnologías de la Información Geográfica para el Desarrollo Territorial*; Servicio de Publicaciones y Difusión Científica de la ULPGC: Las Palmas de Gran Canaria, Spain, 2008.
44. Gobierno de Canarias, C. Plan director reserva natural especial de las dunas de maspalomas. Gobierno de Canarias. Consejería de Medio Ambiente y Ordenación Territorial. In *Videconsejería de Ordenación Territorial*; Dirección General de Ordenación al Territorio: Las Palmas de Gran Canaria, Spain, 2004.
45. Fourqurean, J.W.; Duarte, C.M.; Kennedy, H.; Marbà, N.; Holmer, M.; Mateo, M.A.; Apostolaki, E.T.; Kendrick, G.A.; Krause-Jensen, D.; McGlathery, K.J. Seagrass ecosystems as a globally significant carbon stock. *Nat. Geosci.* **2012**, *5*, 505–509. [[CrossRef](#)]
46. Ruocco, M.; Bertoni, D.; Sarti, G.; Ciccarelli, D. Mediterranean coastal dune systems: Which abiotic factors have the most influence on plant communities? *Estuar. Coast. Shelf Sci.* **2014**, *149*, 213–222. [[CrossRef](#)]
47. Martínez, M.L.; Psuty, N.P. *Coastal Dunes*; Springer Science & Business Media: Berlin, Germany, 2004.
48. Tu, T.M.; Su, S.C.; Shyu, H.C.; Huang, P.S. A new look at ihs-like image fusion methods. *Inf. Fusion* **2001**, *2*, 177–186. [[CrossRef](#)]
49. Padwick, C.; Deskevich, M.; Pacifici, F.; Smallwood, S. Worldview-2 Pan-Sharpener. In Proceedings of the ASPRS 2010 Annual Conference, San Diego, CA, USA, 26–30 April 2010.
50. Wu, B.; Fu, Q.; Sun, L.; Wang, X. Enhanced hyperspherical color space fusion technique preserving spectral and spatial content. *J. Appl. Remote Sens.* **2015**, *9*, 097291. [[CrossRef](#)]
51. Lillo-Saavedra, M.; Gonzalo, C.; Lagosa, O. Toward reduction of artifacts in fused images. *Int. J. Appl. Earth Observ. Geoinf.* **2011**, *13*, 368–375. [[CrossRef](#)]
52. Shridhar, J.D.; Alvarinho, L.J. A spectral index ratio-based antarctic land-cover mapping using hyperspatial 8-band worldview-2 imagery. *Polar Sci.* **2013**, *7*, 18–38.
53. Renda, M.E.; Straccia, U. Web metasearch: Rank vs. Score based rank aggregation methods. In Proceedings of the 2003 ACM symposium on Applied computing, Melbourne, FL, USA, 9–12 March 2003.
54. Blaschke, T.; Lang, S.; Hay, G. *Object-Based Image Analysis: Spatial Concepts for Knowledge-Driven Remote Sensing Applications*; Springer Science & Business Media: Berlin, Germany, 2008.
55. Mountrakis, G.; Im, J.; Ogole, C. Support vector machines in remote sensing: A review. *ISPRS J. Photogramm. Remote Sens.* **2011**, *66*, 247–259. [[CrossRef](#)]
56. Baatz, M.; Benz, U.; Dehghani, S.; Heynen, M.; Höltje, A.; Hofmann, P.; Lingenfelder, I.; Mimler, M.; Sohlbach, M.; Weber, M. *eCognition User Guide*; Definiens Imaging GmbH: Munich, Germany, 2004.




© 2017 by the authors; licensee MDPI, Basel, Switzerland. This article is an open access article distributed under the terms and conditions of the Creative Commons Attribution (CC BY) license (<http://creativecommons.org/licenses/by/4.0/>).







CHAPTER 4. INFLUENCE OF  
PANSHARPENING IN  
OBTAINING ACCURATE  
VEGETATION MAPS





This chapter includes the following published article: E. Ibarrola-Ulzurrun, C. Gonzalo-Martín, J. Marcello. *Influence of pansharpening in obtaining accurate vegetation maps*. Canadian Journal of Remote Sensing, 2017, pp. 1-17.

The work addresses the important process used in many remote sensing applications: classification. The main objective was to study the pansharpening influence in obtaining accurate classification maps. The fused images obtained from the Chapter 3, which is the first pre-processing improvement needed in the data received to generate higher quality information, were used in order to obtain reliable thematic maps. Next, several supervised classification models were applied in the seven different fused multispectral images, using two different classification approaches: pixel and object-based classification techniques.

The overall accuracies obtained from the different classification maps, corroborate the results obtained in Chapter 3, in which the most suitable pansharpening technique was the WAT $\otimes$ FRAC technique for a land ecosystem, the Teide National Park, at pixel and object-based level. Finally, after an extensive pansharpening and classification assessment, the paper demonstrated the good performance of the final methodology selected in a heterogeneous ecosystem with small and mixed vegetation, obtaining challenging thematic maps in land-protected areas.

In summary, the main conclusions and contributions are:

- The importance of the pansharpening step in ecosystems with small and mixed vegetation, where the spatial information is critical and should be well incorporated in order to generate accurate thematic maps.
- Both classification approaches have their own limitations. The main drawback of the pixel-based approach is the presence of mixed pixels located in boundaries between classes, as well as the quantity of data to be processed, higher than in the OBIA approach, in which objects are processed instead of pixels. Regarding OBIA, there is a high dependency on the segmentation parameters.
- Bayes classifier is the most suitable after the segmentation stage, however, SVM obtained the highest overall accuracy, despite the high computation time.
- A methodology was presented that achieves good performance in these heterogeneous regions with small and mixed shrubs, obtaining challenging vegetation maps to study the state of conservation of natural resources.





## Influence of Pansharpening in Obtaining Accurate Vegetation Maps

Eduarne Ibarrola-Ulzurrun<sup>a,b</sup>, Consuelo Gonzalo-Martín<sup>b</sup>, and Javier Marcello<sup>a</sup>

<sup>a</sup>Instituto de Oceanografía y Cambio Global (IOCAG), Universidad de Las Palmas de Gran Canaria (ULPGC), Parque Científico Tecnológico Marino de Taliarte, s/n, 35214, Telde, Las Palmas, Spain; <sup>b</sup>Escuela Técnica Superior de Ingenieros Informáticos, Universidad Politécnica de Madrid, UPM, Campus de Montegancedo, 28223, Pozuelo de Alarcón, Madrid, Spain

### ABSTRACT

In recent decades, there has been a decline in ecosystem services. Thus, the development of reliable methodologies to monitor ecosystems is becoming important. In this context, the availability of very high resolution sensors offer practical and cost-effective means for good environmental management. However, improvements in the data received are becoming necessary to obtain higher quality information in order to get reliable thematic maps. One improvement is pansharpening, which enhances the spatial resolution of the multispectral bands by incorporating information from a panchromatic image. The main goal of this work was to assess the influence of pansharpening techniques in obtaining precise vegetation maps. Thus, pixel- and object-based classification techniques were implemented and applied to fused imagery using different pansharpening algorithms. Worldview-2 high resolution imagery was used due to its excellent spatial and spectral characteristics. The Teide National Park, in The Canary Islands (Spain), was chosen as the study area since it is a vulnerable heterogeneous ecosystem. The vegetation classes of interest considered were established by the National Park conservation managers. Weighted Wavelet 'à trous' through Fractal Dimension Maps pansharpening algorithm demonstrated a superior performance in the image fusion preprocessing step, while the most appropriate classifier to generate accurate vegetation thematic maps in heterogenic and mixed ecosystems was the Bayes method after the segmentation stage, even though Support Vector Machine achieved the highest overall accuracy.

### RÉSUMÉ

Au cours des dernières décennies, les ressources naturelles ont diminué. Pour ces raisons, le développement de méthodologies fiables de surveillance des écosystèmes devient de plus en plus important. Dans ce contexte, la disponibilité de satellites à très haute résolution offre des moyens pratiques et rentables pour une bonne gestion environnementale. Cependant, il est d'abord nécessaire d'introduire des améliorations dans l'acquisition de données afin d'obtenir des informations de meilleure qualité permettant la création des cartes thématiques fiables. Une de ces améliorations est le "pansharpening", qui augmente la résolution spatiale des bandes multispectrales en incorporant de l'information à partir de l'image panchromatique. Le but principal de ce travail était d'évaluer l'influence des techniques de pansharpening dans l'obtention de cartes de végétation précises. Pour ce faire, on a mis en place des techniques de classification par pixel et orientée-objet, et on les a appliquées à l'imagerie fusionnée en utilisant différents algorithmes de "pansharpening". L'imagerie à haute résolution Worldview-2 a été utilisée en raison de ses excellentes caractéristiques spatiales et spectrales. On a choisi le Parc National du Teide, aux Canaries (Espagne), comme zone d'étude, étant donné qu'il s'agit d'un écosystème vulnérable et hétérogène. Les classes de végétation considérées ont été établies par les responsables de la conservation du Parc National. L'algorithme de pansharpening "Weighted Wavelet 'à trous' through Fractal Dimension Maps" a démontré la précision la plus élevée à l'étape de prétraitement de fusion d'images, alors que le classificateur le plus approprié pour générer des cartes précises de végétation, dans les écosystèmes hétérogènes et mixtes, a été la méthode Bayes, après l'étape de segmentation, bien que *Support Vector Machine* a obtenu le plus haut précision globale.

### ARTICLE HISTORY

Received 1 February 2017  
Accepted 9 August 2017

## Introduction

Biodiversity supports a wide variety of ecological functions together with the services provided by ecosystems (Isbell et al. 2011). Its conservation is related to global environmental changes, such as the land use changes,

climate change, and sustainable developments. However, during the last century, human activity gave raise to alterations in ecosystems and thus, biodiversity is suffering a fast decline (Khare and Ghosh 2016). This creates a demand to preserve environmental resources

(Pakzad et al. 2003). Remote sensing has become an essential tool for evaluating and monitoring ecosystems. It is able to provide consistent data on the Earth at various scales, reducing the collection of field data and ground-based observations (Khare and Ghosh 2016), making it a cost-effective tool for land-cover classification, monitoring, and environmental management (Aplin 2004). Procedures for both classifying land cover and monitoring land cover changes are extensively used in environmental management. However, classifying remotely sensed data in a thematic map remains a challenge because of the many factors involved, which may affect the success of the classification (Lu and Weng 2007), i.e., the complexity and heterogeneity of small species in the ecosystem, quality of the remotely sensed data available, as well as the image preprocessing and classification approaches. Remote sensing classification involves the selection of training samples, image pre-processing, a suitable classification model, post-classification processing, and accuracy assessment (Lu and Weng 2007). In this context, pixel-based and object-based classification approaches can be distinguished.

In the traditional pixel-based classification approaches, each pixel is identified by comparing its spectral signature value with the training samples and that pixel is labeled with the proper class based on a certain supervised algorithm (Gao et al. 2009), but neither spatial concepts nor contextual information are incorporated. Thus, the misclassification rate could be high due to the spectral similarity characteristics of some classes, the spectral variability of the canopy reflectance and the presence of mixed pixels located on the boundary between classes (Peña-Barragán et al. 2011). On the other hand, object-based image analysis or OBIA, in the geographic context (GEOBIA), was proposed as a new classification approach due to the launch of very high resolution (VHR) sensors. It offers a methodological framework, from a machine-based interpretation of complex classes, defined by the spectral, spatial, structural and hierarchical properties (Blaschke et al. 2008; Goodin et al. 2015, Oruc et al. 2004). The idea of OBIA is the segmentation of the image followed by successive analyses, usually at different hierarchical levels, in order to create relationships within segments or objects (Garcia-Pedrero et al. 2015; Lantz and Wang, 2013; Peña-Barragán et al. 2011). Given that, segmentation could be defined as a bottom-up region-merging process in which the image is subdivided into homogeneous regions according to several parameters (band weights, scale, color, shape, texture, etc.) defined by the operator, with the objective of creating object delimiting borders (Peña-Barragán et al. 2011). However, segmentation could be a challenge because the quality of the classification results depends largely on the

segments obtained, thus, it is necessary to establish a balance between efficacy and efficiency (Garcia-Pedrero et al. 2015).

As previously mentioned, remote sensing imagery requires a number of corrections and enhancements, before starting with the classification approach. Since, VHR sensors provide both a multispectral image and a panchromatic band, the quality enhancement would be carried out using an image fusion technique (pansharpening algorithm) in which the spatial resolution of the multispectral image can be improved by incorporating information from the panchromatic image (Carper et al. 1990; Chavez et al. 1991; Shettigara 1992). Extensive research into image fusion has been carried out during the last decades. Image fusion can be categorized into 3 levels: pixel level, feature level, and knowledge or decision level. Specifically, pansharpening is performed at pixel level and ideal pansharpening algorithm should have 2 main attributes (Li et al. 2012): (i) enhancing high spatial resolution; and (ii) reducing spectral distortion. The simplest pansharpening methods, at the conceptual and computation level, are Intensity-Hue-Saturation (IHS; Carper et al. 1990; Shettigara 1992), Principal Component Analysis (PCA; Chavez et al. 1991) and Brovey Transforms (Gillespie et al. 1987). However, these techniques have problems because they provide spectral distorted fused images. New approaches such as Wavelet transformation and the High Pass Filtering (Alimuddin et al. 2012; Alparone et al. 2016; Chavez et al. 1991; González-Audicana et al. 2004; Kpalma et al. 2014; Marcello et al. 2013; Pohl 2014; Vivone et al. 2015) have been proposed to address particular problems with the previous techniques (Aiazzi et al. 2002, 2006; Nuñez et al. 1999).

In addition, images acquired from VHR sensors require atmospheric corrections to transform the top of atmosphere radiance into ground reflectance by removing the atmosphere absorption and scattering effects (Marcello et al. 2016), and image orthorectification, as the topographic relief decreases or increases the radiance illuminated because of the difference in land elevation in some areas. Once images have been corrected and enhanced, the generation of products for the management of natural resources can be carried out.

In this context, the main goal in this study was to implement and assess pixel- and object-based classifiers on VHR imagery that were fused using different pansharpening techniques. Thus, the influence of fusion on the classification results was analyzed. The ultimate purpose was the development of a reliable processing methodology which, when applied to remote sensing imagery, serves to obtain accurate vegetation maps and information for the conservation of natural resources.

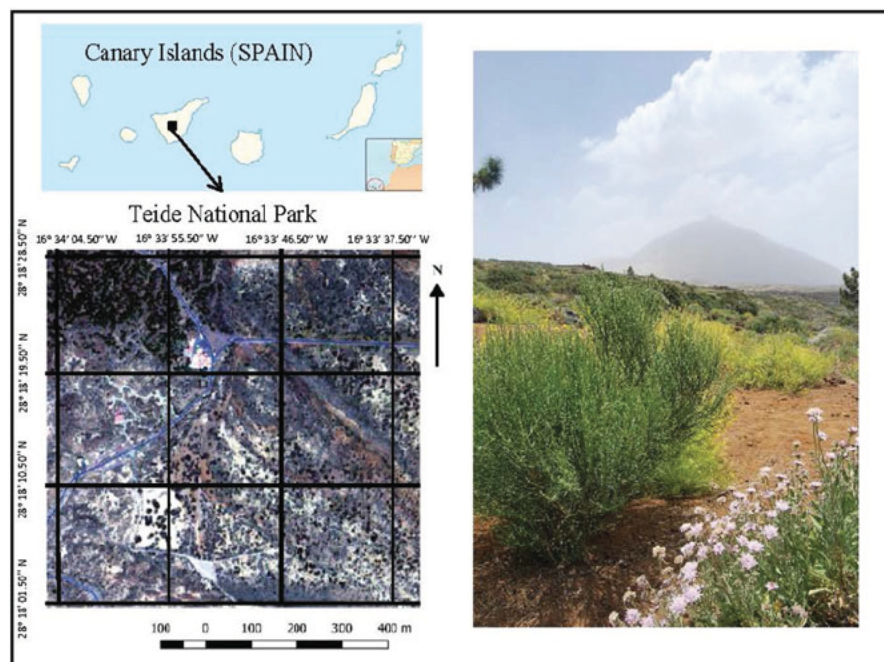


**Figure 1.** Study area of Teide National Park (Canary Islands, Spain).

Specifically, a very complex shrubland ecosystem has been selected to perform the analysis.

The article is structured as follows: The 2nd section includes the study area and a description of the data sets, the image fusion methods, and the different classification techniques applied at pixel- and object-based levels. The analysis and evaluation of the different techniques, as well as the thematic maps obtained are presented in the 3rd section. Finally, the last section includes a critical analysis of the results and summarizes the main outcomes and contributions.

## Material and methods

### Study area and dataset

A heterogeneous ecosystem of The Canary Islands ( $28^{\circ} 06' N$ ;  $16^{\circ} 33' W$ ) was selected for this study: the Teide National Park located on the island of Tenerife (Figure 1). The Teide National Park, created in 1954, is a protected area with 18,990 hectares (Martín-Osorio et al. 2005), located on the island of Tenerife. The Teide National Park area is a giant crater situated in the center of the island. Teide is made up by several overlapping volcanoes in the middle of the giant crater, making it the highest mountain in Spain (3,718 m; González-Lemus et al. 2009). As already mentioned, the vegetation is vulnerable to environmental changes. Thus, the plants respond to thermic and hydric stress, a characteristic of a mountain ecosystem with a shrub physiognomy (Arozena-Concepción and Beltrán-Yanes 2006).

The following non-herbaceous vegetation species were selected for the study by the experts of the National Park, due to their abundance and importance at the ecological level: *Spartocytisus supranubius* (Teide broom), *Pteroccephalus lasiospermus* (Rosalillo de cumbre), *Descurainia bourgaeana* (Hierba pajonera), and *Pinus canariensis* (Canarian pine; Figure 2). All of them are addressed in this article as “vegetation classes.” Moreover, urban, road, and bare soil classes were also included in the classification.

The Teide broom (*Spartocytisus supranubius*; Bonet et al. 2009) is a broom-like shrub reaching a height of 2 m–3 m, moreover it is a strong competitor and its growth is a major factor affecting the composition of plant species (Kyncl et al. 2006). *S. supranubius* is 1 of the most important plant species as is *Pteroccephalus lasiospermus* (Rosalillo de cumbre) and *Descurainia bourgaeana* (Hierba pajonera; Arozena-Concepción and Beltrán-Yanes 2006). *P. lasiospermus* is a small shrub characterized by pink flowers appearing in the spring and *D. bourgaeana* is a shrub that can be easily distinguished by its semi-spherical shape and its flowers of yellow petals. Another significant plant species is the Canary pine (*Pinus canariensis*), the only native pine in the archipelago, which is found in the northern area of the park. This species has a great resistance to fire and cold temperatures (Garzón-Machado et al. 2011; Otto et al. 2012; Wildpret de la Torre 2001). Other similar shrubland ecosystems can be identified around the world, for example: Pico do Pico in the Azores, Mt. Halla in South Korea, and Hawaii or the Galapagos Islands, some areas





**Figure 2.** Vegetation field campaign in the Teide National Park: (a) *Spartocytisus supranubius*; (b) *Pteroccephalus lasiospermus*; (c) *Descurainia bourgaeana*; and (d) *Pinus canariensis*.

of Okanagan Desert in Canada. Thus, the importance of studying this ecosystem is its similarity to other Mediterranean, temperate or tropical parts of the world (Ruocco et al. 2014).

Worldview-2 (WV-2) orthoready imagery was used in the study. The WV-2 satellite, launched by DigitalGlobe on October 8, 2009, was the first commercial satellite to have a very high spatial resolution sensor with 1 panchromatic and 8 multispectral bands. The Teide image was acquired on May 16, 2011, in the spring season as the vegetation species has greater spectral separability (González-Lemus et al. 2009; Wildpret de la Torre 2001).

### Image corrections and enhancements

Numerous methodological problems are associated with the use of data from VHR sensors (Franklin and Wulder 2002), thus, several image enhancements must be carried out in order to reduce these problems and to obtain high quality products which will allow a comprehensive and useful analysis of the natural resources.

### Pansharpening techniques

The first step was to generate a pixel-level fused image, with a high spatial and spectral quality, using a pansharpening process. The enhancement is important in this type of heterogeneous ecosystem due to the small size of some vegetation classes. After a comprehensive review of the state-of-art (Ibarrola-Ulzurrun et al. 2017), 7 pansharpening methods were applied (for detailed information see the references):

- Gram-Schmidt (GS): A low-resolution PAN image is simulated and the GS transformation is performed on the simulated PAN plus the MS bands. Then, the original PAN replaces the first GS band and the inverse transform is applied (Laben and Brower 2000).
- Fast Intensity Hue Saturation (FIHS): It uses the spectral bands and the IHS transformation to estimate the new component  $I$ . The spatial detail is

extracted, computing the difference between the panchromatic band and  $I$ . Finally, it is injected into the multispectral bands (Marcello et al. 2013; Tu et al. 2001; Vivone et al. 2015).

- Hyperspherical Color Sharpening (HCS): It is an algorithm specifically designed for the WV-2 sensor, based on the transformation between any native color space and the hyperspherical color space (Li et al. 2012, 2013; Padwick et al. 2010; Tu et al. 2012; Wu et al. 2015).
- Based Modulation Transfer Function (MTF): The trendy implementations provided by Vivone et al. 2015 (<http://openremotesensing.net/knowledgebase/a-critical-comparison-among-pansharpening-algorithms/>) of 2 different MTF fusion algorithms were used: the one based on Generalized Laplacian Pyramid (MTF\_GLP; Aiazzi et al. 2002, 2006) and the Generalized Laplacian Pyramid plus a High Pass Modulation (MTF\_GLP\_HPM; Burt and Adelson 1983; Aiazzi et al. 2002, 2006; Amro et al. 2011).
- Wavelet 'à trous' (WAVE\_ATROUS): The fused images are obtained by adding the panchromatic wavelet planes to the multispectral image approximation (Amolins et al. 2007; Amro et al. 2011; Dutilleux et al. 1987; Gonzalo-Martín and Lillo-Saavedra 2008; Lillo-Saavedra and Gonzalo 2006; Marcello et al. 2013; Wald et al. 1997).
- Weighted Wavelet 'à trous' method through Fractal Dimension Maps (WAT $\otimes$ FRAC; Lillo-Saavedra and Gonzalo 2006): It is based on the wavelet 'à trous'. A mechanism that controls the trade-off between the spatial and spectral quality by introducing a weighting factor for each band  $\alpha_i(x, y)$  for the panchromatic wavelet coefficients is established and defined as Fractal Dimension Map with the same size as the original image (Lillo-Saavedra et al. 2011). These maps are generated for each of the source images with the box-counting algorithm and by applying a windowing process. Each element in these maps provides a different weighting value for each pixel and each band.

Quality evaluation is a fundamental issue to benchmark and optimize different pansharpening algorithms (Marcello et al. 2013; Rodríguez-Esparragón 2015; Wald 2000; Wang and Bovik 2002). A visual and quantitative assessment was undertaken in order to evaluate the pansharpening results in the different fused images. The quality assessment was carried out for the whole set of bands. In the study, a number of statistical evaluation indices were used to measure the quality of the fused images at the spectral, spatial and global level (Alparone et al. 2008; Kpalma et al. 2014; Shridhar and Alvarinho 2013). The indices applied to measure the spectral quality of the fused images, which take the original multispectral bands as a reference, were: Spectral Angle Mapper (Kruse et al. 1993; best value closer to 0) and Spectral ERGAS (Wald, 2000; best values closer to 0, but usually between 0–3). The spatial quality assesses the spatial detail injected and the panchromatic band was chosen as a reference. The indices considered were: Spatial ERGAS (Lillo-Saavedra et al. 2005; best values closer to 0, but usually between 0–3); Frequency Comparison (Rodríguez-Esparragón et al. 2014; values between 0–1, best closer to 1); and Zhou Index (Zhou et al. 1998; values between 0–1, best closer to 1). Finally, at global level the Q8 index, which is a generalization of the Q index, (Wang and Bovik 2002) and of the Q4 index (Alparone et al. 2004), with values between 0–1 (best closer to 1), was used to measure correlation, mean shifts, and radiometric distortion simultaneously (Marcello et al. 2013).

As the Teide ecosystem is very heterogeneous and composed by small shrubs, pansharpening will be very important to achieve reliable vegetation maps. Also, both qualities will be critical, the spatial to discriminate the small plants and the spectral to differentiate similar covers. As indicated in Thomas et al. (2008), the ideal fusion method does not exist yet, but the fused results generally correspond to a tradeoff between a good geometrical representation of structures and a good representation of spectral information.

#### **Orthorectification and atmospheric correction**

After detailed assessment of different image and model-based atmospheric corrections algorithms using WV-2 imagery and field spectroradiometer data collected simultaneously (Marcello et al. 2016), the FLAASH algorithm (Adler-Golden et al. 1999) achieved the best performance. The appropriate atmospheric parameters were adjusted (atmospheric model, aerosol model, aerosol optical thickness, adjacency, etc.) using climatologic information and field data and the average reflectance estimations achieved a Root Mean Square Error (RMSE) around 3% when compared to the in-situ measurements. Orthorectification, using the Rational Polynomial Coefficients model,

was carried out using ENVI 5.0 software (ENVI 2004) and the average RMSE after the orthorectification was 3.11 m for geodesic points located in the park.

#### **Segmentation at object-based approach**

The OBIA process starts with a segmentation of the input images into local groups of pixels (segments) that become spatial units in the later classifications and accuracy assessment. The object shape, size and spectral properties depend on both the segmentation approach and the research goals. The ideal purpose of the segmentation is to approximate meaningful landscape entities recognizable at a given image resolution (Dronova 2015). Image segmentation in eCognition is not a straightforward process and finding useful segmentation levels is an iterative process (Walsh et al. 2008). The most popular segmentation carried out by eCognition users (Burnett et al. 2003; Dronova 2015; Lu and Weng 2007; Walsh et al. 2008) is *Multiresolution Segmentation*. It is regarded as a region-based algorithm, which starts by considering each pixel as a separate object. Subsequently, pairs of image segments are merged to form bigger segments. The decision to merge is based on the homogeneity criterion, which measures how homogeneous or heterogeneous an image object is within itself. The derived image objects in eCognition are determined by the following parameters (Baatz et al. 2001):

- *Weight* of image channels to assign different importance to each image band.
- *Scale* to determine the maximum heterogeneity of the objects allowed. Smaller scales increase the dimensionality and the division of the objects into the sub-groups, while larger scales combine the multi-segments into 1 (Marangoz et al. 2006).
- *Shape* to adjust the homogeneity of the object generation.
- *Compactness* to determine whether the objects will become more compact or smoother.

Once the *Multiresolution Segmentation* was performed, *Spectral Difference* algorithm was used to merge neighboring image objects when the difference between their layers mean intensities are below the value given by the maximum spectral difference (Baatz et al. 2001).

#### **Classification models**

Several classification techniques were applied in the study. The first step was to determine the classes appearing in the image and to obtain a set of training and testing samples. The size and representativeness of the set of the training samples are critical for image classification (Lu and Weng 2007). The second step was to determine the classification

**Table 1.** Pixel-based and object-based classification algorithms and their parameters.

Classification Approach	Classification Algorithm	Parameters
Pixel-based approach	Maximum Likelihood Mahalanobis Distance Support Vector Machine	Threshold: 0.25 Maximum distance error: None Kernel: Radial basis function Gamma in kernel function: 0.5 Penalty parameter: 200
Object-based approach	Bayes Nearest Neighbor K-Nearest Neighbor Support Vector Machine	eCognition does not allow to set parameters with this classifier eCognition does not allow to set parameters with this classifier K: 20 Kernel: Radial basis function Gamma in kernel function: 0.5 Penalty parameter: 200

model to be used and which classifier apply in each model. An evaluation of the parameters chosen in each classifier was performed. However, these parameters are image dependent, and the user should analyze which parameters are more suitable for their images. The 2 classification approaches considered here were pixel-based, which was carried out using ENVI 5.0 image processing software (Exelis Visual Information Solutions, Inc., a subsidiary of Harris Corporation); and object-based using eCognition Developer (Trimble Geospatial). eCognition is optimized for the cost-effective OBIA classification of VHR imagery.

The classification models selected for carrying out the pixel-based classification approach are Maximum

Likelihood, Mahalanobis Distance, and Support Vector Machine. Regarding the OBIA approach, Bayes, Nearest Neighbor, K-Nearest Neighbor, and Support Vector Machine were selected (Table 1). For choosing the classifiers' parameters, different trials were performed and evaluated until obtaining the most suitable parameter value for each classifier.

Thematic maps were obtained after applying the different classification techniques using the same training samples. Afterwards, the accuracy of the classification was measured by using the testing samples collected. In order to obtain a reliable thematic map, the training and testing samples were selected with the help of Teide

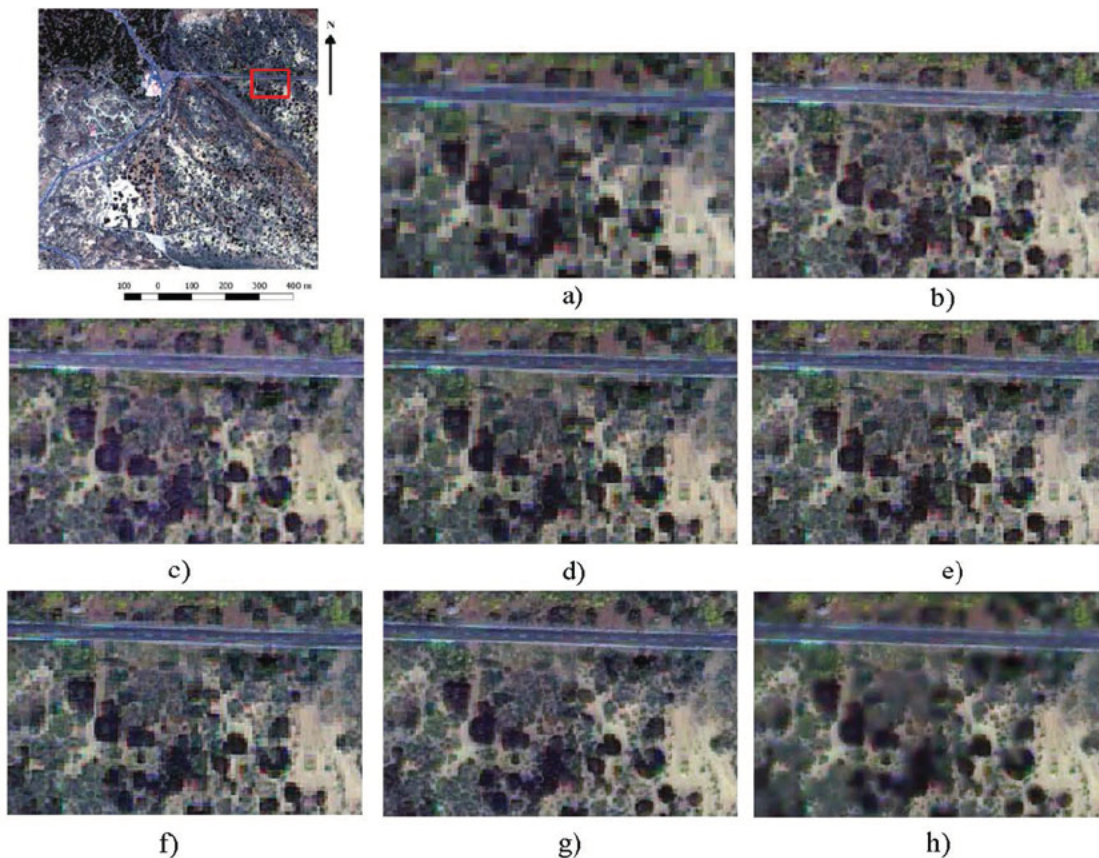


**Figure 3.** True color images of the Teide National Park: (a) original multispectral image; and fused imagery using: (b) GS; (c) FIHS; (d) HCS; (e) MTF\_GLP; (f) MTF\_GLP\_HPM; (g) WAVE\_ATROUS; and (h) WAT $\otimes$ FRAC.

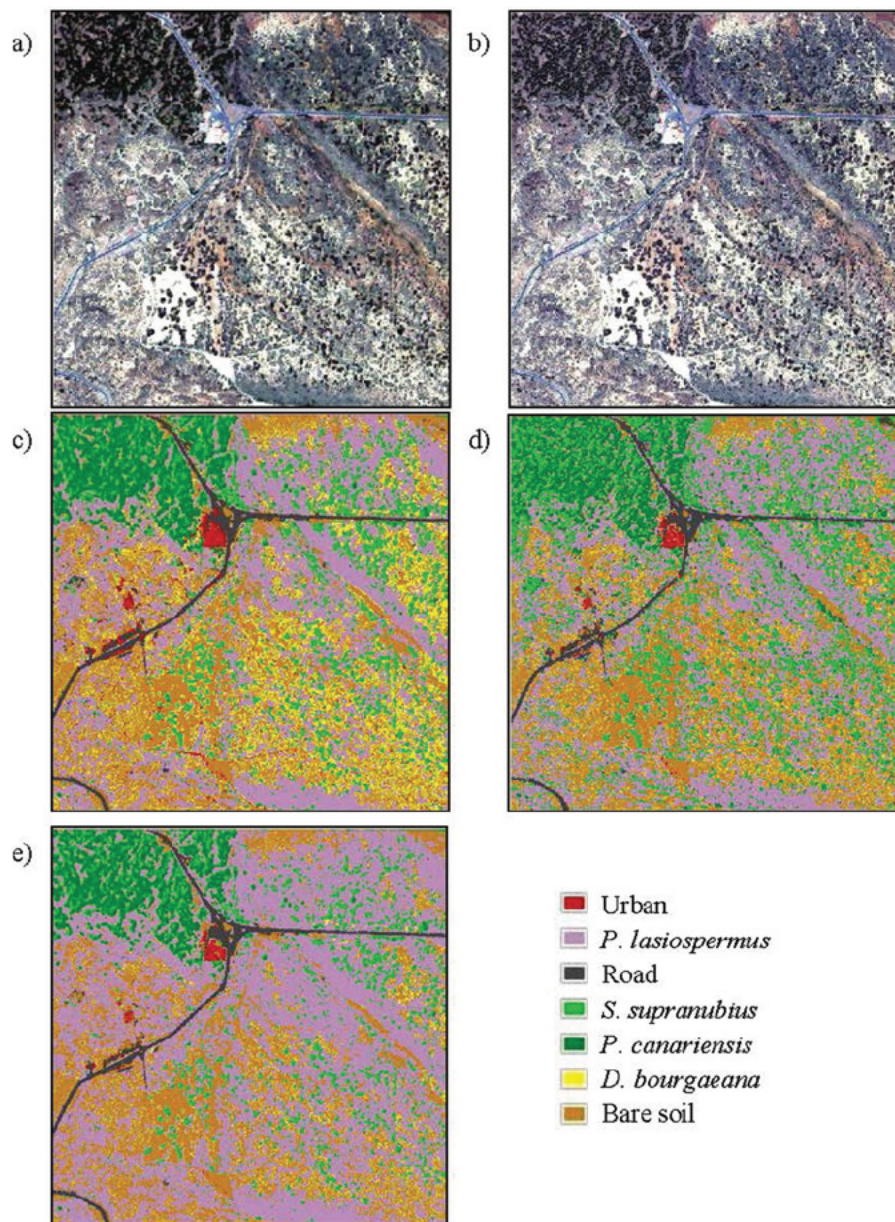


**Figure 4.** RGB color composite: (a) WAT $\otimes$ FRAC fused image and (b) WAVE\_ATROUS fused image; and thematic maps using: (c) Maximum Likelihood in WAT $\otimes$ FRAC fused image; (d) Mahalanobis Distance in WAVE\_ATROUS fused image; and (e) Support Vector Machine in WAT $\otimes$ FRAC fused image.

National Park experts from well-known sites around the park and using the ground truth samples obtained during the fieldwork carried out in the study area, which were used for the training and testing phases in the classification process. The method used for choosing the samples was a random method in which a total of 362,631 pixels (ca. 70% of the total samples) were chosen as training samples and 159,182 pixels (ca. 30% of the total samples) for the testing.

The statistical accuracy assessment technique used in the study was the standardized confusion Error Matrix which reports 2 measurements of accuracy: Overall Accuracy and Kappa coefficient (Congalton 1991). It is

more appropriate in difficult classification approaches, assuming that the map categories are mutually exclusive and exhaustive and that each location belongs to a single category. On the other hand, the Kappa coefficient is a measure of overall statistical agreement, which takes non-diagonal elements into account (Lu and Weng 2007).

### Results and discussion

The following results are presented as: (i) analysis and evaluation of the fused images quality obtained through the different pansharpening techniques; (ii) accuracy of

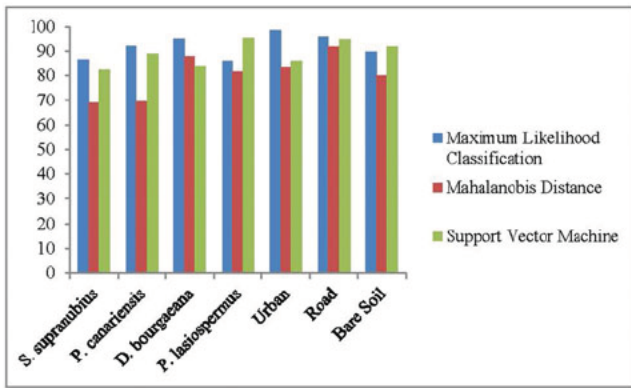


**Figure 5.** Classification overall accuracy in percentage (%) of each class and classifier in the fused imagery. X axis: classes; Y axis: percentage value.

the pixel-based thematic maps obtained for each fused image; and (iii) accuracy of the OBIA classification results obtained for each fused image.

### Pansharpening results

In this section, a visual and a quantitative assessment of the fused images are presented. To facilitate the visual inspection and for a detailed spatial analysis, a zoom of the complete scene is shown in Figure 3.

The visual interpretation at the spectral level in the image indicates that every algorithm seems to correctly preserve the spectral information in the fused image. Moreover, the differences are clearer spatially than spectrally. For HCS and MTF-based techniques, although they maintain the spectral information well, the spatial details are not satisfactorily injected, thus not achieving a good spatial enhancement. This smoothed aspect appearing in the image is because the algorithm makes uniform the areas with a common texture. Thus, Dimensional Fractal Maps are calculated into the MS and the PAN image, giving information regarding roughness in the image areas. Then, a small amount of the spatial information is incorporated in homogeneous areas, maintaining a more homogeneous spectral response, closer to the original multispectral image, avoiding in this way, the 'salt&pepper' effect.

As it was mentioned, in order to carry out an objective evaluation of the pansharpening techniques, 6 quality indices were computed. The results are presented in Table 2. Spectral Quality indices and Q8 confirm that MTF methods provide better spectral performance while WAVE\_ATROUS gets, in general, the lowest spectral quality, even though there is not great difference between the highest and the lowest result. As regards the spatial performance, WAVE\_ATROUS is confirmed as the best spatial quality method. Furthermore, these

results confirm the trade-off between the spectral and spatial quality of pansharpening techniques. As next presented, WAT $\otimes$ FRAC will be the most suitable technique followed by WAVE\_ATROUS, taking into account the balance between a good geometrical representation of structures and a good representation of spectral information (Thomas et al. 2008).

### Pixel-based classification results

Before performing the classification process, the Jeffries-Matusita Distance algorithm was carried out in order to check the ROIs separability. This distance provides for most of the class pairs a value of higher than 1.8, indicating a good separability for most of the ROIs.

Three supervised classification methods were applied to each fused image (Table 1). Table 3 shows the Overall Accuracy as well as the Kappa coefficient for each classification technique applied to each fused image.

The best result for both Maximum Likelihood and Support Vector Machine classification is obtained in the WAT $\otimes$ FRAC fused image, whereas the WAVE\_ATROUS fused image obtains the best accuracy with Mahalanobis Distance classification. Every classifier performs a good classification, which is more significant both in Maximum Likelihood and Support Vector Machine, with Kappa coefficients of 0.76 and beyond. Furthermore, the Support Vector Machine achieves the highest accuracy with the WAT $\otimes$ FRAC fused image. Finally, it is observed how the WAVE\_ATROUS and WAT $\otimes$ FRAC algorithms, which obtain higher values in the quantitative spatial indices (Table 2), improve the classification compared with the original multispectral image and the remaining pansharpening techniques. These results highlight the importance of the spatial information in the Teide National Park where vegetation species are mixed and are limited in size.

In more detail, thematic maps for the best pansharpening algorithm are shown in Figure 4 for Maximum Likelihood, Mahalanobis Distance, and Support Vector Machine.

According to Figure 4c, although the best Maximum Likelihood Classification obtains an Overall Accuracy of 89.12%, some misclassifications appear in this thematic map. For instance, some pixels which are classified as urban (red) appear in bare soil areas, as well as some road pixels in areas of bare soil. Moreover, due to the field observations and information from the Teide managers, an excess of *D. bourgaeana* appears in the classified image (too many yellow pixels). In addition, *S. supranubius* must be less abundant around *P. canariensis* in the ecosystem (top left in the thematic map). For the best Mahalanobis Distance method, similar misclassified pixels to those of the Maximum Likelihood Classification

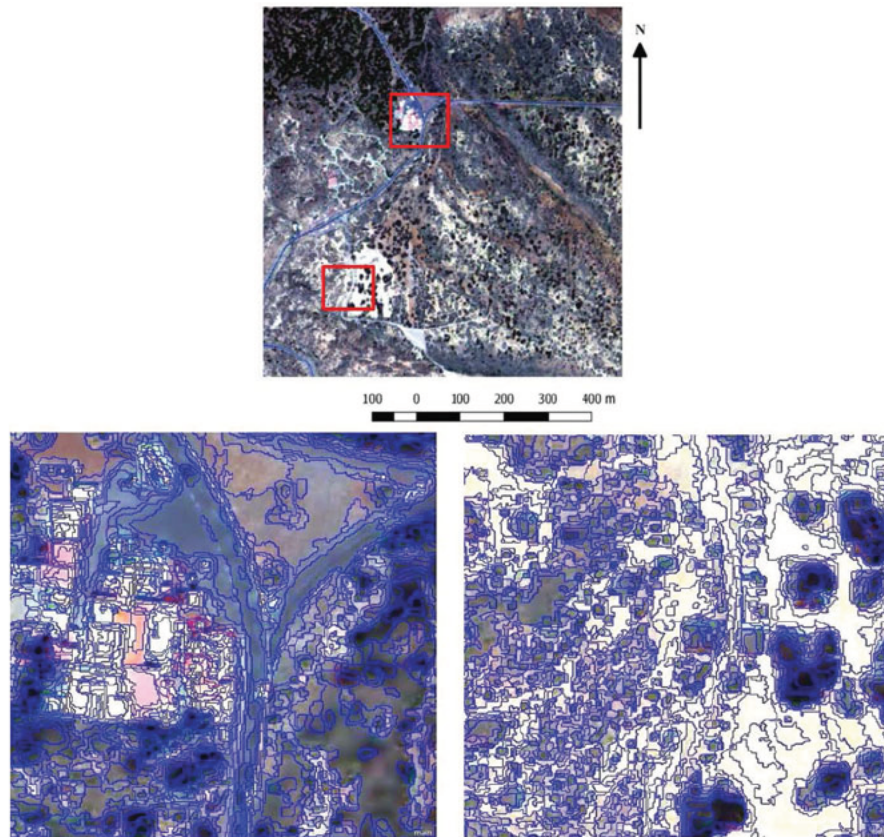


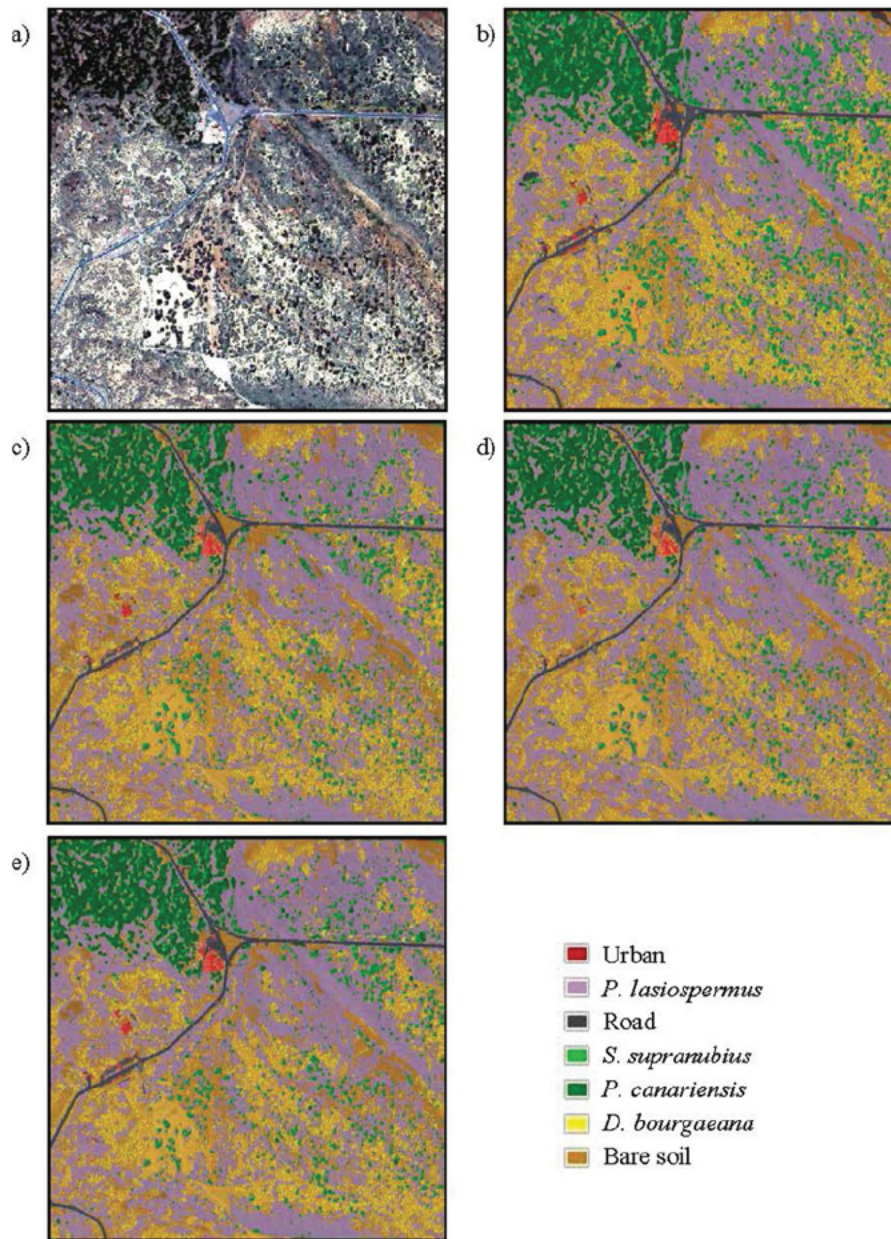
Figure 6. Multiresolution segmentation and spectral difference segmentation results.

Table 2. Quality results for the complete WV-2 bands (best results in bold).

	Spectral Quality		Spatial Quality			Global Quality
	SAM	Spectral ERGAS	Spatial ERGAS	FC	Zhou	Q
GS	4.098	1.704	0.899	0.842	0.736	0.935
FIHS	3.781	1.683	0.894	0.840	0.719	0.898
HCS	3.516	0.387	0.908	0.775	0.669	0.932
MTF_GLP	<b>3.212</b>	1.245	0.903	0.785	0.650	<b>0.961</b>
MTF_GLP_HPM_NM	3.872	<b>0.334</b>	0.888	0.809	0.706	0.921
WAVE_ATROUS	4.588	1.753	<b>0.749</b>	<b>0.935</b>	<b>0.994</b>	0.879
WAT⊗FRAC	4.187	1.445	0.824	0.864	0.892	0.901

Table 3. Accuracy assessment of the pixel-based classification algorithms for each fused image (the best results are in bold).

Classification Techniques	Maximum Likelihood		Mahalanobis Distance		Support Vector Machine	
	Overall Accuracy	Kappa	Overall Accuracy	Kappa	Overall Accuracy	Kappa
Pansharpening Algorithms						
Multispectral	85.06%	0.79	72.89%	0.64	89.60%	0.85
GS	82.73%	0.76	74.28%	0.65	88.45%	0.85
FIHS	83.71%	0.77	76.14%	0.67	88.83%	0.84
HCS	82.99%	0.76	74.33%	0.65	88.90%	0.84
MTF_GLP	85.36%	0.8	74.87%	0.66	88.51%	0.83
MTF_GLP_HPM	82.78%	0.76	73.68%	0.64	88.64%	0.83
WAVE_ATROUS	88.74%	0.84	<b>80.79%</b>	<b>0.73</b>	92.15%	0.89
WAT⊗FRAC	<b>89.12%</b>	<b>0.85</b>	80.41%	0.73	<b>92.75%</b>	<b>0.89</b>



**Figure 7.** (a) WAT@FRAC RGB color composite; and thematic maps: (b) Bayes; (c) Nearest Neighbor; (d) K-Nearest Neighbor; and (e) Support Vector Machine.

appear. Nevertheless, the abundance of pixels classified as *D. bourgaeana* decreases compared with the Maximum Likelihood result while *S. supranubius* class increases in some areas where, according to expert opinion, it does not have to appear in these areas. Finally, the Support Vector Machine thematic map achieves the highest Overall Accuracy (92.75%). Despite the improvement using the Support Vector Machine classifier, the computation time with it was significantly higher, more than 24 hours, than the other 2 classifiers, which took a few minutes in the same computer.

In order to identify the best methodology (pansharpening + classification model) to properly discriminate

the vegetation classes, Figure 5 displays the classification overall accuracy chart for each class in each pixel-based approach for the pansharpening algorithm achieving the best performance. Observing the classes, it is noted that Maximum Likelihood classifier obtains higher values in the different classes than other classifiers except for *P. lasiospermus* and bare soil, even though the best Overall Accuracy and Kappa coefficient is achieved by Support Vector Machine classifier. This fact is important due to the aim of the study, which is to obtain the best plant species classification map. However, as it was mentioned, Figure 4c shows some misclassifications when using Maximum Likelihood classifier.

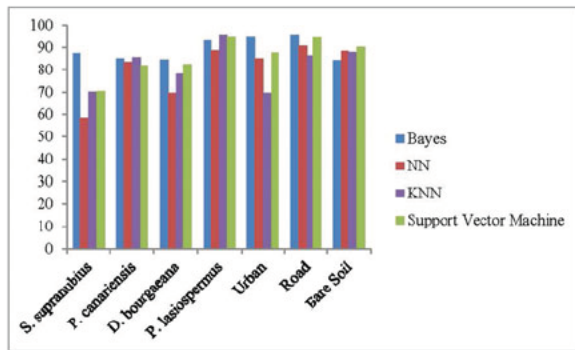


**Figure 8.** Classification overall accuracy in percentage (%) of each class and classifier in the fused image. X axis: classes; Y axis: percentage value.

### Object-based classification results

#### Image segmentation

The image was segmented using the aforementioned *Multiresolution Segmentation* technique to generate first, 8 different object-oriented segmentations to select the most suitable Image Layer Weight and Scale parameters. The segmentation parameters were selected by a visual evaluation and applying a Support Vector Machine classification technique with the training and testing samples obtained in the field work. Both the Overall Accuracy and the Kappa coefficient were analyzed in order to evaluate the most suitable segmentation parameters. The greater the accuracy, the better the adjustment of the segmentation parameters with the image objects. Tables 4 and 5 details some of the Scale parameters and criterion combinations used, as well as the classification accuracy obtained in each segmentation. Test Number 8 shows the most suitable segmentation for the Image Layer Weights and Scale parameters, which is revealed in the classification results.

Figure 6 shows a zoom of the segmentation results, in which objects preserve small shrubs which are difficult to delimitate.

#### OBIA classification

Once the objects are obtained from the segmentation techniques, classification algorithms can be applied. The classification algorithms analyzed and the parameters used are shown in Table 1.

Table 6 shows the Overall Accuracy and the Kappa coefficient for each object-based classification technique applied to each fused image. By analyzing the table, every classifier obtains the best accuracy result in the WAT $\otimes$ FRAC fused image. Overall Accuracy and Kappa coefficient values are similar to the pixel-based classification results (Table 3), with the Support Vector Machine classifier, once again, obtaining the best overall accuracy result. The table shows how the classification accuracy is, in general, improved in images fused with

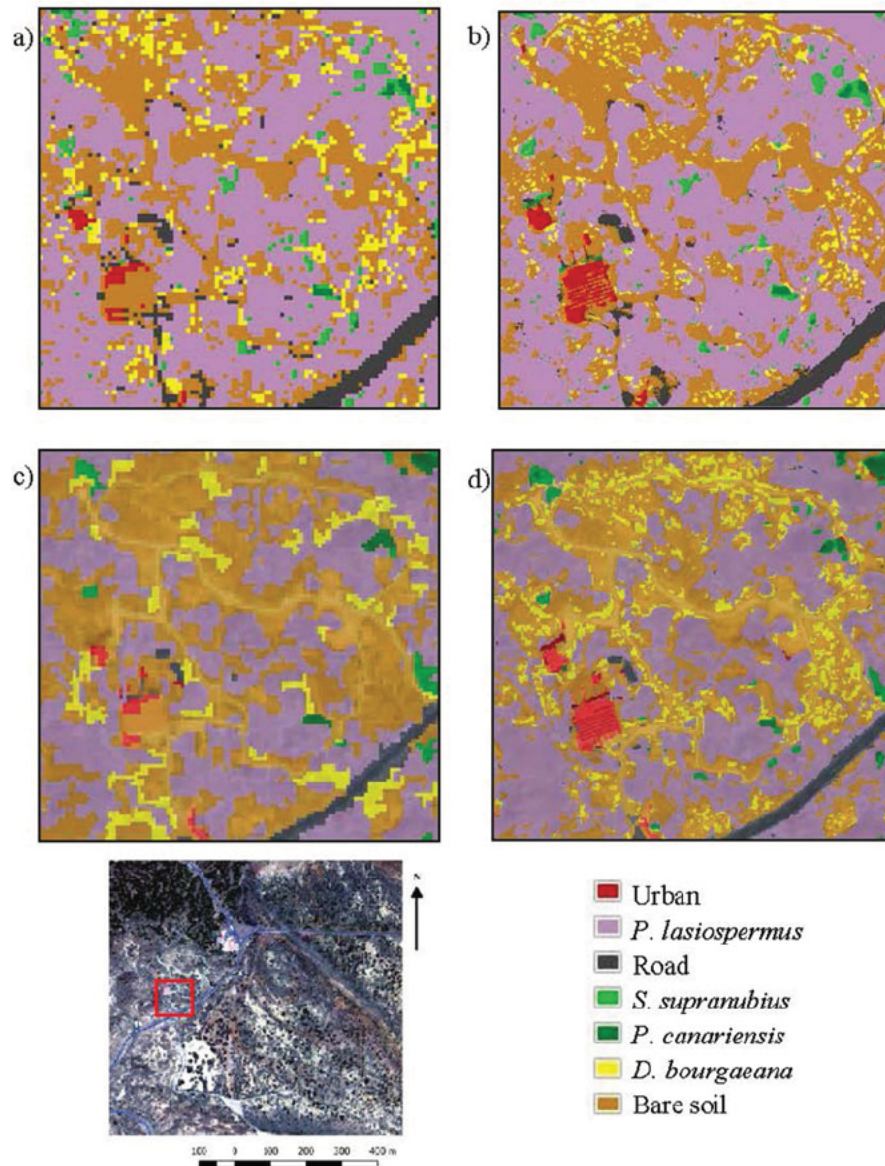
algorithms that preserve the spatial and spectral quality (WAVE\_ATROUS and WAT $\otimes$ FRAC), compared with the original multispectral image. The most accurate thematic maps of each classifier are shown in Figure 7.

Figure 7 shows the WAT $\otimes$ FRAC fused image and each classification map using Bayes, Nearest Neighbor, K-Nearest Neighbor, and Support Vector Machine. In the case of the Bayes classifier some objects which are classified as urban areas appear as bare soil areas and road objects in areas of bare soil, like the Maximum Likelihood Classification in the pixel-based approach. In the Nearest Neighbor classification, the misclassifications obtained in the Bayes classifier are resolved, observing a more accurate thematic map at first sight, as well as K-Nearest Neighbor classifier, which shows a similar thematic map. Finally, the Support Vector Machine map is similar to the previous ones.

Figure 8 summarizes the classification overall accuracy, in percentage, of each class and for each OBIA classification approach applied to the WAT $\otimes$ FRAC fused image. Bayes provides a high percentage of accuracy, obtaining the highest results for most of the vegetation classes. While the Nearest Neighbor, the vegetation classes have a lower percentage of accuracy, achieving the lowest for *S. supranubius*. Regarding the K-Nearest Neighbor classifier, it achieves a high degree of accuracy for *P. lasiospermus*, which is a significant class of interest for the ecosystem management of this region. On the other hand, the misclassifications obtained in the other 3 types of vegetation improved with respect to the Nearest Neighbor classification. Support Vector Machine, even though achieving the highest Overall Accuracy and Kappa coefficient (Table 6), these results do not appear in the ones obtained in the classification accuracy of each class (Figure 8).

It is important to note the good results obtained using the WAT $\otimes$ FRAC algorithm in both pixel-based and object-based approaches. Although the best overall accuracy is obtained by the Support Vector Machine in both cases, not only the computation times for the pixel-based approach are much higher than for the OBIA approach but Maximum Likelihood Classification and Bayes classifier obtain higher accuracies for the majority of vegetation classes of interest. However, as it was mentioned, the visual assessment obtained with Maximum Likelihood classification does not fully correspond with the experts' opinion. This leads to the Bayes classification, at OBIA approach, applied to the WAT $\otimes$ FRAC fused image being the most suitable classifier in order to obtain fast and accurate thematic maps of these difficult heterogeneous shrub-land ecosystems. Even though it does not achieve the highest overall accuracy (Table 6), it is closer to the Support Vector Machine classifier but obtaining higher classification accuracies for each class.





**Figure 9.** Zoom of the thematic maps obtained by the SVM classifier applied at pixel-based approach in: (a) Original multispectral image and (b) WAT ⊗ FRAC fused image; and at OBIA approach in: (c) Original multispectral image and (d) WAT ⊗ FRAC fused image.

**Table 4.** Accuracy assessment of Image Layer Weight (Worldview-2 bands), and scale segmentation parameters (best result appears in bold).

Number	Segmentation				Classification	
	Image Layer Weights	Scale	Shape	Compactness	Overall Accuracy	Kappa Coefficient
1	1,1,1,1,1,1	5	0.1	0.5	78.67%	0.70
2	1,1,1,1,1,1	10	0.1	0.5	88.11%	0.83
3	1,1,1,1,1,1	15	0.1	0.5	87.97%	0.83
4	1,1,1,1,1,1	20	0.1	0.5	88.00%	0.83
5	1,1,1,1,1,1	12	0.1	0.5	88.08%	0.83
6	1,1,1,2,1,1	12	0.1	0.5	88.20%	0.83
7	1,1,1,1,2,1	12	0.1	0.5	87.92%	0.83
<b>8</b>	<b>1,1,1,1,1,2,2</b>	<b>12</b>	<b>0.1</b>	<b>0.5</b>	<b>88.29%</b>	<b>0.83</b>

**Table 5.** Accuracy assessment of compactness and shape segmentation parameter using the Image Weight Layer: 1, 1, 1, 1, 1, 2, 2 and with a Scale: 12 (best result appears in bold).

		Shape								
		0.1	0.2	0.3	0.4	<b>0.5</b>	0.6	0.7	0.8	0.9
Compactness	0.1	88.44	88.40	88.59	88.72	<b>88.83</b>	88.46	88.06	87.96	85.63
	0.2	87.68	88.30	88.72	88.67	88.34	88.69	88.00	87.20	86.14
	0.3	88.07	88.36	88.58	88.50	88.21	88.47	87.95	87.00	84.85
	0.4	87.90	88.70	87.85	88.70	88.54	88.54	87.80	86.69	84.97
	0.5	88.11	88.06	88.78	88.57	88.30	87.99	87.97	86.46	84.85
	0.6	88.54	87.67	88.42	88.79	88.58	87.84	87.41	86.36	84.28
	0.7	88.36	88.08	88.16	88.80	88.35	88.00	87.17	85.88	83.44
	0.8	88.47	88.46	87.86	88.18	88.24	86.86	86.89	85.53	83.77
	0.9	88.33	88.07	87.97	88.14	87.43	86.08	86.74	85.67	84.40

**Table 6.** Accuracy assessment of the object-based classification algorithms for each fused and segmented (Multiresolution Segmentation and Spectral Difference) image (the best results are in bold).

Classification Techniques	Bayes		NN		K-NN		Support Vector Machine	
	Ov. Acc.	Kappa	Ov. Acc.	Kappa	Ov. Acc.	Kappa	Ov. Acc.	Kappa
Pansharpening Algorithms								
Multispectral	79.48%	0.71	77.58%	0.67	77.67%	0.67	80.61%	0.72
GS	77.80%	0.69	77.93%	0.68	81.50%	0.73	82.41%	0.74
FIHS	81.92%	0.74	79.25%	0.70	82.77%	0.75	83.72%	0.76
HCS	78.27%	0.70	79.1%	0.70	82.30%	0.74	82.72%	0.74
MTF_GLP	75.12%	0.66	76.37%	0.66	81.16%	0.73	83.14%	0.75
MTF_GLP_HPM	78.27%	0.70	77.92%	0.68	82.55%	0.74	83.18%	0.75
WAVE_ATROUS	86.04%	0.80	82.84%	0.75	85.22%	0.78	87.68%	0.82
WAT $\otimes$ FRAC	<b>89.14%</b>	<b>0.84</b>	<b>84.07%</b>	<b>0.77</b>	<b>88.54%</b>	<b>0.83</b>	<b>89.39%</b>	<b>0.85</b>

Note. Ov. Acc. = Overall Accuracy.

**Table 7.** Computation times (minutes) of the different classifiers in pixel based (using ENVI) and in OBIA (using eCognition) approaches.

	Pixel-Based Approach			OBIA Approach			
	Maximum Likelihood	Mahalanobis Distance	Support Vector Machine	Bayes	NN	KNN	Support Vector Machine
Computation Time (min)	8	11	1,518	0.18	1.2	1.3	1.6

Table 7 shows the computation times of each classifier in both approaches, using a computer with Windows 10 of 64 bits, Intel<sup>®</sup> Core<sup>™</sup> i7-490 CPU @ 360 GHz with 32.0 GB of RAM. Note that the computation times of OBIA classifiers were significantly lower than the ones using the pixel-based approach, especially the Support Vector Machine, which took hours to obtain the classification maps in the pixel-based approach.

In order to visually assess how the pansharpening process improves the result in the thematic maps, a final figure (Figure 9) shows zooms of the thematic maps obtained using both Support Vector Machine algorithm on the original multispectral and the WAT $\otimes$ FRAC fused images in both pixel and OBIA approaches. We have decided to show Support Vector Machine results because it obtained the most suitable classification in the pixel-based approach and, thus, it is possible to compare the same classification result using the same classifier in the 2 different approaches (pixel- and object-based). The importance of pansharpening is observed as some classes

of interest are not well labeled in the original multispectral thematic maps (Figure 9a). On the other hand, buildings are erroneously classified as bare soil in the original multispectral image and road limits are stepped due to the pixel size in the original image. Moreover, the poor quality of the classification is appreciated when applying OBIA to the Multispectral image, however, when it is applied to the fused image, the contours of the covers are smoother and it reduces the salt and pepper effect.

## Conclusions

The main objective of the presented work was to study the pansharpening influence on obtaining accurate thematic maps, applying pixel-based and OBIA classification techniques on VHR imagery from a complex and heterogeneous ecosystem. Thus, 7 different pansharpening techniques (GS, FIHS, HCS, MTF\_GLP, MTF\_GLP\_HPM, WAVE\_ATROUS, and WAT $\otimes$ FRAC) were applied to achieve the highest spatial resolution of the multispectral

bands while preserving its original spectral information. Several classification algorithms were next applied at the pixel-based level (Maximum Likelihood Classification, Mahalanobis Distance, and Support Vector Machine) and at the object-based level (Bayes, Nearest Neighbor, K-Nearest Neighbor, and Support Vector Machine).

First, visual and quantitative quality assessment of the 7 pansharpening techniques was performed. A good compromise between the spatial and spectral quality is a requirement of the study. This compromise is noted after analyzing the results from the 6 quality metrics. MTF methods achieve the best spectral performance, while WAVE\_ATROUS achieves the best spatial quality. WAT $\otimes$ FRAC provides a suitable balance between the geometrical representation of structures and representation of original spectral information.

Next, detailed accuracy results were performed for the classified maps. We conclude the importance of the pansharpening step in ecosystems with small and mixed vegetation, where the spatial information is critical and should be well incorporated in order to generate accurate thematic maps. It is important to highlight the difficulty in classifying some types of vegetation due to the complexity of this heterogeneous shrubland ecosystem with small vegetation species such as *D. bourgaeana*. Hence, the major impact on the mapping of different types of vegetation is the misclassification created within the plant species, due to their spectral similarity and the mixing contributions from different covers in some pixels. Thus, it is important to create a reliable training sample database, which allows an accurate supervised classification to be made. As mentioned, experts from the Teide National Park helped to obtain the ground truth samples used for training and testing. This assumption leads us back to the importance of obtaining a fused image with a high spatial quality that allows us to differentiate some species from others, avoiding pixel misclassification but also preserving the original spectral information.

In both classification approaches, the WAT $\otimes$ FRAC fused image achieves the best thematic map with every classification method except for Mahalanobis Distance using the pixel-based approach. The highest Overall Accuracy is obtained by the Support Vector Machine, applied to the WAT $\otimes$ FRAC fused image for both approaches, having similar results with Maximum Likelihood in the pixel-based approach and with Bayes in the OBIA approach. Moreover, Maximum Likelihood, as well as Bayes, obtained the highest accuracies for most vegetation classes, even though the visual results in the Maximum Likelihood classification are not fully satisfactory. In addition, the computation time of the Support Vector Machine is higher than other classifiers, being considerably high in the pixel-based approach. Thus, we conclude

that Bayes classifier applied in an object-based approach is the most suitable algorithm for this ecosystem area.

Despite the accurate classification results obtained, some limitations for both studied approaches have to be mentioned. In the case of the pixel approach, the main limitation is the presence of mixed pixels located in boundaries between classes. Moreover, the quantity of data to be processed is higher than in the OBIA approach, in which objects are processed instead of pixels. On the other hand, in the OBIA approach there is a high dependency on the segmentation parameters, which are specific for each image. There is no global protocol for setting the segmentation parameters and the user must analyze which segmentation parameters are more suitable depending on the image.

In conclusion, after an extensive testing of pansharpening and classification algorithms, we have obtained a methodology that provides a good performance in these heterogeneous regions with small and mixed shrubs, obtaining challenging thematic maps of land-protected areas for studying the state of conservation of natural resources.

Future research will include ancillary data, such as Lidar and SAR imagery, as well as specific vegetation indices and texture parameters in the classification approach in order to obtain more accurate thematic maps not only in shrubland ecosystems, but also in coastal and shallow water natural areas. This methodology could be applied not only to Teide National Park ecosystem but to other similar ecosystems around the world.

## Acknowledgments

We wish to acknowledge the Teide National Park conservation managers (Jose Luis Martín Esquivel and Manuel Marrero Gómez) for defining the classes of interest and examining the results obtained, and Ángel Garcia-Pedrero for his implementation of the HCS code.

## Funding

This research has been supported by the ARTEMISAT (CGL2013-46674-R) and ARTEMISAT-2 (CTM2016-77733-R) project, funded by the Spanish *Ministerio de Economía y Competitividad* and *Fondo Europeo de Desarrollo Regional* (FEDER). This work was completed while E. I-U was a Ph.D. student in the IOCAG Doctoral Program in Oceanography and Global Change and funded by the Spanish *Ministerio de Economía y Competitividad* with a FPI grant (BES-2014-069426).

## ORCID

Consuelo Gonzalo-Martín  <http://orcid.org/0000-0002-0804-9293>


## References

- Adler-Golden, S.M., Matthew, M.W., Bernstein, L.S., Levine, T.Y., Berk, A., Richtsmeier, S.C., Acharya, P.K., Anderson, G.P., Felde, J.W., and Gardner, J. 1999. "Atmospheric correction for shortwave spectral imagery based on MODTRAN4." In *Proceedings of SPIE, Imaging Spectrometry V* (Vol. 3753), edited by M. R. Descour and S. S. Shen, pp. 61–69. Bellingham, WA: SPIE.
- Aiazzi, B., Alparone, L., Baronti, S., and Garzelli, A. 2002. "Context-driven fusion of high spatial and spectral resolution images based on oversampled multiresolution analysis." *IEEE Transactions on Geoscience and Remote Sensing*, Vol. 40: pp. 2300–2312.
- Aiazzi, B., Alparone, L., Baronti, S., Garzelli, A., and Selva, M. 2006. "MTF-tailored multiscale fusion of high resolution MS and Pan imagery." *Photogrammetric Engineering and Remote Sensing*, Vol. 72: pp. 591–596.
- Alimuddin, I., Sumantyo, J.T.S., and Kuze, H. 2012. "Assessment of pan-sharpening methods applied to image fusion of remotely sensed multi-band data." *International Journal of Applied Earth Observation and Geoinformation*, Vol. 18: pp. 165–175.
- Alparone, L., Aiazzi, B., Baronti, S., Garzelli, A., Nencini, F., and Selva, M. 2008. "Multispectral and panchromatic data fusion assessment without reference." *Photogrammetric Engineering and Remote Sensing*, Vol. 74(No. 2): pp. 193–200.
- Alparone, L., Baronti, S., Aiazzi, B., and Garzelli, A. 2016. "Spatial methods for multispectral pansharpening: Multiresolution analysis demystified." *IEEE Transactions on Geoscience and Remote Sensing*, Vol. 54(No. 5): pp. 2563–2576.
- Alparone, L., Baronti, S., Garzelli, A., and Nencini, F. 2004. "A global quality measurement of pan-sharpened multispectral imagery." *Geoscience and Remote Sensing Letters*, Vol. 1(No. 4): pp. 313–317.
- Amolins, K., Zhang, Y., and Dare, P. 2007. "Wavelet based image fusion techniques—An introduction, review and comparison." *ISPRS Journal of Photogrammetry and Remote Sensing*, Vol. 62(No. 4): pp. 249–263.
- Amro, I., Mateos, J., Vega, M., Molina, R., and Katsaggelos, A.K. 2011. "A survey of classical methods and new trends in pansharpening of multispectral images." *EURASIP Journal on Advances in Signal Processing*, Vol. 1: p. 79.
- Aplin, P. 2004. "Remote sensing: Land cover." *Progress in Physical Geography*, Vol. 28(No. 2): pp. 283–293.
- Arozena-Concepción, M., and Beltrán-Yanes, E. 2006. "Geografía de la vegetación de las coladas domáticas del atrio de las Cañadas del Teide (Tenerife. I. Canarias)." *Serie Geográfica—Biogeografía: Distribuciones, Dinámicas y Diversidad*, Vol. 13: pp. 43–64.
- Baatz, M., Benz, U., Dehghani, S., Heynen, M., Höltje, A., Hofmann, P., Lingenfelder, I., Mimler, M., Sohlbach, M., and Weber, M. 2001. *eCognition User Guide*. Munich, Germany: Definiens Imaging GmbH.
- Blaschke, T., Lang, S., and Hay, G. 2008. *Object-Based Image Analysis: Spatial Concepts for Knowledge-Driven Remote Sensing Applications*. Berlin, Germany: Springer Science and Business Media.
- Bonet, F.J., Zamora, R., Gastón, A., Molina, C., and Bariego, P. 2009. "Matorrales pulvulares orófilos europeos meridionales." *VV. AA., Bases ecológicas preliminares para la conservación de los tipos de hábitat de interés comunitario en España*. Gobierno de España. Ministerio de Medio Ambiente, y Medio Rural y Marino.
- Burnett, C., Aaviksoo, K., Lang, S., Langanke, T., and Blaschke, T. 2003. "An object-based methodology for mapping mires using high resolution imagery." In *Proceedings of Ecohydrological Processes in Northern Wetlands*, edited by A. Jarvet and E. Lode, pp. 239–244. Tallinn, Estonia: Tartu University Press.
- Burt, P.J., and Adelson, E.H. 1983. "The Laplacian pyramid as a compact image code." *IEEE Transactions on Communications*, Vol. 31(No. 4): pp. 532–540.
- Carper, W., Lillesand, T., and Kiefer, R. 1990. "The use of intensity–hue–saturation transformations for merging SPOT panchromatic and multispectral image data." *Photogrammetric Engineering and Remote Sensing*, Vol. 56: pp. 459–467.
- Chavez, P.S., Stuart, J., Sides, C., and Anderson, J.A. 1991. "Comparison of three different methods to merge multiresolution and multispectral data: Landsat TM and SPOT panchromatic." *Photogrammetric Engineering and Remote Sensing*, Vol. 57: pp. 259–303.
- Congalton, R.G. 1991. "A review of assessing the accuracy of classifications of remotely sensed data." *Remote Sensing of Environment*, Vol. 37(No. 1): pp. 35–46.
- Dronova, I. 2015. "Object-based image analysis in wetland research: A review." *Remote Sensing*, Vol. 7(No. 5): pp. 6380–6413.
- Dutilleul, P., Aiguier, C., and Joliot, R. 1987. "An implementation of the 'algorithm à trous' to compute the wavelet transform." In *Wavelets: Time-Frequency Methods and Phase Space* (2nd ed.), edited by J.M. Combes, A. Grossman, and Ph. Tchamitchian. New York, NY: Springer-Verlag.
- ENVI. 2004. *ENVI User's Guide*. Boulder, CO: Research Systems Inc.
- Franklin, S., and Wulder, M. 2002. Remote sensing methods in medium spatial resolution satellite data land cover classification of large areas. *Progress in Physical Geography*, Vol. 26(No. 2): pp. 173–205.
- Gao, B.C., Montes, M.J., Davis, C.O., and Goetz, A.F. 2009. "Atmospheric correction algorithms for hyperspectral remote sensing data of land and ocean." *Remote Sensing of Environment*, Vol. 113: pp. S17–S24.
- García-Pedrero, A., Gonzalo-Martin, C., Fonseca-Luengo, D., and Lillo-Saavedra, M. 2015. "A GEOBIA methodology for fragmented agricultural landscapes." *Remote Sensing*, Vol. 7(No. 1): pp. 767–787.
- Garzón-Machado, V., Del Arco-Aguilar, M.J., and Pérez-De-Paz, P.L. 2011. "A tool set for description and mapping vegetation on protected natural areas: An example from the Canary Islands." *Biodiversity and Conservation*, Vol. 20(No. 14): pp. 3605–3625.
- Gillespie, A.R., Kahle, A.B., and Walker, R.E. 1987. "Color enhancement of highly correlated images-II. Channel ratio and 'chromaticity' transform techniques." *Remote Sensing of Environment*, Vol. 22: pp. 343–365.
- González-Audiciana, M., Saleta, J.L., Catalán, R.G., and García, R. 2004. "Fusion of multispectral and panchromatic images using improved IHS and PCA mergers based on wavelet decomposition." *IEEE Transactions on Geoscience and Remote Sensing*, Vol. 42: pp. 1291–1299.


- González-Lemus, N., Carracedo-Gómez, J.C., and Durbán-Villonga, M. 2009. "El Parque Nacional del Teide: Patrimonio mundial de la UNESCO." *Anuario de Estudios Atlánticos*, Vol. 1(No. 55): pp. 519–568.
- Gonzalo-Martín, C., and Lillo-Saavedra, M. 2008. "Influence of source images spatial characteristics on the global quality of fused images." *Revista de Teledetección*, Vol. 30: pp. 33–46.
- Goodin, D.G., Anibas, K.L., and Bezymenyyi, M. 2015. "Mapping land cover and land use from object-based classification: An example from a complex agricultural landscape." *International Journal of Remote Sensing*, Vol. 36(No. 18): pp. 4702–4723.
- Ibarrola-Ulzurrun, E., Gonzalo-Martín, C., Marcello-Ruiz, J., García-Pedrero, A., and Rodríguez-Esparragon, D. 2017. "Fusion of high resolution multispectral imagery in vulnerable coastal and land ecosystems." *Sensors*, Vol. 17(No. 2): p. 228.
- Isbell, F., Calcagno, V., Hector, A., Connolly, J., Harpole, W.S., Reich, P.B., Scherer-Lorenzen, M., Schmid, B., Tilman, D., and Van Ruijven, J. 2011. "High plant diversity is needed to maintain ecosystem services." *Nature*, Vol. 477(No. 7363): pp. 199–202.
- Khare, S., and Ghosh, S. 2016. "Satellite remote sensing technologies for biodiversity monitoring and its conservation." *International Journal of Advanced Earth Science and Engineering*, Vol. 5(No. 1): pp. 375–389.
- Kpalma, K., El-Mezouar, M.C., and Taleb, N. 2014. "Recent trends in satellite image pan-sharpening techniques." Paper presented at the 1st International Conference on Electrical, Electronic and Computing Engineering, Vrnjačka Banja, Serbia, June 2014.
- Kruse, F., Lefkoff, A., Boardman, J., Heidebrecht, K., Shapiro, A., Barloon, P., and Goetz, A. 1993. "The spectral image processing system (SIPS)—Interactive visualization and analysis of imaging spectrometer data." *Remote Sensing of Environment*, Vol. 44(No. 2): pp. 145–163.
- Kyncl, T., Suda, J., Wild, J., Wildová, R., and Herben, T. 2006. "Population dynamics and clonal growth of *Spartocytisus supranubius* (Fabaceae), a dominant shrub in the alpine zone of Tenerife, Canary Islands." *Plant Ecology*, Vol. 186(No. 1): pp. 97–108.
- Laben, C.A., and Brower, B.V. 2000. "Process for enhancing the spatial resolution of multispectral imagery using pan-sharpening." U.S. Patent No. 6,011,875. Washington, DC: U.S. Patent and Trademark Office.
- Lantz, N.J., and Wang, J. 2013. "Object-based classification of Worldview-2 imagery for mapping invasive common reed, *Phragmites australis*." *Canadian Journal of Remote Sensing*, Vol. 39(No. 4): pp. 328–340.
- Li, X., He, M., and Zhang, L. 2013. "Hyperspherical color transform based pansharpening method for WorldView-2 satellite images." Paper presented at the IEEE 8th Conference on Industrial Electronics and Applications, Melbourne, Australia, June 2013.
- Li, X., Li, L., and He, M. 2012. "A novel pansharpening algorithm for WorldView-2 satellite images." Paper presented at the International Conference on Industrial and Intelligent Information, Singapore, March 2012.
- Lillo-Saavedra, M., and Gonzalo, C. 2006. "Spectral or spatial quality for fused satellite imagery: A trade-off solution using the wavelet à trous algorithm." *International Journal of Remote Sensing*, Vol. 27(No. 7): pp. 1453–1464.
- Lillo-Saavedra, M., Gonzalo, C., Arquero, A., and Martínez, E. 2005. "Fusion of multispectral and panchromatic satellite sensor imagery based on tailored filtering in the Fourier domain." *International Journal of Remote Sensing*, Vol. 26(No. 6): pp. 1263–1268.
- Lillo-Saavedra, M., Gonzalo, C., and Lagos, O. 2011. "Toward reduction of artifacts in fused images." *International Journal of Applied Earth Observation and Geoinformation*, Vol. 13: pp. 368–375.
- Lu, D., and Weng, Q. 2007. "A survey of image classification methods and techniques for improving classification performance." *International Journal of Remote Sensing*, Vol. 28(No. 5): pp. 823–870.
- Marangoz, A.M., Oruç, M., Karakiş, S., and Şahin, H. 2006. "Comparison of pixel-based and object-oriented classification using IKONOS imagery for automatic building extraction—Safranbolu testfield." Paper presented at the Fifth International Symposium Turkish-German Joint Geodetic Days, Berlin, Germany, March 2006.
- Marcello, J., Eugenio, F., Perdomo, U. and Medina, A. 2016. "Assessment of atmospheric algorithms to retrieve vegetation in natural protected areas using multispectral high resolution imagery." *Sensors*, Vol. 16(No. 10): p. 1624.
- Marcello, J., Medina, A., and Eugenio, F. 2013. "Evaluation of spatial and spectral effectiveness of pixel-level fusion techniques." *Geoscience and Remote Sensing Letters*, Vol. 10(No. 3): pp. 432–436.
- Martín-Osorio, V.E., Wildpret-De La Torre, W., and Hernández-Bolaños, B. 2005. "Avances significativos en la elaboración de la base de datos georreferenciada de Flora y Vegetación del Parque Nacional del Teide, Tenerife, Islas Canarias mediante un Sistema de Información Geobotánica." *Vieraea: Folia Scientiarum Biologiarum Canariensisium*, Vol. 33: pp. 345–358.
- Núñez, J., Otazu, X., Fors, O., Prades, A., Palà, V., and Arbiol, R. 1999. "Multiresolution-based image fusion with additive wavelet decomposition." *IEEE Transactions on Geoscience and Remote Sensing*, Vol. 37: pp. 1204–1211.
- Oruc, M., Marangoz, M., and Buyuksalih, G. 2004. "Comparison of pixel-based and object-oriented classification approaches using Landsat-7 ETM spectral bands." Paper presented at the XX ISPRS Congress, Istanbul, Turkey, July 2004.
- Otto, R., García-Del-Rey, E., Méndez, J., and Fernández-Palacios, J.M. 2012. "Effects of thinning on seed rain, regeneration and understory vegetation in a *Pinus canariensis* plantation (Tenerife, Canary Islands)." *Forest Ecology and Management*, Vol. 280: pp. 71–81.
- Padwick, C., Deskevich, M., Pacifici, F., and Smallwood, S. 2010. "WorldView-2 pan-sharpening." Paper presented at the ASPRS 2010 Annual Conference, San Diego, CA, April 2010.
- Pakzad, K., Lúcio, G., Mota, A., Meirelles, M.S., Luiz, H., Coutinho, C., and Feitosa, R.Q. 2003. "Automatic interpretation of vegetation areas in Brazil." Paper presented at the Joint Workshop of ISPRS Working Groups I/2, I/5, IC WG II/IV and the EARSeL Special Interest Group, Hannover, Germany, October 2003.
- Peña-Barragán, J.M., Ngugi, M.K., Plant, R.E., and Six, J. 2011. "Object-based crop identification using multiple vegetation indices, textural features and crop phenology." *Remote Sensing of Environment*, Vol. 115(No. 6): pp. 1301–1316.

- Pohl, C. 2014. "Challenges of remote sensing image fusion to optimize earth observation data exploitation." *European Scientific Journal*, Vol. 9: pp. 355–365.
- Rodríguez-Esparragón, D. 2015. *Evaluación y desarrollo de métricas de calidad espacial y espectral para aplicaciones de fusión de imágenes multiespectrales de teledetección de alta resolución*. Thesis, Universidad Las Palmas de Gran Canaria, Gran Canaria, Spain.
- Rodríguez-Esparragón, D., Marcello-Ruiz, J., Medina-Machín, A., Eugenio-González, F., Gonzalo-Martín, C., and García-Pedrero, A. 2014. "Evaluation of the performance of the spatial assessment of pansharpened images." Paper presented at the IEEE International Geoscience and Remote Sensing Symposium (IGARSS), Quebec City, Canada, July 2014.
- Ruocco, M., Bertoni, D., Sarti, G., and Ciccarelli, D. 2014. "Mediterranean coastal dune systems: Which abiotic factors have the most influence on plant communities?" *Estuarine, Coastal and Shelf Science*, Vol. 149: pp. 213–222.
- Shettigara, V.K. 1992. "A generalized component substitution technique for spatial enhancement of multispectral images using a higher resolution data set." *Photogrammetric Engineering and Remote Sensing*, Vol. 58: pp. 561–567.
- Shridhar, J.D., and Alvarinho, L.J. 2013. "A spectral index ratio-based Antarctic land-cover mapping using hyperspatial 8-band WorldView-2 imagery." *Polar Science*, Vol. 7(No. 1): pp. 18–38.
- Thomas, C., Ranchin, T., Wald, L., and Chanussot, J. 2008. "Synthesis of multispectral images to high spatial resolution: A critical review of fusion methods based on remote sensing physics." *IEEE Transactions on Geoscience and Remote Sensing*, Vol. 46(No. 5): pp. 1301–1312.
- Tu, T.M., Hsu, C.L., Tu, P.Y., and Lee, C.H. 2012. "An adjustable pan-sharpening approach for IKONOS/QuickBird/GeoEye-1/WorldView-2 imagery." *IEEE Journal of Selected Topics in Applied Earth Observations and Remote Sensing*, Vol. 5(No. 1): pp. 125–134.
- Tu, T.M., Su, S.C., Shyu, H.C., and Huang, P.S. 2001. "A new look at IHS-like image fusion methods." *Information Fusion*, Vol. 2(No. 3): pp. 177–186.
- Vivone, G., Alparone, L., Chanussot, J., Dalla Mura, M., Garzelli, A., Licciardi, G., Restaino, R., and Wald, L. 2015. "A critical comparison among pansharpening algorithms." *IEEE Transactions on Geoscience and Remote Sensing*, Vol. 53(No. 5): pp. 2565–2586.
- Wald, L. 2000. "Quality of high resolution synthesised images: Is there a simple criterion?" In *Proceedings of the Third Conference Fusion of Earth Data: Merging Point Measurements, Raster Maps and Remotely Sensed Images*, edited by T. Ranchin and L. Wald, pp. 99–103 Nice, France: SEE/URSICA.
- Wald, L., Ranchin, T., and Mangolini, M. 1997. "Fusion of satellite images of different spatial resolutions: assessing the quality of resulting images." *Photogrammetric Engineering and Remote Sensing*, Vol. 63(No. 6): pp. 691–699.
- Walsh, S.J., Mcclary, A.L., Mena, C.F., Shao, Y., Tuttle, J.P., González, A., and Atkinson, R. 2008. "QuickBird and Hyperion data analysis of an invasive plant species in the Galapagos Islands of Ecuador: Implications for control and land use management." *Remote Sensing of Environment*, Vol. 112(No. 5): pp. 1927–1941.
- Wang, Z., and Bovik, A.C. 2002. "A universal image quality index." *IEEE Signal Letter*, Vol. 9(No. 3): p. 4.
- Wildpret de la Torre, W. 2001. "Consideraciones sobre la fitobiodiversidad de las cañadas del Teide." Paper presented at the Curso de acreditación de conocimientos para ejercer de guía en el Parque Nacional del Teide, Tenerife, Spain.
- Wu, B., Fu, Q., Sun, L., and Wang, X. 2015. "Enhanced hyperspherical color space fusion technique preserving spectral and spatial content." *Journal of Applied Remote Sensing*, Vol. 9(No. 1): pp. 097291–097291.
- Zhou, J., Civco, D., and Silander, J. 1998. "A wavelet transform method to merge Landsat TM and SPOT panchromatic data." *International Journal of Remote Sensing*, Vol. 19(No. 4): pp. 743–757.





CHAPTER 5. ASSESSMENT  
OF COMPONENT SELECTION  
STRATEGIES IN  
HYPERSPECTRAL IMAGERY







This chapter includes the following published article: E. Ibarrola-Ulzurrun, J. Marcello, C. Gonzalo-Martín. *Assessment of component selection strategies in hyperspectral imagery*. Entropy, 2017, 19(2).

This work is the first one in which HS the Thesis considering HS data. Specifically, the HS image provided by INTA, in Reborio (Asturias, Spain), is used. As it was mentioned in Chapter 2, HS dimensionality reduction is usually necessary before performing a classification to obtain accurate thematic maps.

In this context, the first objective of the paper was to perform a comparative assessment of classic dimensionality reduction techniques. Moreover, different strategies were proposed to determine the suitable number of components in the transformed spaces obtained from the dimensionality reduction techniques. The strategies studied for selecting the suitable number of components for a later classification, were: eigenvalues analysis, texture measurements, transformed signatures of the classes, and classes separability in the transformed space. The study showed that entropy measurement, transformed signatures of the classes, and ROIs separability strategies are more appropriate for the components selection.

The second objective of the paper referred to a new dimensionality reduction approach by splitting the HS image into different spectral regions (Visible, Red Edge, NIR 1 and NIR 2). After applying a dimensionality reduction technique in each spectral region, components for the different regions were selected. The selected components in the transformed space were next stacked and analyzed in order to asses if dimensionality reduction techniques, applied independently for each spectral region, improves the final classification. It was observed that this approach slightly improve the components selection.




The main contributions and conclusions of the study were:

- Comparative evaluation of classical dimensionality reduction techniques (PCA, MNF, and ICA).
- Analysis of different strategies for selecting the most suitable number of component, in which, entropy measurement, transformed signatures of the classes, and ROIs separability strategies are more appropriate for the components selection.
- When a supervised classification is carried out, the transformed signatures of each class, and the ROIs separability values, in the transformed space, are the most suitable strategies.
- A dimensionality reduction approach of the HSI considering a spectral division in different regions was proposed, in order to analyze if the number of components selected were more suitable to generate a final thematic map.



Article

# Assessment of Component Selection Strategies in Hyperspectral Imagery

Edurne Ibarrola-Uizurrún <sup>1,\*</sup> , Javier Marcello <sup>1</sup>  and Consuelo Gonzalo-Martin <sup>2</sup> 

<sup>1</sup> Instituto de Oceanografía y Cambio Global, IOCAG, Universidad de Las Palmas de Gran Canaria, ULPGC, Parque Científico Tecnológico Marino de Taliarte, s/n, 35214 Telde, Spain; javier.marcello@ulpgc.es

<sup>2</sup> Center of Biomedical Technology, Universidad Politécnica de Madrid, UPM, Campus de Montegancedo, Pozuelo de Alarcón, 28223 Madrid, Spain; chelo@fi.upm.es

\* Correspondence: edurne.ibarrola101@alu.ulpgc.es; Tel.: +34-928-457-365

Received: 23 October 2017; Accepted: 1 December 2017; Published: 5 December 2017

**Abstract:** Hyperspectral imagery (HSI) integrates many continuous and narrow bands that cover different regions of the electromagnetic spectrum. However, the main challenge is the high dimensionality of HSI data due to the ‘Hughes’ phenomenon. Thus, dimensionality reduction is necessary before applying classification algorithms to obtain accurate thematic maps. We focus the study on the following feature-extraction algorithms: Principal Component Analysis (PCA), Minimum Noise Fraction (MNF), and Independent Component Analysis (ICA). After a literature survey, we have observed a lack of a comparative study on these techniques as well as accurate strategies to determine the number of components. Hence, the first objective was to compare traditional dimensionality reduction techniques (PCA, MNF, and ICA) in HSI of the Compact Airborne Spectrographic Imager (CASI) sensor and to evaluate different strategies for selecting the most suitable number of components in the transformed space. The second objective was to determine a new dimensionality reduction approach by dividing the CASI HSI regarding the spectral regions covering the electromagnetic spectrum. The components selected from the transformed space of the different spectral regions were stacked. This stacked transformed space was evaluated to see if the proposed approach improves the final classification.

**Keywords:** remote sensing; hyperspectral sensor; feature-extraction; texture measurement; classification; ecosystem management

## 1. Introduction

Hyperspectral imagery (HSI) has significantly contributed to the progress of remote sensing studies. HSI contains multiple continuous and narrow spectral bands, which cover different regions of the electromagnetic spectrum [1–4]. These sensors provide high detail, which permits the discrimination of small spectral variations [4] and allow the better characterization of materials, making HSI suitable for source separation and classification processes [5]. However, HSI also increases the computational load due to the enhancement of spectral resolution, which gives a high level of data dimensionality that can demean the results of the classification process [5]. In addition, the high number of spectral bands associated with HSI changes the ratio between the number of training samples and the number of bands, causing a decrease of a classifier’s accuracy [6]. This fact produces the ‘Hughes’ phenomenon [7], which specifies that the size of the training sample set or Regions Of Interest (ROIs) needed for a given classifier increases exponentially with the number of spectral bands [8]. One common method to solve this issue is the reduction of the dimensionality, which becomes necessary to obtain more precise thematic maps [2,9]. In other words, dimensionality reduction decreases the feature dimensionality by removing redundant information while keeping the important information in the feature vector [10].

Several techniques have been proposed in the last several years to overcome the 'Hughes' phenomenon. Feature-selection and feature-extraction are traditional approaches for reducing the dimensionality of HSI [9,11,12]. This study is focused on the traditional feature-extraction techniques for HSI dimensionality reduction, *Principal Component Analysis* (PCA), *Minimum Noise Factor* (MNF), and *Independent Component Analysis* (ICA). These techniques significantly reduce the number of extracted features compared to the original dimension [1]. However, the selection of the adequate number of components remains an open issue. Besides that, a lack of a comparative study on traditional techniques used in HSI dimensionality reduction has been observed as well as an accurate approach for component selection in the transformed space. There exist studies comparing PCA, MNF, and ICA with new methodologies [9,13–15], as well as other studies that analyze their behavior or improve these techniques [1,2,5,11,16–18], without making a comparison with the existing methods. Additionally, previous studies [8,19,20] have used a small number of components to obtain adequate classification maps. However, in such studies, the most common approach used to select components is to determine them through eigenvalues, which are the measure of the variance explained by the components obtained from the dimensionality reduction techniques.

In this context, our first objective was to carry out a comparative assessment of the classical dimensionality reduction techniques (PCA, MNF, and ICA) and to assess different strategies for selecting the most suitable number of components in order to study their performance in the classification of high spatial resolution imagery of the Compact Airborne Spectrographic Imager (CASI) sensor. To evaluate the dimensionality reduction techniques, a robust classification approach, known as the Support Vector Machine (SVM) [21,22] algorithm, was used as a reference, which is an efficient technique for HSI classification [6,23,24]. For this objective, the classic eigenvalues analysis, texture measurements, the transformed signatures of the classes, and ROIs separability in the transformed space, were analyzed to identify the best approach for the selection of an adequate number of components that contain sufficient information for a later classification stage. The second objective was to propose a new dimensionality reduction approach by dividing CASI HSI into different spectral regions. The selected components from each spectral region were stacked. This new stacked transformed space was evaluated in order to see if the best dimensionality reduction technique, applied independently for each region of the electromagnetic spectrum, improves the final classification.

The paper is structured as follows: Section 2 includes the study area description, datasets, and the dimensionality reduction methodology followed in the analysis. Section 3 presents the classification results of each dimensionality reduction technique, as well as the component selection results and the spectral division assessment. Finally, a critical analysis of the results and a summary of the main outcomes and contributions are included in Section 4.

## 2. Materials and Methods

### 2.1. Study Area and Data Set

The study area is situated in a coastal area of northern Spain, specifically in Reborio (Asturias). The image was acquired and processed in 2011 through the CASI sensor by the Instituto Nacional de Técnica Aeroespacial (INTA). The image was radiometrically corrected and georeferenced, and it has 144 spectral bands and a spatial resolution of 1 m. The classes selected for the classification were forest, meadow, road, shadows, sand, bare soil, urban, water, and waves.

### 2.2. Dimensionality Reduction Methodology

A preliminary analysis based on three different dimensionality reduction methods—PCA, MNF, and ICA—was performed to determine the number of valuable components containing most of the statistical information. Next, a brief description of them is included.

### 2.2.1. Dimensionality Reduction Techniques

PCA is often used for the dimensionality reduction of HSI [3,25–30]. It is a mathematical orthogonal transformation that changes a set of observations of possibly correlated variables into a set of uncorrelated variables called principal components [31]. PCA retains most of the information of the original data in a low-dimensional space [13]. Conventional PCA faces three main challenges: (1) obtaining a covariance matrix in an extremely large spatial dimension; (2) dealing with the high computational cost required for the analysis of a large dataset; and (3) retaining locally structured elements that appear in a small number of bands for improved discriminant ability when feature bands are globally extracted as principal components [1]. Besides this, PCA equates variance with information and is based on the assumption that the data structure can be described by a multidimensional normal distribution. The performance of PCA depends on the noise characteristics. When noise variance is larger than the signal variance in one band or when the noise is not uniformly distributed between each band, PCA does not guarantee that the amount of information decreases for principal components with a lower ranking [32].

MNF is a noise-adjusted principal component transform that equalizes and estimates the amount of noise in each image band to ensure that the output components are ordered by their information amount [33]. The MNF transform, like PCA, is an eigenvector procedure based on the covariance structure of the noise in the image dataset. MNF is a linear transform consisting of two different steps: (1) computation of the covariance matrix to decorrelate and rescale the noise in the data; and (2) the performance of a standard PCA transform of the decorrelated and rescaled noise data. The goal of the MNF transform is to select components such they maximize the Signal-to-Noise Ratio (SNR), which compares the level of the signal to the level of the background noise rather than the information content [13]. The fact of ordering the components according to the amount of information results in a more reliable identification and elimination of noisy components, and allows for the preservation of components that contain useful information [9,13].

ICA has a wide range of potential applications [32]. Its goal is to decompose a multivariate random measured signal into a linear combination of independent source signals [2]. In contrast with PCA, ICA not only decorrelates second-order statistics but also reduces higher-order statistical dependencies, attempting to make the signals as independent as possible. It is an alternative approach to PCA for dimensionality reduction because it is designed to search for more independent factors that can linearly generate the returns instead of searching for principal components, which allow us to represent the maximum of the return dispersion [5].

### 2.2.2. Component Selection Strategies

Different strategies were evaluated to select the suitable number of components which contained the most statistical information for each dimensionality reduction method (Figure 1):

- Transformation statistics: it is the most common method used in the bibliography to select the suitable number of components. The eigenvalues of the obtained components were analyzed [34]. Components with large eigenvalues contain a higher amount of data variance, while components with lower eigenvalues contain less data information and more noise [31].
- Texture measurements: texture parameters, as entropy, are simple mathematical representations of image features. These features represent high-level information that can be used to describe the objects in and structure of images [10,35], and in consequence can be applied to select the components providing important information. An entropy first-order texture filter is applied based on a co-occurrence matrix [31]. The Equation (1) from Anys et al. [36] was used to compute the entropy using the pixel values in a kernel centered at the current pixel. Entropy is calculated based on the distribution of the pixel values in the kernel. It measures the disorder of the kernel

values, where  $N_g$  is the number of distinct grey levels in the image, and  $P(i)$  is the probability of each pixel value.

$$\text{Entropy} = - \sum_{i=0}^{N_g} P(i) * \ln P(i) \quad (1)$$

- Signatures of the classes in the transformed space (transformed signatures): the classes considered in the study will have values in the components with information, but they will not be distinguished within each other if the component is mainly noise. Moreover, spatially, in components without noise, objects' shapes are recognizable, while in noisy components, only a "salt and pepper" effect appears. A visual assessment is used in order to determine from which components the classes cannot be distinguished within each other, being that those components are mainly noise. However, transformed signatures are dependent on the classes determined by each user as well as the type of image.
- ROIs separability in the transformed space: during the supervised classification procedure, training and testing regions were selected for each class of interest. The evaluation of the separability in different numbers of components could benefit the selection procedure. This strategy is class-dependent. An ROI's separability was determined through the Transformed Divergence (TD) measure (2). This separability index exponentially takes into account the mean and the covariance, and its value ranges from 0 to 2 to indicate how well the selected ROI pairs are statistically separable. Values greater than 1.8 indicate that an ROI pair has good separability [31].

$$\text{TD} = 2 \left( 1 - e^{-\frac{D}{8}} \right) \quad (2)$$

Finally, the evaluation was performed using as a reference the accuracy of the classifications carried out for different numbers of components. The method used for the classifications' validation is known as cross-validation, in which the input data is divided into randomly selected training and testing (ROIs) samples. The testing samples were evaluated against the classified pixels to check if the classifier can properly reproduce the output. The Overall Accuracy (OA), given as a percentage, is obtained from the standardized confusion Error Matrix that compares the thematic map and the rest of the samples selected.

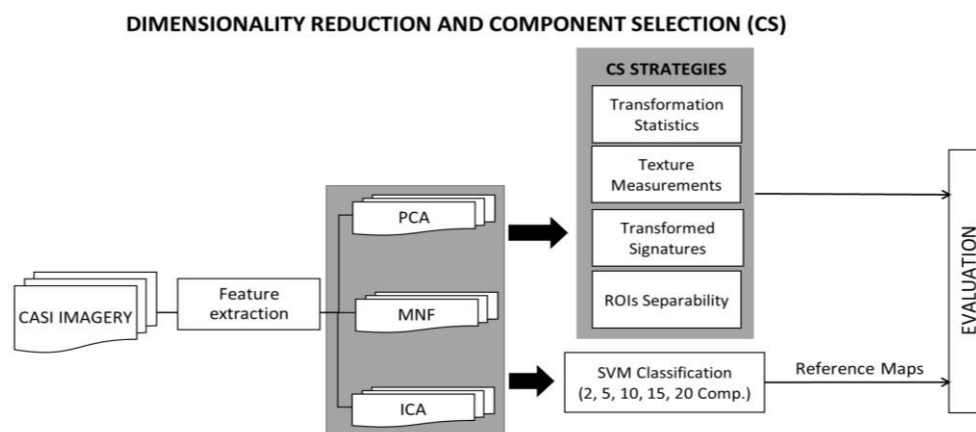


**Figure 1.** Flow diagram of the methodology proposed for evaluation of component selection strategies. CASI: Compact Airborne Spectrographic Imager; PCA: Principal Component Analysis; MNF: Minimum Noise Factor; ICA: Independent Component Analysis; ROI: region of interest; SVM: Support Vector Machine.

A Support Vector Machine (SVM) algorithm was used in order to evaluate a dimensionality reduction method's performance. It has been widely used for HSI classification and relies on training data for model optimization [1,3,26]. SVM is one of the most used kernel learning algorithms,

which carries out a robust non-linear classification of the image' pixels using the kernel trick. The idea is to find a separating hyperplane in a higher dimensionality feature space induced by the kernel function while all the computations are done in the original space [3,22]. In other words, it aims to find a hyperplane that makes the average classification error of the training data reach its minimum. As was mentioned, the kernel function is the key factor of the SVM classifier. Typical kernels are the linear, the polymodal, the sigmoid and the radial basis function (RBF) kernel functions [2]. The RBF kernel function, a type of feed-forward Neural Network [26], is selected in the study because it is considered a robust kernel function for remote sensing imagery [37–39].

### 2.2.3. Spectral Division Analysis

Apart from the previous analysis, another study was conducted in order to assess if applying a dimensionality reduction technique independently to different regions of the spectrum (Figure 2) could improve the classification performance in the final transformed space obtained

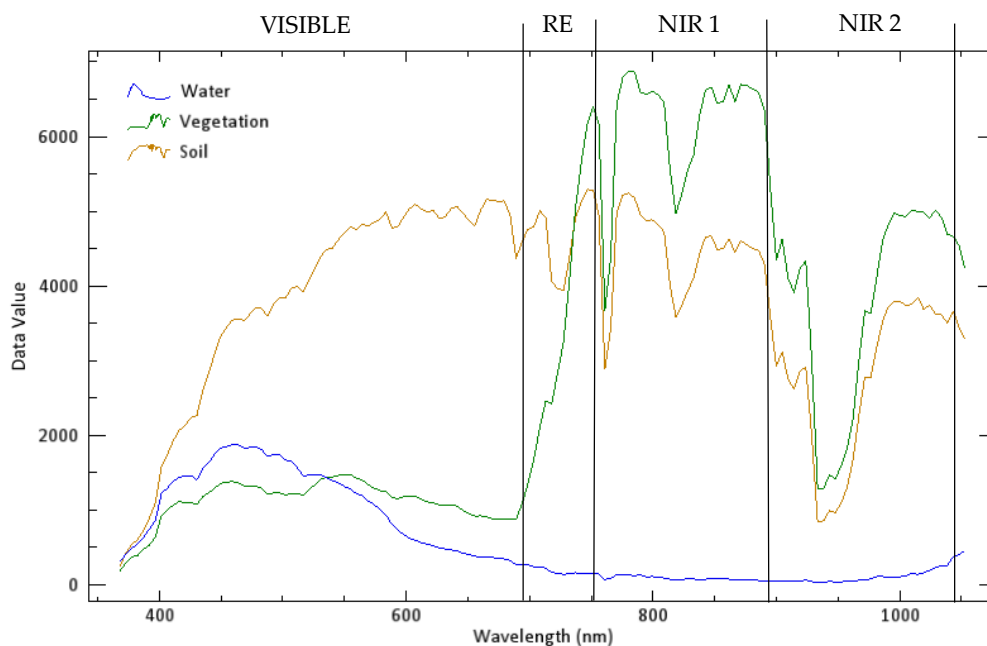


**Figure 2.** Representative spectral reflectance curves for several common Earth surface materials over the visible light to the reflected infrared spectral range (VISIBLE: Visible region; RE: Red Edge region; NIR 1: Near Infrared 1 Region; NIR 2: Near Infrared 2 Region).

We call “spectral division” a division where the CASI spectral bands are separated into four groups. The four groups are (1) the Visible region: bands 1 to 70 (368.3–698.7 nm), (2) the Red Edge region: bands 71 to 80 (705.5–751.5 nm), (3) the NIR1 (Near Infrared 1) region: bands 81 to 111 (751.5–895.6 nm), and (4) the NIR2 (Near Infrared 2) region: bands 112 to 144 (899.9–1052.7 nm).

Figure 3 shows the flow diagram of the spectral division analysis as part of the dimensionality reduction process. After the preliminary assessment, the best reduction technique was selected for this analysis (the MNF technique, as will be discussed in Section 3). Once the different spectral regions were selected, a dimensionality reduction transformation was performed independently on each of them. Then, different numbers of components were selected using the component selection strategies described in Section 2.2.2. After selecting the different numbers of components, a layer stacking was carried out for obtaining a transformed space with the selected number of components of each spectral region. Moreover, SVM classifications were performed on the components selected in each region group and in the transformed space obtained from the selected component stacks.



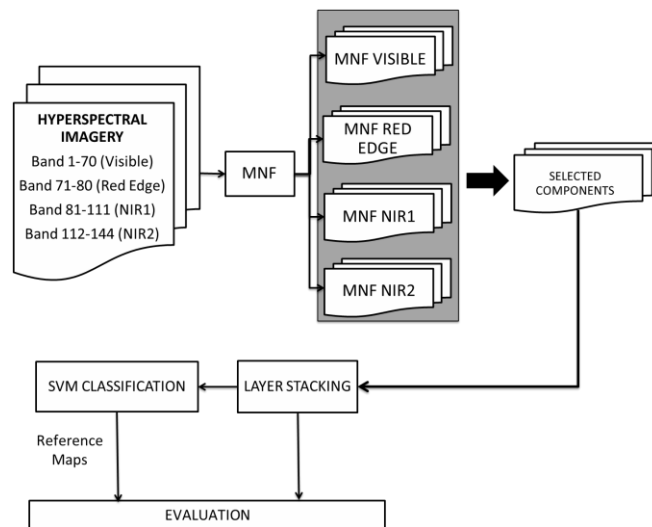


**Figure 3.** Diagram flow of the spectral division analysis.

### 3. Results and Discussion

#### 3.1. Dimensionality Reduction Techniques

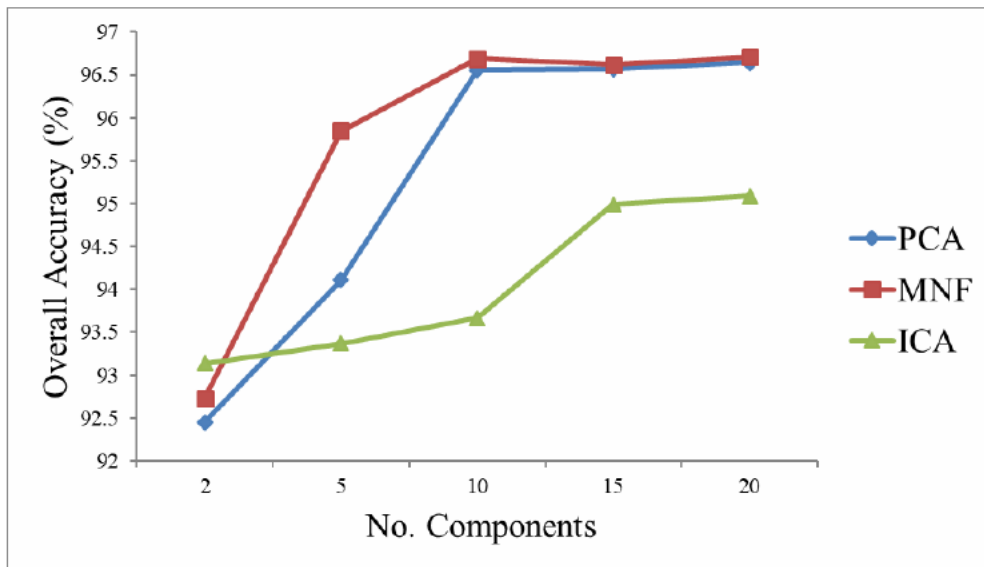
This section includes the results obtained from the methodology shown in Figure 1. Section 3.1.1 shows the results obtained from the SVM classification, while Section 3.1.2 shows the results of the different component selection strategies.

##### 3.1.1. Classification Results for Each Technique

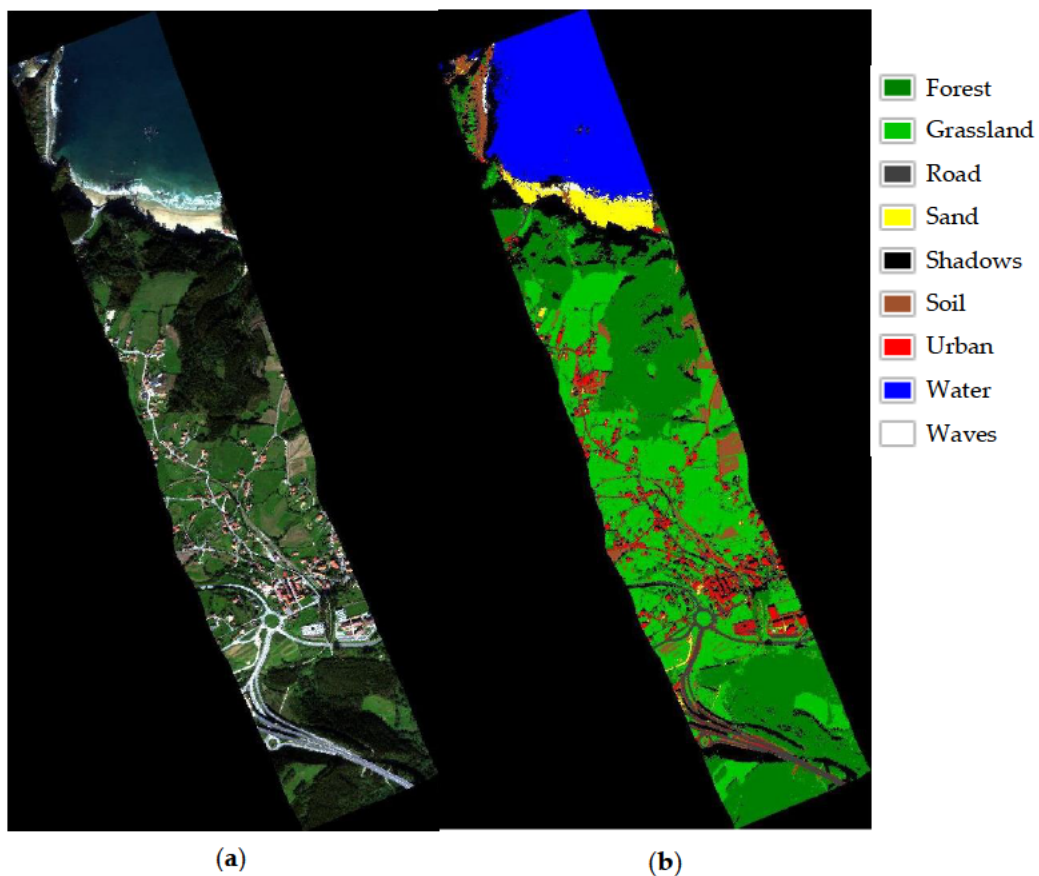
The samples chosen for the classification were taken randomly. 70% of the samples were used for training and 30% for testing. The classes chosen were forest (4797 pixels), meadow (6501 pixels), road (1226 pixels), shadows (2428 pixels), sand (1574 pixels), bare soil (760 pixels), urban (1090 pixels), water (6886 pixels), and waves (141 pixels). The SVM classifier, using the RBF kernel and the appropriate parameters ( $\gamma = 0.1$ ;  $\text{penalty} = 100$ ), was trained with a different number of components from the three dimensionality reduction methods considered. The evaluation was carried out by choosing the 2, 5, 10, 15, and 20 first components after performing the three dimensionality reduction methods (PCA, MNF, and ICA). Due to the noise of the last components chosen, it is expected that the accuracy results should decrease when adding more components.

Figure 4 shows the OA for each method and for a given number of components. It can be observed that MNF achieves the highest accuracy. The OA in the PCA transformed space and the OA in the MNF transformed space are stabilized using 10 components, whereas ICA needs at least 15 components to stabilize the OA, but with a lower OA than the PCA transformed space and the MNF transformed space. Figure 5 shows the thematic map obtained from the best SVM classification, which uses the MNF transformed space with 10 components (OA: 96.68%).

This information about the minimum number of components required to achieve the best performance will be the reference information to assess the different component selection methods.



**Figure 4.** The Support Vector Machine (SVM) Algorithm’s Overall Accuracy for 2, 5, 10, 15, and 20 components.



**Figure 5.** (a) RGB (Red Green Blue) color composite; (b) SVM classification map obtained from the 10 first components of the Minimum Noise Fraction (MNF) transform.

### 3.1.2. Results for the Component Selection Strategies

As indicated in Figure 1, four component selection strategies were analyzed.

In this context, the first strategy is based on the calculation of eigenvalues. Figure 6 shows the eigenvalues obtained after carrying out PCA, MNF, and ICA transforms. Eigenvalues with higher values provide more information than eigenvalues with values close to zero, which contain mainly noise. Thus, visually, only 2 components concentrate most of the information for PCA, 10 for MNF, and 2 for ICA.

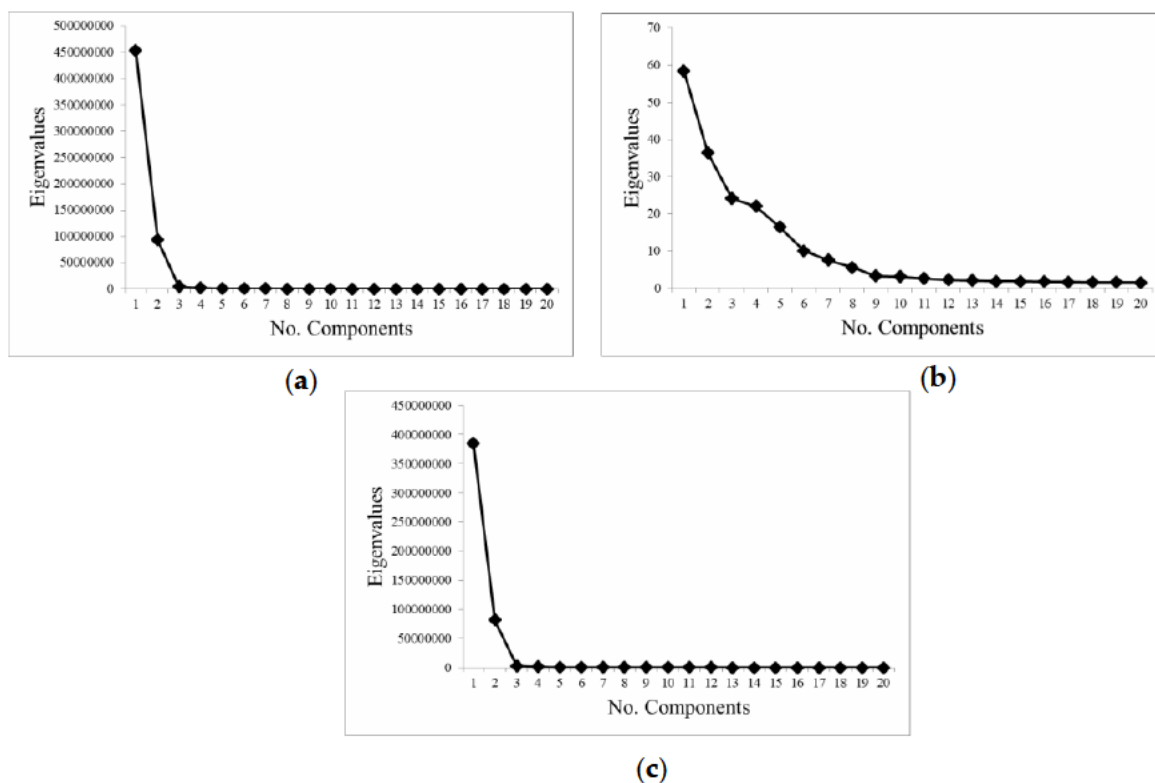


**Figure 6.** Eigenvalues of the first 20 components: (a) Principal Component Analysis (PCA); (b) MNF; and (c) Independent Component Analysis (ICA).

The texture measurement of each component was extracted using the entropy. From the experiments, it can be observed that the mean of the entropy does not show an appropriate pattern for component selection but the standard deviation does (Figure 7). In this case, the components with the highest information obtain higher standard deviation values (the figure is shown in a logarithmic scale in order to offer a better visualization). It is observed that, around the 10th component, the logarithmic curve changes its slope in PCA and MNF, while in ICA it changes around the 15th component.

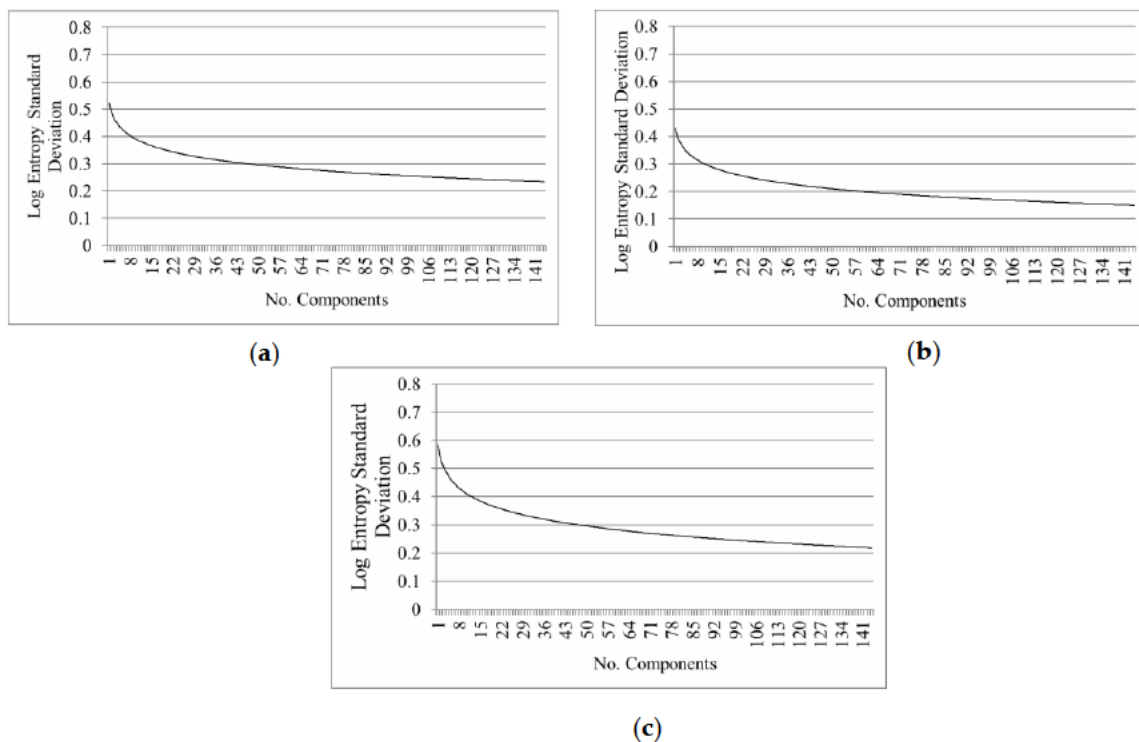


Figure 7. Entropy standard deviation: (a) PCA; (b) MNF; and (c) ICA.

Figure 8 shows the transformed signatures of the different classes. Since the different dimensionality reduction techniques give different results, the scale is different. Only components 1 to 20 are presented to facilitate the observation of the classes difference in the first components. Figure 8 shows how signatures in the transformed space allow us to discriminate some classes from others, but only for the first components. This result is consistent with Figure 9, where the separability measures of each class are shown as a function of the number of components. The greatest separability of the ROIs is from the 10 components for PCA and MNF and the 15 for ICA, which is in agreement with the results shown in Figure 4.

Table 1 shows a qualitative assessment, summarizing the quantitative results for determining the component selection strategy that most closely matches with the results obtained in the classifications. ‘Good’ means that the strategy achieves a good agreement with the number of components determined by the SVM algorithm, ‘Wrong’ means that the number of bands selected by the strategy does not match with the SVM algorithm’s results. Thus, we can observe which measurement may be the most adequate to determine the number of components to be used for the dimensionality reduction of HSI.

Table 1. Results comparison of SVM classification and strategies to determine components (comp.).

		PCA	MNF	ICA
EVALUATION	SVM Classification	Good (10 comp)	Best (10 comp)	Medium (15 comp)
	Eigenvalues	Wrong (2 comp)	Good (9 comp)	Wrong (2 comp)
COMPONENT SELECTION STRATEGIES	Entropy	Good (10 comp)	Good (10 comp)	Good (15 comp)
	Signatures of the classes	Good (9 comp)	Good (10 comp)	Medium (11 comp)
	ROIs separability	Good (10 comp)	Good (10 comp)	Good (15 comp)

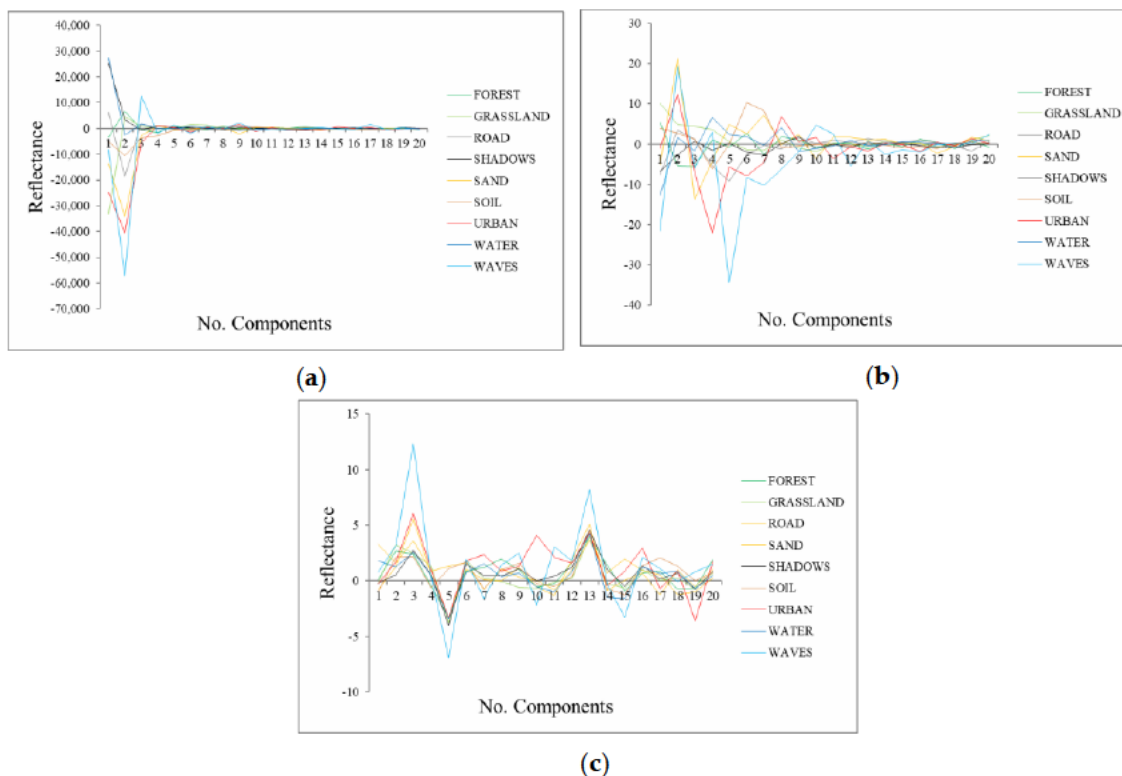


Figure 8. Transformed signatures of each class in: (a) PCA; (b) MNF; and (c) ICA.

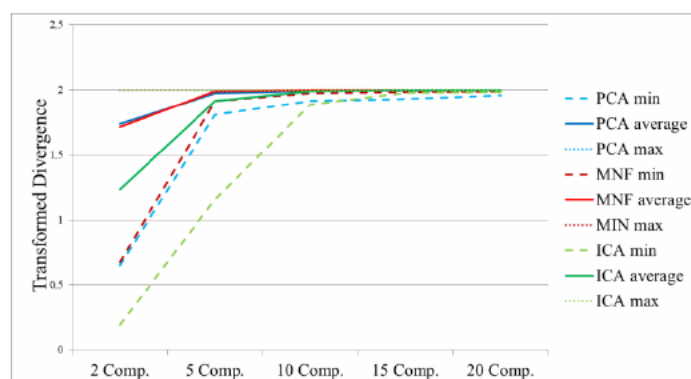


Figure 9. ROIs separability in the transformed space of PCA, MNF, and ICA. Comp: components.

From the results summarized in Table 1, as indicated in the first row, it is observed that MNF and PCA are more reliable techniques, because they do not need a great number of components in the classification, as is the case with the ICA technique. Moreover, PCA and MNF obtained similar OA values, being slightly better those of MNF. On the other hand, the best classification results regarding the different numbers of components (PCA 10 comp., MNF 10 comp., and ICA 15 comp.) are taken as a reference to determine the suitable strategy for selecting an adequate number of components. Thus, as indicated, if the number of components determined by a particular strategy is equal or very close to the number of components for which the best SVM classification result is attained, the strategy is labeled as ‘Good’. Hence, the eigenvalues with information obtained for PCA and ICA (two components in both techniques) do not match with the result of the classification. On the other hand, the remaining different dimensionality reduction techniques got a good determination of components using the entropy measurement (PCA and MNF the logarithmic curve changes around the 10th component while it changes around the 15th component for the ICA technique).

Finally, it can be observed that the entropy, transformed signatures of the classes, and the ROIs separability in the transformed space match with the results obtained for the classification with the SVM algorithm, and are suitable methods for selecting an adequate number of components with more statistical information.

### 3.2. Spectral Division Analysis Results

From the results shown in Section 3.1, MNF is the most suitable dimensionality reduction technique. Thus, it was chosen for the second part of the study, where the HSI was divided into groups according to different regions of the electromagnetic spectrum (the Visible, Red Edge, NIR1, and NIR2 regions). In this part of the study, MNF was applied separately to the each of them.

Figure 10 shows the eigenvalues for each spectral region. Figures 11 and 12 show the entropy’s standard deviation and the transformed signatures of the classes, respectively. Figure 11 shows the ROIs separability results when taking different numbers of components in the transformed space. Table 2 shows the components selected for each region regarding the eigenvalue, entropy, transformed signatures of the classes, and ROIs separability approaches.

**Table 2.** Selected components of each region regarding the Eigenvalues, Entropy, Transformed signatures of classes, and ROIs separability in the transformed space.

REGIONS	EIGENVALUES	ENTROPY	SIGNATURES OF CLASSES	ROIS SEPARABILITY
Visible	5 comp.	5 comp.	5 comp.	4 comp.
Red Edge	3 comp.	3 comp.	3 comp.	3 comp.
NIR1	3 comp.	3 comp.	3 comp.	3 comp.
NIR2	2 comp.	3 comp.	2 comp.	3 comp.

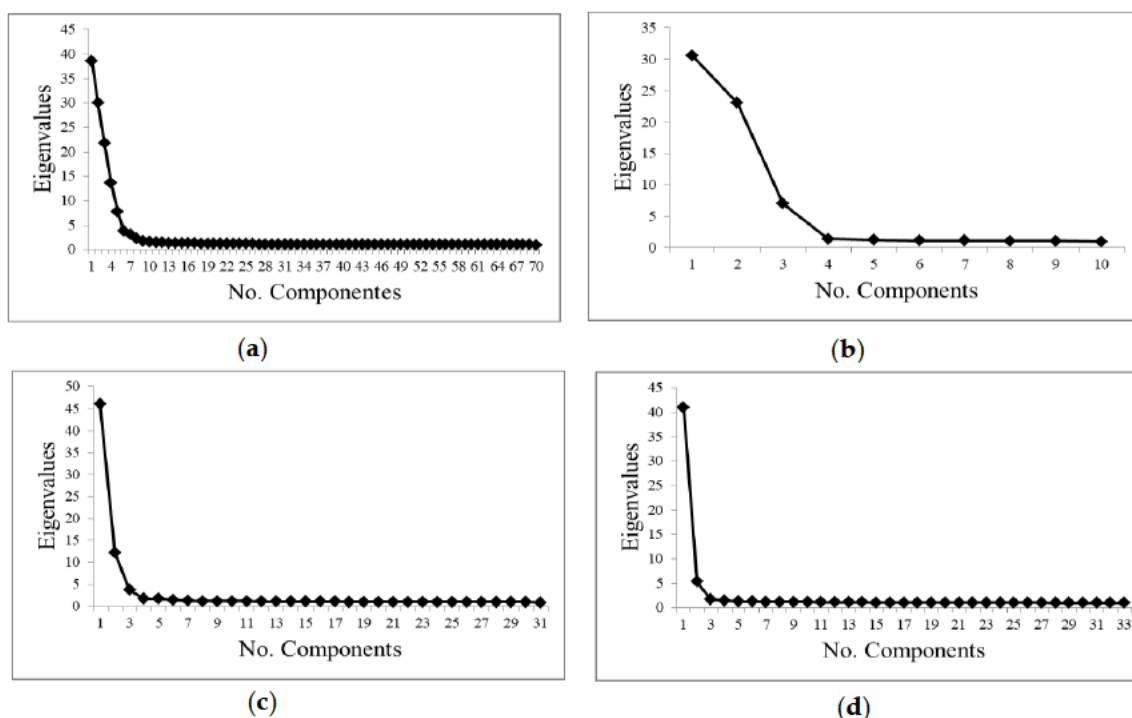


**Figure 10.** Eigenvalues obtained from the MNF transformation: (a) Visible region; (b) Red Edge region; (c) NIR 1 region; and (d) NIR 2 region.

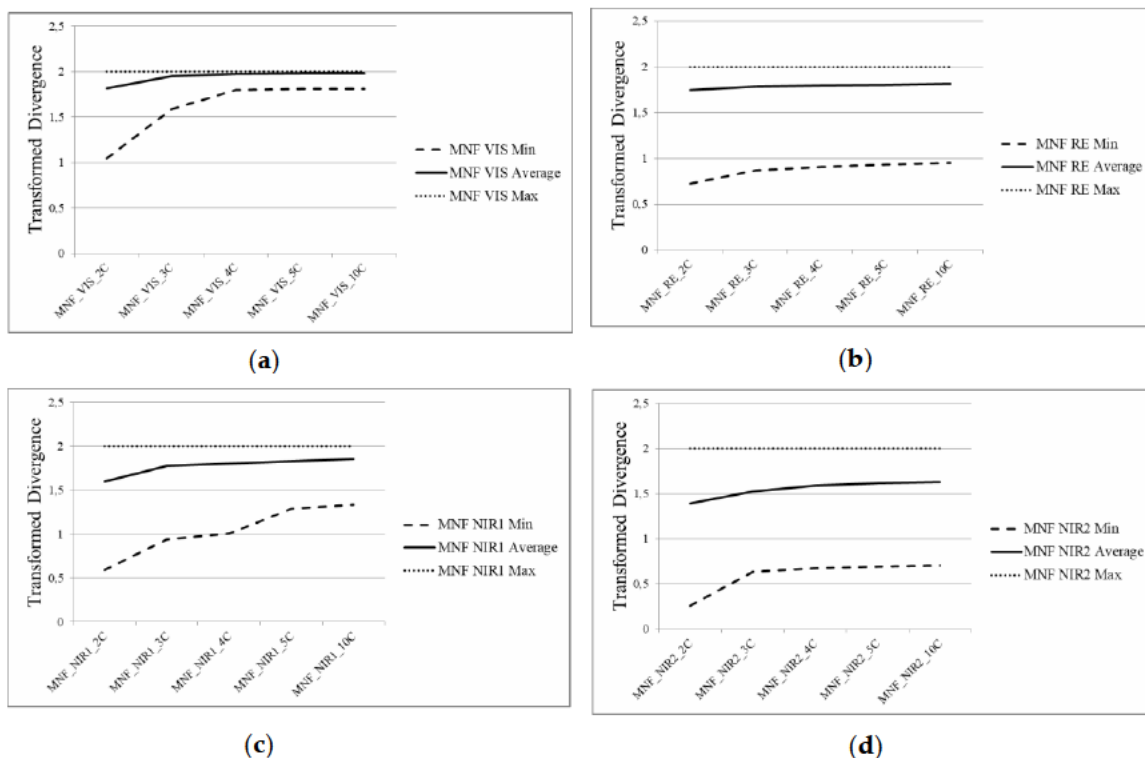


**Figure 11.** ROIs separability in the transformed space of: (a) the Visible region (MNF\_VIS\_XC, X: no. of components); (b) the Red Edge region (MNF\_RE\_XC); (c) the NIR1 region (MNF\_NIR1\_XC); and (d) the NIR2 region (MNF\_NIR2\_XC).

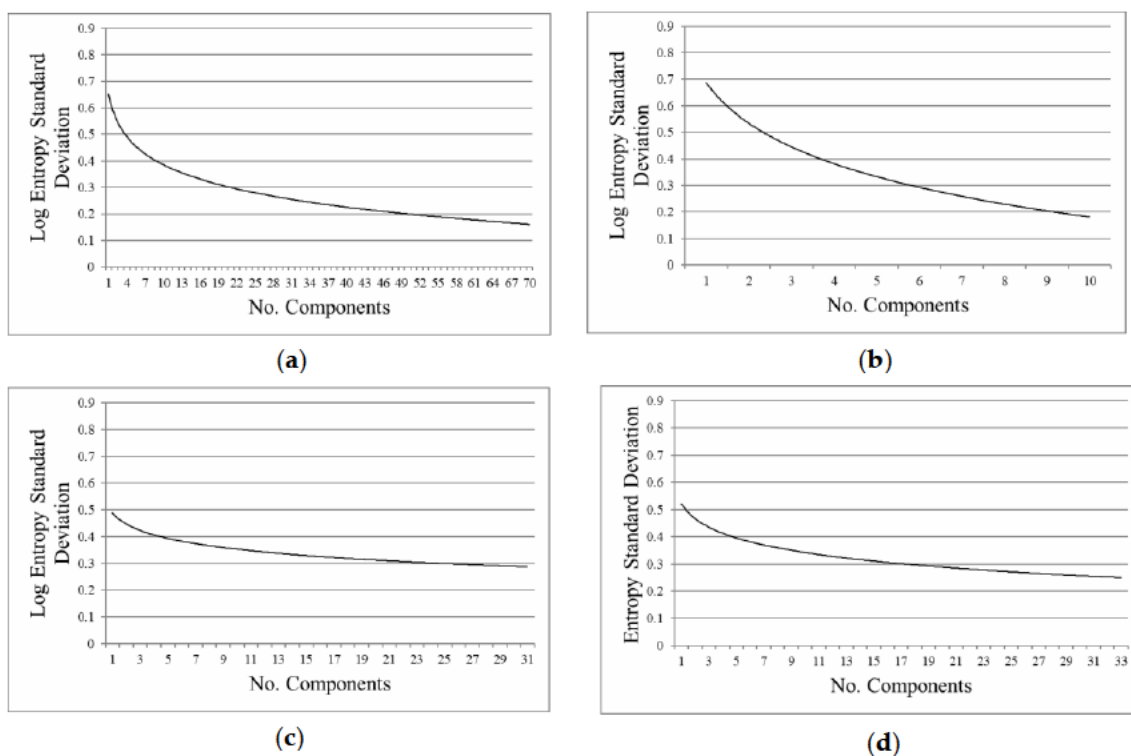


**Figure 12.** Entropy Standard Deviation: (a) Visible region; (b) Red Edge region; (c) NIR1 region; and (d) NIR2 region.

Regarding the eigenvalues strategy, the numbers of components selected for each region are: five for the Visible region, three components for the Red Edge region and for the NIR1 region, and finally only two components have information for the NIR2 region, (Figure 10 and Table 2). Concerning the entropy's standard deviation, the components with the highest information obtain higher standard deviation values, being five in the Visible region, three in the Red Edge and NIR1 regions, and three in the NIR2 region (Figure 12, Table 2). Observing the transformed signatures of the classes, five components are selected for the Visible region, again three components for the Red Edge and NIR1 regions, and two components are selected for the NIR2 region (Figure 13, Table 2). Finally, in Figure 11, the ROIs separability results are stabilized using four components in the Visible region, and three components for Red Edge, NIR1, and NIR2 spectral regions (Table 2).

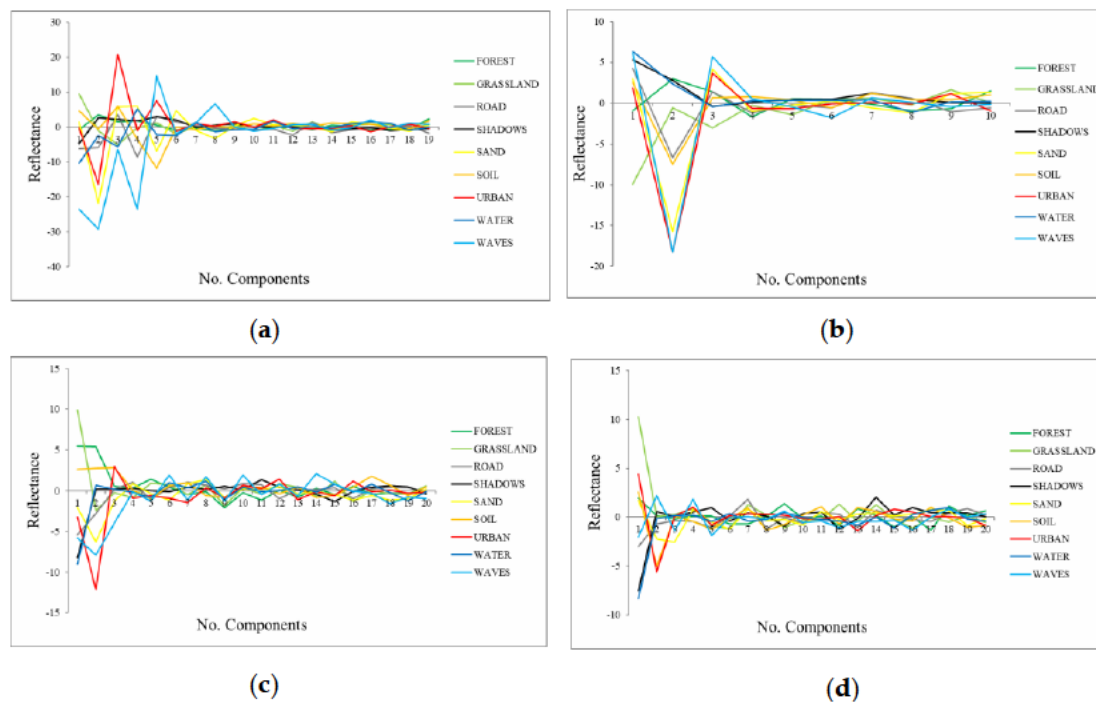


**Figure 13.** Transformed signatures of each class in: (a) the Visible region; (b) the Red Edge region; (c) the NIR1 region; and (d) the NIR2 region.

As observed in Table 2, there are some disagreements in the number of components for the Visible and the NIR2 regions, where finally five and two components were selected, respectively. Thus, we decided to create a stacked transformed space with five components for the Visible region, three for the Red Edge and NIR1 regions, and two for the NIR2 region.

Once the MNF stacked transformed space with 13 components was generated, the ROIs separability of the components selected in each spectral division group, as well as in the stacked transformed space, was computed (Figure 14). Moreover, the signatures in the stacked transformed space were obtained (Figure 15). Finally, SVM classifier was applied to the components selected in each spectral division group and in the stacked transformed space (Figure 16). Then, the SVM accuracies were compared with the SVM classifications obtained in Section 3.1 in order to evaluate not only which methodology is more suitable for obtaining an accurate thematic map but also to assess the influence of using the appropriate components in the classification process.



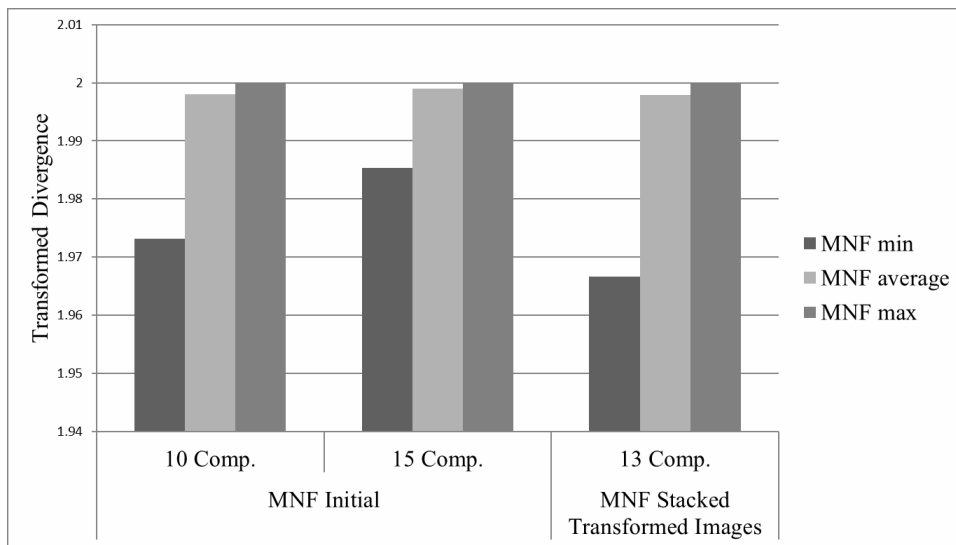


Figure 14. ROIs separability of the MNF transformed space of the initial transformation (spectral division not applied) using 10 and 15 components and from the stacked transformed space (13 comp.).

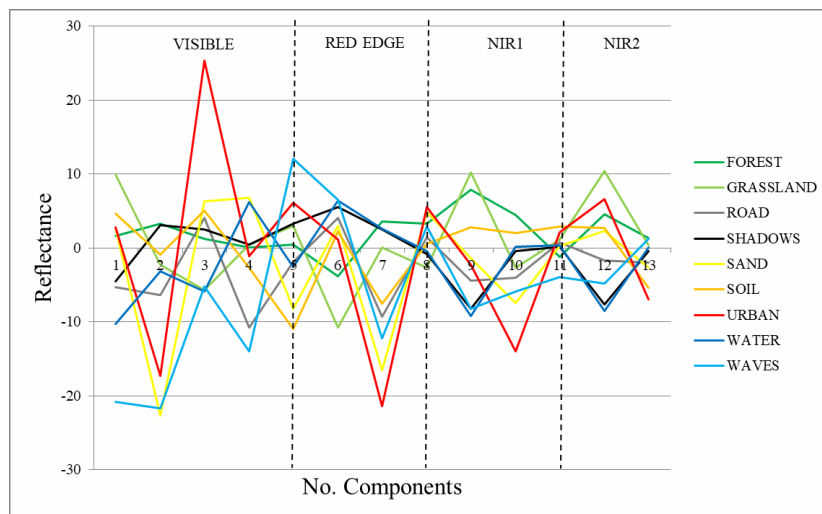


Figure 15. Transformed signatures of the classes in the stacked MNF transformed space: 13 comp.

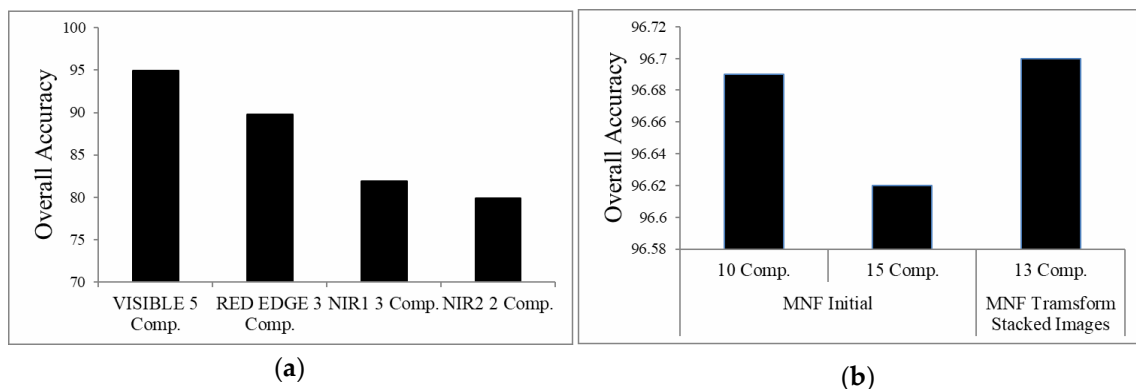


Figure 16. Overall Accuracy (%) of SVM classification of MNF transformed space for: (a) the components selected in each spectral region; and (b) MNF initial transformation (spectral division not applied) using 10 and 15 components and from the stacked transformed space (13 comp.).

Figure 14 shows the ROIs separability results from the MNF initial transformation using 10 and 15 components and in the stacked transformed space with 13 components. The minimum value for every transformed space is above 1.9. However, the minimum value in the stacked transformed space is a bit lower than in the original MNF transformations.

The transformed signatures of the classes in the stacked MNF transformed space (Figure 15) reveal, as well, how the visible region discriminates them slightly better, as is the case with the ROIs separability (Figure 11a).

It is again observed, in Figure 16a, how the Visible region obtains a better OA. Regarding the classification accuracy in the MNF transformed spaces, Figure 16b also shows the OA of the SVM classification applied in the MNF initial transformation using 10 and 15 components (see Figure 4), in order to compare with this second approach. SVM classification applied in the stacked MNF transformed space with 13 components obtains the highest accuracy (96.7%), being a bit higher than the original MNF transformation with 10 components (96.69%).

#### 4. Conclusions

The objectives of this study were to carry out a comparative evaluation of classical dimensionality reduction techniques (PCA, MNF, and ICA) in HSI and to assess different strategies for selecting the most suitable number of components. At the same time, we proposed to carry out a dimensionality reduction approach considering a spectral division of the HSI in order to analyze if the number of components selected was more suitable for generating a final thematic map.

In the first part of the study, according to the SVM classification results, MNF was the most suitable dimensionality reduction technique. Regarding the component selection strategies, entropy measurement, transformed signatures of the classes, and ROIs separability strategies are more appropriate for the components' selection. However, the transformed signatures of the classes and ROIs separability strategies need a manual ROIs selection for each class. In contrast, it was demonstrated that eigenvalues are not the most appropriated method to select a suitable number of components containing most of the statistical information.

On the other hand, the second part of the study proposed a spectral division of the HSI, and then performed an MNF transformation independently on the different regions of the electromagnetic spectrum. Once this MNF transformation was carried out, the components with more information were selected according to the different strategies. It can be observed that using this spectral division approach, when comparing it with the traditional MNF transformation, only slightly improves the components' selection.

Therefore, after the evaluation, the standard deviation values of the entropy are proposed to determine the appropriate number of components. However, if a supervised classification is carried out, in which the classes and the corresponding ROIs are determined, the transformed signatures of each class as well as the ROIs separability values, in the transformed space, are a good choice. In this way, the selection of components would be adjusted to each user and each classification problem.

A more comprehensive study should be carried out to evaluate if this method would be recommended as a component selection strategy. In consequence, this study is currently being performed using different types of HSI, since these results could be influenced by the imagery considered.

**Acknowledgments:** The authors want to acknowledge INTA (Instituto Nacional de Técnica Aeroespacial) for providing the CASI imagery. This research has been supported by the ARTEMISAT-2 (CTM2016-77733-R) project, which was funded by the Spanish *Agencia Estatal de Investigación* (AEI) and by the *Fondo Europeo de Desarrollo Regional* (FEDER). This work was completed while E. I-U was a Ph.D. student in the IOGAG Doctoral Program in Oceanography and Global Change (ULPGC), and it was funded by the Spanish *Ministerio de Economía y Competitividad* with a FPI grant (BES-2014-069426).

**Author Contributions:** All of the authors contributed extensively to the work, developing the methodology, and analyzing the results. Edurne Ibarrola-Ulzurrun processed the hyperspectral data, carried out the dimensionality reduction techniques, analyzed the different component selection strategies, and wrote the overall paper, supervised by Javier Marcello and Consuelo Gonzalo-Martin, who were also involved in the manuscript's discussion and revision.

**Conflicts of Interest:** The authors declare no conflict of interest. The founding sponsors had no role in the design of the study; in the collection, analyses, or interpretation of data; in the writing of the manuscript, and in the decision to publish the results.


## References

1. Ren, J.; Zabalza, J.; Marshall, S.; Zheng, J. Effective feature extraction and data reduction in remote sensing using hyperspectral imaging. *IEEE Signal Process. Mag.* **2014**, *31*, 149–154. [[CrossRef](#)]
2. Li, C.; Yin, J.; Zhao, J. Using improved ICA method for hyperspectral data classification. *Arabian J. Sci. Eng.* **2014**, *39*, 181–189. [[CrossRef](#)]
3. Benediktsson, J.A.; Ghamisi, P. *Spectral-Spatial Classification of Hyperspectral Remote Sensing Images*; Artech House: Boston, MA, USA, 2015.
4. Ballanti, L.; Blesius, L.; Hines, E.; Kruse, B. Tree species classification using hyperspectral imagery: A comparison of two classifiers. *Remote Sens.* **2016**, *8*, 445. [[CrossRef](#)]
5. Villa, A.; Chanussot, J.; Jutten, C.; Benediktsson, J.A.; Moussaoui, S. On the use of ICA for hyperspectral image analysis. In Proceedings of the IEEE International Geoscience and Remote Sensing Symposium (IGARSS), Cape Town, South Africa, 12–17 July 2009; Volume 4, pp. 97–100.
6. Melgani, F.; Bruzzone, L. Classification of hyperspectral remote sensing images with support vector machines. *IEEE Trans. Geosci. Remote Sens.* **2004**, *42*, 1778–1790. [[CrossRef](#)]
7. Hughes, G. On the mean accuracy of statistical pattern recognizers. *IEEE Trans. Inf. Theory* **1968**, *14*, 55–63. [[CrossRef](#)]
8. Ghamisi, P.; Benediktsson, J.A.; Phinn, S. Land-cover classification using both hyperspectral and Lidar data. *Int. J. Image Data Fusion* **2015**, *6*, 189–215. [[CrossRef](#)]
9. Fassnacht, F.E.; Neumann, C.; Förster, M.; Buddenbaum, H.; Ghosh, A.; Clasen, A.; Joshi, P.K.; Koch, B. Comparison of feature reduction algorithms for classifying tree species with hyperspectral data on three central European test sites. *IEEE J. Sel. Top. Appl. Earth Obs. Remote Sens.* **2014**, *7*, 2547–2561. [[CrossRef](#)]
10. Ibrahim, R.W.; Moghaddasi, Z.; Jalab, H.A.; Noor, R.M. Fractional differential texture descriptors based on the Machado entropy for image splicing detection. *Entropy* **2015**, *17*, 4775–4785. [[CrossRef](#)]
11. Licciardi, G.A.; Frate, F. In A comparison of feature extraction methodologies applied on hyperspectral data. In Proceedings of the 2010 Hyperspectral Workshop, Frascati, Italy, 17–19 March 2010; pp. 17–19.
12. Wang, L.; Zhao, C. *Hyperspectral Image Processing*; Springer: Berlin, German, 2016.
13. Luo, G.; Chen, G.; Tian, L.; Qin, K.; Qian, S.-E. Minimum noise fraction versus principal component analysis as a preprocessing step for hyperspectral imagery denoising. *Can. J. Remote Sens.* **2016**, *42*, 106–116. [[CrossRef](#)]
14. Chang, C.-I.; Du, Q.; Sun, T.-L.; Althouse, M.L. A joint band prioritization and band-decorrelation approach to band selection for hyperspectral image classification. *IEEE Trans. Geosci. Remote Sens.* **1999**, *37*, 2631–2641. [[CrossRef](#)]
15. Cheryadat, A.; Bruce, L.M. Why principal component analysis is not an appropriate feature extraction method for hyperspectral data. In Proceedings of the IEEE International Geoscience and Remote Sensing Symposium, IGARSS, Toulouse, France, 21–25 July 2003; pp. 3420–3422.
16. Du, H.; Qi, H.; Wang, X.; Ramanath, R.; Snyder, W.E. Band selection using independent component analysis for hyperspectral image processing. In Proceedings of the IEEE Applied Imagery Pattern Recognition Workshop, Washington, DC, USA, 15–17 October 2003; Volume 32, pp. 93–98.
17. Lennon, M.; Mercier, G.; Mouchot, M.; Hubert-Moy, L. Independent component analysis as a tool for the dimensionality reduction and the representation of hyperspectral images. In Proceedings of the IEEE International Geoscience and Remote Sensing Symposium (IGARSS), Sydney, Australia, 9–13 July 2001; pp. 2893–2895.
18. Wang, J.; Chang, C.-I. Independent component analysis-based dimensionality reduction with applications in hyperspectral image analysis. *IEEE Trans. Geosci. Remote Sens.* **2006**, *44*, 1586–1600. [[CrossRef](#)]
19. Liao, W.; Vancoillie, F.; Devriendt, F.; Gautama, S.; Pizurica, A.; Philips, W. Fusion of pixel-based and object-based features for classification of urban hyperspectral remote sensing data. In Proceedings of the 5th International Conference on Geographic Object-Based Image Analysis (GEOBIA), Thessaloniki, Greece, 21–24 May 2014; pp. 179–184.


20. Múcher, C.A.; Kooistra, L.; Vermeulen, M.; Borre, J.V.; Haest, B.; Haveman, R. Quantifying structure of natura 2000 heathland habitats using spectral mixture analysis and segmentation techniques on hyperspectral imagery. *Ecol. Indic.* **2013**, *33*, 71–81. [[CrossRef](#)]
21. Cortes, C.; Vapnik, V. Support vector machine. *Mach. Learn.* **1995**, *20*, 273–297. [[CrossRef](#)]
22. Mountrakis, G.; Im, J.; Ogole, C. Support vector machines in remote sensing: A review. *ISPRS J. Photogramm. Remote Sens.* **2011**, *66*, 247–259. [[CrossRef](#)]
23. Rojas, M.; Dópido, I.; Plaza, A.; Gamba, P. Comparison of support vector machine-based processing chains for hyperspectral image classification. *Proc. SPIE* **2010**, *78100B*. [[CrossRef](#)]
24. Denghui, Z.; Le, Y. Support vector machine based classification for hyperspectral remote sensing images after minimum noise fraction rotation transformation. In Proceedings of the IEEE International Conference Internet Computing & Information Services (ICICIS), Hong Kong, China, 17–18 September 2011; pp. 32–135.
25. Rodarmel, C.; Shan, J. Principal component analysis for hyperspectral image classification. *Surv. Land Inf. Sci.* **2002**, *62*, 115.
26. Chandrashekar, G.; Sahin, F. A survey on feature selection methods. *Comput. Electr. Eng.* **2014**, *40*, 16–28. [[CrossRef](#)]
27. Wiersma, D.J.; Landgrebe, D.A. Analytical design of multispectral sensors. *IEEE Trans. Geosci. Remote Sens.* **1980**, *GE-18*, 180–189. [[CrossRef](#)]
28. Drumetz, L.; Veganzones, M.A.; Gómez, R.M.; Tochon, G.; Dalla Mura, M.; Licciardi, G.A.; Jutten, C.; Chanussot, J. Hyperspectral local intrinsic dimensionality. *IEEE Trans. Geosci. Remote Sens.* **2016**, *54*, 4063–4078. [[CrossRef](#)]
29. Kaewpijit, S.; Le-Moige, J.; El-Ghazawi, T. Hyperspectral Imagery Dimension Reduction Using Principal Component Analysis on the HIVE. In Proceedings of the Science Data Processing Workshop, Greenbelt, MD, USA, 26–28 February 2002.
30. Vidal, M.; Amigo, J.M. Pre-processing of hyperspectral images. Essential steps before image analysis. *Chemom. Intell. Lab. Syst.* **2012**, *117*, 138–148. [[CrossRef](#)]
31. Richards, J.A. *Remote Sensing Digital Image Analysis*; Springer: Berlin, Germany, 1999; Volume 3.
32. Hyvärinen, A.; Oja, E. Independent component analysis: Algorithms and applications. *Neural Netw.* **2000**, *13*, 411–430. [[CrossRef](#)]
33. Green, A.A.; Berman, M.; Switzer, P.; Craig, M.D. A transformation for ordering multispectral data in terms of image quality with implications for noise removal. *IEEE Trans. Geosci. Remote Sens.* **1988**, *26*, 65–74. [[CrossRef](#)]
34. Francis, J.G. The QR transformation—Part 2. *Comput. J.* **1962**, *4*, 332–345. [[CrossRef](#)]
35. Padmanaban, R.; Bhowmik, A.K.; Cabral, P.; Zamyatin, A.; Almegdadi, O.; Wang, S. Modelling urban sprawl using remotely sensed data: A case study of Chennai city, Tamilnadu. *Entropy* **2017**, *19*, 163. [[CrossRef](#)]
36. Anys, H.; Bannari, A.; He, D.; Morin, D. Texture analysis for the mapping of urban areas using airborne MEIS-II images. In Proceedings of the First International Airborne Remote Sensing Conference and Exhibition, Strasbourg, France, 12–15 September 1994; Environmental Research Institute of Michigan: Ann Arbor, MI, USA, 1994; pp. 231–245.
37. Huang, X.; Zhang, L. An SVM ensemble approach combining spectral, structural, and semantic features for the classification of high-resolution remotely sensed imagery. *IEEE Trans. Geosci. Remote Sens.* **2013**, *51*, 257–272. [[CrossRef](#)]
38. Pal, M.; Mather, P.M. Assessment of the effectiveness of support vector machines for hyperspectral data. *Future Gener. Comput. Syst.* **2004**, *20*, 1215–1225. [[CrossRef](#)]
39. Braun, A.C.; Weidner, U.; Hinz, S. Support vector machines for vegetation classification—A revision. *Photogramm. Fernerkund. Geoinf.* **2010**, *2010*, 273–281. [[CrossRef](#)]







CHAPTER 6.  
HYPERSENSPECTRAL  
CLASSIFICATION THROUGH  
UNMIXING ABUNDANCE  
MAPS ADDRESSING THE  
SPECTRAL VARIABILITY





This chapter includes the following published article: E. Ibarrola-Ulzurrun, L. Drumetz, J. Marcello, C. Gonzalo-Martín, J. Chanussot. *Hyperspectral classification through unmixing abundance maps addressing the spectral variability*. IEEE Transactions on Geoscience and Remote Sensing. Accepted.

As it was explained in Chapter 2, once the HS imagery pre-processing is executed, two processing steps can be carried out, spectral unmixing and classification. The paper is focused on spectral unmixing models in which the spectral variability was considered, as well as the spatial information. Its main objectives of the paper are: (i) analysis of the spectral variability of the endmembers; (ii) analysis of the use of classification maps, to assess the performance of the unmixing models; and (iii) obtaining accurate classification maps using a small training set.

Usually, the HS image acquired from airbornes or drones cover narrow stripes with different radiometric values. Moreover, if a mountainous area is covered by the image, the reflectance value of a same material varies depending on the orientation with respect the sun and the sensor angles. Thus, to efficiently apply an unmixing model, it is necessary to correctly identify the spectral response of each endmember. Besides, the hyperdimensionality of this type of imagery, as well as the presence mixed pixels, must be taken into account. Thus, it is necessary to develop different strategies that consider this spectral variability of the materials. Reasonable abundances maps were obtained and used to get accurate thematic maps.

The main contributions and conclusions of this study are:

- Assessment of different spectral unmixing methods: linear mixing models as FCLSU, and models that consider the spectral variability of the classes, as SCLSU, ELMM and RELMM.
- The importance to use unmixing models which consider the spectral variability in areas with topographic changes, radiometric disturbances, etc.
- The good performance of the classification maps obtained from the abundance maps, as a tool for evaluating the unmixing models as well as for providing accurate classifications results.
- When applying unmixing models which consider the spectral variability, it is not necessary a high number of training samples for obtaining accurate classifications using the abundances maps. Thus, the “Hughes” phenomenon is avoided.
- The main outcome of this chapter is the final thematic maps obtained from HS imagery of the Teide National Park.





# Hyperspectral Classification through Unmixing Abundance Maps Addressing Spectral Variability

Edurne Ibarrola-Ulzurrun, Lucas Drumetz, *Member, IEEE*, Javier Marcello, *Senior Member, IEEE*, Consuelo Gonzalo-Martín, and Jocelyn Chanussot, *Fellow, IEEE*

**Abstract**— Climate change and anthropogenic pressure are causing an indisputable decline in biodiversity; therefore, the need of environmental knowledge is important to develop the appropriate management plans. In this context, remote sensing and, specifically, hyperspectral imagery (HSI) can contribute to the generation of vegetation maps for ecosystem monitoring. To properly obtain such information and to address the mixed pixels inconvenience, the richness of hyperspectral data allows the application of unmixing techniques. In this sense, a problem found by the traditional linear mixing model (LMM), a Fully Constrained Least Squared Unmixing (FCLSU), is the lack of ability to account for spectral variability. This study focuses on assessing the performance of different spectral unmixing models depending on the quality and quantity of endmembers. A complex mountainous ecosystem with high spectral changes was selected. Specifically, FCLSU and 3 approaches, which consider the spectral variability, were studied: Scaled Constrained Least Squares Unmixing (SCLSU), Extended LMM (ELMM) and Robust ELMM (RELMM). The analysis includes two study cases: (i) robust endmembers and (ii) non-robust endmembers. Performances were computed using the reconstructed Root Mean Square Error (RMSE) and classification maps taking the abundances maps as inputs. It was demonstrated that advanced unmixing techniques are needed to address the spectral variability to get accurate abundances estimations. RELMM obtained excellent RMSE values and accurate classification maps with very little knowledge of the scene and minimum effort in the selection of endmembers, avoiding the curse of dimensionality problem found in HSI.

**Index Terms**— CASI, hyperspectral image classification, spectral unmixing, Hughes phenomenon, endmembers, spectral variability.

## I. INTRODUCTION

**D**URING the last decades, the increasing loss of biodiversity has become a global concern [1]. For instance, variations in vegetation lead to an alteration of the habitat structure, causing changes in the ecosystem biodiversity. Thus, knowledge on the conservation status and habitat structure of natural areas becomes essential for environmental management. Nowadays, most conservation status assessments are based on field observations and/or aerial photo interpretations, being a very labor-intensive and time-consuming processes. Instead, remote sensing is a valuable, accurate and repeatable tool for mapping and monitoring ecosystems and to study their conservation status [2, 3]. Specifically, hyperspectral image analysis techniques have significantly contributed to these tasks. However, it remains a challenge, requiring sensors and methods which

can deal with complex habitats structures present in ecosystems [1, 4].

Hyperspectral imagery (HSI) are built by hundreds of narrow and contiguous spectral bands covering the electromagnetic spectrum, typically from the visible to the near-infrared, and sometimes also shortwave infrared spectral bands (0.3-2.5  $\mu\text{m}$ ) [5, 6]. The rich spectral information available in HSI increases the capability of precisely discriminating the materials or covers of interest [7, 8].

Hyperspectral image classification has been a very active area of research in the last years [9, 10]. Even though HSI is a suitable tool for source separation and classification processes, conventional HSI classification methods suffer from important limitations for detailed ecosystem mapping due to the limited degree of detail that can be mapped. It also increases the computational load because of the enhancement of spectral resolution, which leads to high dimensional data that can degrade the classification process [11]. Another limitation of HSI classification is the little availability of ground truth data in practice. For instance, supervised classification is generally a difficult task due to the ratio between the high dimensionality of the data and the limited availability of labeled training samples [7]. The rule of thumb is that the required number of training samples is linearly related to the dimensionality of the data. This problem is called the *curse of dimensionality*, or *Hughes phenomenon* [10, 12], which specifies that the size of training samples set required for classification increases exponentially with the number of spectral bands [13].

On the other hand, when more details are required in the classification process, the more difficulties arise, such as *mixed pixels*, leading to lower accuracy in classification maps [2]. Besides, the spatial resolution of a sensor could be too low to distinguish materials, leading to a composite of individual spectra in the same pixel. Thus, the recognition of pixels is frequently a combination of numerous materials which introduces a need to quantitatively decompose, or *unmix*, this mixture [14]. In this context, hyperspectral unmixing may be the right tool to move beyond the pixel-based limitations for ecosystem mapping and monitoring [2].

Spectral unmixing refers to any process that retrieves the pure spectral components, called *endmembers*, and a set of fractional *abundances*, that indicate the proportion of each endmember [7, 14]. Endmembers are, generally, assumed to represent the pure materials present in the image, whereas

the set of abundances at each pixel, represents the percentage of each endmember present in the pixel [5, 7]. The potential of spectral unmixing to estimate the spatial distribution and abundances of invasive species and vegetation has been studied [2, 15-17]. Thus, spectral unmixing could be a suitable methodology for environmental management. However, there are some issues found in unmixing techniques: (i) the notion of a pure material can be subjective and problem dependent, hence leading to a definition of endmembers that depends on the application and spatial resolution [5]; (ii) most studies assume that a proportion represents the percentage of material associated with an endmember present in a pixel. However, Hapke [18] states that the abundances in a linear mixture represent the relative area of the corresponding endmembers in a pixel [5].

Unmixing models can be, either, linear or nonlinear [5]. In most applications, Linear Mixing Model (LMM) is assumed considering that contributions of each endmember sum up in a linear way [5]. According to the LMM definition, data lie into a simplex whose vertices are defined by the endmembers [19]. However, LMM is not accurate since many real physical processes are inherently nonlinear, e.g. multiple scattering and intimate mixing, contribute to the measured radiance or reflectance. The most important source of error in LMM lies in the lack of ability to account for sufficient temporal and spatial spectral variability. This can result in significant estimation errors being propagated throughout the unmixing process [6, 20-22].

The paper focuses on spectral unmixing models in which the spectral variability is considered, as well as the spatial information. The main objectives can be divided into:

- Analysis of the endmember variability: the endmember spectral signature can change depending on the geometry and topography of the scene, atmospheric effects, noise in the image or variation of a hidden parameter (e.g. water content in vegetation). Considering endmember variability, a significant improvement can be achieved.
- Analysis of the use of classification maps, to assess the performance of the unmixing models.
- Obtaining accurate classification maps in a mountainous ecosystem with high spectral variability using few training samples, solving the issues caused by the hyperdimensionality of the data.

In this context, different unmixing models are evaluated: (i) Fully Constrained Least Squares Unmixing (FCLSU), a traditional LMM; (ii) Scaled Constrained Least Squares Unmixing (SCLSU) approach [19, 23]; (iii) Extended Linear Mixing Model (ELMM), that extends the LMM by considering endmember variability while preserving the LMM framework, and allowing the pixelwise variation of the endmembers according to scaling factors [19, 24]; and finally, (iv) Robust ELMM (RELMM) [25], a refined formulation of ELMM. The effects of the endmembers' purity and quantity for each class are also analyzed. Accurate classification maps are obtained, taking the abundance maps as inputs, to avoid the *Hughes phenomenon*, and using a hard classification method.

The paper is structured as follows: Section II contains the study area and the description of the data sets. Section

III presents the analyzed unmixing algorithms. Section IV describes the applied methodology. Section V includes the main results and a critical analysis. Finally, Section VI summarizes the main outcomes and contributions.

## II. STUDY AREA

The study is focused in a volcanic vulnerable and heterogenic ecosystem of Tenerife island (Canary Islands, Spain), the Teide National Park (28°06'N 15°24'W). The climate of the National Park is conditioned by the extreme altitude conditions (ranging between 2000 and 3718 m), strong insolation and thermal variations. It can be defined as a subalpine continental climate, very different from the prevailing one in the low and middle areas of the island [26]. It is a remarkable biodiversity hotspot with high variability of endemic species vulnerable to environmental changes [27], making Teide National Park an ecosystem with a high interest of study from an ecological point of view. The discrimination of the heterogeneous vegetation communities found in the study area is a challenging task because the different vegetation may have similar spectral response and even the same plant species has phenological changes depending on its location in the Park. Besides, due to climate change and the increment of the European rabbit population, *Spartocytisus supranubius*, a very important species in Teide National Park, is showing a negative density-damage, leading to an absence of rejuvenation, while *Pterocephalus lasiospermus* has increased its distribution and abundance despite the presence of a non-native generalist herbivore [28]. For these reasons, it is important to carry out a detailed study of Teide National Park, in order to develop a suitable management plan by the managers of the Park.

The non-herbaceous vegetation species, selected for the study due to their abundance and importance at ecological level, were: *Pinus canariensis*, *Spartocytisus supranubius*, *Pterocephalus lasiospermus* and *Descurainia bourgaeana*. The period of the year was an important factor in the selection of the acquisitions, since the relevant species bloom during spring and species are at their greatest point of spectral difference. However, plant individuals do not bloom at the same time in every part of the study area, due to climatic differences through the Park, leading to an additional spectral variation within the same plant species.

In this context, the image used for this study was acquired on 1<sup>st</sup> of June, 2017 through the CASI (Compact Airborne Spectrographic Imagery) sensor configured with 68 spectral bands, covering a range from 0.3969 to 1.0390  $\mu\text{m}$  and a spatial resolution of 0.75 meters. It was radiometrically and atmospherically corrected as well as georeferenced (Product Level 2c) [29]. Four different subsets (Fig. 1) were selected to evaluate the algorithms in an image with spectral variability related with the topography changes due to the mountainous ecosystem (Areas 3 and 4) and radiometric changes between different swaths which appear when acquiring the CASI imagery (Areas 2 and 4). Area 1 was chosen as a control subset in a zone without either topographic or radiometric changes. Finally, the four subsets have another intrinsic spectral variability due to the blooming of plant individuals.

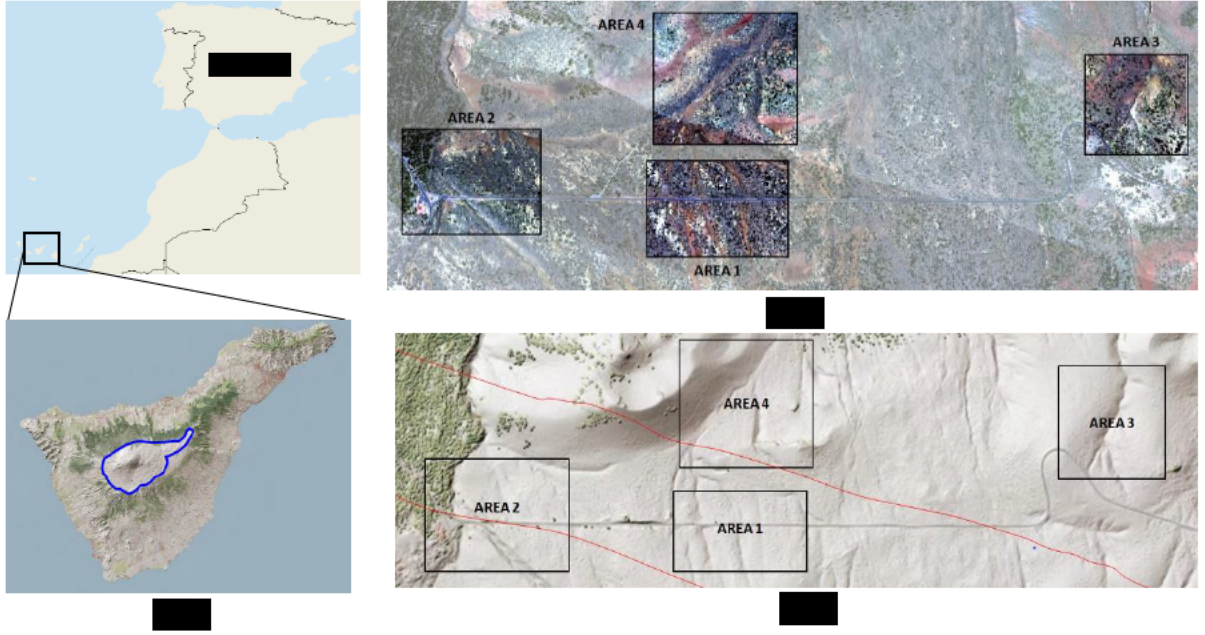


Fig. 1. Teide National Park: (a) geographic location, (b) true color composite (CASI bands X, Y Z nm) highlighting the 4 subsets used in the study and (c) digital elevation model and the swath limits in red.

### III. UNMIXING ALGORITHMS

#### A. Linear Mixing Model

Several studies have investigated the mixing scales and linearity. Singer and McCord [30] found that if the scale of the mixing is large (macroscopic), mixing occurs in a linear fashion. For microscopic or intimate mixtures, the mixing is generally nonlinear [30, 31]. The Linear Mixing Model (LMM) assumes no interaction within materials: the incident light interacts with just one material [5]. LMM considers a linear combination of the pure spectral of the materials located in the pixel area, weighted by their fractional abundance (Eq. 1).  $P$  is the number of endmembers considered,  $s_p$  is a reference endmember providing the direction of a straight line joining the origin at that point on which each local endmember lies,  $a_{pn}$  is the abundance coefficient of the endmember in pixel  $n$ ,  $e_n$  is additive noise.

$$x_n = \sum_{p=1}^P a_{pn}s_p + e_n \quad (1)$$

However, LMM shows some limitations such as nonlinearities in the mixing processes and material variability. Endmember variability comprehends that each material cannot be completely represented by a single spectrum, being a subject of intra-class variations [20]. Traditional Fully Constrained Least Squares Unmixing (FCLSU) [32] has been used in this work.

In the literature, endmember variability has been addressed using endmember bundles [33], which incorporate variability by representing each endmember by a set of spectra, each of which could reasonably be the reflectance of an instance of the endmember. Thus, endmember unmixing needs to be extended to bundle unmixing and using multiple signatures for each endmember class may provide more accurate fractions [34, 35]. In this context, several studies have implemented different methods which deal with the endmember spectral variability, such as Multiple Endmember Spectral Mixture Analysis (MESMA)

[36], AutoMCU [37], Perturbed Linear Mixing Model (PLMM) algorithm [6].

#### B. The Scaled Constrained Least Squares Unmixing

The Scaled Constrained Least Squares Unmixing (SCLSU) (Eq. 2) model is based on LMM. It uses the nonnegative least squares to estimate the spectral variability [19, 23].  $\psi_k$  is added as a scaling factor considering the brightness changes in the spectral signature of a pixel.

$$x_n = \psi_k \sum_{p=1}^P a_{pn}s_p + e_n \quad (2)$$

Yet, SCLSU cannot consider other types of variability than scaling factors. It is a simple approach to address spectral variability assuming a scaling factor that affects equally to all the endmembers present in a pixel. Thus, a more complex version was proposed, the ELMM, which is next described.

#### C. Extended Linear Mixing Model

Spectral variability can be modeled using an accurate radiative transfer-based model such as the Hapke model [18]. This physical model allows accessing the reflectance value of a material for one wavelength, knowing the corresponding single scattering albedo, the photometric parameters of the material and the incidence, emergence, and azimuth angles during the acquisition. ELMM was derived from this model using simplifying physical assumptions [38]. ELMM [19, 24] allows a pixelwise variation of each endmember (The code is available in: <http://openremotesensing.net/knowledgebase/spectral-variability-and-extended-linear-mixing-model/>). The data points are assumed to lie in a convex cone spanned by the reference endmembers. The scaling factors, combined with the ASC (Abundance Sum-to-one Constraint) and ANC (Abundance Non-negativity Constraint), constrain each pixel to lie in a simplex whose vertices are variants of the reference endmembers, situated on straight lines joining the

origin and each of the reference endmembers, thus defining the simplex orientation in the cone. In [24], a criterion to perform spectral unmixing using the ELMM is defined in Eq. 3, where  $\psi$  is the scaling factor rearranged in a  $\mathbb{R}^{P \times N}$  matrix and by  $\underline{S} = [S_n]$  being  $n = 1, \dots, N$ , the collection of pixel-dependent endmember matrices,  $A \in \Delta_p$  means that each abundance vector  $a_n \in \mathbb{R}^P$  in each pixel belongs to the unit simplex with  $P$  vertices,  $S_0$  is a matrix containing reference endmembers,  $\|\cdot\|_F$  denotes the Frobenius norm. The term  $\lambda_S \|S_n - S_0 \psi_n\|_F^2$ , forces each endmember to be close (but not equal) to scaled versions of the (unit norm) representatives of the reference directions depending on the value  $\lambda_S$ , which is regularization parameter on the ELMM tightness. The scaling factors capture illumination induced variability, while  $S_n$  can further consider the intrinsic variability effects. Spatial regularizations incorporate two regularization parameters to tune,  $R(A)$  and  $R(\psi)$ , which are applied to the abundances and the scaling factors, respectively.  $R(A)$  is the total variation regularization term on the abundances, promoting smooth abundances while allowing sharp discontinuities when necessary (at the border between objects for instance);  $R(\psi)$  is a Tikhonov regularization on the gradient of the abundances, to promote spatial smoothness in the scaling factors. They penalize the norm of the spatial gradient of the abundance maps or scaling factors, using the total variation regularization related for the scaling factors and incorporate the constraints on the variables to enforce spatial smoothing:

$$J(A, S, \psi) = \frac{1}{2} \sum_{n=1}^N (\|x_n - S_n a_n\|_2^2 + \lambda_S \|S_n - S_0 \psi_n\|_F^2) + R(A) + R(\psi). \quad (3)$$

The data lies in a convex cone, whose edges are the endmembers and each pixel belong to a simplex (Fig. 2). However, this formulation relies on the reference endmembers,  $S_0$ , and if they are poor representatives of the spectra of the materials, they can cause errors in the estimation of the unmixing parameters. Hence, a new Robust ELMM (RELMM) is proposed [25], which does not rely on the reference endmembers.

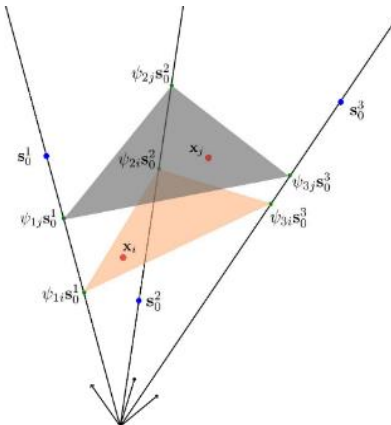


Fig. 2. Geometric interpretation of the ELMM in the case of three endmembers. Red: two data points; blue: reference endmembers; green: the scaled versions for the two considered pixels [33].

#### D. Robust Extended Linear Mixing Model

RELMM [25] shows endmembers as directions in the feature space, as directional data. The added values of RELMM are the iterative update of  $S_0$  using the volume regularized [39], adapted to a conic model via the unit norm constraints. It allows to iteratively adjust the position of the reference endmember lines in the feature space. Thus, it is proposed a new model [25] (Eq. 4), where  $tr$  denotes the trace of a matrix, and  $V = P I_P - \mathbb{1}_P \mathbb{1}_P^T$  ( $\mathbb{1}_P$ , being a column vector of  $P$  ones), such that  $tr(S_0 V S_0^T) = \sum_{i=1}^{P-1} \sum_{j=i+1}^P \|s_{0i} - s_{0j}\|_2^2$ .  $\lambda_S$  and  $\lambda_{S_0}$  are regularization parameters.

$$J(A, S, \psi, S_0) = \frac{1}{2} \sum_{n=1}^N (\|x_n - S_n a_n\|_2^2 + \lambda_S \|S_n - S_0 \psi_n\|_F^2) + \frac{\lambda_{S_0}}{2} tr(S_0 V S_0^T) + R(A) + R(\psi) \quad (4)$$

The fact that the reference endmembers are normalized has also the advantage of easily allowing to compare the magnitude of the scaling factors across different materials and images. Moreover, spatial regularizations ( $R(A)$  and  $R(\psi)$ ) can be added as in the ELMM model.

RELMM has the same geometric interpretation as ELMM, however, the reference endmembers in RELMM lie on the unit hypersphere leading to be more accurate than ELMM even when the initialization is poor [25].

## IV. METHODOLOGY

### A. Study Cases

The analysis can be divided in two different study cases. First, the different abundances maps were obtained by FCLSU, SCLSU, ELMM and RELMM, using robust reference endmembers with many representative pixels for each class under different conditions and second, using very few non-robust endmembers (Fig. 3).

For the first part of the study, an extensive field campaign was carried out and field observation data were acquired to provide accurately located and quantitative ground reference data. Then, Regions of Interest (ROIs) were manually selected in the original HSI to create accurate training and testing sample sets. Candidate pixels were selected in areas where the vegetation types appeared to be pure and were relatively homogeneous. This procedure was difficult to implement due to the small scale of species spatial distribution and the small size of some vegetation patches. Thus, samples from the vegetation species mentioned above were identified in the HSI, as well as bare soil and road endmembers. The set of ROIs was divided into a training set, to obtain the robust reference endmembers (in average 1400 pixels per class), and the testing set, to provide an independent dataset to evaluate the classification performances (in average 4500 pixels per class). Robust endmembers used in the first study case were calculated getting the average value of each class for the whole training set of ROIs. Fig. 4 shows the spectral signature of each endmember as well as picture of each vegetation class. Thus, the robust endmembers used in this part of the study consider every type of spectral variability found in the different classes.

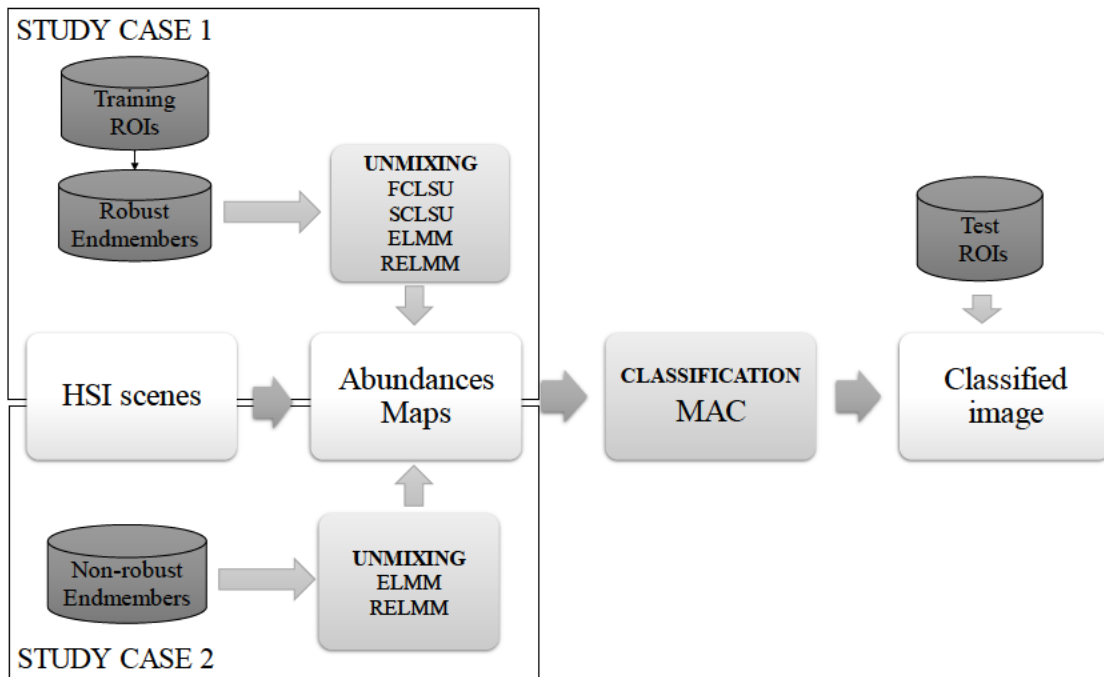


Fig. 3. Flowchart of the unmixing and classification assessment procedure.

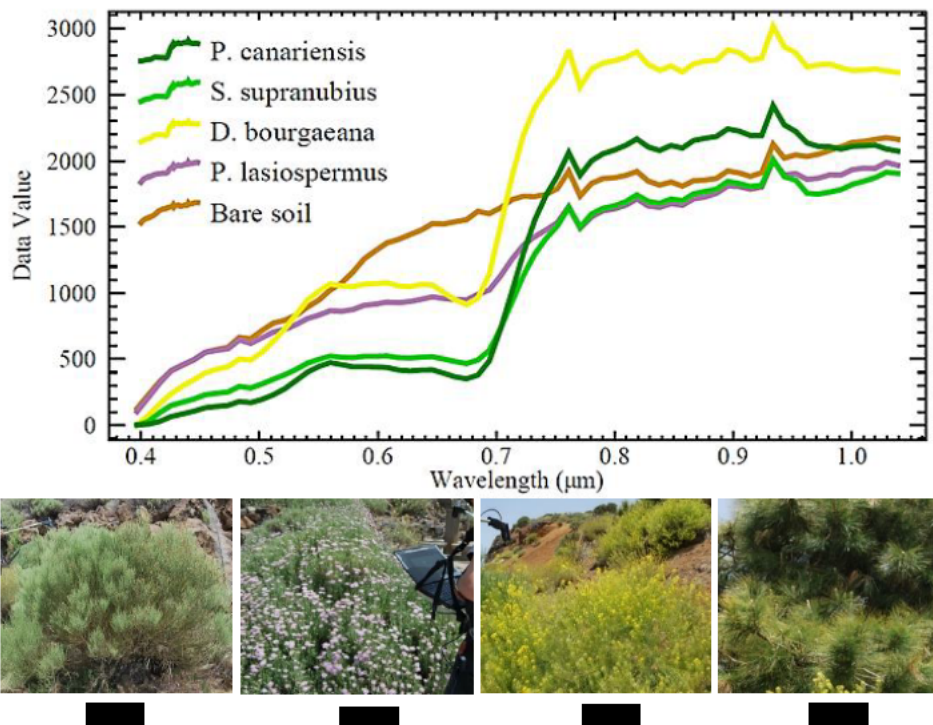


Fig. 4. Endmember spectral signatures used in the study and vegetation of interest: (a) *S. supranubius*, (b) *P. lasiospermus*, (c) *D. bourgaeana* and (d) *P. canariensis*.

In the second part of the study the performances of ELMM and RELMM are investigated, in order to show the necessity to apply unmixing models, which take the spectral variability into account, for obtaining good unmixing results. Thus, non-robust endmembers were acquired getting the average of 1, 3, 5 and 10 pixels per class. They are called non-robust endmembers because using 1 or 3 pixels for each class, spectral variability is not considered. For instance, non-robust endmembers obtained from 10 pixels will higher consider spectral variability (its robustness

increase) rather than non-robust endmembers obtained from 1 pixel. Thus, it might be seen how ELMM and RELMM models can properly adjust the non-robust endmembers, allowing to refine and correct those endmembers [25].

#### B. Methodology assessment

The quality of the unmixing results can be measured by the reconstruction error calculated by the Root Mean Squared Error (RMSE) given the set of the original pixels ( $x_{true}$ ) and the reconstruction data from the corresponding

abundances obtained from the pixels and the mixing model ( $\hat{x}_{ln}$ ).  $N$  and  $L$  are the given pixel and band, respectively [24, 40] (Eq. 5).

$$RMSE = \frac{1}{N} \sum_{n=1}^N \sqrt{\frac{1}{L} \sum_{l=1}^L (x_{lntrue} - \hat{x}_{ln})^2} \quad (5)$$

However, RMSE is an indirect measure which only shows how the model fits the data, though it is possible to achieve good reconstruction errors with poor abundance and/or spectral variability retrieval. In this context, classification maps were additionally used to assess the methodology. Even though, there exists some studies using abundances maps as inputs for classification [41, 42], classification maps are used as another evaluation process of the different unmixing models as well as to solve the hyperdimensionality of the data.

### C. HSI hyperdimensionality solving proposal

As dimensionality increases in HSI, more training samples is demanded to obtain thematic maps with higher accuracy. In literature [10, 43-46], to solve this curse of dimensionality problem, data reduction through band selection or feature extraction, reduces dimensionality without the need to increase the number of training samples [43, 47, 48]. Usually, feature extraction and feature selection methods were used by selecting the optimal bands or the optimal subset from the HSI [3]. These techniques significantly reduce the number of suitable components compared to the original dimension [49]. During the last decades, researchers have studied several approaches to alleviate the Hughes phenomenon such as Principal Component Analysis (PCA), Minimum Noise Fraction (MNF) or Independent Component Analysis (ICA). On the other hand, Kernel-based methods, such as Support Vector Machine (SVM), have demonstrated their performance in handling high-dimensional data [50].

Thus, the study proposed to use spectral unmixing models which consider the spectral variability of the different classes in order to obtain reasonable abundances maps that will be used for obtaining accurate thematic maps.

In this context, Maximum Abundance Classification (MAC) is proposed, which takes in the abundance maps, the largest abundance vector into the pixel, to set it as a class. Finally, the performance of the classification maps is assessed both in terms of visual comparisons with general field information on known vegetation structures and using the confusion matrix, whose information is summarized by the Overall Accuracy, OA, defined as the ratio of the number of validation pixels that are correctly classified to the total number of validation pixels irrespective of the class [51]. In order to obtain the confusion matrices, the testing samples obtained in the first study case were used.

## V. RESULTS AND DISCUSSION

This section presents the results of the different spectral unmixing methods in the different scenes.

The first step was to set the spatial regularization parameters for ELMM and RELMM. Specifically, the

values used were,  $\lambda_s=0.01$ ,  $\lambda_a=0.01$  and  $\lambda_{psi}=0.02$ , which are part of  $S_k$ ,  $\mathcal{R}(A)$  and  $\mathcal{R}(\psi)$  in Eq. 3 and 4, for ELMM and RELMM and  $\lambda_{s_0} = 10$ , in the RELMM model. They were selected by trial and error, leaving at the beginning  $\lambda_a$  and  $\lambda_{psi}$  at zero, in order to set a suitable  $\lambda_s$ , which is the most crucial parameter to tune. It is observed visually both the abundance and scaling factor maps. A high value of  $\lambda_s$  means that local variants of the endmembers will not drift too far away from the (scaled) reference, whereas a small value means that the local endmembers will get further away from the actual lines. In the last case, the data fit will be better, and the abundance maps will be sparser as a result, since local endmembers will tend to match individual pixels. To get an insight of what happens, scatterplot of the data and local endmembers should be performed, using the first three principal components. Once  $\lambda_s$  is well set up, it is better to choose small  $\lambda_a$  and  $\lambda_{psi}$  values. If they look very similar to the ones without the spatial regularizations, the values can be increased. On the other hand, if the abundance maps look too smooth (or even completely uniform), they are way too large and the user could decrease both  $\lambda_a$  and  $\lambda_{psi}$ .

Next, the results of the two study cases are presented.

### A. Study case 1: Spectral Unmixing using robust endmembers

As it was explained in Section III, the study is divided in two study cases. This subsection shows the results of the different spectral unmixing methodologies when robust endmembers are used as inputs.

Table I shows the average reconstructed RMSE obtained for the four different methods in the different scenes (in bold appears the best RMSE value for each scene) while Fig. 5 shows the RMSE maps. ELMM and RELMM outperform the FCLSU and SCLSU approaches as it was expected. It can be clearly appreciated the worst accuracy of FCLSU and SCLSU in areas with considerably spectral variation (Areas 2, 3 and 4) and the good performances of ELMM and RELMM even in such complex scenes. The spatial regularization on the abundances improves the results for ELMM and RELMM, being more robust to noise on the measured data, as well as on the spectral signatures. The spatial regularization allows to precisely estimate the spatially correlated abundances, removing the noise and the uncertainty that affects to FCLSU and SCLSU [24].

TABLE I  
RMSE VALUES FOR EACH SCENE USING ROBUST ENDMEMBERS  
FOR THE UNMIXING ( $\times 10^{-3}$ ).

	AREA 1	AREA 2	AREA 3	AREA 4
FCLSU	70.21	79.97	183.48	121.65
SCLSU	5.44	5.77	11.37	8.61
ELMM	0.61	0.63	1.09	<b>0.66</b>
RELMM	<b>0.57</b>	<b>0.61</b>	<b>1.07</b>	0.72

A visual representation of the extracted abundances for Area 2 is shown in Fig. 6. Regarding the abundance maps, every model, except for FCLSU, obtain plausible estimations at visual level. However, most of endmembers are purer for RELMM and ELMM than for SCLSU. The scaling factors extracted by SCLSU, ELMM and RELMM are displayed in Fig. 7. They show the spectral variation of the different classes.

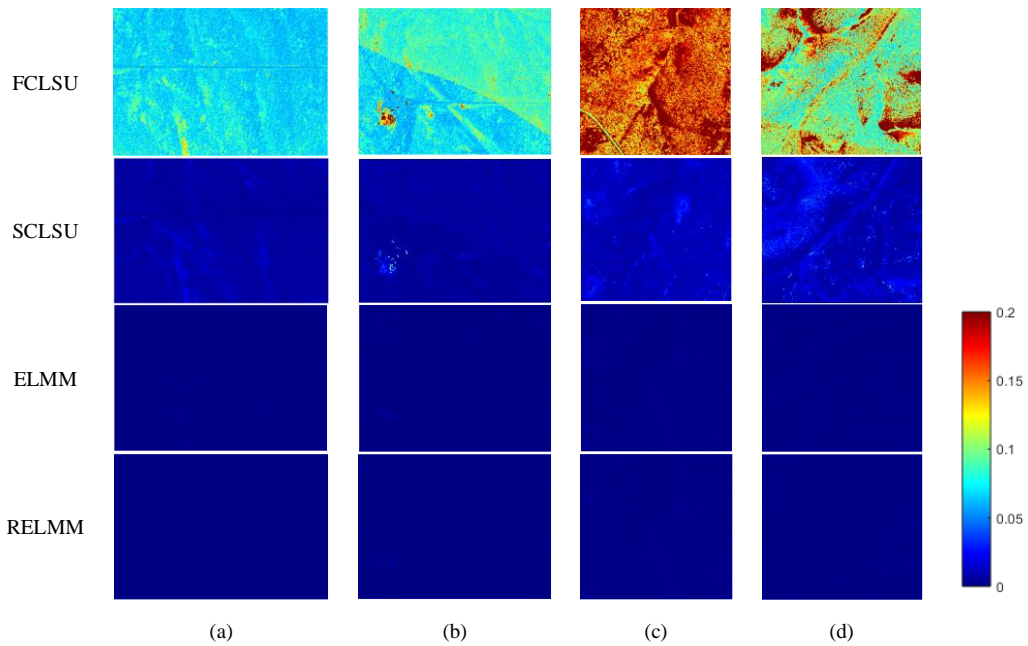


Fig. 5. RMSE maps for: FCLSU, SCLSU, ELMM and RELMM of (a) Area 1, (b) Area 2, (c) Area 3 and (d) Area 4.

As extracting spectral variability is difficult or even impossible when the materials have low abundances, pixels with abundance below 0.5 are removed from the scaling factor maps for a better interpretation. SCLSU scaling factor maps are difficult to interpret as only one scaling factor is estimated for all the endmembers. ELMM and RELMM scaling factor maps show correlation with radiometric and topographic changes, being more evident in *P. lasiospermus* and bare soil maps. In case of Area 2, RELMM gets higher values regarding the radiometric variability due to the sensor pass, being more evident in *P. lasiospermus* map, leading ELMM and RELMM to deal with the induced spectral variability. Again, RELMM obtains higher scaling factor values than ELMM, due to its ability to better adjust the references. Therefore, ELMM and RELMM obtain the best results in terms of abundance estimation, as well as spectral variability recovery.

In the case of ELMM and RELMM, the spatial coherency of the abundances and the scaling factors allows to recover the parameters more precisely. Besides, the explicit computation of a different scaling factor for each pixel and material allows obtaining sparser variability maps, which also makes ELMM and RELMM stronger in terms of interpretability. Moreover, the spatial regularization parameters of ELMM and RELMM allow to estimate the spatially correlated abundances, removing the noise and the uncertainty, which affects SCLSU, when two endmember variations of two different materials share a common global shape, and can look quite similar after appropriate scaling [24].

Fig.8 shows a scatterplot of the dataset (in blue) and the endmembers generated by the model (in red) using the first three components of a Principal Component Analysis (PCA) for Area 2. It can be observed that the different materials are equally affected by the spectral variability, being the shape of the variability (red data) or the manifold of the endmember variants, complex. All materials are affected by spectral variability and the conic model advocated by the ELMM and RELMM seems to fit the data. Besides, RELMM scatterplot is sparser than ELMM, meaning that

RELMM can adjust the reference and thus, is able to obtain sparser abundances maps.

Finally, Table II and Fig. 9 show the overall accuracy (OA) values and the MAC classifications maps obtained from the abundance maps of the unmixing models, respectively. As it was expected, ELMM and RELMM obtain the highest OA, while FCLSU obtains the lowest OA. Area 1 shows less differences within the OA obtained from the different unmixing models, as this area lacks spectral variability. The difference between the OA values obtained from ELMM and RELMM abundances maps is small (less than 2% in case of Area 1 and less than 0.36% in Areas 2, 3 and 4). Regarding the classification maps, there is no great visual differences within SCLSU, ELMM and RELMM, whereas, FCLSU classification map clearly shows the radiometric change in the scene, showing how the model does not consider the spectral variability. Regarding the results presented in Fig. 9, some misclassifications can be identified. For instance, some pixels classified as urban (red) or roads (black) appear in bare soil areas. Moreover, in the FCLSU map, *S. supranubius* is incorrectly assigned to urban and road pixels in some areas. Specifically, classes with lower classification accuracy in the four areas analyzed are *S. supranubius* and urban (ca. 60% well classified versus ca. 80% for the remaining classes). Finally, analyzing the overall accuracy (OA%) results, it is obvious how SCLSU, ELMM and RELMM are considering the spectral variability regarding the blooming of plant individuals.

TABLE II  
OA VALUES IN PERCENTAGE (%) RESULTING FROM THE ABUNDANCES  
MAPS OBTAINED WITH ROBUST ENDMEMBERS.

	AREA 1	AREA 2	AREA 3	AREA 4
FCLSU + MAC	76.06	78.81	85.63	64.81
SCLSU + MAC	77.08	86.95	87.43	92.62
ELMM + MAC	77.09	<b>87.23</b>	87.82	<b>92.84</b>
RELMM + MAC	<b>78.78</b>	87.00	<b>88.18</b>	92.7



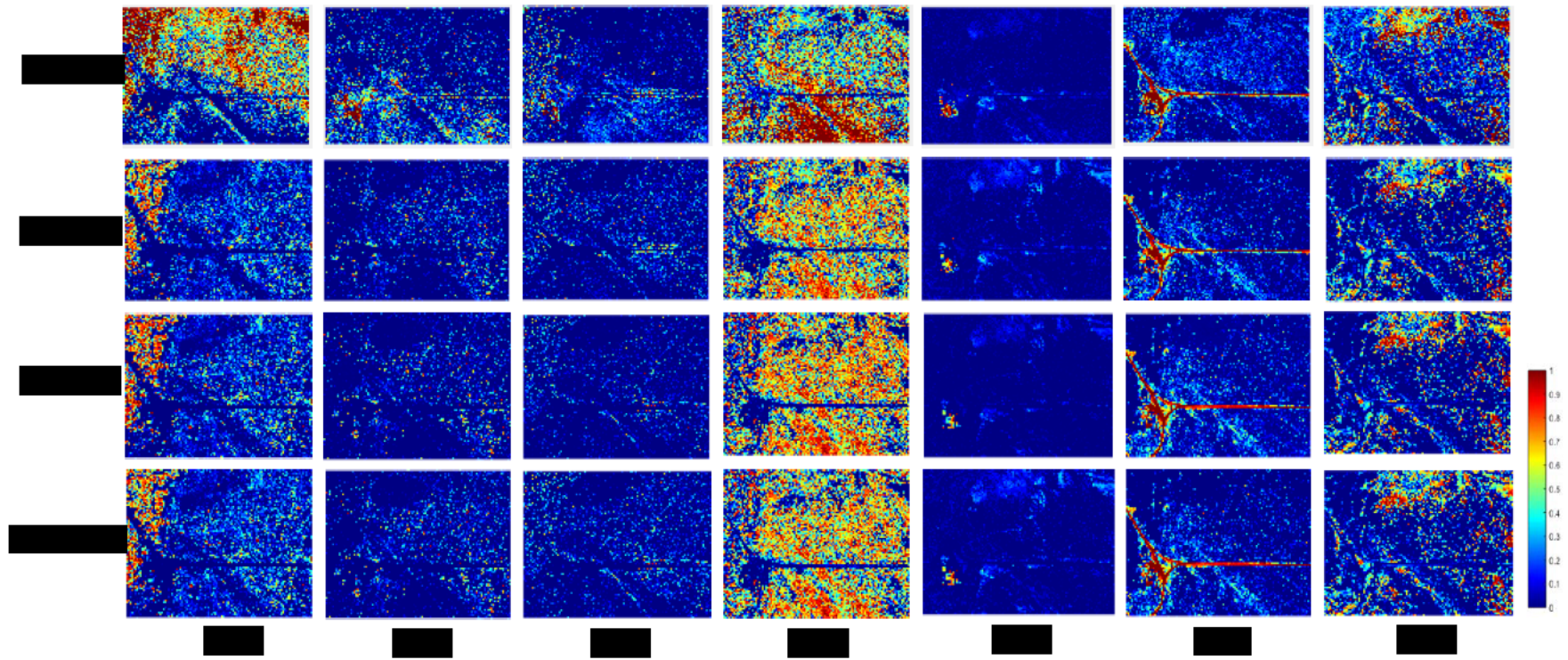


Fig. 6. Abundance maps estimated by FCLSU, SCLSU, ELMM and RELMM of Area 2. (a) *P. canariensis*, (b) *S. supranubius*, (c) *D. bourgaeana*, (d) *P. lasiospermus*, (e) Urban, (f) Road and (g) Bare soil.

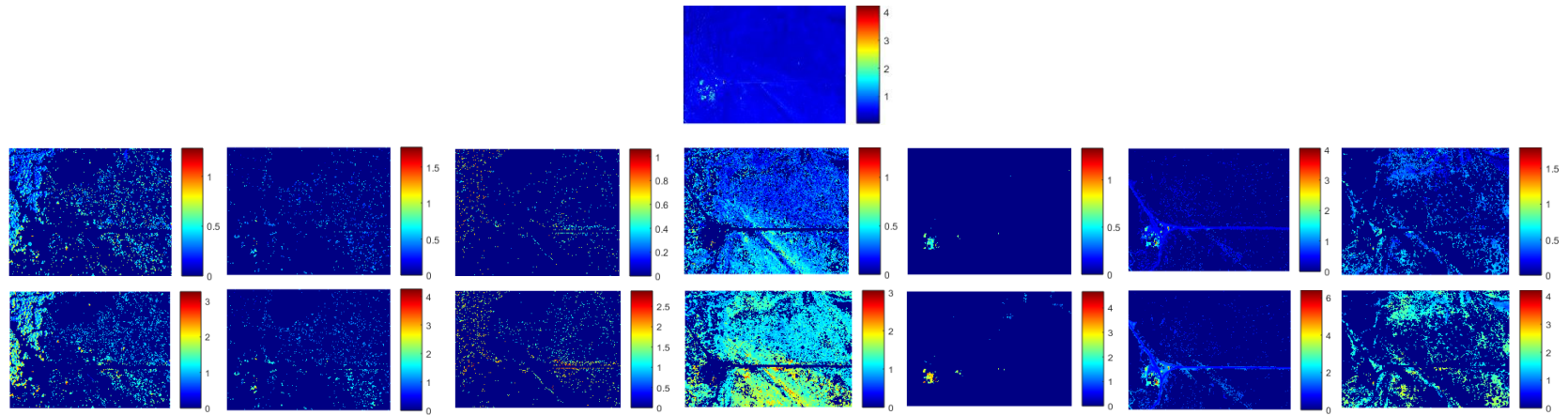


Fig. 7. Scaling factor maps from SCLSU (one scaling factor for all the endmembers), ELMM and RELMM with  $> 0.5$  abundances of Area 2. (a) *P. canariensis*, (b) *S. supranubius*, (c) *D. bourgaeana*, (d) *P. lasiospermus*, (e) Urban, (f) Road and (g) Bare soil.

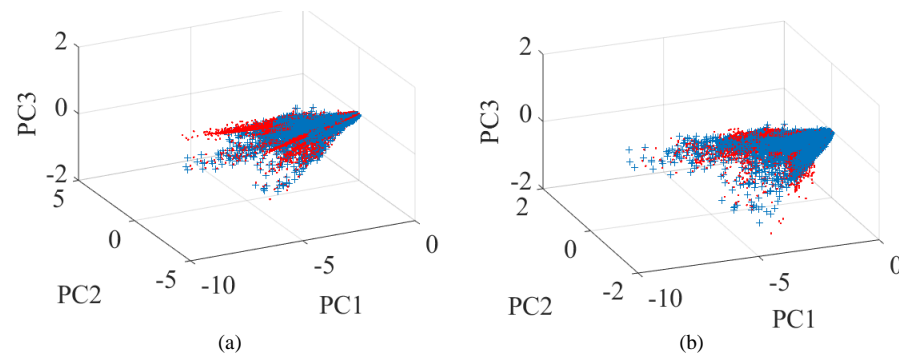


Fig. 8. PCA scatterplot for (a) ELMM and (b) RELMM of Area 2. In blue the data and in red the extracted endmembers.

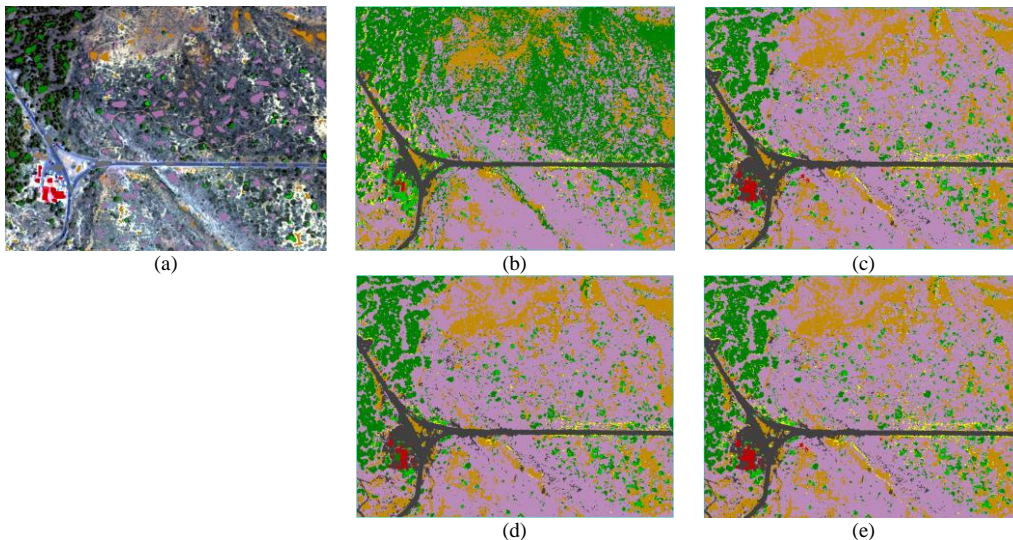


Fig. 9. (a) Ground Truth Samples and Classification maps obtained by: (b) FCLSU, (c) SCLSU, (d) ELMM and (e) RELMM after applying a MAC classification in Area 2.

### B. Study case 2: Spectral Unmixing using non-robust endmembers.

As it was observed in Tables I and II, even though ELMM and RELMM got better results, there is not too much difference between them. Both models consider the spectral variability of endmembers, but if this spectral variability is included in the model by taking many robust endmembers, the robustness of RELMM is not significant. Thus, it seems RELMM will not improve the results much, leading to even slightly worse performance.

Besides, as it is explained in [24], if the abundance of one material is low in a pixel, a different scaling factor for this material will change the orientation of the simplex related to this pixel, but the edge of the simplex, linking the other two (scaled) endmembers, will not change. Hence, the abundance coefficients for the other two materials will not change much either. In this context, both ELMM and RELMM do not require pure pixels to extract the spectral variability of a material efficiently, but only a significant abundance contribution of this material in the considered pixel, or in the neighboring area. Taking this fact into consideration, in this part of the study, non-robust endmembers were acquired selecting 1, 3, 5 and 10 pixels per class. In this way, the spectral variability is not considered in the endmembers. Since, the objective was to observe the robustness of RELMM and ELMM, only both models are included in this study case.

Table III shows the RMSE values for ELMM and RELMM using 1, 3, 5 and 10 pixels to obtain and average endmember for each class. The RMSE values are mostly the same for both methods, except in some cases (Area 2 and Area 3), where RELMM got slightly better RMSE. Moreover, the values show a minimum change when more than 1 pixel is taken as reference endmember.

TABLE III  
RMSE VALUES FOR EACH SCENE USING NON-ROBUST ENDMEMBERS FOR THE UNMIXING ( $\times 10^{-4}$ ).

	AREA 1	AREA 2	AREA 3	AREA 4
ELMM_1p	7.96	9.80	14.90	<b>7.87</b>
RELMM_1p	<b>7.17</b>	<b>7.41</b>	<b>13.52</b>	8.01
ELMM_3p	6.08	7.39	12.14	<b>7.21</b>
RELMM_3p	<b>5.60</b>	<b>6.19</b>	<b>10.92</b>	7.45
ELMM_5p	5.73	6.98	11.42	7.61
RELMM_5p	<b>5.66</b>	<b>6.29</b>	<b>10.77</b>	<b>7.55</b>
ELMM_10p	5.83	6.67	11.51	<b>7.26</b>
RELMM_10p	<b>5.71</b>	<b>6.27</b>	<b>10.68</b>	7.53

Abundances and scaling factor maps (removing abundances  $< 0.5$ ) for ELMM and RELMM using endmembers from 1 and 10 pixels in Area 4 are shown in Fig. 10 and 11, respectively. It can be observed that even considering 1 or 10 pixels to obtain the reference endmembers, both methods obtain plausible abundances, although abundances values are higher in the case of taking 10 pixels for the reference endmember. Finally, we can assume the good performance of both methods as the radiometric change is solved even taking only 1 pixel for each class and using it as a reference endmember. Regarding the scaling factor maps, it is observed that the values decrease if 10 pixels are considered for the references endmembers that is when more spectral variability is taken for the reference endmembers. In this case, *S. supranubius*, *P. lasiospermus* and bare soil get lower scaling factors in the center of the ravine, as well as in the bottom of the image where sensor swath changes, again, both models have to deal with the induce spectral variability.

The qualitative results of Area 4, using scatterplots of the data in the recovered endmembers of ELMM and RELMM using endmembers obtained from 1 and 10 pixels, are shown in Fig. 12. It is observed how the endmembers in red are close to the edge of the cone defined by the data when the number

of averaged endmembers is higher, meaning that they capture more spectral variability. Moreover, RELMM scatterplots are sparser than ELMM, as it occurs in Fig. 8, leading to a better adjustment of the reference endmembers.

OA results obtained from MAC classification are shown in Table IV. Accurate classification maps with OA over 70% and achieving values over 84% for the best case depending on the area. Moreover, in most of the cases, RELMM outperforms ELMM. Finally, Fig. 13 shows that classification goodness, using ELMM and RELMM, does not improve when the robustness of the endmembers increases. 3-5 pixels are enough to generate the reference endmembers in order to obtain an accurate classification map.

TABLE IV  
OA VALUES IN PERCENTAGE (%) RESULTING FROM THE  
ABUNDANCES MAPS OBTAINED WITH NON-ROBUST  
ENDMEMBERS.

	AREA 1	AREA 2	AREA 3	AREA 4
ELMM_1p + MAC	72.44	82.89	<b>72.55</b>	90.86
RELMM_1p + MAC	<b>73.61</b>	<b>83.64</b>	72.14	<b>90.99</b>
ELMM_3p + MAC	91.25	83.68	84.91	94.21
RELMM_3p + MAC	<b>91.55</b>	<b>84.34</b>	<b>85.35</b>	<b>94.31</b>
ELMM_5p + MAC	91.29	82.04	85.26	94.86
RELMM_5p + MAC	<b>92.37</b>	<b>82.40</b>	<b>85.70</b>	<b>95.17</b>
ELMM_10p + MAC	<b>88.44</b>	82.36	87.69	95.06
RELMM_10p + MAC	88.35	<b>82.85</b>	<b>87.93</b>	<b>95.11</b>

It is observed how in this part of the study, it is not necessary to get an accurate set of training samples as in the first study case. Only few pixels per class are needed for the spectral unmixing and none for the classification, obtaining accurate classification maps with few knowledge and information of the scene and less effort, avoiding the *Hughes phenomenon*.

## VI. CONCLUSIONS

The paper analyzes different spectral unmixing models: a traditional LMM, the FCLSU, and three models in which the spectral variability as well as the spatial information are considered, SCLSU, assuming a scaling factor that affects equally to all the endmembers present in a pixel, and ELMM and RELMM that assume different scaling factors for each endmembers. The study has been conducted in an ecosystem with high spectral variability within the endmembers due to topography changes, sensor's radiometric change and an intrinsic spectral variability due to the blooming of plant individuals. In order to evaluate the methods, quantitative results using reconstructed RMSE, as well as classification maps obtained from the abundances maps, are presented.

The analysis has been divided in two different study cases. In the first one, the four models were analyzed by taking a robust set of endmembers that considers the spectral variability of the classes. Regarding the challenge that the ecosystem represents, ELMM and RELMM have shown good performance in terms of abundance estimation and spectral variability retrieval, obtaining a significant lower RMSE than FCLSU and SCLSU and higher OA in the classification. Thus, both models can be successfully applied in images with high spectral variability due to topographic changes, but also in images with radiometric differences in each track during the

airborne image sensing and the intrinsic spectral variability of plant species blooming, being experimentally confirmed to be well modelled by them.

The second study case proves that ELMM and specifically, RELMM, are useful techniques for obtaining accurate classification maps with both a minimum knowledge of the scene and less effort. Thus, very few pixels were taken to obtain an average reference endmember for each class. In case, this RMSE does not decrease when increasing the endmembers robustness (from endmembers obtained from 1 pixels to 10 pixels), meaning that increasing the endmembers robustness does not increase the precision of the abundance maps. Moreover, classification maps resulted by taking the abundance maps as inputs, using a hard classification model, RELMM obtains higher OA rather than ELMM, demonstrating that RELMM is more precise in an image with high spectral variability. Thus, the second study case allows analyzing the properties of each pixel, including additional information about the characterization of mixed pixels in the HSI by adding spectral variability. Hence, it proves that RELMM is robust to the absence of pure pixels in the scene, as well as to noise. Moreover, it is confirmed that classification does not improve when the robustness of the endmembers increases. Therefore, it is not necessary a high number of training samples, avoiding the *Hughes phenomenon* by using the abundances maps.

Consequently, an analysis of the endmember variability has been carried out in both study cases, confirming the importance to use unmixing models which consider the spectral variability. Moreover, it can be concluded from the study, the good performance of the classification maps obtained from the abundance maps, as a tool for evaluating the unmixing models as well as for providing accurate classifications results. Nowadays, obtaining accurate thematic maps are very important in order to study climate changes concerns, population dynamics, anthropogenic pressure, etc., which are essential issues for developing ecosystem management plans.

Finally, it would be interesting to test both ELMM and RELMM on other habitats with high heterogeneity and spectral variability. Future research would be devoted to study the spectral variability not only produced by the topographic changes but also by the health status of the species, drought effects and vegetation canopy. Besides, both models will be analyzed using drone imagery with higher spatial resolution (ca. 10 cm) in which the swath width is narrower and radiometric changes are more evident, as well as the topographic changes and the different structures of plant species, i.e. leaves, branches, flowers and shadows.

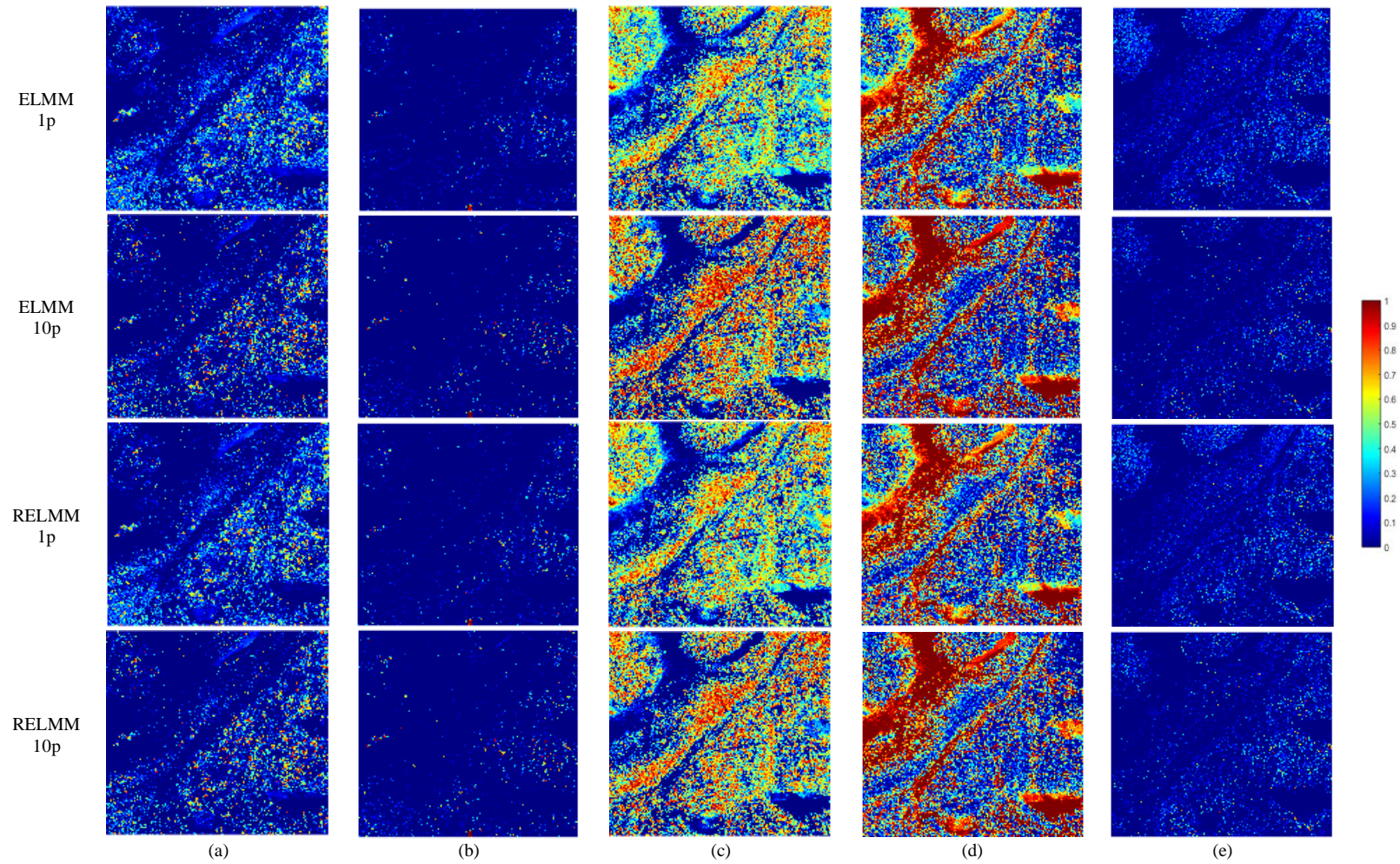


Fig. 10. Abundance maps estimated in ELMM and RELMM of Area 4 using 1 and 10 pixels for averaging the reference endmembers. (a) *S. supranubius*, (b) *P. canariensis*, (c) *P. laiospermus*, (d) Bare soil and (e) *D. bourgaeana*.

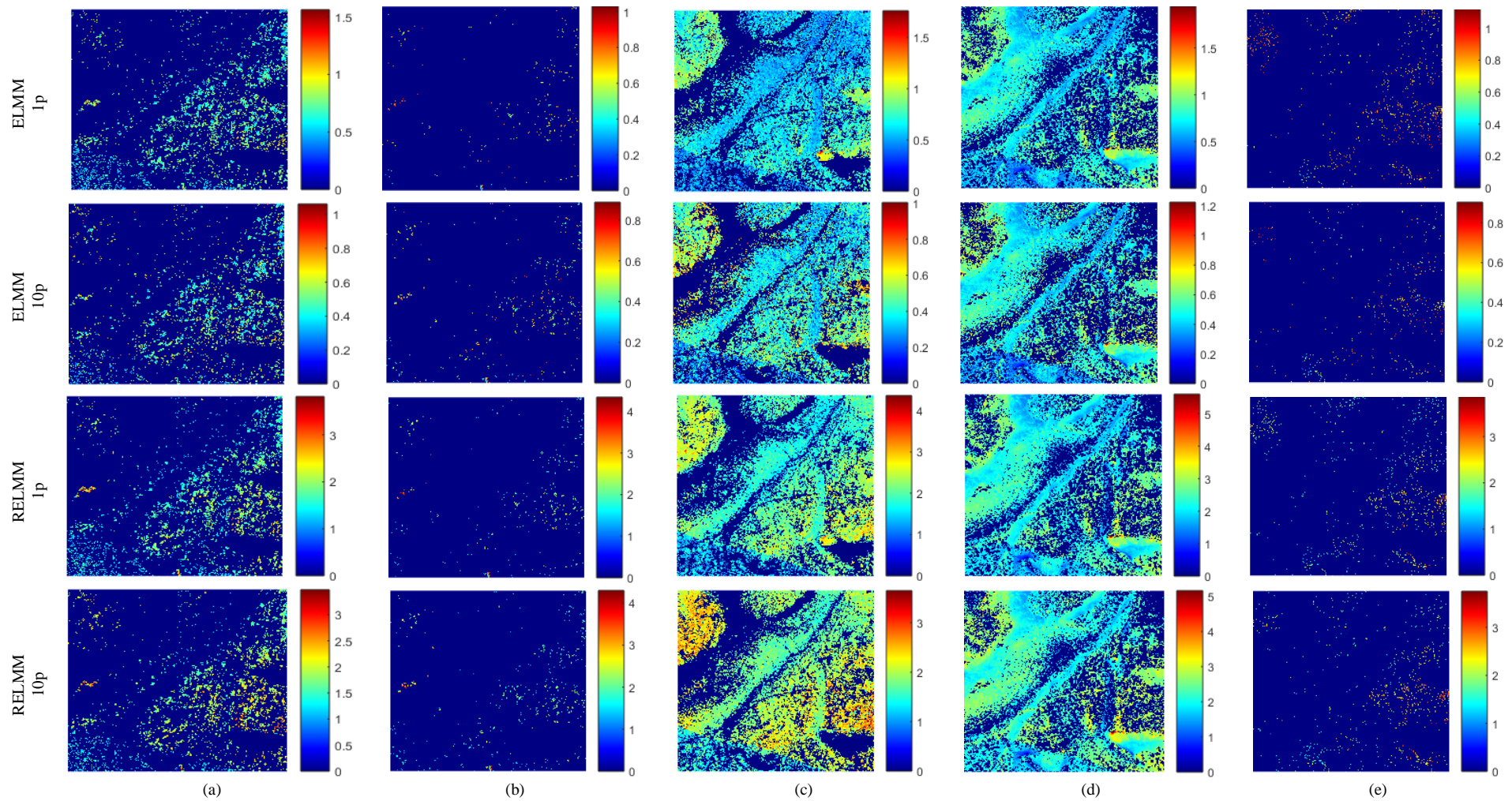


Fig. 11. Scaling Factor Maps estimated by ELMM and RELMM in Area 4 using 1 and 10 pixels for averaging the reference endmembers. (a) *S. supranubius*, (b) *P. canariensis*, (c) *P. laiospermus*, (d) Bare soil and (e) *D. bourgaeana*.

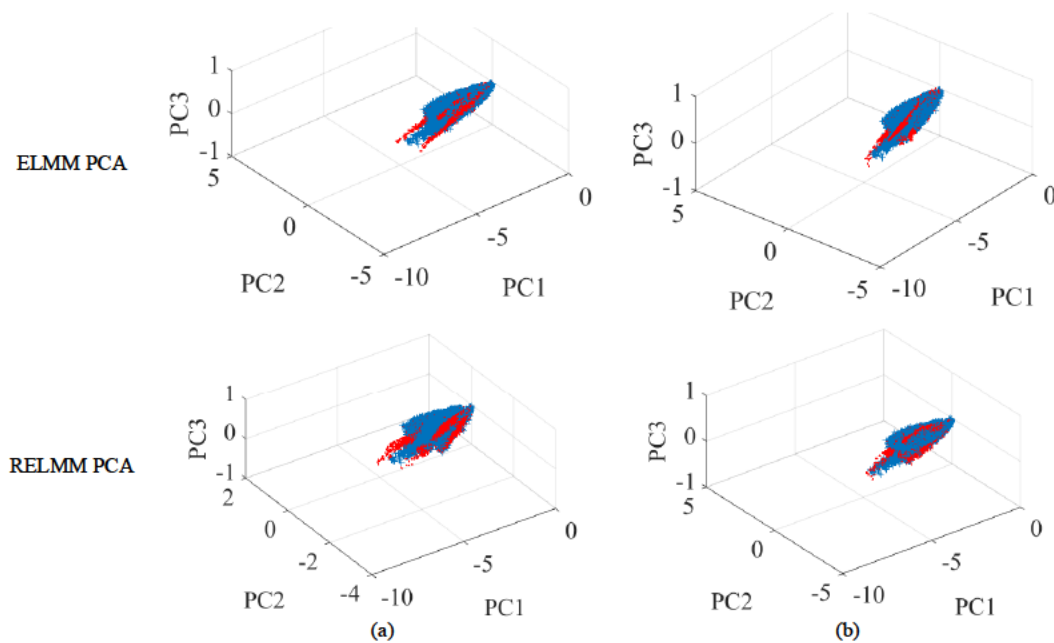


Fig. 12. PCA scatterplot for ELMM and RELMM of Area 4 using: (a) 1 and (b) 10 pixels for averaging the reference endmembers. In blue the data and in red the extracted endmembers.

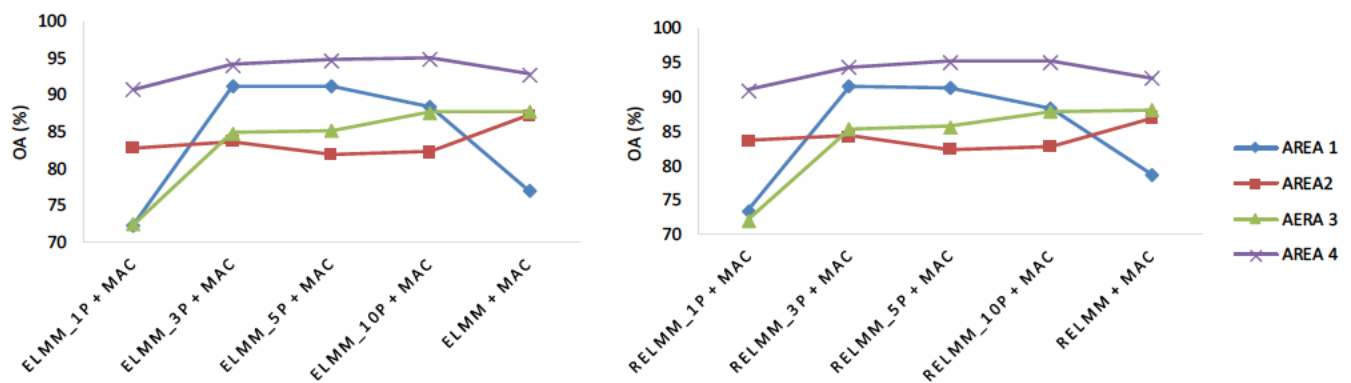


Fig. 13. Overall Accuracies results from MAC classification applied to (a) ELMM and (b) RELMM abundances maps from non-robust to robust endmembers in each area of study.

#### ACKNOWLEDGMENT

The authors want to acknowledge INTA (Instituto Nacional de Técnica Aeroespacial) for providing the CASI imagery. This work was completed while E. I-U was a Ph.D. student in the IOCAG Doctoral Program in Oceanography and Global Change (ULPGC).


#### REFERENCES

- [1] C. A. Múcher, L. Kooistra, M. Vermeulen, J. V. Borre, B. Haest, and R. Haveman, "Quantifying structure of Natura 2000 heathland habitats using spectral mixture analysis and segmentation techniques on hyperspectral imagery," *Ecological indicators*, vol. 33, pp. 71-81, 2013.
- [2] S. Delalieux, B. Somers, B. Haest, T. Spanhove, J. V. Borre, and C. Múcher, "Heathland conservation status mapping through integration of hyperspectral mixture analysis and decision tree classifiers," *Remote Sensing of Environment*, vol. 126, pp. 222-231, 2012.
- [3] Y. Dian, Z. Li, and Y. Pang, "Spectral and texture features combined for forest tree species classification with airborne hyperspectral imagery," *Journal of the Indian Society of Remote Sensing*, vol. 43, pp. 101-107, 2015.
- [4] L. Ballanti, L. Blesius, E. Hines, and B. Kruse, "Tree species classification using hyperspectral imagery: A comparison of two classifiers," *Remote Sensing*, vol. 8, p. 445, 2016.
- [5] J. M. Bioucas-Dias, A. Plaza, N. Dobigeon, M. Parente, Q. Du, P. Gader, et al., "Hyperspectral unmixing overview: Geometrical, statistical, and sparse regression-based approaches," *IEEE Journal of Selected Topics in Applied Earth Observations and Remote Sensing*, vol. 5, pp. 354-379, 2012.
- [6] P.-A. Thouvenin, N. Dobigeon, and J.-Y. Tourneret, "Hyperspectral unmixing with spectral variability using a perturbed linear mixing model," *IEEE Transactions on Signal Processing*, vol. 64, pp. 525-538, 2016.
- [7] I. García-Dópido, "New Techniques for Hyperspectral Image Classification," Departamento de tecnología de los computadores y de las comunicaciones, Universidad de Extremadura, 2013.
- [8] M. Fauvel, Y. Tarabalka, J. A. Benediktsson, J. Chanussot, and J. C. Tilton, "Advances in spectral-spatial classification of hyperspectral images," *Proceedings of the IEEE*, vol. 101, pp. 652-675, 2013.
- [9] G. Camps-Valls, D. Tuia, L. Bruzzone, and J. A. Benediktsson, "Advances in hyperspectral image classification: Earth monitoring with statistical


- learning methods," *IEEE Signal Processing Magazine*, vol. 31, pp. 45-54, 2014.
- [10] P. Ghamisi, J. Plaza, Y. Chen, J. Li, and A. J. Plaza, "Advanced spectral classifiers for hyperspectral images: A review," *IEEE Geoscience and Remote Sensing Magazine*, vol. 5, pp. 8-32, 2017.
- [11] A. Villa, J. Chanussot, C. Jutten, J. A. Benediktsson, and S. Moussaoui, "On the use of ICA for hyperspectral image analysis," in *Geoscience and Remote Sensing Symposium, 2009 IEEE International, IGARSS 2009*, 2009, pp. IV-97-IV-100.
- [12] G. Hughes, "On the mean accuracy of statistical pattern recognizers," *IEEE transactions on information theory*, vol. 14, pp. 55-63, 1968.
- [13] P. Ghamisi, J. A. Benediktsson, and S. Phinn, "Land-cover classification using both hyperspectral and LiDAR data," *International Journal of Image and Data Fusion*, vol. 6, pp. 189-215, 2015.
- [14] N. Keshava and J. F. Mustard, "Spectral unmixing," *IEEE Signal Processing Magazine*, vol. 19, pp. 44-57, 2002.
- [15] E. L. Hestir, S. Khanna, M. E. Andrew, M. J. Santos, J. H. Viers, J. A. Greenberg, et al., "Identification of invasive vegetation using hyperspectral remote sensing in the California Delta ecosystem," *Remote Sensing of Environment*, vol. 112, pp. 4034-4047, 2008.
- [16] C. Zhang, "Applying data fusion techniques for benthic habitat mapping and monitoring in a coral reef ecosystem," *ISPRS Journal of Photogrammetry and Remote Sensing*, vol. 104, pp. 213-223, 2015.
- [17] M. Garcia and S. L. Ustin, "Detection of interannual vegetation responses to climatic variability using AVIRIS data in a coastal savanna in California," *IEEE Transactions on Geoscience and Remote Sensing*, vol. 39, pp. 1480-1490, 2001.
- [18] B. Hapke, *Theory of reflectance and emittance spectroscopy*: Cambridge university press, 2012.
- [19] M. A. Veganzones, L. Drumetz, G. Tochon, M. Dalla Mura, A. Plaza, J. M. Bioucas-Dias, et al., "A new extended linear mixing model to address spectral variability," in *IEEE Workshop on Hyperspectral Image and Signal Processing Evolution in Remote Sensing (WHISPERS 2014)*, 2014.
- [20] B. Somers, G. P. Asner, L. Tits, and P. Coppin, "Endmember variability in spectral mixture analysis: A review.," *Remote Sensing of Environment*, vol. 115, pp. 1603-1616, 2011.
- [21] A. Zare and K. Ho, "Endmember variability in hyperspectral analysis: Addressing spectral variability during spectral unmixing," *IEEE Signal Processing Magazine*, vol. 31, pp. 95-104, 2014.
- [22] X. Zhang, J. Zhang, C. Li, C. Cheng, L. Jiao, and H. Zhou, "Hybrid Unmixing Based on Adaptive Region Segmentation for Hyperspectral Imagery," *IEEE Transactions on Geoscience and Remote Sensing*, vol. 56, pp. 3861 - 3875, 2018.
- [23] C. L. Lawson and R. J. Hanson, *Solving least squares problems*: SIAM, 1995.
- [24] L. Drumetz, M.-A. Veganzones, S. Henrot, R. Phlypo, J. Chanussot, and C. Jutten, "Blind hyperspectral unmixing using an Extended Linear Mixing Model to address spectral variability," *IEEE Transactions on Image Processing*, vol. 25, pp. 3890-3905, 2016.
- [25] L. Drumetz, J. Chanussot, and A. Iwasaki, "Endmembers as directional data for robust material variability retrieval in hyperspectral image unmixing," *IEEE International Conference on Acoustics, Speech and Signal Processing (ICASSP)*, pp. 1-5, 2018.
- [26] N. González-Lemus, J. C. Carracedo-Gómez, and M. Durbán-Villonga, "El Parque Nacional del Teide: patrimonio mundial de la UNESCO," *Anuario de Estudios Atlánticos*, vol. 1, pp. 519-568, 2009.
- [27] V. Garzón-Machado, M. J. del Arco-Aguilar, and P. L. Pérez-de-Paz, "A tool set for description and mapping vegetation on protected natural areas: an example from the Canary Islands," *Biodiversity and Conservation*, vol. 20, pp. 3605-3625, 2011.
- [28] J. Cubas, J. L. Martín-Esquivel, M. Nogales, S. D. Irl, R. Hernández-Hernández, M. López-Darías, et al., "Contrasting effects of invasive rabbits on endemic plants driving vegetation change in a subtropical alpine insular environment," *Biological Invasions*, vol. 20, pp. 793-807, 2018.
- [29] E. de Miguel, A. Fernández-Renau, E. Prado, M. Jiménez, Ó. G. de la Cámara, C. Linés, et al., "The processing of CASI-1500I data at INTA PAF," *EARSeL eProceedings*, vol. 13, pp. 30-37, 2014.
- [30] R. B. Singer and T. B. McCord, "Mars-large scale mixing of bright and dark surface materials and implications for analysis of spectral reflectance," in *Lunar and Planetary Science Conference Proceedings*, 1979, pp. 1835-1848.
- [31] D. Nash and J. Conel, "Spectral reflectance systematics for mixtures of powdered hypersthene, labradorite, and ilmenite," *Journal of Geophysical Research*, vol. 79, pp. 1615-1621, 1974.
- [32] D. C. Heinz, "Fully constrained least squares linear spectral mixture analysis method for material quantification in hyperspectral imagery," *IEEE transactions on geoscience and remote sensing*, vol. 39, pp. 529-545, 2001.
- [33] S. Henrot, J. Chanussot, and C. Jutten, "Correction to "Dynamical Spectral Unmixing of Multitemporal Hyperspectral Images"[Jul 16 3219-3232]," *IEEE Transactions on Image Processing*, vol. 25, pp. 4443-4443, 2016.
- [34] C. A. Bateson, G. P. Asner, and C. A. Wessman, "Endmember bundles: A new approach to incorporating endmember variability into spectral mixture analysis," *IEEE transactions on geoscience and remote sensing*, vol. 38, pp. 1083-1094, 2000.
- [35] B. Somers, M. Zortea, A. Plaza, and G. P. Asner, "Automated extraction of image-based endmember bundles for improved spectral unmixing," *IEEE Journal of Selected Topics in Applied Earth Observations and Remote Sensing*, vol. 5, pp. 396-408, 2012.
- [36] D. A. Roberts, M. Gardner, R. Church, S. Ustin, G. Scheer, and R. Green, "Mapping chaparral in the Santa Monica Mountains using multiple endmember spectral mixture models," *Remote sensing of environment*, vol. 65, pp. 267-279, 1998.
- [37] G. P. Asner and D. B. Lobell, "A biogeophysical approach for automated SWIR unmixing of soils and vegetation," *Remote sensing of environment*, vol. 74, pp. 99-112, 2000.
- [38] L. Drumetz, "Endmember variability in hyperspectral image unmixing," Université de Grenoble Alpes, 2016.
- [39] M. Berman, H. Kiiveri, R. Lagerstrom, A. Ernst, R. Dunne, and J. F. Huntington, "ICE: A statistical approach to identifying endmembers in hyperspectral images," *IEEE transactions on Geoscience and Remote Sensing*, vol. 42, pp. 2085-2095, 2004.
- [40] M. A. Veganzones, G. Tochon, M. Dalla-Mura, A. J. Plaza, and J. Chanussot, "Hyperspectral image segmentation using a new spectral unmixing-based binary partition tree representation," *IEEE Transactions on Image Processing*, vol. 23, pp. 3574-3589, 2014.
- [41] J. Sigurdsson, M. O. Ulfarsson, and J. R. Sveinsson, "Total variation and  $\ell_1$  based hyperspectral unmixing for feature extraction and classification," in *Geoscience and Remote Sensing Symposium (IGARSS), 2015 IEEE International*, 2015, pp. 437-440.
- [42] A. Medina-Machín, J. Marcello, A. Hernández-Cordero, J. Martín-Abasolo, and F. Eugenio, "Vegetation species mapping in a coastal-dune ecosystem using high resolution satellite imagery," *GIScience & Remote Sensing*, pp. 1-23, 2018.
- [43] F. E. Fassnacht, C. Neumann, M. Förster, H. Buddenbaum, A. Ghosh, A. Clasen, et al., "Comparison of feature reduction algorithms for classifying tree species with hyperspectral data on three central European test sites," *IEEE Journal of Selected Topics in Applied Earth Observations and Remote Sensing*, vol. 7, pp. 2547-2561, 2014.
- [44] G. A. Licciardi and F. Frate, "A comparison of feature extraction methodologies applied on hyperspectral data," in *Proc. Hyperspectral 2010 Workshop, Frascati, Italy*, 2010, pp. 17-19.
- [45] L. Wang and C. Zhao, *Hyperspectral Image Processing*: Springer, 2016.
- [46] J. M. Bioucas-Dias, A. Plaza, G. Camps-Valls, P. Scheunders, N. Nasrabadi, and J. Chanussot, "Hyperspectral remote sensing data analysis and future challenges," *IEEE Geoscience and remote sensing magazine*, vol. 1, pp. 6-36, 2013.
- [47] M. L. Clark, D. A. Roberts, and D. B. Clark, "Hyperspectral discrimination of tropical rain forest tree species at leaf to crown scales," *Remote sensing of environment*, vol. 96, pp. 375-398, 2005.
- [48] C. Li, J. Yin, and J. Zhao, "Using Improved ICA Method for Hyperspectral Data Classification," *Arabian Journal for Science & Engineering (Springer Science & Business Media BV)*, vol. 39, 2014.
- [49] J. Ren, J. Zabalza, S. Marshall, and J. Zheng, "Effective feature extraction and data reduction in remote sensing using hyperspectral imaging [applications corner]," *IEEE Signal Processing Magazine*, vol. 31, pp. 149-154, 2014.
- [50] G. Camps-Valls and L. Bruzzone, "Kernel-based methods for hyperspectral image classification," *IEEE Transactions on Geoscience and Remote Sensing*, vol. 43, pp. 1351-1362, 2005.
- [51] E. Belluco, M. Camuffo, S. Ferrari, L. Modenese, S. Silvestri, A. Marani, et al., "Mapping salt-marsh vegetation by multispectral and hyperspectral remote sensing," *Remote sensing of environment*, vol. 105, pp. 54-67, 2006.







CHAPTER 7. TEMPORAL  
DYNAMIC ANALYSIS OF A  
MOUNTAIN ECOSYSTEM  
BASED ON MULTI-SOURCE  
AND MULTI-SCALE REMOTE  
SENSING DATA





This chapter includes the following article: E. Ibarrola-Ulzurrun, J. Marcello, C. Gonzalo-Martín, J. Martín-Esquivel. *Temporal dynamic analysis of a mountain ecosystem based on multi-source and multi-scale remote sensing data*. Ecosphere. Under review.

This work is the final stage of the Thesis. After applying different pre-processing and classification techniques in the different types of imagery, and once the final products are obtained, a change detection analysis can be performed. Those final products obtained during the Thesis are not useful if they cannot be applicable in real scenarios. In this case, all the work performed during the Thesis has been used for the environmental management of a natural protected study area.

This article proposes a framework to monitor complex ecosystems using remote sensing imagery. Firstly, a pre-processing of the data is needed in order to be able to compare multi-source imagery (MS and HS). Then, accurate thematic maps were obtained after applying advanced classifications algorithms to the multi-temporal data. Once the classification maps were generated, they can be compared by a post-classification analysis, to detect changes in the vegetation during different years, not only for a global vegetation coverage, but a species level.

In summary, an analysis of the ecosystem changes was carried out, with the support of J. Martín-Esquivel, the conservation manager from Teide National Park.

The paper results corroborate and strengthen what it is directly observed in nature, analyzed by the Teide Managers. It is demonstrated that *P. lasiospermus* has extended rapidly, while *S. supranubius* has decrease its population during the last decades. Thus, thanks to remote sensing, it has been possible to study these changes in a large area, as well as obtaining quantitative results of how the species coverage has changed during years.

The main contribution of this paper were:

- A complete methodological framework to study changes in ecosystems through multi-sensor and multi-temporal remote sensing techniques was proposed.
- This framework make possible to study large areas, and to obtain quantitative results of the coverage change of the species during a period of time.
- Moreover, the framework proposed is ecological relevant, statistical credibility, effective, flexible and transferable to other systems.



# TEMPORAL DYNAMIC ANALYSIS OF A MOUNTAIN ECOSYSTEM BASED ON MULTI-SOURCE AND MULTI-SCALE REMOTE SENSING DATA

Edurne Ibarrola-Ulzurrun 1,\* , Javier Marcello 1, Consuelo Gonzalo-Martín 2 and José Luis Martín-Esquivel 3

<sup>1</sup> Instituto de Oceanografía y Cambio Global (IOCG), Universidad de Las Palmas de Gran Canaria (ULPGC), Parque Científico Tecnológico Marino de Taliarte, 35214, Telde, Las Palmas (Spain).

<sup>2</sup> Department of Computer Architecture and Technology, Universidad Politécnica de Madrid (UPM), Campus de Montegancedo, Boadilla del Monte, 28660, Madrid (Spain).

<sup>3</sup> Parque Nacional del Teide, C/Sixto Perera González 25, 38300, La Orotava, Tenerife, Islas Canarias (Spain)

\* Correspondence: edurne.ibarrola101@alu.ulpgc.es; Tel.: +34-928457365

## ABSTRACT

During the last decades, ecosystems have suffered a decline in natural resources due to climate change and anthropogenic pressure. Specifically, the European rabbit introduced by humans, as well as drought episodes, have led to a change in the vegetation structure of a mountainous ecosystem: Teide National Park (Spain). Teide managers studied, with field-based traditional methods, how the two keystone vegetation species, *Spartocytisus supranubius* and *Pteroccephalus lasiospermus* have changed their dynamics in this vulnerable and heterogenic ecosystem. However, remote sensing is an important tool for classifying, monitoring and managing large areas in a fast and economic way. This work proposes a methodological framework to monitor the changes produced in this protected area using multi-source remote sensing imagery. The results strengthen and extend the analysis followed by the National Park managers, demonstrating that *S. supranubius* has decreased its population while *P. lasiospermus* has increased. Moreover, this study presents thematic maps of the species of interest, as well as its specific coverage at different dates, providing quantitative data difficult to get with traditional approaches.

**Keywords:** remote sensing imagery, change detection, multispectral, hyperspectral, Support Vector Machine, invasive species.

## INTRODUCTION

Ecosystems are exposed to high pressure due to intensification of agricultural land use, tourism, development and climate change, being highly dynamic in space and time. Specifically, climate change is producing important variations in entire communities in those areas where it manifests most intensely, such as regions at greater latitude and areas of higher altitude. Thus, ecosystem deterioration has a strong negative impact in the local biodiversity, and might put rare and threatened species at a serious extinction risk (Pepin and Lundquist 2008, Spanhove et al. 2012).

In this context, to understand ecosystem dynamics and its consequences is vital for the success of their conservation and restoration, especially on the services they provide (Mueller and Geist 2016). Hence, it is important to implement accurate monitoring methodologies of land surface attributes, as it is critical for dealing with uncertainty in the management of large-ecosystems (Coppin et al. 2004, Förster et al. 2014). Hence, for large-scale monitoring efforts, two general approaches have been defined (Manley et al. 2000): retrospective and predictive. Retrospective monitoring seeks to detect changes in status or condition, while predictive monitoring seeks to detect indications of undesirable effects before they have a chance to occur or become serious. Both, retrospective and predictive monitoring deal about detecting changes in a large-scale area. In that regard, change detection could be defined as the process of identifying differences in the state of a phenomenon at different times (Singh 1989). The time and accuracy of change detection on the Earth's surface can provide guidance for resources management by using multi-temporal datasets related to state of changes (Lu et al. 2004).

An ecological monitoring program should ideally consider ecological relevance, statistical credibility, cost-effectiveness, flexibility and transferability to other systems, as the most important criteria (Mueller and Geist 2016, Mason et al. 2017). In this context, remote sensing could be an important tool to monitor ecosystems, at community and species level to detect population trends, that guide in the establishment of conservation objectives with the purpose of avoiding the transition to undesirable situations (Mason et al. 2017).

Remote sensing can contribute to a better understanding of natural habitats, their spatial distribution and their conservation status, being considered an ideal data source for land cover classifications in large areas (Corbane et al. 2013). Hence, it is a valuable tool for monitoring and managing ecosystems, as it allows the acquisition of data in remote and inaccessible areas (Spanhove et al. 2012, Förster et al. 2014). Besides, it has been successfully used for many ecological studies, such as detecting land-cover changes, monitoring crops, deforestation, forest fires, estimating carbon sequestration, detecting vegetation stress and other applications (Aplin 2004, Spanhove et al. 2012, Alqurashi and Kumar 2013). This technology is

important since traditional field-based assessment methods are sometimes subjective, time consuming, data lagged and often too expensive. Thus, remote can complement and add information to traditional field-based methods providing indicators for different spatial and temporal scales and involving varying temporal revisit frequencies up to daily observations (Xie et al. 2008, Nunez-Casillas et al. 2012, Förster et al. 2014).

The area of study is the Teide National Park (Tenerife, Spain), a vulnerable high mountain ecosystem strongly stressed by climate change. This study describes a methodology framework to monitor non-herbaceous species of this ecosystems using remote sensing imagery. The conservation managers have analyzed how the two keystone species have changed their population dynamic due to the abundance of European rabbits and recurrent drought episodes. Specifically, the study proposes a post-classification analysis to study those dynamics by using remote sensing multi-source and multi-temporal data, in order to complement and add accurate information to the field observations, for a future ecosystem management.

## STUDY CASE DESCRIPTION

### Study Area

The study area is a high mountain ecosystem in the subtropical island of Tenerife (28°06'N 15°24'W), the Teide National Park with 13,679 ha of total extension. The dominant vegetation is a meso-oromediterranean shrub dominated by the endemic broom, *Spartocytisus supranubius* (del Arco Aguilar et al. 2010) (Fig. 1).

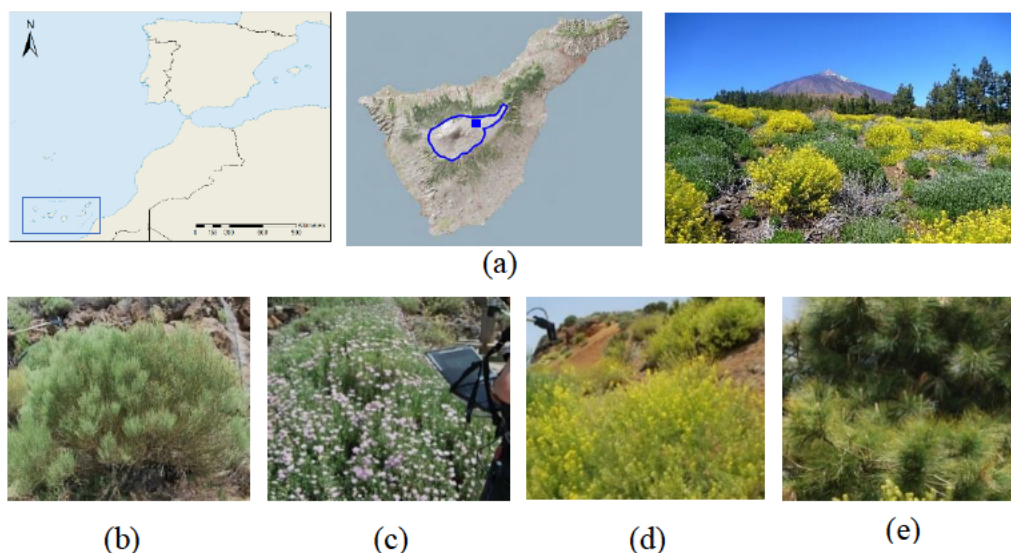


Figure 1. (a) Teide National Park, location and species of interest: blue line delimits the total National Park and the blue square the study area. (b) *Spartocytisus supranubius*, (c) *Pterocephalus lasiospermus*, (d) *Descurainia bourgaeana* and (e) *Pinus canariensis*.



The National Park is formed by a large caldera, inside which the Teide volcano rises up to an altitude of 3,718 m, being the highest peak of Spain. According to the records in the database of the Teide National Park, a total of 206 vascular plants, mostly herbaceous, acclimated to the stressed environmental conditions of high altitude, grow up. 7% of these taxons are endemic from Teide National Park, whereas the 15% are endemic from Tenerife and 32% are endemic from Canary Islands. The adaptations to the altitude of these species are manifested in the shape of the leaves (Lausi and Nimis 1986), the canopy and the physiology of the plants (Perera-Castro et al. 2017b), which has been well studied in the case of the *Spartocytisus supranubius* (Teide broom) (González-Rodríguez et al. 2017) and the pine *Pinus canariensis* (Canary pine) (Brito et al. 2014). Indeed, *S. supranubius* is one of the most important plant species, as well as *P. canariensis*, *Descurainia bourgaeana* (Hierba pajonera) and *Pterocephalus lasiospermus* (Rosillo de cumbre). The latter is particularly surprising, since in the middle of the last century, it was considered a very rare species, of which only a few specimens were known (Sventenius 1946). However, nowadays, it is the most abundant species in the National Park, possibly due to its thermophilic character (Perera-Castro et al. 2017a) and its low palatability for herbivores (Cubas et al. 2018). Figure 1 shows the species selected to the study.

#### *Ecosystem description and problematic*

The Teide National Park has been historically object of several human uses, mainly led by the grazing of goats and the extractive activities of soil and wood of *S. supranubius*. Nowadays, goats have been eradicated, while extraction of wood is considered a traditional activity of low intensity, being beekeeping the only remaining activity. The greatest current challenges for the management of the Park are public use, herbivory pressure due to rabbits and droughts episodes and temperature increase (climate change). Regarding public use, it is about making compatible the enjoyment of nature, by more than four million visitors a year, with its conservation.

The presence of herbivores continues to be a factor of pressure on the flora, especially the European rabbit (*Oryctolagus cuniculus*). The rabbits were introduced on Canary Islands during XV-XVI centuries by the Castilian conquerors, but their populations have increased in the last decades, reaching densities of up to 3 rabbits/ha some years, because the climate in the summit is becoming less cold (Martín et al. 2012). They play a key role in the functioning of the ecological systems (Chapuis et al. 2004). *Oryctolagus* affects ecosystems by producing changes in the structure and composition of the soil, as well as in the richness and diversity of plant species. Cubas et al. 2018 studied how rabbits influenced the population dynamics of two of the most abundant plants of this habitat, *S. supranubius* and *P. lasiospermus*, demonstrating an antagonistic effect: while rabbits limited the expansion of *S. supranubius* because when feeding on their seedlings prevented the regeneration of the plant, at the same time they favored the expansion of *P. lasiospermus* because

this plant was able to take advantage of the extra nutrients contribution from the latrines of the herbivore and it was less palatable than the brooms. This study was made in small areas of the Park through traditional field-based assessment methods.

*S. supranubius* is the key species of the high mountain ecosystem of Tenerife. Its populations were reduced at the beginning of the last century until the declaration of the Teide National Park led to the suppression of pastoral activities in the sixties. Since then, their populations experienced a considerable recovery, however, this positive trend slowed down in the 1980s, when episodes of death began to appear matching with a strong increase in temperature, drought episodes and, probably, an increase in rabbit populations. Extinction events of *S. supranubius* affect the entire National Park but are most notable in the southern area where extreme drought severely reduced the secondary growth of brooms (Olano et al. 2017, Cubas et al. 2018). The dendrochronological analyses, elaborated by Olano et al. 2017, studied the impact of the droughts of 2008 and 2012, underlining that they were one important stress factors behind the death of *S. supranubius*.

Remote sensing can complement and add relevant information to Cubas et al. 2018 work, covering a larger area of study and quantifying the surface area of the same species considered in this study, as well as other important species of the Teide National Park.

#### *Remote sensing framework*

Remote sensing involves measuring electromagnetic radiation from features on the Earth's surface, providing a basic representation of land cover variation (Aplin 2004). In this context, change detection is one of the most important applications in remote sensing (Mouat et al. 1993, Petit and Lambin 2001, Volpi et al. 2013). It aims to identify the changes occurred by jointly analyzing two or more images over the same geographical scene at different times (Gong et al. 2016).

The ideal situation would be to have data from the same sensor, same dates during different years and under same conditions; however this is not always possible, so the use of multi-source data is the best approximation. In fact, the integration of multi-source and multi-temporal remote sensed imagery is one of the most challenging task and an active area in the field of change detection (Lu et al. 2004, Jianya et al. 2008, Volpi et al. 2013, Gong et al. 2016). Moreover, the use of multi-source images for change detection is worth to be considered and researched deeply, while multi-temporal imagery has the potential to compensate for possible bias in the spectral information caused by the plants being in different phenological phases.

Besides, the type of imagery is a major factor in the classification analysis, and hence, in change detection studies. The evolution of spaceborne remote sensing has led to the introduction of advanced multispectral (MS) and hyperspectral (HS)

imagery from the visible to the near infrared spectrum (400 – 2500 nm). MS satellite imagery with three to eight bands is commonly used in land cover classification, vegetation studies, texture, land cover changes, forest fires and others (Rodríguez-Galiano et al. 2012, Feilhauer et al. 2013). The launch, in the last decades, of high spatial resolution satellite sensors (i.e. IKONOS, Quickbird, Worldview, etc) have been an advance of remote sensing in biodiversity analysis and monitoring. Also, for more heterogeneous ecosystems, such as the shrublands or tropical forests, high spatial resolution HS images are ideal for habitat monitoring (Jiménez-Michavila 2011) because the availability of tens to hundreds of spectral bands provides more information to discriminate and analyze the status of different species. The lack of HS satellite imagery with high spatial resolution has led to the use of airborne HS sensors. HS airborne imagery allows the simultaneous acquisition of spectral bands with high spatial resolution, increasing the possibility of accurately discriminating the land covers of interest (Fauvel et al. 2013, Ballanti et al. 2016). However, HS imagery is more expensive and requires higher computational cost.

In this context, classifying the species of the Teide National Park require a spatial resolution less than 1 meter in order to discriminate at species level due to the complexity of the ecosystem, with mixed vegetation and small shrubs. Therefore, the change detection study, covering 15 years, was carried out using multi-source and multi-temporal data. Three different very high resolution images were used in the study, two MS provided by the Quickbird (QB) and Worldview-2 (WV-2) sensors, and one HS recorded by the CASI 1550i sensor (Compact Airborne Spectrographic Imager) (Table 1 and Fig. 2).

Table 1. Specifications of the multispectral images: Quickbird and Worldview-2; and the hyperspectral image: CASI.

	<b>Spatial resolution</b>	<b>Spectral resolution</b>	<b>Acquisition date</b>	<b>Product</b>	<b>References</b>
QB	MS: 2.4 m PAN: 0.65 m	4 MS bands 1 PAN band	26 <sup>th</sup> May 2002	Orthoready	(Digital Globe)
WV-2	MS: 1.85 m PAN: 0.48 m	8 MS bands 1 PAN band	16 <sup>th</sup> May 2011	Orthoready	(Digital Globe)
CASI	0.75 m	68 HS bands	1 <sup>st</sup> June 2017	Level 2c	(de Miguel et al. 2014)

Level 2c: Radiometrically and atmospherically corrected, and orthorectified.

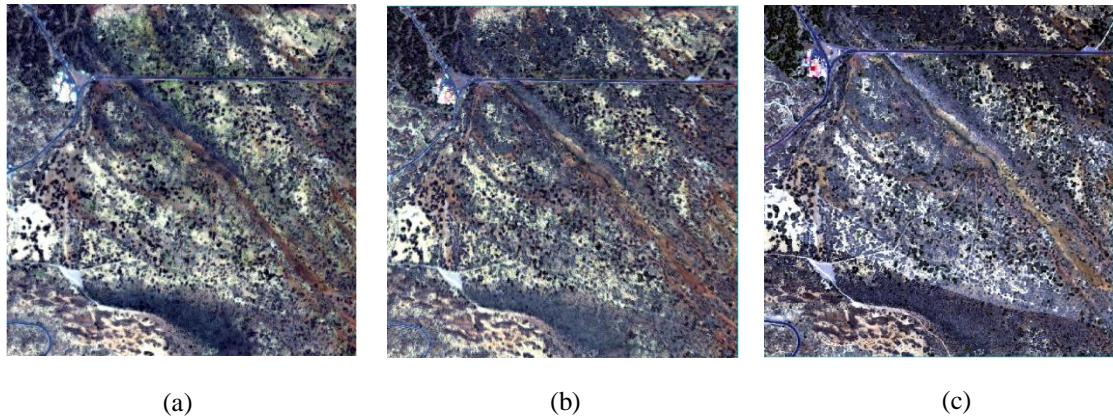


Figure 2. Remote sensing imagery in RGB color composite: (a) Quickbird of 2002 (R: 3, G: 2, B: 1); (b) Worldview-2 of 2011 (R:5, G: 3, B: 2); (c) CASI of 2017 (R:29, G: 20, B: 12).

The date is an important factor in the selection of the imagery to be analyzed. Thus, the Teide images acquisition were done during the end of the spring season as the vegetation species have greater spectral separability.

## METHODOLOGY

When implementing a change detection project, the following major steps are involved (Lu et al. 2004): (1) image pre-processing; (2) classification; (3) selection of suitable techniques to implement change detection analyses; and (4) accuracy assessment. The methodology framework followed in the study is shown in Fig. 3. It was implemented using ENVI 5.1 image processing software (Exellis Visual Information Solutions) and Matlab software (The MathWorks, Inc.).

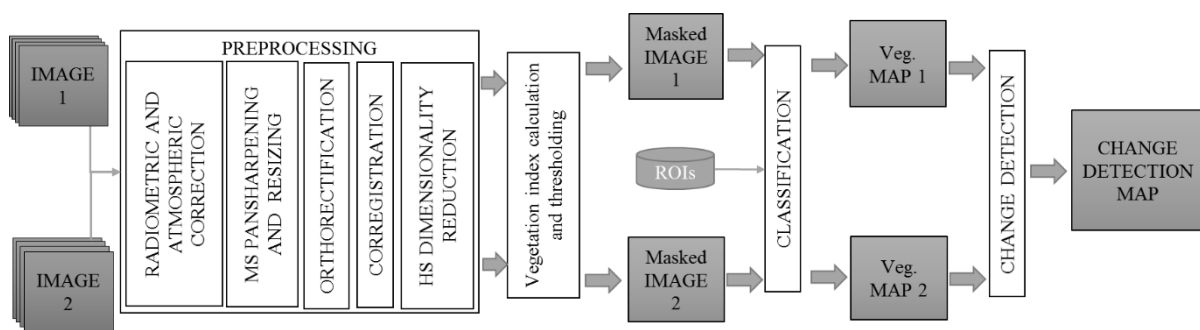


Figure 3. Diagram followed in the change detection study.

### *Pre-processing*

Prior to a land cover change analysis, some pre-processing steps are necessary to standardize the multi-source and multi-temporal images. Remote sensors provide raw data images; thus, it is necessary to apply correction techniques and to

perform image pre-processing in order to obtain high quality imagery (Ibarrola-Ulzurrun et al. 2018).

*Radiometric and Atmospheric correction.* Apart from the radiometric calibration to convert digital numbers to radiance values, there are different ways of correcting remote sensing data for atmospheric effects: simple image-based methods and more complex algorithms based on a radiative transfer model of the atmosphere. In this work, complex models were applied. Specifically, the Fast Line-of-sight Atmospheric Analysis of Spectral Hypercubes (FLAASH) to the satellite data (Marcello et al. 2016), and the Atmospheric Correction (ATCOR-4) to the airborne imagery (de Miguel et al. 2014).

*Pansharpening and Resizing.* High resolution MS platforms record data simultaneously by using MS and panchromatic (PAN) sensors, providing both types of imagery of the same scene with different spatial and spectral resolution. The MS image is characterized by having higher spectral resolution, while the PAN image obtained from this sensor has a higher spatial resolution. Image fusion, or pansharpening, allows to improve the spatial quality of the MS image. Thus, the pansharpening data fusion technique is defined by the process of merging MS and PAN images to create new MS fused images with higher spatial resolution. This process is very important in the analysis of heterogeneous and mixed shrublands ecosystems, where the size of the plants to be analyze is small.

After a detailed review of the state-of-art in pansharpening techniques, pansharpening algorithms achieving optimal performance were assessed and selected in previous studies performed for the Teide National Park (Ibarrola-Ulzurrun et al. 2017a, Ibarrola-Ulzurrun et al. 2017b). Thus, it was decided to use the Wavelet '*à trous*' algorithm to perform the pansharpening process in QB and WV-2 imagery to increase the spatial resolution by a factor of 4 with the minimum degradation of the spectral information.

The CASI imagery does not have a PAN image, however, as it appears in Table 1, its spatial resolution is higher than both MS images (QB and WV-2) because CASI flies on board an aircraft instead of a satellite at much higher altitude. Thus, a pixel resizing was performed in order to obtain the same pixel size (0.5 meters), using Nearest Neighbor algorithm (ENVI 2004), to avoid the mixing of information from neighboring pixels.

*Orthorectification.* Orthorectification schemes were applied in order to minimize the distortions manly induced by the topography. Some geometric error sources could be the variation of the movement in the platform and in the measuring instruments, the viewing angles of the sensor, the atmosphere conditions, Earth curvature and rotation, topographic effects, etc. In this context, orthorectification was necessary as we are dealing with a mountainous ecosystem. A RPC (Rational Polymodal

Orthorectification) model was performed which replaces the rigorous sensor model with an approximation of the ground-to-image relationship (ENVI 2004). The orthorectification errors in each scene were compared visually with images obtained from GRAFCAN (Cartografía de Canarias S.A.) and quantitatively with existing geodesic points (<http://visor.grafcan.es/visorweb/>). The CASI image was orthorectified by georeferenced hemispherical-directional reflectance factor (de Miguel et al. 2014).

*Co-registration.* Image co-registration is the process of geometrically aligning two or more images. Precise co-registration of the images is required in change detection studies. The importance of accurate spatial co-registration is obvious because large spurious results of change detection will be produced if there is misregistration. It is difficult to achieve high accuracy in the co-registration between multi-temporal and multi-source images due to many factors, i.e. imaging models, imaging angles, topography, curvature and rotation of the Earth or sensor type and data acquisition. For these reasons, in a mountainous area, an orthorectification is needed first (Jianya et al. 2008), as it was performed in this study. The geometric relationship between the warp image to register and the base image was obtained through a number of representative and well distributed tie points and, then, applying the corresponding geometric transform. In the case of this study, a minimum of 40 distributed ground control point (GCPs) were collected for each pair of images, considering the WV-2 data as the base image. A polynomial method was used with a Nearest Neighbor resampling (ENVI 2004) to fit the images in the overlapping areas,

*Dimensionality reduction for CASI imagery.* Regarding HS image, due to the high number of spectral bands, an additional pre-processing step is sometimes required. HS classification is a challenging task due to the presence of redundant features, the imbalance among the limited number of available training samples for the supervised classification, and the high dimensionality of the data (Ghamisi et al. 2017). Therefore, the high level of data dimensionality in HS imagery poses a problem for classifications because of the unbalance between the high dimensionality of the input data and the number of training samples used in the supervised classification process, known as the 'Hughes phenomenon' (Hughes 1968). Hence, when the number of spectral bands (dimensionality) increases, with a constant number of training samples, the accuracy of the statistics estimation decreases (Ghamisi et al. 2015). To solve this issue, data reduction through band selection decreases dimensionality without the need to increase the amount of training samples.

In a previous study, Ibarrola-Ulzurrun et al. 2017c compare the performance of different dimensionality reduction techniques and assessed strategies for selecting the most suitable number of components to increase the performance in the classification of CASI imagery. The study concluded that Minimum Noise Fraction (MNF) was the most suitable dimensionality reduction technique, which has also

been supported by other authors (Melgani and Bruzzone 2004, Tarabalka et al. 2010, Ibarrola-Ulzurrun et al. 2017c).

#### *Vegetation Index Masking.*

Once the pre-processing steps were completed, images with different spectral bands at 50 cm of spatial resolution providing reflectance values of the Earth surface were obtained. The next step was to create a mask to eliminate non-vegetation pixels. The reflectance curves (spectral signatures) for the different wavelengths of healthy green plants have a characteristic shape that is dictated by various plant attributes (Fig. 4).

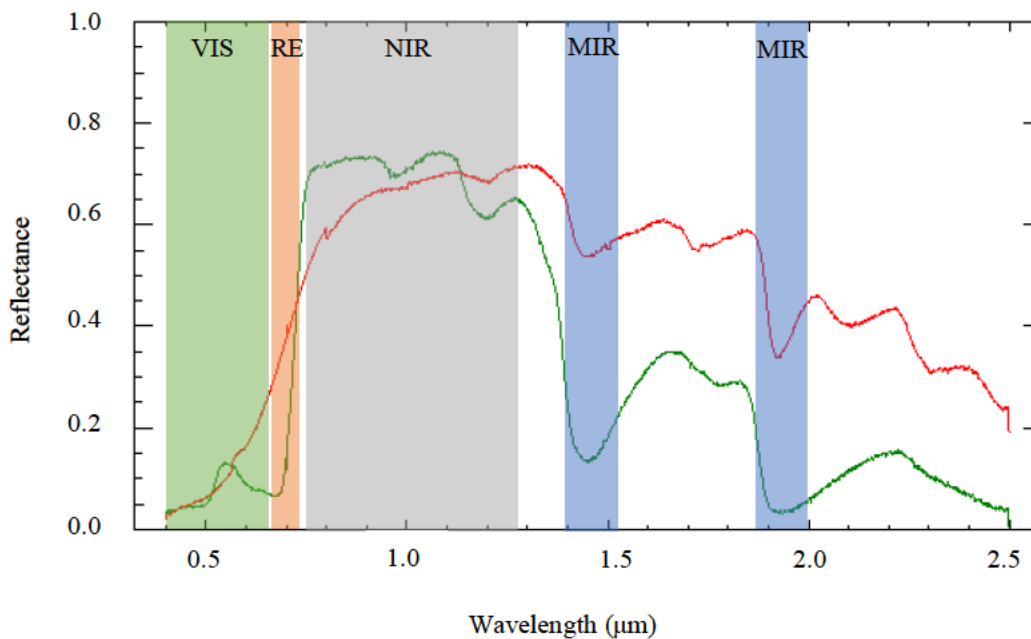


Figure 4. Vegetation spectral signature. Green signature: healthy vegetation; Red signature: dry vegetation. Shaded areas - VIS: visible wavelength corresponding to the chlorophyll peak; RE: red edge; NIR: Near Infrared wavelength corresponding with cell structure; MIR: Middle Infrared corresponding to the water absorptions wavelengths.

Due to the characteristic vegetation spectral signature, vegetation indices are common to enhance vegetation information (Yamano et al. 2003). The Normalized Difference Vegetation Index (NDVI) (Rouse Jr et al. 1974) and the Modified Soil Adjusted Vegetation Index (MSAVI2) (Huete 1988) are the most suitable for estimating quantitative characteristics of vegetation in dry and semi-dry regions (Galvão et al. 1999, Wang and Tenhunen 2004, Medina-Machín et al. 2018). NDVI is the ratio between the Red (RED) and the Near Infrared (NIR) regions (Eq. 1), while MSAVI2 is a more complex index applied to areas with high degree of exposed soil surface (Eq. 2).

$$NDVI = \frac{(NIR - RED)}{(NIR + RED)} \quad (1)$$

$$MSAVI2 = \frac{2NIR + 1 - \sqrt{(2NIR + 1)^2 - 8(NIR - RED)}}{2} \quad (2)$$

After calculating both vegetation indices, boxplot analyses were obtained in order to select the most suitable vegetation index to distinguish between vegetation and non-vegetation areas. Then, the vegetation index threshold was used to create a mask to remove the non-vegetation pixels to subsequently, classify vegetation areas at species level.

### *Classification*

Remote sensing classification assigns a unique label to each pixel vector so that it is well-defined by a given class with a degree of uncertainty (Xie et al. 2008, Bioucas-Dias et al. 2013). The major steps involved in the classification step may include determination of a suitable classification system, such as selection of training samples, selection of a suitable classification model, and accuracy assessment. The user needs the scale of the study area, the economic state, and the analyst skills, are important factors influencing the selection of the data, the design of the classification procedure, and the quality of the classification results (Lu and Weng 2007).

Supervised classification methods are based on learning an established classification from a training dataset, which contains the predictor variables measured in each sampling unit and assigns prior classes to the sampling units (Xie et al. 2008). Training samples are usually collected from fieldwork or using fine spatial resolution images. In the case of this study, several field observations campaigns were carried out, to provide accurately located and quantitative ground reference data for each vegetation species of interest. Random sampling was used to select both training and testing Regions of Interest (ROIs) for the classification. This procedure was difficult to implement because of the variability of species spatial distribution and the small vegetation patches.

The first step in the classification process was to determine the classes appearing in the study area and obtain the database set of training and testing ROIs for each one. The classes were chosen according to criteria of representativity and abundance. The selected species were: *S. supranubius*, *P. lasiospermus*, *D. bourgaeana* and *P. canariensis* (Fig. 1). In order to obtain reliable classification maps, the training and testing samples were selected during the field observations in well-known sites around the study area.



Regarding the classification model, Support Vector Machines (SVM) (Cortes and Vapnik 1995) have demonstrated their effectiveness in several remote sensing applications as well as in HS classification (Camps-Valls et al. 2008, Ballanti et al. 2016). SVM contain a machine learning algorithm that separates classes by defining the optimal hyperplane between them, based on support vectors that are defined by training data (Mountrakis et al. 2011). Specifically, several researches address the problem of very high resolution classification by using SVM with a lower computational cost (Bruzzone and Carlin 2006, Ibarrola-Ulzurrun et al. 2017b, Xia et al. 2017). SVM was also selected because another previous study carried out in the same study area (Ibarrola-Ulzurrun et al. 2017b), comparing different algorithms, demonstrates the SVM capability to obtain accurate classification maps.

Evaluation of classification results is an important process in the mapping procedure. Thus, the statistical accuracy assessment used in the study was the standardized confusion Error Matrix. The confusion matrix approach is the most widely used and reports two global accuracy measurements, Overall Accuracy and Kappa coefficient. Kappa coefficient describes the proportion of correctly classified validation sites after random agreements are removed (Rosenfield and Fitzpatrick-Lins 1986). Moreover, it is recognized as a powerful method for analyzing a single error matrix and for comparing the differences between various error matrices (Lu and Weng 2007). Finally, combining classification with preliminary feature extraction and reduction techniques increase the classification accuracy.

### *Change Detection Analysis*

The final step in the framework (Fig. 3) is the analysis of changes. After a revision of the state-of-art of different change detection methods, the post-classification technique was decided as the most suitable method for the study. It is a useful technique for extracting land used and land cover information, which independently classifies each image and compares the classified maps on a pixel-by-pixel basis to identify changes. Besides, it minimizes the impacts of atmospheric, sensor and environmental differences between multi-temporal and multi-source images. Thus, no precise atmospheric correction is strictly required during the pre-processing of each scene. Moreover, it is useful because it provides details about changes and avoids selecting appropriate thresholds (Coppin et al. 2004, Alqurashi and Kumar 2013).

## **RESULTS**

### *Pre-processing results*

After the radiometric and atmospheric corrections, the wavelet 'à trous' pansharpening technique was applied. The spatial resolution obtained after the pansharpening step and the resizing was 0.5 meters for both MS and HS imagery.

Fig. 5 shown the spatial improvement of the MS bands and the importance of this step due to the small size of vegetation. Afterwards, orthorectification was carried out, achieving an improved error around 2-2.5 meters (reference image error ca. 36 meters) (Fig. 6). Once both satellites images were orthorectified, a precise image co-registration was performed to almost achieve subpixel accuracy.

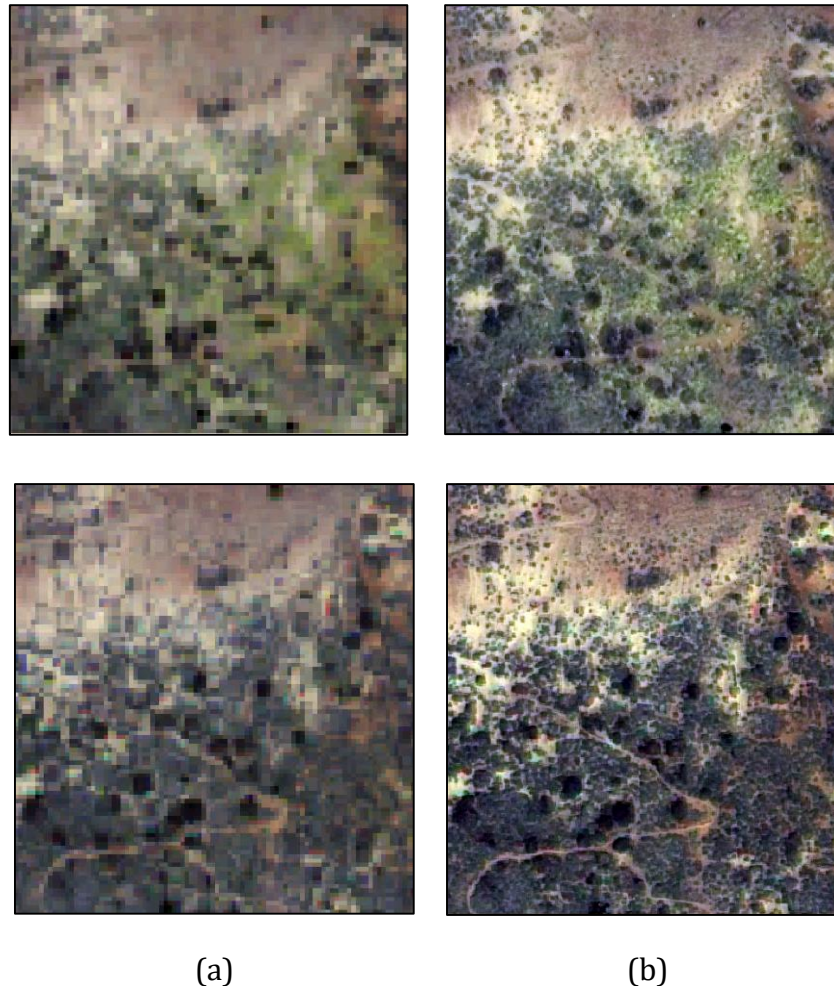


Figure 5. (a) Original Multispectral image and (b) fused image. Up: Quickbird images; Down: Worldview-2 images.

Regarding the dimensionality reduction of CASI imagery, a selection of the suitable components was carried out analyzing the eigenvalues and the standard deviation values of the entropy (Ibarrola-Ulzurrun et al. 2017c). Besides, a visual assessment of the MNF components was made to determine which components are spatially coherent and which contain noise. Based on this procedure, a total of 8 components (Fig. 7) were chosen without losing relevant information for the vegetation classification for the final classification, instead of the original 68 bands.

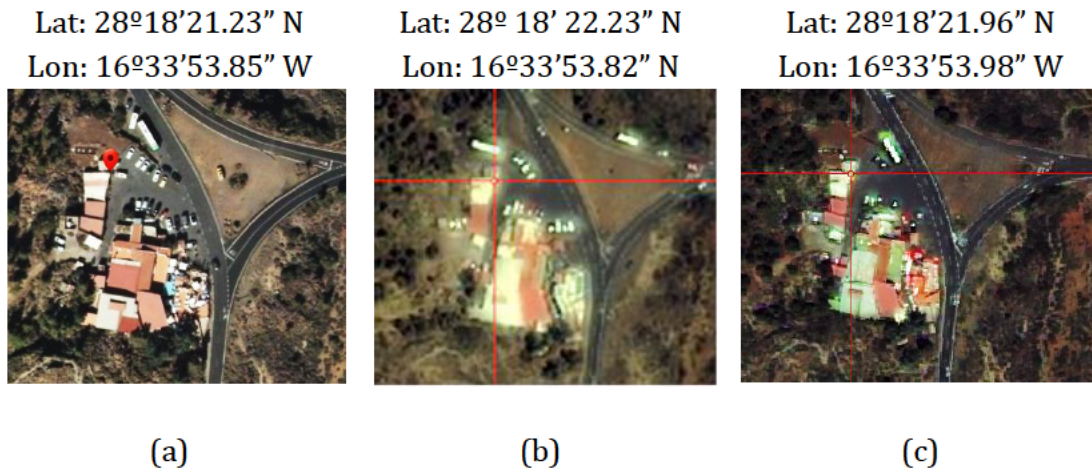


Figure 6. (a) Orthophoto of GRAFCAN and images after orthorectification: (b) Quickbird image and (c) Worldview-2 image.

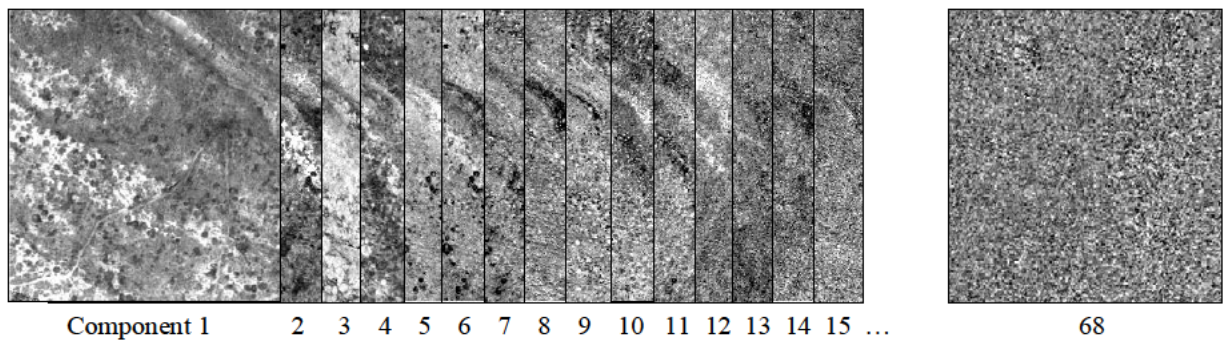


Figure 7. MNF components of the CASI image.

Concerning the generation of a vegetation mask, analysis of NDVI and MSAVI-2 values was accomplished. Boxplot diagrams (Fig. 8) were obtained to study the behavior of NDVI and MSAVI2 values in vegetated (162,538 pixels) and non-vegetated (69,164 pixels) areas, covering the different plant species, as well as the different types of bare soil, road and urban areas. The threshold was set in the first quartile of each index. Even though it was not possible to set an exact threshold to separate vegetated and non-vegetated areas, due to the spatial resolution of the imagery and to the presence of mixed pixels, NDVI more precisely discriminates vegetated and non-vegetated areas than MSAVI2. Therefore, NDVI was chosen to generate the vegetation mask configuration (Table 2).

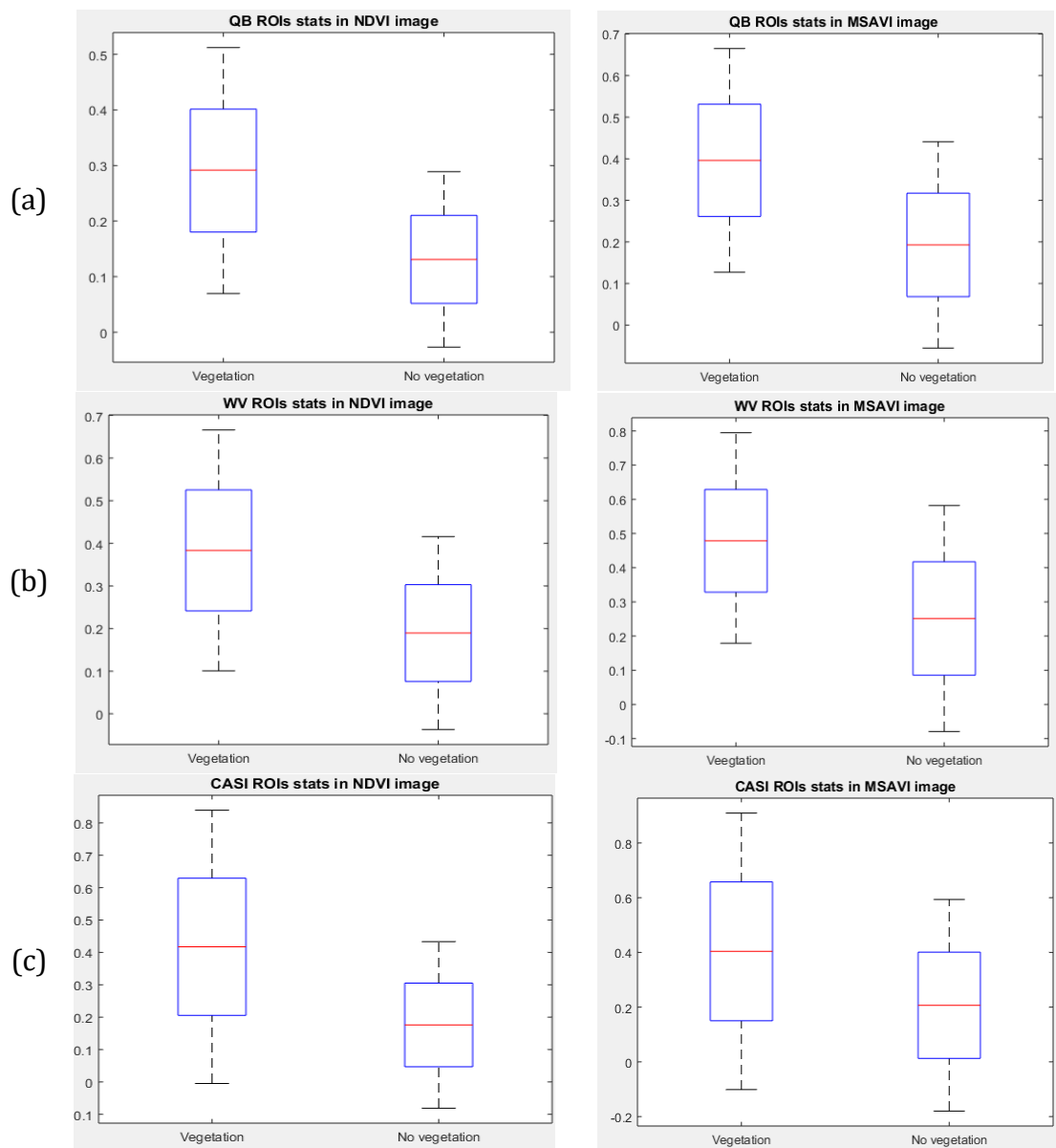


Figure 8. NDVI and MSAVI boxplot diagrams for: (a) QB, (b) WV-2 and (c) CASI.

Table 2. NDVI threshold to discriminate vegetated and non-vegetated areas in each image.

	<b>Threshold</b>
QB 2002	0.18
WV 2011	0.22
CASI 2017	0.20

Finally, Fig. 9 (up) shows the pre-processed and masked images used for the classification step. It can be appreciated how the vegetated area has increased from 2002 to 2017.

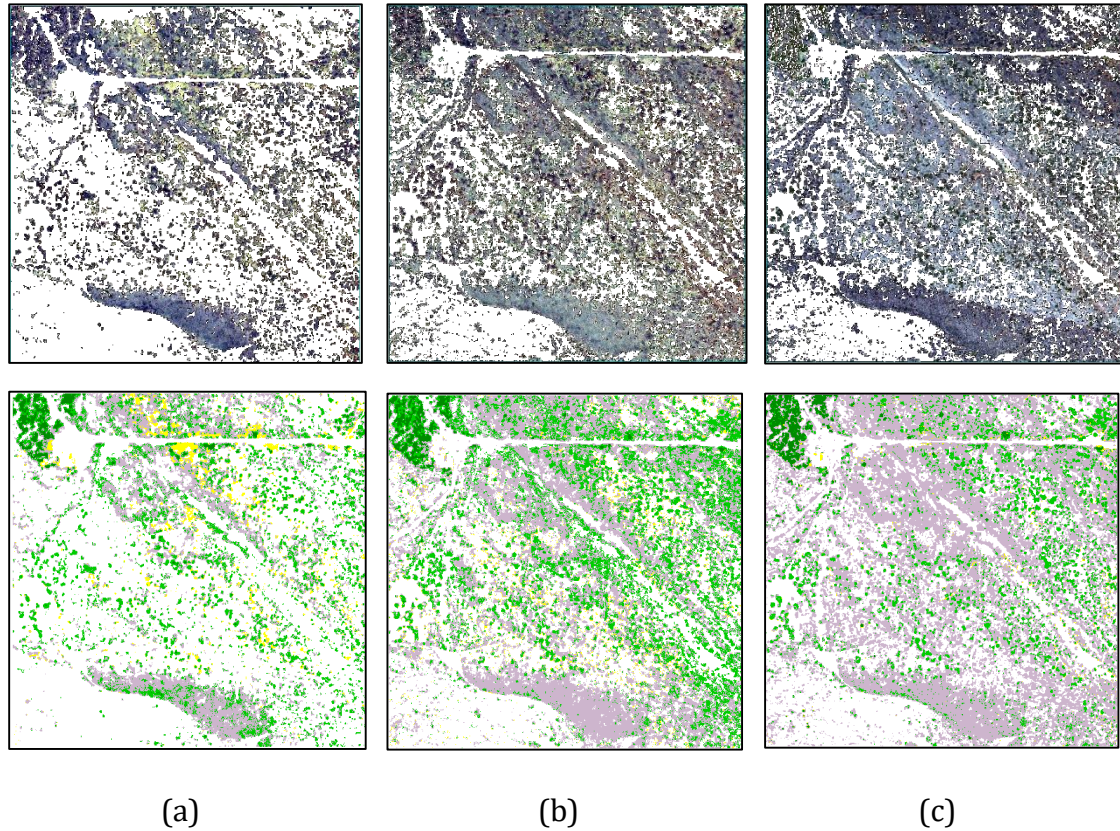


Figure 9. Up: Masked and pre-processed images: (a) QB, (b) WV-2 and (c) CASI. Down: Classification maps: (a) Quickbird, (b) Worldview-2 and (c) CASI imagery (light green: *S. supranubius*; dark green: *P. canariensis*; violet: *P. lasiospermus*; yellow: *D. bourgaeana*).

### *Classification results*

It is important to highlight the difficulty in classifying some types of vegetation due to the complexity of this heterogeneous shrubland ecosystem with mixed and small vegetation species such as *D. bourgaeana*. Hence, the major impact on the mapping of different types of vegetation is the misclassification created within the plant species, due to their spectral similarity and the mixing contributions from different covers in some pixels. Thus, it is important to create a reliable training sample database, which allows an accurate supervised classification to be made. This assumption leads us back to the importance of obtaining a fused image with the maximum spatial quality that allows to differentiate some small size species from others, avoiding pixel misclassification but also preserving the original spectral information.

A visual inspection of each classification was carried out to identify areas of potential error contrast between classifications. Moreover, the results of the classification were quantitatively assessed using the confusion matrices and the Overall Accuracy and Kappa coefficient.

Table 3 shows the SVM classification Overall Accuracy and the Kappa coefficient. It can be observed that accuracy increases depending on the type of imagery, being CASI imagery the most suitable sensor to obtain accurate thematic map, followed by WV-2 imagery. The main reason is the higher available number of spectral bands for the classification. Fig. 9 (down) presents the thematic maps for each scene. It is visually observed, the increase of *S. supranubius* in 2015, followed by a decrease in 2017. *P. lasiospermus* increases its coverage area from 2002 to 2017. *D. bourgaeana* seems to suffer a reduction of its cover area too, while *P. canariensis* remains stable.

Table 3. SVM classification Overall Accuracy and Kappa coefficient.

	Overall Accuracy (%)	Kappa coefficient
QB	77.99	0.632
WV-2	85.03	0.741
CASI	95.77	0.922

### Change Detection Analysis

Table 4 and Fig. 10 show the total vegetation and species coverage in the different years. Knowing the spatial resolution (0.5 m of pixel size) of each scene, it is possible to obtain specific coverage values in km<sup>2</sup>. It is observed how the total vegetation has almost doubled since 2002. Moreover, it is demonstrated that *P. canariensis* and *D. bourgaeana* have barely changed their coverage area, as it was expected taking into account the previous works of Olano et al. 2017 and Cubas et al. 2018. On the other hand, *P. lasiospermus* has increased from 2002 to 2017, tripling its initial extent in the last 15 year; while *S. supranubius* has experienced an increase of 0.032 km<sup>2</sup> from 2002 to 2011, however, its population has decreased by 2017 to lower values than in 2002, with a net loss of 0.014 km<sup>2</sup> in the 15 years analyzed.

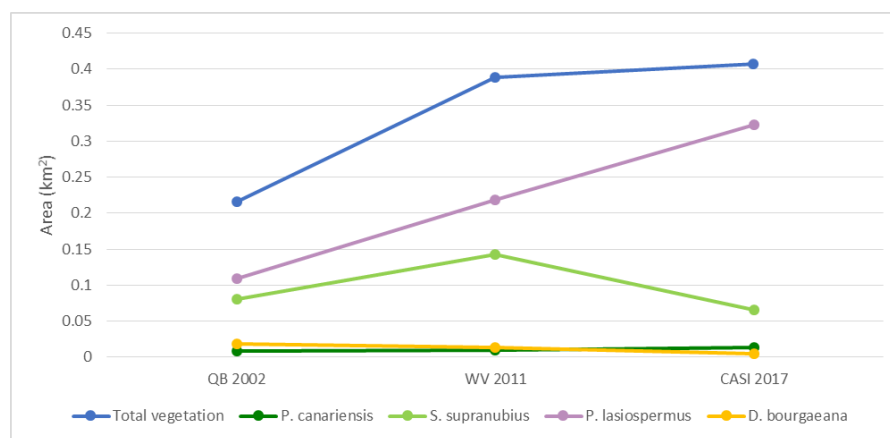


Figure 10. Vegetated area and plant species coverage in 2002, 2011 and 2017 in the different scenes.

Table 4. Vegetation and plant species coverage in % and km<sup>2</sup> in the different scenes.

	<b>QB 2002</b>		<b>WV 2011</b>		<b>CASI 2017</b>	
	%	km <sup>2</sup>	%	km <sup>2</sup>	%	km <sup>2</sup>
<b><i>Total vegetation</i></b>	31.33	0.215	56.61	0.388	59.38	0.407
<b><i>P. canariensis</i></b>	1.16	0.008	1.24	0.009	1.90	0.013
<b><i>S. supranubius</i></b>	11.69	0.080	16.35	0.112	9.65	0.066
<b><i>P. lasiospermus</i></b>	15.83	0.109	34.05	0.234	47.16	0.323
<b><i>D. bourgaeana</i></b>	2.66	0.018	4.97	0.034	0.68	0.005

The results are influenced by the many factors: sensor spatial resolution, mixing of species, classification accuracies, etc. However, they provide quite accurate information about the dynamics of the Teide ecosystem and it is possible to obtain reasonable trends of the vegetation changes in the habitat.

## DISCUSSION

A complex ecosystem, with mixed vegetation and small size, was analyzed using remote sensing data, being a challenging methodological framework. Specifically, it was observed the necessity to perform accurate pre-processing steps in order to improve the spectral and spatial quality of the imagery. Vegetation indices were also applied to improve the final mapping accuracy. After performing the specific pre-processing steps, it was possible to obtain quite reliable thematic maps applying the SVM algorithm, properly trained and parameterized, which were used for the change detection study.

Multi-source and multi-temporal remote sensing imagery were used to complement and add accurate information to field observations for a future ecosystem management. Important outcomes of the study are the increase in the coverage of vegetation (practically doubled) in 15 years, the dominance of *P. lasiospermus* whose extension has almost tripled, and the decline of *S. supranubius* (despite the rebound of 2011), corroborating the works by Olano et al. 2017 and Cubas et al. 2018, for specific test locations. It surprises the rapid expansion of *P. lasiospermus*, a very rare species several decades ago, whose current predominance is accelerated vigorously, altering the landscape in this sector of the high mountain ecosystem. Undoubtedly, the aforementioned facilitating effect of herbivores, their better resistance to herbivory, and their own thermophilic character, are factors that help explaining their considerable increase in a warming scenario.

Thanks to remote sensing, it has been possible to study those changes in a larger area, as well as obtaining quantitative results of how the species coverage and location have changed during years. However, some advanced tasks have to be

undertaken before satisfactory results can be achieved (i.e. suitable data, pre-processing, develop accurate classification models, knowledge of the study area, and time and cost restrictions). In conclusion, the remote sensing framework proposed is ecological relevant, statistical credible, cost-effective, flexible and transferability to other systems giving a guidance to environmental managers to consider remote sensing as a useful tool. Moreover, hints and advices are given to facilitate the framework application to other habitats and ecosystems.

Future studies will include the systematic change detection monitoring in the whole Teide National Park, using Worldview-2 and Worldview-3 imagery, in order to obtain more accurate results and with a continuity during years. Moreover, vegetation features, habitat heterogeneity, species richness, species-area relationships can be extracted from this study. Thus, specific research plans could be implemented following the proposed framework.

## **ACKNOWLEDGEMENTS**

This research has been supported by the ARTEMISAT-2 (CTM2016-77733-R) project, which was funded by the Spanish Agencia Estatal de Investigación (AEI) and by the Fondo Europeo de Desarrollo Regional (FEDER). This work was completed while E. I-U was a Ph.D. student in the IOCAG Doctoral Program in Oceanography and Global Change (ULPGC), and it was funded by the Spanish Ministerio de Economía y Competitividad with a FPI grant (BES-2014-069426).

## **LITERATURE CITED**

- Alqurashi, A. F., and L. Kumar. 2013. Investigating the use of remote sensing and GIS techniques to detect land use and land cover change: A review. *Advances in Remote Sensing* **2**:193.
- Aplin, P. 2004. Remote sensing: land cover. *Progress in Physical Geography* **28**:283-293.
- Ballanti, L., L. Blesius, E. Hines, and B. Kruse. 2016. Tree species classification using hyperspectral imagery: A comparison of two classifiers. *Remote Sensing* **8**:445.
- Bioucas-Dias, J. M., A. Plaza, G. Camps-Valls, P. Scheunders, N. Nasrabadi, and J. Chanussot. 2013. Hyperspectral remote sensing data analysis and future challenges. *IEEE Geoscience and remote sensing magazine* **1**:6-36.
- Brito, P., J. R. Lorenzo, Á. M. González-Rodríguez, D. Morales, G. Wieser, and M. S. Jimenez. 2014. Canopy transpiration of a *Pinus canariensis* forest at the tree line: implications for its distribution under predicted climate warming. *European journal of forest research* **133**:491-500.
- Bruzzzone, L., and L. Carlin. 2006. A multilevel context-based system for classification of very high spatial resolution images. *IEEE Transactions on Geoscience and Remote Sensing* **44**:2587-2600.
- Camps-Valls, G., L. Gómez-Chova, J. Muñoz-Marí, J. L. Rojo-Álvarez, and M. Martínez-Ramón. 2008. Kernel-based framework for multitemporal and multisource remote sensing data classification and change detection. *IEEE Transactions on Geoscience and Remote Sensing* **46**:1822-1835.



- Coppin, P., I. Jonckheere, K. Nackaerts, and B. Muys. 2004. Digital Change Detection Methods in Ecosystem Monitoring: a review. *International Journal of Remote Sensing* **25**:1565-1596.
- Corbane, C., S. Alleaume, and M. Deshayes. 2013. Mapping natural habitats using remote sensing and sparse partial least square discriminant analysis. *International Journal of Remote Sensing* **34**:7625-7647.
- Cortes, C., and V. Vapnik. 1995. Support vector machine. *Machine learning* **20**:273-297.
- Cubas, J., J. L. Martín-Esquivel, M. Nogales, S. D. Irl, R. Hernández-Hernández, M. López-Darias, M. Marrero-Gómez, M. J. del Arco, and J. M. González-Mancebo. 2018. Contrasting effects of invasive rabbits on endemic plants driving vegetation change in a subtropical alpine insular environment. *Biological Invasions* **20**:793-807.
- Chapuis, J.-L., Y. Frenot, and M. Lebouvier. 2004. Recovery of native plant communities after eradication of rabbits from the subantarctic Kerguelen Islands, and influence of climate change. *Biological Conservation* **117**:167-179.
- de Miguel, E., A. Fernández-Renau, E. Prado, M. Jiménez, Ó. G. de la Cámara, C. Linés, J. A. Gómez, A. I. Martín, and F. Muñoz. 2014. The processing of CASI-1500I data at INTA PAF. *EARSeL eProceedings* **13**:30-37.
- del Arco Aguilar, M.-J., R. González-González, V. Garzón-Machado, and B. Pizarro-Hernández. 2010. Actual and potential natural vegetation on the Canary Islands and its conservation status. *Biodiversity and Conservation* **19**:3089-3140.
- Digital Globe, U. S. Digital Globe Satellite Information  
<https://www.digitalglobe.com/resources/satellite-information>.
- ENVI. 2004. ENVI User's Guide. Research System Inc.
- Fauvel, M., Y. Tarabalka, J. A. Benediktsson, J. Chanussot, and J. C. Tilton. 2013. Advances in spectral-spatial classification of hyperspectral images. *Proceedings of the IEEE* **101**:652-675.
- Feilhauer, H., F. Thonfeld, U. Faude, K. S. He, D. Rocchini, and S. Schmidlein. 2013. Assessing floristic composition with multispectral sensors—A comparison based on monotemporal and multiseasonal field spectra. *International Journal of Applied Earth Observation and Geoinformation* **21**:218-229.
- Förster, M., M. Zebisch, I. Wagner-Lücker, T. Schmidt, K. Renner, and M. Neubert. 2014. Remote sensing-based monitoring of potential climate-induced impacts on habitats. Pages 95-113 *Managing Protected Areas in Central and Eastern Europe Under Climate Change*. Springer.
- Galvão, L. S., Í. Vitorello, and R. Almeida Filho. 1999. Effects of band positioning and bandwidth on NDVI measurements of tropical savannas. *Remote Sensing of Environment* **67**:181-193.
- Ghamisi, P., J. A. Benediktsson, and S. Phinn. 2015. Land-cover classification using both hyperspectral and LiDAR data. *International Journal of Image and Data Fusion* **6**:189-215.
- Ghamisi, P., J. Plaza, Y. Chen, J. Li, and A. J. Plaza. 2017. Advanced spectral classifiers for hyperspectral images: A review. *IEEE Geoscience and remote sensing magazine* **5**:8-32.
- Gong, M., P. Zhang, L. Su, and J. Liu. 2016. Coupled dictionary learning for change detection from multisource data. *IEEE Transactions on Geoscience and Remote Sensing* **54**:7077-7091.

- González-Rodríguez, Á. M., P. Brito, J. R. Lorenzo, A. Gruber, W. Oberhuber, and G. Wieser. 2017. Seasonal cycles of sap flow and stem radius variation of *Spartocytisus supranubius* in the alpine zone of Tenerife, Canary Islands. *Alpine Botany* **127**:97-108.
- Huete, A. R. 1988. A soil-adjusted vegetation index (SAVI). *Remote Sensing of Environment* **25**:295-309.
- Hughes, G. 1968. On the mean accuracy of statistical pattern recognizers. *IEEE transactions on information theory* **14**:55-63.
- Ibarrola-Ulzurrun, E., C. Gonzalo-Martin, J. Marcello-Ruiz, A. Garcia-Pedrero, and D. Rodriguez-Esparragon. 2017a. Fusion of High Resolution Multispectral Imagery in Vulnerable Coastal and Land Ecosystems. *Sensors* **17**:228.
- Ibarrola-Ulzurrun, E., C. Gonzalo-Martín, and J. Marcello. 2017b. Influence of pansharpening in obtaining accurate vegetation maps. *Canadian Journal of Remote Sensing* **43**:528-544.
- Ibarrola-Ulzurrun, E., J. Marcello, and C. Gonzalo-Martin. 2017c. Assessment of Component Selection Strategies in Hyperspectral Imagery. *Entropy* **19**:666.
- Ibarrola-Ulzurrun, E., J. Marcello, and C. Gonzalo-Martin. 2018. Advanced Classification of Remote Sensing High Resolution Imagery. An Application for the Management of Natural Resources. Pages 1-13 *Developments and Advances in Intelligent Systems and Applications*. Springer.
- Jianya, G., S. Haigang, M. Guorui, and Z. Qiming. 2008. A review of multi-temporal remote sensing data change detection algorithms. *The International Archives of the Photogrammetry, Remote Sensing and Spatial Information Sciences* **37**:757-762.
- Jiménez-Michavila, M. 2011. Cartografía de especies de matorral de la Reserva Biológica de Doñana mediante el sistema hiperespectral aeroportado INTA-AHS. Implicaciones en el estudio y seguimiento del matorral de Doñana. Universidad Autónoma de Madrid.
- Lausi, D., and P. L. Nimis. 1986. Leaf and canopy adaptations in a high-elevation desert on Tenerife, Canary Islands. *Vegetatio* **68**:19-31.
- Lu, D., P. Mausel, E. Brondizio, and E. Moran. 2004. Change detection techniques. *International Journal of Remote Sensing* **25**:2365-2401.
- Lu, D., and Q. Weng. 2007. A survey of image classification methods and techniques for improving classification performance. *International Journal of Remote Sensing* **28**:823-870.
- Manley, P. N., W. J. Zielinski, C. M. Stuart, J. J. Keane, A. J. Lind, C. Brown, B. L. Plymale, and C. O. Napper. 2000. Monitoring ecosystems in the Sierra Nevada: the conceptual model foundation. *Environmental Monitoring and Assessment* **64**:139-152.
- Marcello, J., F. Eugenio, U. Perdomo, and A. Medina. 2016. Assessment of Atmospheric Algorithms to Retrieve Vegetation in Natural Protected Areas Using Multispectral High Resolution Imagery. *Sensors* **16**:1624.
- Martín, J. L., J. Bethencourt, and E. Cuevas-Agulló. 2012. Assessment of global warming on the island of Tenerife, Canary Islands (Spain). Trends in minimum, maximum and mean temperatures since 1944. *Climatic Change* **114**:343-355.
- Mason, T., D. Keith, and A. Letten. 2017. Detecting state changes for ecosystem conservation with long-term monitoring of species composition. *Ecological Applications* **27**:458-468.

- Medina-Machín, A., J. Marcello, A. Hernández-Cordero, J. Martín-Abasolo, and F. Eugenio. 2018. Vegetation species mapping in a coastal-dune ecosystem using high resolution satellite imagery. *GIScience & Remote Sensing*:1-23.
- Melgani, F., and L. Bruzzone. 2004. Classification of hyperspectral remote sensing images with support vector machines. *IEEE Transactions on Geoscience and Remote Sensing* **42**:1778-1790.
- Mouat, D. A., G. G. Mahin, and J. Lancaster. 1993. Remote sensing techniques in the analysis of change detection. *Geocarto International* **8**:39-50.
- Mountrakis, G., J. Im, and C. Ogole. 2011. Support vector machines in remote sensing: A review. *ISPRS Journal of Photogrammetry and Remote Sensing* **66**:247-259.
- Mueller, M., and J. Geist. 2016. Conceptual guidelines for the implementation of the ecosystem approach in biodiversity monitoring. *Ecosphere* **7**:e01305.
- Nunez-Casillas, L., F. Micand, B. Somers, P. Brito, and M. Arbelo. 2012. Plant species monitoring in the Canary Islands using WorldView-2 imagery. *ISPRS-International Archives of the Photogrammetry, Remote Sensing and Spatial Information Sciences*:301-304.
- Olano, J. M., P. Brito, Á. M. González-Rodríguez, J. L. Martín-Esquivel, M. García-Hidalgo, and V. Rozas. 2017. Thirsty peaks: Drought events drive keystone shrub decline in an oceanic island mountain. *Biological Conservation* **215**:99-106.
- Pepin, N., and J. Lundquist. 2008. Temperature trends at high elevations: patterns across the globe. *Geophysical Research Letters* **35**.
- Perera-Castro, A., P. Brito, and A. González-Rodríguez. 2017a. Changes in thermic limits and acclimation assessment for an alpine plant by chlorophyll fluorescence analysis:  $F_v/F_m$  vs.  $R_{fd}$ . *Photosynthetica*:1-10.
- Perera-Castro, A. V., P. Brito, and A. M. Gonzalez-Rodriguez. 2017b. Light response in alpine species: Different patterns of physiological plasticity. *Flora* **234**:165-172.
- Petit, C., and E. Lambin. 2001. Integration of multi-source remote sensing data for land cover change detection. *International Journal of Geographical Information Science* **15**:785-803.
- Rodriguez-Galiano, V., M. Chica-Olmo, F. Abarca-Hernandez, P. Atkinson, and C. Jeganathan. 2012. Random Forest classification of Mediterranean land cover using multi-seasonal imagery and multi-seasonal texture. *Remote Sensing of Environment* **121**:93-107.
- Rosenfield, G. H., and K. Fitzpatrick-Lins. 1986. A coefficient of agreement as a measure of thematic classification accuracy. *Photogrammetric engineering and remote sensing* **52**:223-227.
- Rouse Jr, J. W., R. Haas, J. Schell, and D. Deering. 1974. Monitoring vegetation systems in the Great Plains with ERTS.
- Singh, A. 1989. Review article digital change detection techniques using remotely-sensed data. *International Journal of Remote Sensing* **10**:989-1003.
- Spanhove, T., J. V. Borre, S. Delalieux, B. Haest, and D. Paelinckx. 2012. Can remote sensing estimate fine-scale quality indicators of natural habitats? *Ecological Indicators* **18**:403-412.
- Sventenius, E. R. 1946. Notas sobre la flora de Las Cañadas de Tenerife. Instituto Nacional de Investigaciones Agronómicas, Centro de las Islas Canarias.

- Tarabalka, Y., J. Chanussot, and J. A. Benediktsson. 2010. Segmentation and classification of hyperspectral images using watershed transformation. *Pattern Recognition* **43**:2367-2379.
- Volpi, M., D. Tuia, F. Bovolo, M. Kanevski, and L. Bruzzone. 2013. Supervised change detection in VHR images using contextual information and support vector machines. *International Journal of Applied Earth Observation and Geoinformation* **20**:77-85.
- Wang, Q., and J. D. Tenhunen. 2004. Vegetation mapping with multitemporal NDVI in North Eastern China transect (NECT). *International Journal of Applied Earth Observation and Geoinformation* **6**:17-31.
- Xia, J., N. Falco, J. A. Benediktsson, P. Du, and J. Chanussot. 2017. Hyperspectral Image Classification With Rotation Random Forest Via KPCA. *IEEE Journal of Selected Topics in Applied Earth Observations and Remote Sensing* **10**:1601-1609.
- Xie, Y., Z. Sha, and M. Yu. 2008. Remote sensing imagery in vegetation mapping: a review. *Journal of plant ecology* **1**:9-23.
- Yamano, H., J. Chen, and M. Tamura. 2003. Hyperspectral identification of grassland vegetation in Xilinhot, Inner Mongolia, China. *International Journal of Remote Sensing* **24**:3171-3178.





# CHAPTER 8. CONCLUSIONS AND FUTURE RESEARCH





## 8.1. CONCLUSIONS AND CONTRIBUTIONS

The general objective of the Thesis was the study of processing methodologies which, when applied to very high resolution multispectral and hyperspectral remote sensing imagery, serve to obtain accurate information for the conservation of natural areas. Advanced processing methodologies, applied to remote sensing data, have been reviewed, studied and evaluated for the subsequent monitoring and management of land resources in several complex and vulnerable ecosystems of Canary Islands (Spain).

Novel and suitable methodologies have been compiled on: the acquisition of data of the study area and plant communities, the pre-processing (pansharpening, orthorectification, dimensionality reduction in HS imagery, etc.) and classification of MS and HS data at both pixel and object levels. In this context, pre-processing techniques, as well as spectral unmixing and classification methodologies for both MS and HS data, have been the main topics addressed in the Thesis.

One of the most challenging aspect of this Thesis was the generation of reliable and accurate products in heterogeneous and complex ecosystems with plant species with small size and low leaf area. Usually, remote sensing are applied in non-complex ecosystems, with well-differentiated classes and without high spectral variability within the image, such as different blooming dates within species, plant species variability due to the area, topographic changes, etc. Thus, it is shown during the whole manuscript the importance of the pre-processing techniques in this type of complex ecosystems.

Specific conclusions have been discussed in the different chapters, but to summarize:

1. Regarding the selection of the appropriate data for the characterization of the ecosystems to be analyzed, we can conclude the importance to choose the suitable imagery, depending on the final study purpose. For instance, it is demonstrated how Worldview satellite imagery would be the most suitable data to perform change detection studies at specific level in the considered ecosystem, covering a large area and achieving a good compromise between the spectral and spatial resolutions.  
Moreover, *in-situ* measures and ancillary data were essential during the processing of the data, such as ground truth data for the supervised classification, DEMs for the orthorectification, orthophotos for HS sharpening, etc.
2. The second specific objective was to analyze, validate and apply advanced pre-processing algorithms to generate imagery with high spatial and spectral quality. During the Thesis, it was shown that the selection of accurate pre-processing techniques is critical to improve the spectral and spatial quality



information of the imagery (atmospheric correction, image sharpening, orthorectification, etc.).

Specifically, advanced pansharpening methods in MS imagery are important to obtain image with finer spatial detail, fundamental due to the small size of the plants to be discriminated. Moreover, pansharpening is studied not only as the most suitable technique for different ecosystems, but also as an essential step for high resolution imagery, in order to obtain accurate thematic maps. On the other hand, the fusion of airborne HS imagery with higher spatial resolution data (orthophotos, drone, etc.) can be an important pre-preprocessing for the monitoring of complex ecosystems. A comprehensive assessment has been carried out and the benefits and drawbacks of HS sharpening methods have been identified.

3. Concerning the objective of developing specific products for the management of land resources, it has been highlighted during the whole work the challenge of obtaining accurate vegetation maps in some vulnerable and heterogenic ecosystems, as Teide National Park. As it was said in the specific objectives, the research difficulty is the generation of a robust and automatic methodology for the systematic mapping of heterogeneous ecosystems. In this context, the first remark is that those mixed ecosystems need advanced processing techniques and very high resolution data. For instance, object-based classification provides better results in heterogenic ecosystems using VHR MS imagery. On the other hand, advanced unmixing techniques are needed to address the spectral variability of heterogenic and mixed ecosystems using HS imagery. In this case, it is possible to get suitable abundance estimations and accurate thematic maps, without applying hyperdimensionality reduction techniques, and thus, avoiding the “Hughes” effect.

Regarding the classification methodologies, they have not been only used to obtain the vegetation maps at species level, but also as an indirect method to evaluate the importance of pansharpening, to assess the suitable number of components in HS data and to analyze the performance of spectral unmixing techniques. The most suitable and robust classification algorithm to apply in the MS and HS data was identified.

4. The last specific objective was to study the variability of natural resources in the Teide National Park. The specific conclusions of this objective are described in detail in Chapter 7, in which a frame work selected for change detection in heterogenic land ecosystems was identified, after testing different options. Thus, we can conclude that remote sensing is an important tool for detecting changes in large areas in an automatic, continuous and effective way. It provides quantitative results of the species coverage and how they have changed during a temporal period.

We can confirm that the Thesis provides important information of the performance of algorithms at different levels of the pre-processing chain. In

addition, a general framework for the processing of very high resolution MS and HS data has been developed, that could be used as a reference for the generation of land products in similar ecosystems. It has been shown that the thematic maps obtained by different methodologies, are accurate enough. Moreover, the potential used of the vegetation maps, at species level, for carrying out an environmental plan has been discussed. The information provided in this work is used at operational level by the Teide National Park managers.

As a final though, the current society has effects on the natural environment, not only negative effects such as using the natural resources and degrading ecosystems, but also positive effects, protecting natural areas of interest. This Thesis allows the analysis of fundamental environmental parameters for different sectors of high socio-economic interest, since the economic impact of the natural resources used by humans is linked to tourism, pollution, loss of biodiversity, sustainable management of plant resources and climate change.

## **8.2. FUTURE RESEARCH**

The outcome of the Thesis allows the scientific community to have a number of image processing techniques applicable to multi-source sensors. This enables the development of studies at the highest possible resolution and increases the potential of research for environmental management, especially in vulnerable and complex ecosystems. However, additional improvements can be undertaken.

In this context, future research could be to:

- Obtain accurate land products using HS drone imagery at a very high spatial resolution (for instance, less than 10 cm). This will lead to studies of specific conditions of the shrubs appearing in the ecosystems studied during the Thesis. Due to the ultra-high spatial resolution, chemical components of the small leaves can be analyzed and studied, the hydric stress of the plant species and the health status, as well as several physiological parameters.
- Include ancillary data, such as orthophotos, LiDAR and SAR imagery, in the framework described during the Thesis, to improve:
  - Change detection using textural parameters from orthophotos from several decades ago, when RGB information was not available, until the present.
  - Use LiDAR and SAR data, which can complement MS and HS imagery. For instance, LiDAR can be used to obtain improved DEMs on each study, to analyze the geomorphological structures from the land, to study the height of specific plant species, calculate the biomass, detection of areas prone to fire propagation, detection of soil moisture, identification and analysis of ecosystem degradation, etc.

- On the other hand, high resolution SAR data combined with the optical and infrared information can improve the classification accuracies.
- Study changes in other areas of interest of the Teide National Park, using the same type of imagery (i.e. Worldview-2 and Worldview-3), which could have a continuity on time during years. Besides, study the dynamics in land resources over time and its possible relationship with climate change or anthropogenic factors in Teide National Park.
- Validate the whole framework in other study areas of interest in the Canary Islands or other similar regions around the world.
- Analyze and validate deep learning approaches for both MS and HS classification, such as CNNs.

### **8.3. SCIENTIFIC CONTRIBUTIONS**

Next, the publications derived from this thesis are shown:

#### **8.3.1. Publications**

- J. Marcello, E. Ibarrola-Ulzurrun, C. Gonzalo-Martín, J. Chanussot, G. Vivone. Assessment of hyperspectral sharpening for the monitoring of natural areas using multiplatform remote sensing imagery. *Transactions on Geoscience and Remote Sensing*. Under review.
- E. Ibarrola-Ulzurrun, J. Marcello, C. Gonzalo-Martín, J.L. Martín-Esquivel. Temporal dynamics analysis of a mountain ecosystem based on multi-source and multi-scale remote sensing data. *Ecosphere Journal*. Under review.
- E. Ibarrola-Ulzurrun, L. Drumetz, J. Marcello, C. Gonzalo-Martín, J. Chanussot. Hyperspectral Classification through Unmixing Abundance Maps Addressing Spectral Variability. *Transactions on Geoscience and Remote Sensing*. Accepted.
- E. Ibarrola-Ulzurrun, J. Marcello, C. Gonzalo-Martín. Assessment of Component Selection Strategies in Hyperspectral Imagery. *Entropy*, 2017, 19(2).
- E. Ibarrola-Ulzurrun, C. Gonzalo-Martín, J. Marcello. Influence of pansharpening in obtaining accurate vegetation maps. *Canadian Journal of Remote Sensing*, 2017, pp. 1-17.
- E. Ibarrola-Ulzurrun, C. Gonzalo-Martín, J. Marcello-Ruiz, García-Pedrero, A., Rodríguez-Esparragón, D, 2016. Fusion of High Resolution Multispectral images in vulnerable coastal and land ecosystems. *Sensors* 2017, 17(2), pp. 228.

#### **8.3.2. Book Chapters**

- E. Ibarrola-Ulzurrun, J. Marcello, C. Gonzalo-Martín. Advanced Classification of Remote Sensing High Resolution Imagery. *An Application for the Management*

of Natural Resources. In *Developments and Advances in Intelligent Systems and Applications 2018*, pp. 1-13. Springer, Cham.

### 8.3.3. Conferences

- E. Ibarrola-Ulzurrun, L. Drumetz, J. Chanussot, J. Marcello-Ruiz, C. Gonzalo-Martín. Classification using unmixing models in areas with substantial endmember variability. WHISPERS, September 2018. Amsterdam (Netherlands).
- E. Ibarrola-Ulzurrun, L. Drumetz, J. Chanussot, C. Gonzalo-Martín, J. Marcello-Ruiz. Extended Linear Mixing Model in an ecosystem with high spectral variability. IGARSS, July 2018. Valencia (Spain).
- E. Ibarrola-Ulzurrun, J. Marcello-Ruiz, C. Gonzalo-Martín, J. Chanussot. Evaluation of hyperspectral classification maps in heterogeneous ecosystem. IGARSS, July 2018. Valencia (Spain).
- E. Ibarrola-Ulzurrun, C. Gonzalo-Martín, J. Marcello-Ruiz. Evaluación de técnicas de reducción de la dimensionalidad en imágenes hiperespectrales y su aplicación para la clasificación de ecosistemas terrestres. AET Conference, October 2017. Murcia (Spain).
- E. Ibarrola-Ulzurrun, J. Marcello, C. Gonzalo-Martín. Cartografiado de un ecosistema costero vulnerable mediante clasificación basada en objetos en imágenes de muy alta resolución. AET Conference, October 2017. Murcia (Spain).
- E. Ibarrola-Ulzurrun, C. Gonzalo-Martín, J. Marcello-Ruiz. Vulnerable land ecosystems classification using spatial context and spectral indices. SPIE Remote Sensing Conference, September 2017. Warsaw (Poland).
- E. Ibarrola-Ulzurrun, J. Marcello, C. Gonzalo-Martín. Evaluation of dimensionality reduction techniques in hyperspectral imagery and their application for the classification of terrestrial ecosystems. SPIE Remote Sensing Conference, September 2017. Warsaw (Poland).
- E. Ibarrola-Ulzurrun, J. Marcello-Ruiz, C. Gonzalo-Martín. Sea floor mapping of coastal ecosystems using very high resolution imagery and OBIA classification. International Congress Energy and Environmental Engineering and Management, July 2017. Las Palmas de Gran Canaria (Spain).
- E. Ibarrola-Ulzurrun, C. Gonzalo-Martín, J. Marcello-Ruiz. Influence of pansharpening techniques in obtaining accurate vegetation thematic maps. SPIE Remote Sensing Conference, September 2016. Edinburgh (United Kingdom).
- E. Ibarrola-Ulzurrun, J. Marcello-Ruiz, C. Gonzalo-Martín. Pansharpening in coastal ecosystems using Worldview-2 imagery. SPIE Remote Sensing Conference, September 2016. Edinburgh (United Kingdom).
- Ulzurrun, E. I., Martín, C. G., & Ruiz, J. M. Analysis of Land and marine resources by processing high resolution satellite images. In *11th Iberian Conference on Information Systems and Technologies (CISTI)* (pp. 1-4), June 2016. Gran Canaria (Spain).

- J. Marcello, F. Marqués, F. Eugenio, A. Medina y E. Ibarrola. Selección de información espacial para mejorar la clasificación temática en imágenes de alta resolución. AET Conference, October 2015. Sevilla (Spain).
- A. García-Pedrero, D. Rodríguez-Esparragón, J. Marcello-Ruiz, E. Ibarrola-Ulzurrun, M. Lillo-Saavedra and J. Marcello-Ruiz. Automatic identification of shrub vegetation of the Teide National Park. IWOB1, July 2015. San Sebastian (Spain).

**ACRONYMS**

6S: Second Simulation of the Satellite Signal in the Solar Spectrum

AE: Autoencode

ANN: Artificial Neural Networks

ACORN: Atmosphere CORrection Now

ATCOR: Atmospheric and Topographic Correction

AutoMCU: Auto Monte Carlo Unmixing

AVHRR: Advanced Very High Resolution Radiometer

BT: Brovey Transform

CART: Classification and Regression Trees

CASI: Compact Airborne Spectrographic Imager

CC: Correlation coefficient

CDL: Coupled Dictionary Learning

CNMF: Coupled Nonnegative Matrix Factorization

CNN: Convolutional Neural Networks

CVA: Change Vector Analysis

DBN: Deep Belief Network

DCT: Discrete Cosine Transform

DEM: Digital Elevation Model

ELMM: Extended Linear Mixing Model

EM: Expectation Maximization

ERGAS: Spectral Relative Dimensionless Global Error (erreur relative globale adimensionnelle de synthèse)

FC: Frequency Comparison

FCLSU: Fully Constrained Least Squared Unmixing

FDM: Fractal Dimension Map

FIHS: Fast Intensity Hue Saturation

FLAASH: Fast one-of-sight Atmospheric Analysis of Spectral Hypercubus

FSC: Fast Sample Consensus

GCPs: Ground Control Points  
GEOBIA: Geographic Object-based image analysis  
GFPCA: Guided Filter PCA  
GIS: Geographic Information Systems  
GLCM: Gray Level Co-occurrence Matrix  
GLP: Generalized Laplacian Pyramid  
GPS: Global Position System  
GS: Gram-Schmidt  
GSA: GS Adaptive  
HCS: Hyperspherical Color Sharpening  
HPF: High-Pass-Filtering  
HPM: High-Pass-Modulation  
HS: Hyperspectral  
HSI: Hyperspectral imagery  
ICA: Independent Component Analysis  
IHS: Intensity-Hue-Saturation  
IM: Intensity Modulation  
INTA: Instituto Nacional de Técnica Aeroespacial  
IOCAG: Instituto de Oceanografía y Cambio Global  
KPCA: Kernel PCA  
KT: Kauth-Thomas  
LMM: Linear Mixing Model  
LT: Linear Transforming  
MAC: Maximum Abundance Classification  
MESMA: Multiple Endmember Spectral Mixture Analysis  
MIR: Middle Infrared  
MNF: Minimum Noise Fraction  
MODTRAN: MODerate spectral resolution atmospheric TRANsmittance  
MS: Multispectral

MSAVI2: Modified Soil Adjusted Vegetation Index

MTF: Modulation Transfer Function

MVPCA: Maximum-Variance PCA

NDVI: Normalized Difference Vegetation Index

NIR: Near Infrared

OA: Overall Accuracy

OBIA: Object-based image analysis

PAN: Panchromatic

PCA: Principal Component Analysis

PLMM: Perturbed Mixing Model

QB: Quickbird

QNR: Quality with No Reference

QUAC: Quick Atmospheric Correction

RANSAC: RANdom SAmple Consensus

RBMs: Restricted Boltzmann Machines

RE: Red Edge

RED: Red

RELMM: Robust ELMM

RGB: Red – Green – Blue

RMSE: Root Mean Square Error

ROI: Region of interest

RPC: Rational Polymodal Coefficients

SAM: Spectral Angle Mapper

SCLSU: Scaled Constrained Least Squares Unmixing

SFIM: Smoothing Filter-based Intensity Modulation

SPCA: Data Slicing PCA

SVM: Support Vector Machine

TD: Transformed Divergence



TM: Thematic Mapper

ULPGC: Universidad Las Palmas de Gran Canaria

UPM: Universidad Politécnica de Madrid

VHR: Very High Resolution

VHSR: Very High Spatial Resolution

VIS: Visible

WAT $\otimes$ FRAC: Weighted Wavelet '*à trous*' through Fractal Dimension Maps

WAVE\_ATROUS: Wavelet '*à trous*'

WV-2: Worldview-2



